A Dissertation

entitled

The Development of Alternative Green Sample Preparation Approaches for Analysis of Unconventional Environmental Pollutants

by

Ronald V. Emmons

Submitted to the Graduate Faculty as partial fulfillment of the requirements for the

Doctor of Philosophy Degree in

Chemistry

Dr. Emanuela Gionfriddo, Committee Chair

Dr. Dragan Isailovic, Committee Member

Dr. Jon R. Kirchhoff, Committee Member

Dr. Erin Prestwich, Committee Member

Dr. Scott Molitor, Dean
College of Graduate Studies

The University of Toledo
May 2023

An Abstract of

The Development of Alternative Green Sample Preparation Approaches for Analysis of Unconventional Environmental Pollutants

by

Ronald V. Emmons

Submitted to the Graduate Faculty as partial fulfillment of the requirements for the Doctor of Philosophy Degree in Chemistry

The University of Toledo

May 2023

The need for more robust, high-throughput sample preparation methodologies continues to grow as the analytical challenges of the modern world progress. This is apparent from the lowering advisory limits of environmental contaminants to the generation of novel anthropogenic wastes. Solid phase microextraction (SPME) technologies present unique qualities that enable it to tackle these challenges from an alternative approach. To date, there are a variety of matrices, contaminants and analytical tools that are still not well understood or reliably accounted for in the literature. This work advances the field of sample preparation with the development of novel extraction and separation workflows for the quantitative analyses of complex environmental matrices.

The first project of this work develops a sample preparation method for crude (4-methylcyclohexylmethanol (MCHM), a chemical blend commonly used in the coal industry for the separation of coal from rock, debris and coal dust by froth flotation. This mixture contains (4-methylcyclohexyl)methanol (68–89%), 4-(methoxymethyl)cyclohexanemethanol (4–22%); methyl 4-

methylcyclohexanecarboxylate (5%), dimethyl-1,4-cyclohexanedicarboxylate (1%), and 1,4-cyclohexanedimethanol (1–2%), which all occur in the cis and trans diastereoisomeric forms; along with water (4–10%) and methanol (1%). Significant attention regarding the impact of these compounds on human health arose in 2014, when a spill of crude MCHM into the Elk River resulted in the contamination of drinking water for over 300,000 residents in West Virginia and Kentucky in the United States. In response, a series of studies aimed to investigate the mixture's capacity for long-term exposure by determining the sorption properties of crude MCHM to pipes and linings. Sorbed MCHM was demonstrated to readily desorb from polyethylene into water at levels above the odor threshold, confirming the risk to residents from contaminated tap water pipelines. In light of this, it is imperative to develop analytical tools that enable the detection of crude MCHM components in environmental water samples for routine water monitoring. In this work, two SPME methods, based on fiber and thin film geometry, were developed and validated and coupled to gas chromatography – mass spectrometry (GC-MS). Their performances were compared with a modified solid-phase extraction (SPE) protocol based on EPA Method 522 for the analysis of volatiles in water. Both SPME methods demonstrated lower limits of quantitation (LOQ) compared to the SPE protocol. Thin film solid phase microextraction (TF-SPME), due its superior sensitivity and faster throughput was selected as the optimal extraction approach for 4-MCHM and other constituents of crude MCHM, with LOQ below the odor threshold for aqueous crude MCHM in distilled water at 19–21 °C (0.55 µg L^{-1}).

The second project focuses on the untargeted analysis of unconventional oil and gas waste. Produced water (PW), the primary waste byproduct of these operations, contains

a diverse number of anthropogenic additives together with the numerous hydrocarbons extracted from the well. Due to potential environmental hazards, it is critical to characterize the chemical composition of this type of waste before proper disposal or remediation/reuse. In this work, a TF-SPME approach was developed and optimized to characterize produced water. The thin film device consisted of hydrophilic-lipophilic balance particles embedded in polydimethylsiloxane and immobilized on a carbon mesh surface. These devices were chosen to provide broad extraction coverage and high reusability. Various parameters were evaluated to ensure reproducible results while minimizing analyte loss. This optimized protocol, consisting of a 15 min extraction followed by a short (3 s) rinsing step, enabled the reproducible analysis of produced water without any sample pretreatment. Extraction efficiency was suitable for both produced water additives and hydrocarbons. The developed approach was able to tentatively identify a total of 201 compounds from produced water samples, by using one-dimensional GC-MS and data deconvolution.

The third project continues work on PW. This waste has been shown to contain petroleum distillates, polycyclic aromatic hydrocarbons (PAHs), and organic fracturing additives, along with dissolved salts, heavy metals, and naturally-occurring radioactive materials (NORMs). Identification of these compounds is critical to develop future reuse and disposal protocols to minimize environmental contamination and potential health risks. In this study, versatile extraction methodologies were investigated for the untargeted analysis of PW. TF-SPME with hydrophilic-lipophilic balance particles (HLB) was utilized for the extraction of organic solubles from eight PW samples from the Permian Basin and Eagle Ford formation in Texas. GC-MS analysis found a total of 266 different organic constituents including 1,4-dioxane, atrazine, pyridine, PAHs, and substituted alkyl

chain hydrocarbons. The elemental composition of PW was evaluated using dispersive solid-phase extraction (D-SPE) followed by inductively coupled plasma – mass spectrometry (ICP-MS), utilizing a new coordinating sorbent, poly(pyrrole-1-carboxylic acid). ICP-MS analysis confirmed the presence of 29 elements including major (Mg, Mn, Zn, Se, Ag, Ba) and trace rare earth elements, as well as hazardous metals, such as Cr, Cd, Pb, and U. Utilizing chemometric analysis, both approaches facilitated the discrimination of each PW sample based on their geochemical origin with a prediction accuracy above 90% using partial least squares-discriminant analysis (PLS-DA), paving the way for PW origin tracing in the environment.

In the fourth project, an introduction method for direct ambient mass spectrometry was developed and tested for drugs and pesticides in the environment. Direct ambient mass spectrometry (AMS) methodologies significantly increase sample throughput, can be adapted for onsite analysis and are often regarded as semi-quantitative by most developed protocols. One of the limitations of AMS, especially for onsite analysis applications, is the irreproducibility of the measurements related to the occurrence of transient microenvironments (TME) and variable background interferences. In this work, we report an effective strategy to minimize these effects by hyphenating, for the first time, arrow solid phase microextraction (Arrow-SPME) to mass spectrometry via a thermal desorption unit (TDU) and Direct Analysis in Real Time (DART) source. The developed method was optimized for extracting and analyzing pesticides and pharmaceuticals from surface water. It was demonstrated that the hyphenation of the SPME and TDU-DART resulted in reduced background contamination, indicating the suitability of the method for onsite analysis even in variable and non-ideal environments. Model analytes were quantified in the low µg/L

range with a total analysis time of less than 5 min, linear dynamic ranges (LDR), and interday reproducibility for most compounds being 2.5 – 500 µg/L and 10 %, respectively. The developed approach provides an excellent analytical tool that can be applied for the onsite high-throughput analysis of water samples as well as air and aerosols. Considering the tunability of our extraction process, time-resolved environmental monitoring can be achieved onsite within minutes.

Continuing DART related work, the fifth project develops a strategy for analyzing per- and polyfluoroalkyl substances (PFAS), an emerging toxic class of anthropogenic chemicals that are persistent in the environment, are currently regulated at the low part-per-trillion level worldwide. Quantification and screening of these compounds currently rely mostly on liquid-chromatography hyphenated to mass spectrometry. The growing need for quicker and more robust analysis in routine monitoring has been, in many ways, spearheaded by the advent of direct ambient mass spectrometry (AMS) technologies. Direct analysis in real-time (DART), a plasma-based ambient ionization source that permits rapid automated analysis, has been shown to be effective at ionizing a large range of compound classes, PFAS. This work seeks to evaluate the performance of DART-MS for the screening and quantification of PFAS of different classes, employing a central composite design (CCD) to better understand the interactions of DART parameters on the ionization of PFAS. Furthermore, in-source fragmentation of the model PFAS were evaluated based on the evaluated DART parameters. Preconcentration of PFAS from water samples was achieved by SPME and extracts were analyzed using the optimized DART-MS conditions, which allowed obtaining linear dynamic ranges (LDR) between 10 and 5000 ng/L for the model analytes and LOQs of 10, 25 and 50 ng/L for all analytes.

The sixth project focuses on developing novel strategies for the extraction and chromatographic separation of the cyanoneurotoxin β-N-methylamino-L-alanine (BMAA) and its structural isomers. Effective quantitative analysis of BMAA and its isomers without the need for derivatization has always been an analytical challenge due to their poor retention and separation on various liquid chromatography (LC) stationary phases. Previous studies that utilized conventional hydrophilic interaction chromatography (HILIC) demonstrate false negatives compared to reverse-phase workflows with derivatization. This work evaluates the chromatographic behavior of BMAA and its isomers, in their underivatized forms, on selected stationary phases, in particular fluorophenyl-based columns, to attain effective retention and separation. Detection and quantification were achieved with an ion-trap mass spectrometer. Extraction and preconcentration were achieved via SPME by assessing the effectiveness of multiple extraction phases, including HLB and mixed-mode (MM). A MM extraction phase consisting of C_8 and benzene sulfonic acid moieties permitted the ideal extraction performance of BMAA and its isomers (2,4-diaminobutyric acid, DABA; N-(2-aminoethyl) glycine, AEG). Chromatographic separation was achieved within 8 min on a fluorophenyl stationary phase, ensuring high throughput without derivatization, and showing exceptional improvement from conventional HILIC methods. Limits of quantification in water for BMAA and AEG were 2.5 μg L^{-1} and DABA was 5 μg L^{-1}, with linear dynamic ranges from 2.5 μg L^{-1} - 200 μg L^{-1} for BMAA and AEG and 5 μg L^{-1} - 200 μg L^{-1} for DABA.

The final, seventh project continues the work of project six but with more focus on complex matrices. BMAA and its isomers have been demonstrated to bioaccumulate in

aquatic fauna such as blue crab, these same toxins have also been detected in the brains of patients with amyotrophic lateral sclerosis (ALS) and dementia. A sample preparation method is developed in this work for the extraction of these toxins in brain and blue crab utilizing SPME hyphenated to LC-MS. Through an initial solvent-extraction approach, SPME device fouling and matrix effects were found to be acceptable. Further expansion of this workflow should enable the robust extraction of cyanoneurotoxins from complex matrices with consecutive reuse of the SPME device.

This dissertation is dedicated to my parents, family, friends and current and past mentors for all that they do.

Acknowledgements

First I would like to express my gratitude to my advisor Dr. Emanuela Gionfriddo for her guidance and the opportunities given to me in her research group. Without her training, patience and direction this dissertation would have not been possible.

I would also like to acknowledge the faculty and staff at the University of Toledo, particularly my advisory committee Dr. Jon Kirchhoff, Dr. Dragan Isailovic and Dr. Erin Prestwich for all their helpful discussions and teaching the past 5 years. A great acknowledgement to Tom Kina is necessary as he was instrumental in training and assisting me on various instrument maintenance techniques. Thanks to the Chemistry Stockroom staff (Past and Present) for their help and support, particularly Anthony Kaminski and Stephanie Kaetzel. I would also like to thank Charlene Hansen, Pamela Samples and Stephanie Fear for their help navigating 5 years worth of paper work.

Thank you to all my past and present group members for all their help, encouragement and support. A special thanks to Nipunika H. Godage for first training me on a variety of techniques and for her friendship and support the past 5 years. I would like to think my parents, siblings and friends for all their loving support. Finally, a huge thanks to my previous scientific mentors, Drs. Daniel “Gold Finch” Finnen and Erik Larson for giving me the opportunity to find something I am passionate about.

Table of Contents

List of Tables

List of Figures

List of Abbreviations

1-4CHDM 1,4-Cyclohexanedimethanol
4-MCHM.....(4-methylcyclohexyl)methanol
4MMCH.....4-(methoxymethyl)cyclohexanemethanol

AD.....Alzheimer's Disease
AEG .....N-(2-aminoethyl)glycine
ALS .....Alzheimer's Disease
ALS-PDC.....Amyotrophic Lateral Sclerosis-Parkinsonian Dementia Complex
AMDIS.....Automated Mass Spectral Deconvolution and Identification System
AMS.....Ambient Mass Spectrometry
ANOVA .....Analysis of Variance

BMAA.....β-N-methylamino-L-alanine

C18.....Octadecylsilane
CAR .....Carboxen
CCD .....Central Composite Design
CE .....Capillary Electrophoresis
CID.....Collision-Induced Dissociation
CIS .....Cooled Injection System
CN.....Cyanopropylsilane
CRM.....Charged Residue Model

DABA .....2,4-diaminobutyric Acid
DART.....Direct Analysis in Real Time
DBDI.....Dielectric Barrier Discharge Ionization
DESI.....Desorption Electrospray Ionization
DI .....Direct Immersion
DM-1-4-CHC.....Dimethyl-1,4-cyclohexanedicarboxylate
DoE .....Design of Experiments
DOM .....Dissolved Organic Matter
D-SPE .....Dispersive SPE
DVB .....Divinylbenzene

EI.....Electron Impact/Ionization

EIC .....Extracted Ion Chromatogram
ELISA .....Enzyme-Linked Immunosorbent Assay
EPA.....Environmental Protection Agency
ESI.....Electrospray Ionization

FA .....Formic Acid
FDA.....Food and Drug Administration
FDR.....False Discovery Rate
FID .....Flame Ionization Detector
FW.....Flowback Water

GC .....Gas Chromatography
GC-MS.....Gas Chromatography-Mass Spectrometry
GCxGC .....Two-Dimensional Gas Chromatography
GenX.....Hexafluoropropylene Oxide Dimer Acid

HDPE .....High-Density Polyethylene
HILIC.....Hydrophilic Interaction Chromatography
HLB.....Hydrophilic-lipophilic Balance
HLB-WAX.....Flame Ionization Detector
HRMS .....High Resolution Mass Spectrometry
HS .....Headspace

ICP-MS .....Inductively Coupled Plasma-Mass Spectrometry
IEM .....Ion-Evaporation Model
IS .....Internal Standard

LC .....Liquid Chromatography
LC-MS .....Liquid Chromatography-Mass Spectrometry
LIT .....Linear Ion Trap
LLE .....Liquid-Liquid Extraction
LOD .....Limit of Detection
LOOCV.....Leave-One-Out Cross-Validation
LOQ .....Limit of Quantitation

m/z.....Mass-to-Charge Ratio
MCHCA.....Trans-4-Methyl-1-cyclohexanecarboxylic Acid
MCHM.....Crude (4-methylcyclohexyl)methanol
MM .....Mixed-Mode
MMCHC .....Methyl 4-methylcyclohexanecarboxylate
MS.....Mass Spectrometry
MS^n .....Multistage Mass Spectrometry

NIST.....National Institute of Standards and Technology
NORM.....Naturally-Occurring Radioactive Materials
NPLC .....Normal-Phase Liquid Chromatography

P&T.....Purge and Trap
PA .....Polyacrylate
PAHs.....Polycyclic Aromatic Hydrocarbons
PBS .....Phosphate-Buffered Saline
PCA.....Principle Components Analysis
PC.....Principle Component
PDMS.....Polydimethylsiloxane
PFAS .....Per- and Polyfluoroalkyl Substances
PFOA .....Perfluorooctanoic Acid
PFBS Perfluoro-1-Butanesulfonate
PFOS .....Perfluorooctane Sulfonic Acid
PFP.....Fluorophenyl
PLS-DA.....Partial Least Squares-Discriminant Analysis
PPh .....Polyglycol Ethers
PPy-CO_2.....Poly(pyrrole-1-carboxylic Acid)
PTV .....Programmable Temperature Vaporization
PW.....Produced Water

QqQ.....Triple Quadrupole
QuEchERS .....Quick, Easy, Cheap, Effective, Rugged, and Safe

REEs .....Rare-Earth Elements
RF.....Radio Frequency
RI.....Retention Index
RPLC.....Reverse-Phase Liquid Chromatography
RSD.....Relative Standard Deviation
RT .....Retention Time

S/N .....Signal-to-Noise Ratio
SBSE.....Stir Bar Sorptive Extraction
SPE.....Solid Phase Extraction
SPME .....Solid Phase Microextraction
SWD.....Salt Water Disposal

TDS .....Total Dissolved Solids
TDU .....Thermal Desorption Unit
TF.....Thin Film
TME .....Transient Microenvironment
TOC.....Total Organic Content
TOF .....Time-of-Flight
TSS.....Total Suspended Solids

UV.....Ultraviolet

v:v.....Volume-to-Volume

w:w.....Weight-to-Weight
WHO.....World Health Organization
WVAW .....West Virginia America Water

List of Symbols

Δ .....Change/Difference

°C .....Degree Celsius
K.....Kelvin
R^2.....Correlation Coefficient
M.....Parent ion

Chapter 1

An Introduction to Small Molecule Analysis

1.1 Modern Challenges

An increasing number of contaminants and toxins discovered (and created) each year, along with the elucidation of their numerous health effects, has posed a major challenge for modern small molecule analysis. Along with greater regulatory pressure, analytical workflows have been tasked with becoming leaner, with higher-throughputs and lower limits of detection than previously possible with a wide range of complex matrices. To accomplish this, novel approaches from samplings all the way to the detector and subsequent data analysis are required. This chapter will introduce fundamentals of the powerful analytical tools used in these projects, namely solid phase microextraction, liquid and gas chromatography, direct analysis in real time and mass spectrometry.

1.2 Sample Preparation

Various steps are required before detection in any analytical procedure for complex matrices. While there are exceptions, often these steps are comprised of sampling, sample preparation, separation, and finally detection and data interpretation.[1] The integrity and quality of the procedure's results are greatly impacted by each step, the method's sensitivity and accurate characterization of the analyte or matrix hinging on not only each

analytical process but the interplay between them.[2] Sampling is the selection of samples from the bulk matrix in question, ensuring the discrete sample obtained accurately defines the matrix, and is either followed or in parallel with sample preparation. Sample preparation can be comprised of many or few steps, ranging from simple matrix dilution to more extensive techniques such as solid phase extraction (SPE) or QuEchERS (quick, easy, cheap, effective, rugged, and safe).[3–5] The primary objective of sample preparation is to modify the sample in way that allows introduction of the targeted analytes into an analytical instrument. This is accomplished commonly by isolation of the target components from the bulk sample or modifying the matrix in a way that allows it to be compatible with an instrument.[2] Component isolation employs an extraction approach which often permits the amended sample to be enriched with components of interest and, preferentially, leaving behind other components which may interfere with the analysis such salts and phospholipids.[6]

Common extraction techniques used consist of liquid-liquid extraction, purge and trap, and headspace analysis along with solid sorbent-based extraction techniques such as SPE or solid phase microextraction (SPME).[2,7,8] SPE utilizes a cartridge packed with a solid sorbent bed, this sorbent allowing trapping of the analyte and removal of unwanted interferences.[9] Sorbent chemistry for SPE can often be similar to SPME, with many SPME applications utilizing SPE particles for device development. This chemistry can range from functionalities such as C_{18}, NH_2 and multi-mode functionalities such as hydrophilic-lipophilic balance (HLB) with both N-vinylpyrrolidone and divinylbenzene.[10,11] The key differences being the amount of extraction phase and the closed vs open bed sorbent bed geometry of the techniques.[12] As an exhaustive technique, SPE does not require an external

calibration in many cases as most analyte is transferred to the cartridge and eluted.[13] The geometry of the device and the kinetics of the approach, however, disallows certain unique properties that other alternative sorbent-based extraction techniques can embrace such as is the case of SPME.[12]

1.2.1 Solid Phase Microextraction

Since its invention in the early 1990's, SPME has been developed to primarily address the urgency for high throughput sample preparation techniques with automative capabilities.[12,14] First being developed on optical fibers, this geometry was further utilized by coating an extraction phase on a solid fiber-like support, such as fused silica or flexible nitinol wires. Due to the device's geometry and open-bed approach, several analytical steps such as sampling, extraction and preconcentration can be performed in one step.[12] Furthermore, in many cases these devices can be directly introduced to instrumentation. When hyphenated to gas chromatography (GC), a thermally resistant polymer such as polydimethylsiloxane (PDMS) can be used as either an extraction phase or a binder for extractive particles such as divinylbenzene (DVB) or Carboxen (Car). This permits the device to be able to be directly desorbed in the GC inlet with geometries such as fiber and arrow, with large volume inlets allowing desorption of even more geometries such as thin film.[15] Considering this, for GC applications all sample preparation can be easily automated using a similar autosampler that would be used for conventional liquid injections. There have been great advances in direct introduction to liquid chromatography (LC) with in-tube SPME, however, in many circumstances SPME is not hyphenated directly to LC but requires a separate liquid desorption prior to injection.[12,16,17] Contrary to GC applications, for LC extraction phases resistance to organic solvent is necessary.[18]

Further expansion on LC extraction phases, in particular their biocompatibility and resistance to matrix fouling, can be found in Chapter 8, section 8.3.1.

1.2.1.1 Fundamentals

Because the amount of extraction phase used is so small, SPME is non-exhaustive, meaning a relatively small amount of analyte is extracted compared to exhaustive techniques. When exposing the device to a sample, either directly or from its headspace, analyte partition and equilibrate between the sample and the extraction phase. However, molecular kinetics play a major role in analyte uptake and consequently the throughput of the method. Described in Figure 1-1, SPME extraction is facilitated by a concentration gradient between the exposed extraction phase and the bulk sample.[12] In the case of an agitated sample, molecular movement through the sample is primarily driven by convection. This portion of the sample has no concentration gradient, the concentration reflecting the original analyte concentration in the sample (C_s). The sample in contact with the SPME device, however, is stationary. As a result, the portion of the sample surrounding the device is static, molecular movement being driven by a much slower diffusion process. The thickness of this zone, referred to as the boundary layer, is primarily controlled by the viscosity of the sample, thickness of the sampling device and the agitation applied.[7] For example, a 10 µm thick extraction phase in an aqueous solution would have a boundary layer on the order of 10 – 100 µm thick.[12] Minimization of this layer's thickness is necessary for high-throughput applications, practical approaches involving increasing agitation speeds or modifying the matrix (e.g., dilution of honey with water).[19,20]

A unique consequence of this equilibrium-based approach is balanced coverage, the amount of extracted analyte not only being related to their abundance but also their

physicochemical properties.[12,21,22] For example, in the case of extracting from environmental waters, highly-polar constituents will be more likely to be at high concentrations than non-polar constituents due to their increase solubility and affinity for water. However, if an extraction phase with high affinity for non-polar analytes such as DVB/PDMS is utilized, the non-polar analytes at low concentrations will preferentially equilibrate toward the SPME device. This results in balanced coverage, the polar analytes will still be extracted due to their affinity for DVB, yet the amount extracted of both classes of constituents will be relatively similar compared to exhaustive approaches. In doing so, low concentration analyte will be less masked by the dominant constituents in both separation and detection. Multi-class trace analysis and untargeted analysis can easily take advantage of this feature in both simple and complex matrices.

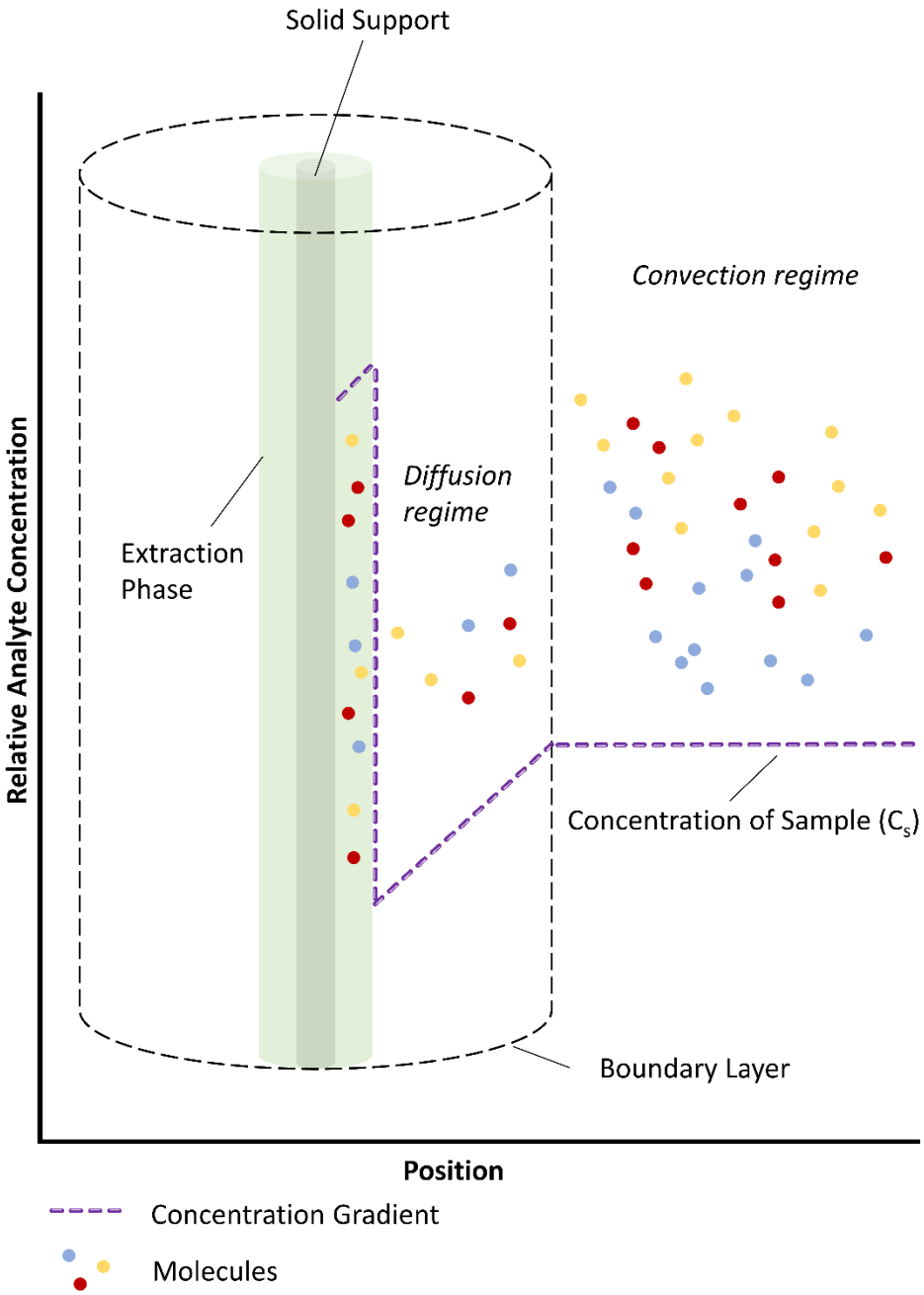

Figure 1-1 Analyte kinetics between the bulk sample, boundary layer and extraction phase for solid phase microextraction (image not to scale).

At equilibrium, the amount of analyte extracted can be expressed by Equation 1-1:

$$n^{eq} = \frac{K_{es}V_eV_s}{K_{es}V_e + V_s}C_s \qquad \textbf{(Equation 1-1)}$$

Where the amount of analyte extracted at equilibrium (n^{eq}) is directly proportional to C_s, the concentration of the sample.[12] This allows robust quantitation as long as the other factors affecting the extraction are accounted for. K_{es}, the partition coefficient of the analyte between the extraction phase and sample, is affected by stationary phase chemistry, temperature of the system and the chemical properties of the matrix. The volume of the extraction phase, V_e, is controlled during SPME device manufacturing. On the other hand, V_s, the volume of the sample, can vary greatly and at times be unknown (e.g., in situ lake monitoring). Due to the small amount of extraction phase used with SPME, in many cases it can be assumed that the sample volume is far greater than the extraction phase volume, even at laboratory scales. Because of this, when $V_s >> K_{fs}V_e$, the volume of the sample is negligible,[12] and Equation 1-1 can be simplified to Equation 1-2:

$$n^{eq} = K_{fs}V_eC_s \qquad \textbf{(Equation 1-2)}$$

Without dependence of the volume of the sample, this technique opens the way for *in situ* air and water monitoring along with *in vivo* biomonitoring. This Equation also allows quantitation for pre-equilibrium conditions, however, careful evaluation of the analytes' equilibria is critical to ensure an optimal approach that considers both analytical throughput and the amount extracted. When the device is first exposed to the sample, the rate of extraction can be expressed in Equation 1-3:

$$\frac{dn}{dt} = \left(\frac{D_sA}{\delta}\right)C_s \qquad \textbf{(Equation 1-3)}$$

Where the amount of analyte extracted (n) per unit of time (t) is proportional to C_s, the diffusion constant of the analyte through the sample matrix (D_s), the surface area of the extraction phase (A), and the thickness of the boundary layer surrounding the SPME device (δ).[12] As one might expect, minimizing the diffusion limited boundary layer enables faster extraction kinetics, along with increasing the device's surface area exposed to the sample. In these pre-equilibrium conditions, referred to as the kinetic region, it is especially critical to control the amount of time the SPME device is exposed to the sample to ensure reproducibility. This is further exemplified by the linear regime with its high slope, indicating that even with small differences in extraction time the amount of analyte extracted can differ greatly. The optimized extraction time must then be carefully considered as a compromise. Extracting until equilibrium will enhance the analytical methods overall sensitivity with more analyte extracted, along with higher reproducibility. Regrettably, this will also lengthen the analytical workflow. Pre-equilibrium extraction will increase throughput at the cost of both sensitivity and reproducibility, many developed protocols choosing to extract at conditions past the linear regime but still in the kinetic region. Due to the automation of SPME, great reproducibility can still be obtained even in the kinetic region. Demonstrated in Equation 1-4:

$$t_e = t_{95\%} = \frac{3\delta(b-a)}{D_s} \qquad \textbf{(Equation 1-4)}$$

The time it takes for analyte to reach equilibrium between the sample and extraction phase, commonly approximated as 95% to complete equilibration, is related only to δ, D_s, and the thickness of the extraction phase (b-a).[12] Extraction kinetics can further be visualized in Figure 1-2, which divides the kinetic and equilibrium regimes by their respective kinetic models. Within the context of the other Equations presented in this

section, it can be demonstrated that when developing new SPME devices the geometry of the extraction phase plays a large role in the amount extracted and the speed of analysis.[15,23] For example, the geometry of a conventional SPME fiber is cylindric. Increasing the thickness of the extraction phase by a factor 2 will increase the amount extracted at equilibrium by a factor of 2 (Equation 2), and the surface area will only slightly change providing negligible changes to extraction at the kinetic region. However, the increased thickness will increase the amount of time it takes for the analyte to reach equilibrium in both extraction and desorption. To avoid these caveats, the geometry of the extraction phase can be changed. In the case of thin film geometry, the extraction phase can be greatly increased (increasing the amount extracted) while still applying a thinner extraction phase (faster to equilibrate) and enhancing surface area (faster kinetics).[15] While a geometry such as this boasts only positives in terms of extraction, in practical terms its automation is not as developed as fiber geometry requires modification to pre-existing hardware, such as large-volume injectors for GC analysis. An overview of common SPME geometries is presented in Figure 1-3.

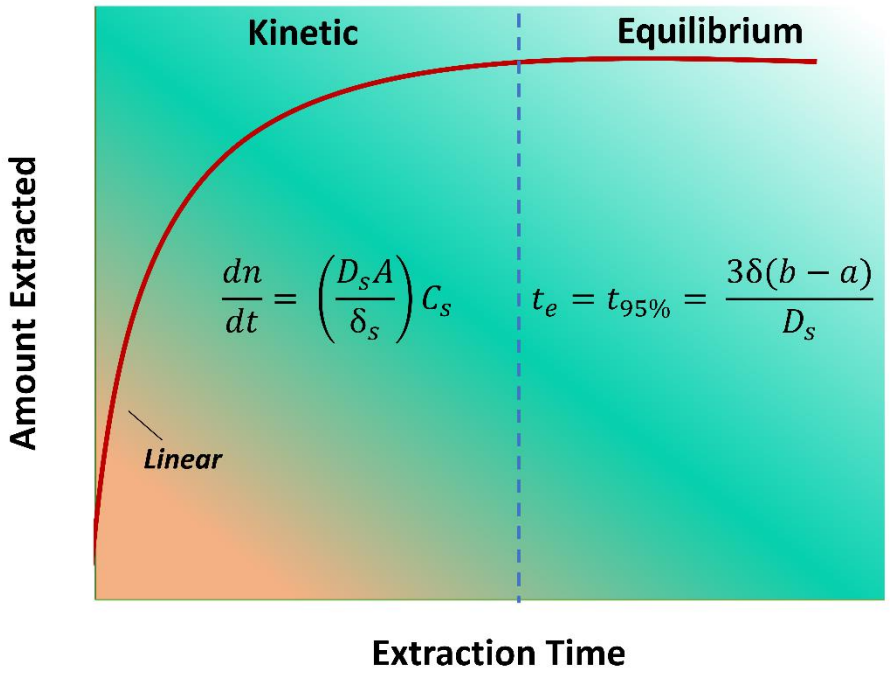

Figure 1-2 Extraction time profile describing analyte uptake in relationship with time, transitioning between kinetic and equilibrium regimes.

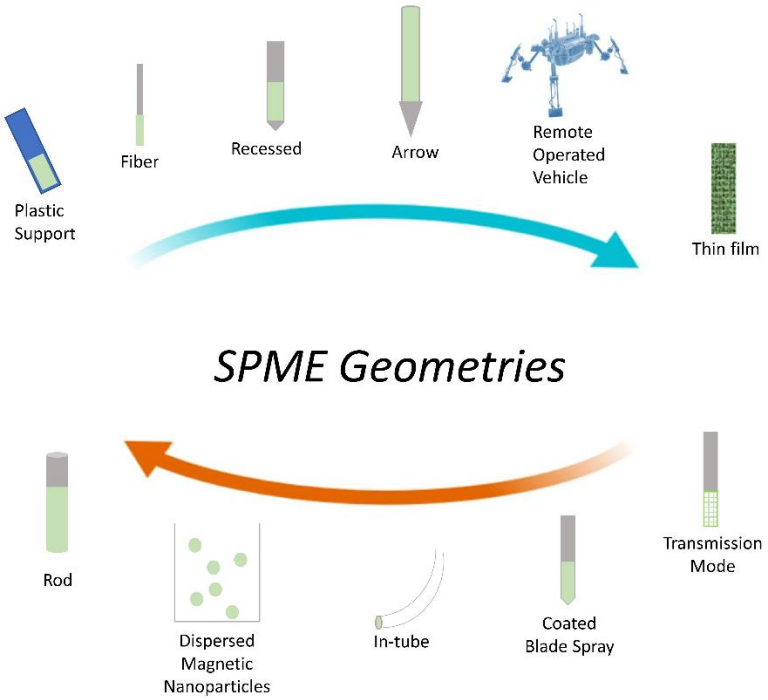

Figure 1-3 Schematic representation of the various SPME geometries (not to scale). Reproduced with permission from Elsevier.[23]

1.2.1.2 Calibration Methods

Many of the same calibration methods for other methods are still applicable to SPME, however, there are small differences in their practical applications. These include methods such as standard addition and internal standard calibration. All quantitative methods in this work were developed utilizing a matrix-matched internal standard calibration approach.[7,12] This method requires the addition of an analyte similar in physicochemical properties to the target analyte. Moreover, the internal standard must be distinguishable from the target analyte and not be present in the analyzed matrix. If available, an isotopically-labelled version of the target analyte satisfies these conditions. The internal standard is then added to both the sample matrix and the calibration matrix at the same concentrations. This calibration matrix consists of analyte-free matrix that closely resembles the sample matrix to be quantitated. Keeping the same internal standard concentration while varying the concentration of target analyte through different calibration matrix levels, a calibration curve is obtained in respect to area of response for analyte/area of response for internal standard. In this way, subsequent analysis of the target sample spiked with only the internal standard allows quantitation based off the ratio of their response areas. As SPME is an equilibration-based technique, it is critical that the extraction conditions between both the real sample and the calibration matrix are conserved.

1.3 Separation and Detection

Separation of matrix constituents and the target analytes is invaluable to enhance method sensitivity and to better characterize unknown compounds. In a way, most of the analytical steps prior to detection in this work can be considered a separation phenomenon.

With SPME, analytes are separated from the bulk matrix leaving behind any unretained matrix components. Furthermore, chromatographic separation enables separation of compounds based on their physicochemical properties. Mass spectrometry, facilitating the separation of produced ions by their mass-to-charge (*m/z*) ratios, permits detection and characterization of the matrix constituents. While there are many different kinds of chromatographic and mass spectrometric systems, this discussion will focus on the methods employed in this work. Chromatography was carried out using gas chromatography (GC) and liquid chromatography (LC), with an electron impact (EI) – single quadrupole MS and electrospray ionization (ESI) – linear ion trap MS used, respectively.

1.3.1 Gas Chromatography

The modern form of gas chromatography has been developed since 1952.[24] Shown in Figure 1-4, a gas chromatograph consists of an injection port, column, column oven and detector, all preceded by a flow controller for the chosen carrier gas. Once a sample is injected into the injection port, the sample vaporizes instantaneously and is carried by the gas into the column. The analytes then partition into the liquid stationary phase coated inside this column (typically PDMS) and are separated by their boiling point, molecular weight and chemical structure.[25] Many previous works have extensively discussed the theory of gas chromatography.[25,26] For the projects discussed in this work, inlet systems must be particularly accounted for.

In a conventional split/splitless inlet (Figure 1-5), gas flow within the inlet is controlled by both the split outlet vent and the septum purge vent.[27] In the case of split injection, when the carrier gas enters the inlet, the gas will enter the column and also pass

through both vents. A split ratio must be set, meaning the ratio of gas allowed to flow between the split vent and column. For example, with a column flow rate of 1 mL/min and a split ratio of 100:1, the inlet flow will be just above 100 mL/min (approximately 103 mL/min). During injection, the volume of gas calculated to exceed 100 mL/min will escape the septum purge to avoid contamination, while 1 mL/min will enter the column and 100 mL/min will flow through the split vent. In this way, a high inlet flow rate is possible with only one part per hundred of the carrier gas entering the column. As the sample vaporizes in the inlet's glass liner, this high flow rate will quickly sweep the sample into the column resulting in a narrow band and sharper chromatographic peaks. However, due to much of the carrier gas leaving the split vent, less sample is injected, reducing method sensitivity. This mode of injection is preferred for samples with non-volatile components and high analyte concentrations.[15,25]

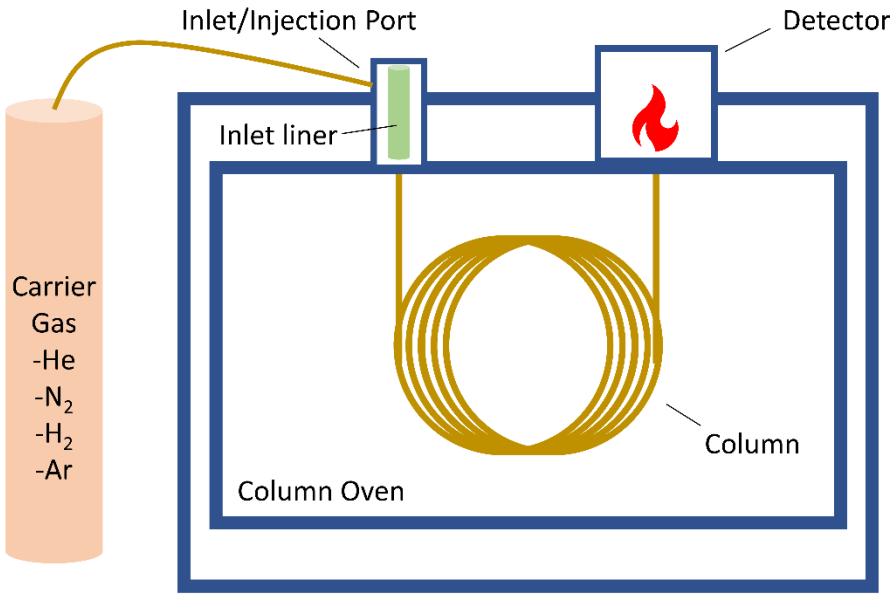

Figure 1-4 Gas chromatograph diagram.

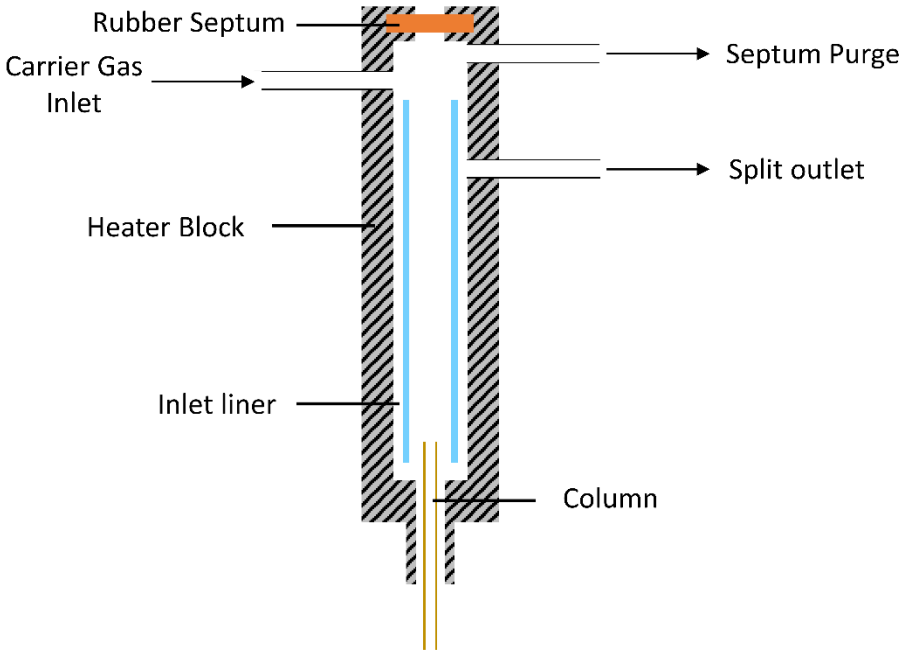

Figure 1-5 Conventional split/splitless injection port of a gas chromatograph system.

On the other hand, splitless injection involves the split vent being entirely closed until the sample completely enters the column. While this increases method sensitivity, the slow inlet gas flow is unable to create the narrow sample band typical with split injections. Furthermore, sample-cleanup is more critical as all volatile and non-volatile components will enter the head of the column. Sample vaporization to column introduction can take upwards to a minute, the analytes diffusing and causing band broadening. On a typical split/splitless inlet, it is common to lower the initial column oven temperature to approximately 35 to 40 °C when using splitless injection to allow analytes to condense at the head of the column.[25] This allows analyte to refocus before separation, resulting in narrower chromatographic peaks. For SPME applications, splitless injection is used due to the sample cleanup it allows and the relatively low amount of analyte injected. If introduced to a typical splitless system, the gas flow would be too slow for efficient thermal desorption

of the analyte from the extraction phase. In light of this, low-volume glass liners are used in conjunction with SPME to facilitate higher gas flow rates within the liner.[12,28]

Larger geometry SPME devices, such as thin film, require large-volume thermal desorption units (TDUs) as opposed to conventional split/splitless GC inlets.[15,29,30] The same principles can be carried over to large-volume injectors, however, because of the volume and increased desorption time a separate focusing stage is necessary.[31] This is accomplished by installing between the column and TDU a programmable temperature vaporization (PTV) inlet, or otherwise known as a cooled injection system (CIS). During thermal desorption, the CIS is cooled (e.g., liquid nitrogen, liquid carbon dioxide, Peltier cooling) to cryofocus the sample band. After desorption, the CIS system is quickly heated, releasing the band into the column resulting in complete introduction of analyte and narrow peaks. This two-stage system approach is highlighted in Figure 1-6.[15] A further advantage of utilizing a separate cryofocusing system is the potential of increased inlet gas flow. With larger extraction phases, high carrier gas flows are needed to efficiently desorb, however, splitless injection is still preferred for ultra-trace analysis. It is important to note that for most TDU-CIS systems, the CIS is responsible for this inlet flow. To accomplish high flow rates with no loss of analyte, the TDU can be set to a splitless injection while the CIS can be set to what is referred to as solvent-vent. This will allow the CIS to vent large of amounts of carrier gas, increasing desorptive flow, while retaining analyte as they are cryofocused on the CIS liner. Once thermal desorption is complete, the TDU is cooled to room temperature and the CIS is increased to 200-300 °C with the solvent-vent valve now closed to facilitate splitless injection. This flexibility allows other injections modes as well, highlighted in Table 1.1.

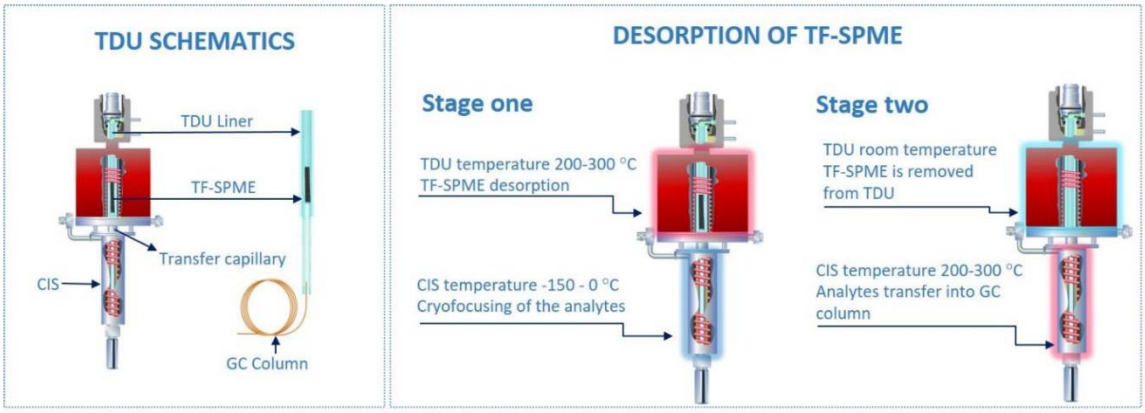

Figure 1-6 Two-stage thermal desorption of large-volume SPME devices into the GC analytical column.[15]

Table 1.1 Configurations and applications of two-stage thermal desorption.

Application	TDU Split	CIS Split	Rationale
Ultra-trace Analysis	Splitless	Solvent-vent/Splitless	Maximum Analyte Injected
High Concentrations	Splitless	Solvent-vent	Prevents Column /Detector Saturation
Unknown Analysis	Split	Split	Protects System from Contamination
Dirty/Watery Sample	Split	Solvent-vent/Splitless	High Sensitivity with Slightly Less Protection

1.3.1.1 Electron Impact – Quadrupole Mass Spectrometry

Mass spectrometers can be divided into three separate components: the ion source, mass analyzer and the detector.[32] While there are different configurations of each component depending on the application, in all forms of mass spectrometry the ion source produces ions, the mass analyzer separates ions based on their mass-to-charge (*m/z*) ratio, and the detector measures the charge or current produced by these ions and converts this to a measurable signal.

The most common ion source used in GC-MS applications is electron ionization (EI) ionization, often referred to as electron impact ionization.[33] With this method, as the eluent leaves the GC column, a filament positioned perpendicular to this gas stream is both heated and applied electric current. This results in thermionic emission of electrons. These electrons are then accelerated to 70 eV, enabling wide-range ionization and extensive fragmentation of molecules.[34] This electron beam collides with the neutral molecules in the gaseous phase under vacuum, causing a molecular ion to be produced along with its fragments. The ionization mechanism can be described in Equation 1-5:

$$M + e^- \rightarrow M^{+\bullet} + 2e^- \qquad \textbf{(Equation 1-5)}$$

Where M is a molecule, e^- is an electron and $M^{+\bullet}$ is the molecular ion. As this is a hard ionization technique, many fragments are formed through further bond dissociation.[33] These ions are then focused toward the mass analyzer by the use of a repeller electrode and in some cases an extracting lens. Schematics of this ionization process are found in Figure 1-7. The mass analyzer, in this case a single quadrupole, filter ions by their *m/z* ratios by quickly altering the radio frequency voltage and DC offset voltage among four parallel metal rods. In this way, for each combination of voltages only one *m/z* value has a trajectory stable enough to pass through the quadrupole allowing satisfactory *m/z* separation.[25] This technique has been extensively used and is highly reproducible, allowing not only quantitation but the development of extensive mass spectral libraries. Putative identification is possible under these conditions, with further investigation necessary for more confident identification such as using analyte standards and high resolution mass spectrometry.

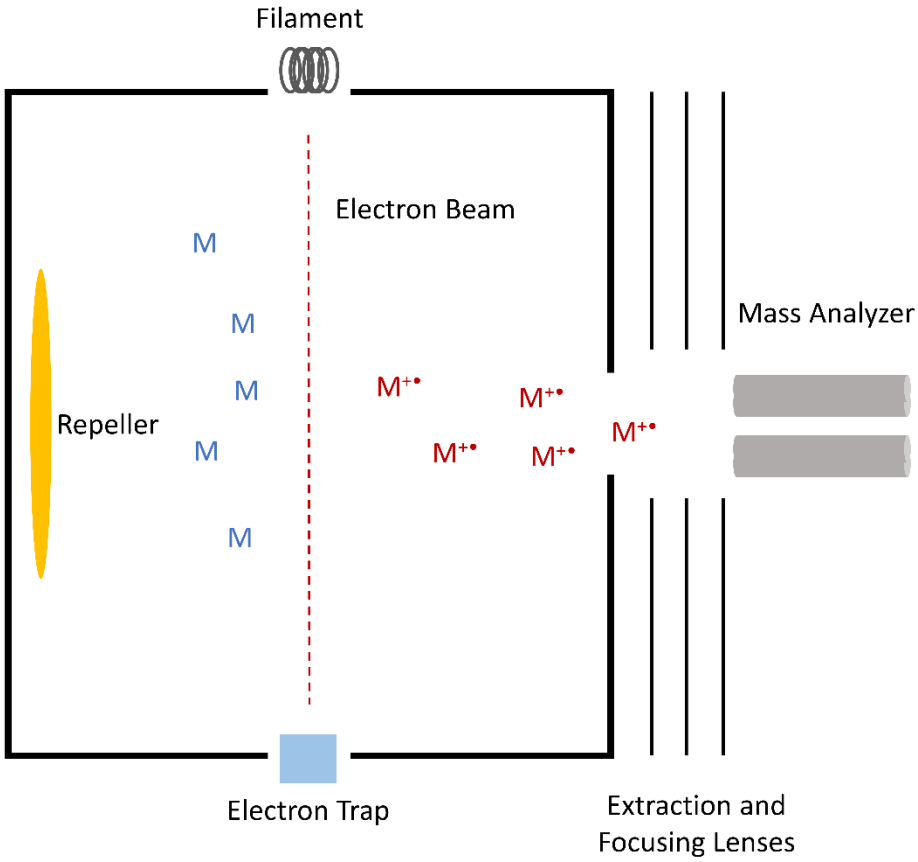

Figure 1-7 Diagram of an electron ionization chamber.

1.3.2 Liquid Chromatography

Modern liquid chromatography (LC) consists of a liquid pumping system that continuously flows solvent through an analytical column and into a detector, allowing both isocratic and gradient elution at high pressures.[35] The analytical column is packed with a stationary phase of a variety of chemistries, the solvent used referred to as mobile phase. Injected compounds are separated based on their chemical interactions between the mobile phase and the stationary phase, changes in selectivity much easier to perform than GC. Changes in solvent composition (e.g., water, methanol, acetonitrile, tetrahydrofuran, isopropyl alcohol) along with additive concentration (e.g., salts, acids) are used to facilitate

unique selectivity and separation, the use of two pumps and mobile phase reservoirs referred to as gradient elution. The mechanism of interaction between analyte and the surrounding mobile and stationary phase is often referred to as its retention mode (Table 1.2).[35–38]

Table 1.2 Retention modes and their applications.

Retention Mode	Stationary Phase	Mobile Phase	Compound Classes
Reverse-phase	C18, C8, C4, Cyano, Amino, Phenyl	Aqueous → Organic	Neutrals, Weak Acids/Bases
Normal-phase	Silica, Cyano, Amino, Diol	Organic → Aqueous	Polar Compounds, Ionic
Ion-exchange	Anion/Cation Exchange Resins	Aqueous → Buffer	Ionic
Size Exclusion	Polystyrene, Silica	Aqueous/Organic	Polymers, High Molecular Weight

For example, reverse-phase separation is performed by using a hydrophobic stationary phase (e.g., C18 coated silica particles) and injecting the liquid sample with high amounts of polar mobile phase. In this way, analyte is able to interact with the analytical column through hydrophobic interactions and are eluted with a less polar solvent such as methanol. In reverse-phase chromatography, more non-polar molecules will interact with the stationary phase more and elute at a later time. Normal-phase separation is the opposite, utilizing a polar stationary phase and starting with an organic mobile phase. There are various subcategories of each major retention mode, a notable normal-phase mode being hydrophilic interaction chromatography (HILIC). With HILIC, a mixture of water and acetonitrile permits a thin layer of water to form on the stationary phase surface (around 90% acetonitrile).[39] Polar analyte preferentially partition into this stationary aqueous layer, essentially making this mode a liquid-liquid separation. While there are clear distinctions between retention modes for many applications, non-specific and perhaps multi-mode

retention is possible. The most infamous example being ionic interaction of charged analyte with the column's stainless steel hardware or unreacted silanol groups resulting in tailing.[40] While many of these multi-mode retention modes were considered deleterious in the past, hybrid stationary phases combining unique chemical selectivity have been introduced to tackle more challenging analytes.[41]

1.3.2.1 Electrospray Ionization – Linear Ion Trap Mass Spectrometry

Electrospray ionization (ESI) is the most common ionization source hyphenated to liquid chromatography.[42] Contrary to the high vacuum EI, ESI is performed at atmospheric pressure and is a soft ionization technique. This ionization method flows the mobile phase into a small needle where a high voltage is applied, producing a Taylor cone (Figure 1-8**).**[43] This cone produces a droplet of mobile phase, this droplet containing a surface charge along with analyte molecules. Through solvent evaporation (commonly facilitated by nitrogen gas or heat), the droplet becomes smaller until its surface charge density becomes too large.[44] Due to the charge density, a Coulomb explosion occurs which creates even smaller droplets and these droplets undergo the same process. The formation of gaseous analyte molecules from these droplets is explained by two major models, the charged residue model (CRM) and ion-evaporation model (IEM).[44] In CRM, which is thought to describe the ionization of larger molecules, it is proposed that droplets become small enough to contain only one analyte molecule. Formation of the gas-phase analyte molecule occurs when the surrounding solvent molecules evaporate completely, the final solvent shell imparting the surface charge to the analyte. Low molecular weight species are expected to follow the IEM. In this model, the analyte charge is a result of an additive present in the mobile phase such as a volatile acid. Once the droplet becomes small enough,

the electric field from the charged surface causes the ejection of the ionized analyte in its gaseous form alongside surrounding gaseous solvent molecules. In both models, the generated ions are $[M + zH]^{z+}$ for positive ionization and $[M - zH]^{z-}$ for negative.[44] While small molecule analysis generally creates singly-charged ions, adducts are common (e.g., Na^+, NH_4^+, K^+, CH_3COO^-) alongside multiple charges with larger molecules such as proteins and carbohydrates.[45] Once formed, these ions then enter the MS orifice due to the potential difference between the MS capillary and the ESI needle.

This work utilizes a linear ion trap (LIT) in conjunction with LC-ESI. A LIT is constructed by the inversion of linear quadrupoles in a geometry (typically circular) that facilitates the confinement of ions in a two-dimensional radio frequency (RF) field (Figure 1-9) alongside an axial electric potential.[46] A consequence of this design is a high degree of ion storage coupled to the ability to filter ions while keeping the target ion in the analyzer. This allows what is referred to as subsequent MS^n experiments. Using this technique, an ion can be initially collided, its fragment collected, and that fragment collected and so forth.[47] MS^n hold great potential for structural identification of components. To isolate a single ion or eject a range of others, the RF voltage of the system can be changed to bring unwanted ions in resonance to an ejection path. Collision and fragmentation of analytes is performed using collision-induced dissociation (CID).[47] An RF voltage is applied to increase the kinetic energy of a specific ion, this increased energy causing the ion to collide with an inert gas (helium) causing fragmentation.

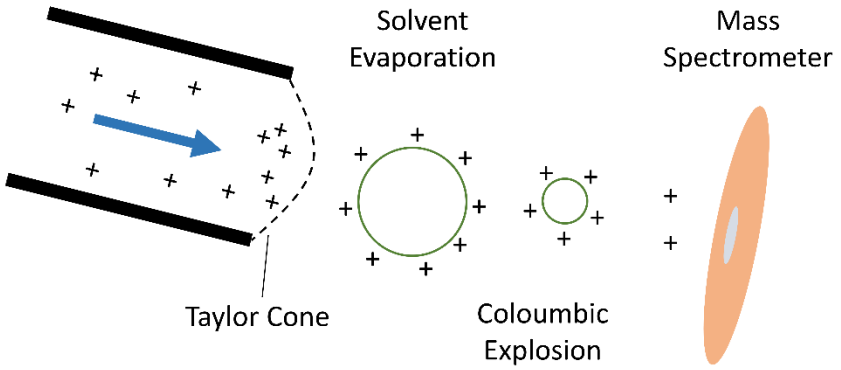

Figure 1-8 Development of droplets and subsequent droplet evaporation and Coulomb explosion in electrospray ionization in positive mode.

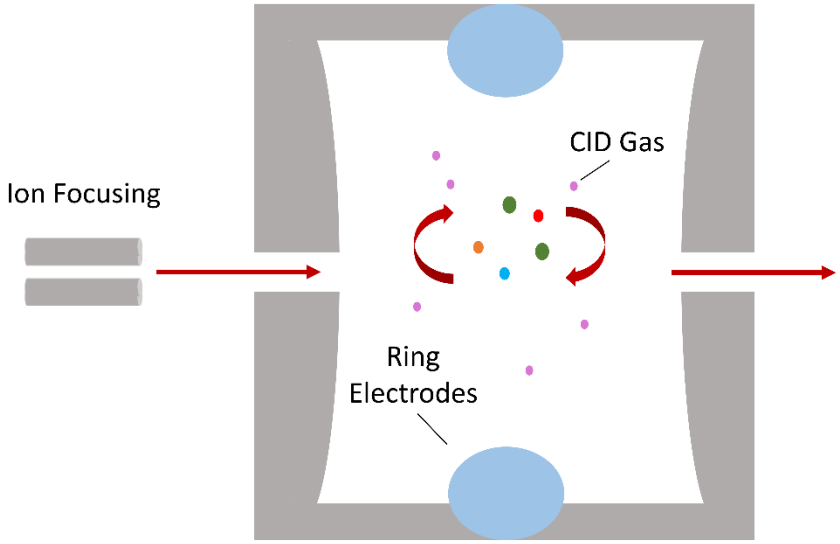

Figure 1-9 Schematic view of a linear ion trap.

1.3.3 Direct Analysis in Real Time

Direct ambient mass spectrometry permits direct introduction of a sample to a mass spectrometer.[48] With the removal of chromatography, these methods permit ultra-fast analysis times, practical capabilities for on site analysis, and the potential for the analysis of unaltered samples. Direct analysis in real time (DART) consists of a heated gas stream which is electrically discharged in the open-air environment.[49] Starting from the gas source (Figure 1-10), either helium or nitrogen is flowed through a needle electrode. A current is applied to this electrode causing a glow discharge, producing ions, electrons and metastable species from the chosen gas. These products are then heated through a ceramic cylinder and ions removed by an electric grid with an applied voltage. Metastables then interact with analyte in the open air environment, enabling efficient ionization prior to MS inlet introduction. The majority of positive ionization applications is thought to be a form of Penning ionization[49,50] with water clusters as an intermediate (Equations 1-6 – 9):

$$M^* + H_2O \rightarrow M + H_2O^{+\bullet} + e^- \qquad \textbf{(Equation 1-6)}$$

$$H_2O^{+\bullet} + H_2O \rightarrow H_3O^+ + OH^\bullet \qquad \textbf{(Equation 1-7)}$$

$$H_3O^{+\bullet} + nH_2O \rightarrow [nH_2O + H]^+ \qquad \textbf{(Equation 1-8)}$$

$$A + [nH_2O + H]^+ \rightarrow [A + H]^+ + nH_2O \qquad \textbf{(Equation 1-9)}$$

In negative ionization mode, the electric grid is applied a negative potential, allowing thermal (or Penning) electrons to react with atmospheric oxygen to produce O_2^-.[49,51] Depending on the analyte, either oxygen mediated radical formation or direct electron capture can occur (Equations 1-10 - 12):

$$O_2 + e^- \rightarrow O_2^{-\bullet} \qquad \textbf{(Equation 1-10)}$$

$$O_2^{-\bullet} + A \rightarrow A^{-\bullet} + O_2 \qquad \textbf{(Equation 1-11)}$$

$$S + e^- \rightarrow S^{-\bullet} \qquad \textbf{(Equation 1-12)}$$

In this work the DART system was hyphenated to the LIT for method development and a triple quadrupole MS for quantitation. The triple quadrupole is similar in design to a single quadrupole system but with three quadrupoles in succession, Q1, q2 and Q3 (Figure 1-11).[52] This configuration allows there to be two mass analyzers with a collision cell, q2, in between. Fragmentation is based on CID similar to a LIT system, with selected ions being collided with collision gas (helium).[47] Scan rates are typically faster with triple quadrupole systems than LIT, a necessity for simultaneous multi-ion monitoring which is required for DART quantitation. A fragment ion or product ion scan is utilized, the parent ion being selected in Q1, fragmented in q2, and fragments analyzed through Q3 before detection.

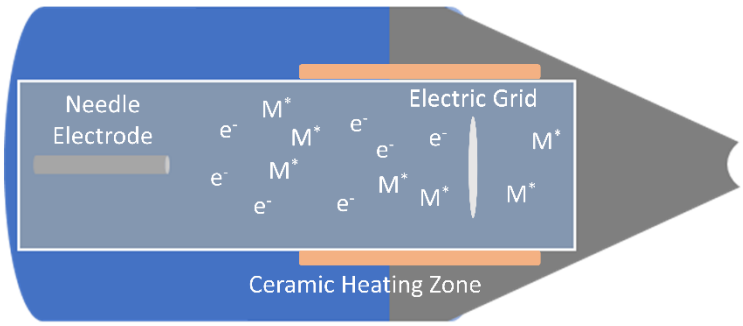

Figure 1-10 Direct analysis in real time apparatus.

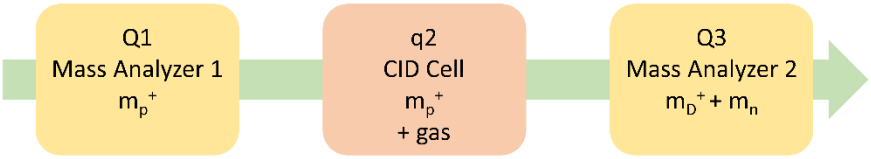

Figure 1-11 Triple quadrupole for tandem mass spectrometry.

1.4 Summary

An overview of the core concepts and technologies used in the work, encompassing SPME, GC-MS, LC-MS and DART-MS were discussed. When viewing an analytical method holistically, understanding the interplay between sample preparation and instrumental analysis is necessary to ensure robust results across a variety of different applications. Analytes from matrices such as water, hydraulic fracturing fluids and brain can be selectively extracted, leaving behind unwanted matrix components and interferences in few steps. Because the extract is clean and preconcentrated with analytes, separation and detection are further enhanced with greater method sensitivity obtained. Chapters 2, 3 and 4 focus on the development of extraction and data approaches for the analysis of aqueous contaminants using thin film SPME coupled to GC-MS. Chapters 5 and 6 discuss the quantitative capabilities of DART-MS after analyte enrichment. Finally, Chapters 7 and 8 discuss cyanoneurotoxins and the development of novel extraction and separation approaches for their determination from water and biological matrices such as crab and brain.

Chapter 2

Exploring the Efficiency of Various Extraction Approaches for Determination of Crude (4-methylcyclohexyl)methanol (MCHM) Constituents in Environmental Samples

Adapted from a paper published in *LCGC North America*[53]

Ronald V. Emmons, Amila M. Devasurendra, Nipunika H. Godage,

Emanuela Gionfriddo

Abstract

Crude (4-methylcyclohexyl)methanol (MCHM) is a chemical blend commonly used in the coal industry for the separation of coal from rock, debris and coal dust by froth flotation. Crude MCHM consists of (4-methylcyclohexyl)methanol (68–89%), 4-(methoxymethyl)cyclohexanemethanol (4–22%); methyl 4-methylcyclohexanecarboxylate (5%), dimethyl-1,4-cyclohexanedicarboxylate (1%); and 1,4-cyclohexanedimethanol (1–2%), which all occur in the cis and trans diastereoisomeric forms; along with water (4–10%) and methanol (1%). Significant attention regarding the

[53]Reprinted from LCGC North America, 2019, 37(S4), 28-34. Copyright © Chromatography Online.

impact of these compounds on human health arose in 2014, when a spill of crude MCHM into the Elk River resulted in the contamination of drinking water for over 300,000 residents in West Virginia and Kentucky of the United States. In response, a series of studies aimed to investigate the mixture's capacity for long-term exposure by determining the sorption properties of crude MCHM to pipes and linings. Sorbed MCHM was demonstrated to readily desorb from polyethylene into water at levels above the odor threshold, confirming the risk to residents from contaminated tap water pipelines. In light of this, it is imperative to develop analytical tools that enable the detection of crude MCHM components in environmental water samples for routine water monitoring. In this work, two solid phase microextraction methods, based on fiber and thin film geometry, were developed and validated. Their performances were compared with a modified SPE method based on EPA Method 522 for the analysis of volatiles in water. Both SPME methods demonstrated lower LOQ compared to the SPE protocol. TF-SPME, due its superior sensitivity and faster throughput was selected as the optimal extraction approach for 4-MCHM and other constituents of crude MCHM, with limits of quantitation below the odor threshold for aqueous crude MCHM in distilled water at 19–21 °C (0.55 µg L^{-1}).

2.1 Introduction

On January 9, 2014, an estimated 37,800 L of a chemical mixture was spilled into the Elk River upriver from Charleston, West Virginia, United States. This mixture, used in a purification process for coal, contained crude (4-methylcyclohexyl)methanol (MCHM; 88.5%) and a proprietary blend of stripped polyglycol ethers (PPh; 7.3%) and water (4.2%). Crude MCHM is composed of (4-methylcyclohexyl)methanol (4-MCHM; 68-89%), 4-

(methoxymethyl)cyclohexanemethanol (4MMCH; 4-22%), methyl 4-methylcyclohexanecarboxylate (MMCHC; 5%), dimethyl-1,4-cyclohexanedicarboxylate (DM-1-4-CHC; 1%), 1,4-cyclohexanedimethanol (1-4CHDM; 1-2%), water (4-10%) and methanol (1%).[54] The drinking water treatment plant located in Charleston, operated by West Virginia America Water (WVAW), was contaminated along with approximately 300,000 residences. 4-MCHM readily adsorbs and desorbs from pipes made from polyethylene materials,[55] creating a risk of chronic exposure for contaminated households. Although analysis was not performed on the day of the spill, levels as high as 2400 μg L^{-1} 4-MCHM were detected exiting WVAW the day after contamination.[56] Concentrations of 4-MCHM in the range of 2-5 μg L^{-1} were found persisting from January 20 to February 2, 2014.[57] Analysis of tap water from households indicated that contamination was not constrained to the WVAW facility only but also affected the entire water distribution system, evidenced by concentrations as high as 420 μg L^{-1} being found in drinking water two weeks after the spill.[58] Tap water from residences with different water suppliers were demonstrated to be contaminated by crude MCHM, with 4-MCHM being detected over 600 km from the spill site in Louisville, Kentucky.[59] Of the approximate 300,000 households directly affected by the spill, an estimated 25,623 households of them exhibited health problems such as rash, skin irritation, respiratory problems, nausea, diarrhea and other symptoms linked to crude MCHM according to the Centers for Disease Control and Prevention.[60] It has been established that 4-MCHM damages DNA, with its metabolites being more toxic due to their potential to cause greater oxidative stress.[61] It has also been shown that low levels of 4-MCHM can be cytotoxic when paired with PPh, with concentrations as low as 1.28 μg L^{-1} 4-MCHM and 1.52 μg L^{-1} PPh.[62] It is thus convenient

to develop analytical methods able to quantitate crude MCHM components and associated metabolites, so as to monitor long term accumulation and release of these contaminants in environmental waters. Previous studies employed liquid-liquid extraction (LLE) coupled with GC-FID and GC-MS.[63,64] Also, headspace (HS) sampling coupled with GC-FID[55,65], purge and trap (P&T) with GC-MS[59] and headspace solid phase microextraction (HS-SPME) coupled to GC-MS[66] have also been used to detect 4-MCHM without consideration for its crude constituents, since these components contribute less in the leaked mixture. In light of new toxicological data,[61,62] accompanied by a lack of adequate research on the toxicology and sorption behavior of the minor constituents of crude MCHM, we herein propose quantitative methods for analysis of 4-MCHM and all compounds associated, including a primary metabolite of 4-MCHM, trans-4-Methyl-1-cyclohexanecarboxylic acid (MCHCA).[67] The goal of this study is to quantify, for the first time, all known components of crude MCHM, comparing the efficiency of various extraction approaches across different methods. The methods developed in this study utilized solid-phase extraction (SPE), direct immersion solid-phase microextraction (DI-SPME) and direct immersion thin-film microextraction (DI-TF-SPME). Each method employed gas chromatography-mass spectrometry (GC-MS) for separation and detection. Among the methods developed, TF-SPME provided the best results in terms of throughput and limits of detection (LOQs) achievable. The TF-SPME based method was thus used for analysis of tap, lake and river water.

2.2 Experimental

2.2.1 Materials and Instrumentation

Reference standards of 4-MCHM, MMCHC, DM1-4CHC and MCHCA were purchased from Sigma Aldrich (St. Louis, MO, USA), along with internal standards toluene-d8 and methyl benzoate-d8. A standard solution of 4MMCH was obtained from Toronto Research Chemicals Inc (Toronto, ON, Canada) and 1,4-CHDM was purchased from Tokyo Chemical Industries Co., Ltd. (Tokyo, Japan). Buffer solutions at pH 4, 6, 8, 10 were purchased from Honeywell Specialty Chemicals (Seelze, Germany). Materials for SPE included Sep-Pak AC2 Plus short Cartridge (400 mg) from Waters (Milford, MA, USA) and Cole-Parmer 2 mL wide neck volumetric vial with PTFE/Silicone lined cap (Vernon Hills, IL, USA). Disposable Falcon tubes (3, 10 and 50 mL) were obtained from Becton (Dickinson and Company, Franklin Lakes, NJ, USA). HPLC grade water, methanol and dichloromethane were bought from Fisher Scientific (Fair Lawn, NJ, USA). SPME fibers were purchased from Supelco (Bellefonte, PA). Car/PDMS thin-films were obtained from GERSTEL (Linthicum, MD, USA). River and tap water samples were collected in glass containers, being completely filled as to minimize headspace. The river sample was collected ~0.5 m below the water surface along the bank of the Ohio River located at Portsmouth, Ohio. The lake water was obtained from the west fork of Keuka Lake near Pulteney, NY in Steuben County, approximately 10 m off shore. The lake water was collected in a plastic container ~1.5 m below the surface. Tap (drinking) water was obtained at a residence in Louisville, Kentucky. Samples were stored in their original containers at 4 °C until analysis. An Agilent 7890 B GC hyphenated to a 5977 B single quadrupole mass spectrometer (Agilent Technologies, Santa Clara, CA, USA) and equipped with a DB-5ms

column (30 m x 250 µm x 0.25 µm, Agilent Technologies), MultiPurpose Sampler, MPS, (GERSTEL, Inc., Linthicum, MD, USA), a cooled injection system, CIS 4, (GERSTEL, Inc., Linthicum, MD, USA) and a thermal desorption unit, TDU, (GERSTEL, Inc., Linthicum, MD, USA) was used for analysis of the crude MCHM constituents. Ultra-pure Helium (99.999%) was used as the carrier gas at a flow of 1.5 mL min^{-1} for each method. For SPE and SPME analysis, the GC oven temperature was set at 50 ^{o}C (held for 2 min) to 220 ^{o}C (held for 2 min) at a rate of 20 ^{o}C min^{-1}. During TF-SPME analysis the GC oven was programmed at an initial temperature of 50 ^{o}C (held for 2 min) to 290 ^{o}C at a rate of 20 ^{o}C min^{-1} (held for 2 min). The mass spectrometer was used in electronic ionization (EI) mode at 70 eV with the MS source being set at 230 ^{o}C and the quadrupole at 150 ^{o}C, collecting full scan mass spectra. All data analysis was performed with Agilent Masshunter Workstation Quantitative Analysis software (Agilent Technologies, Santa Clara, CA, USA) for GC-MS. The response for each analyte was obtained as the sum of individual peak areas for trans and cis isomers, with exception of DM1-4-CHC and MCHCA.

2.2.2 SPE Protocol

The SPE extractions were conducted according to a modified-protocol based on EPA method 522 [68] before GC-MS analysis. SPE cartridges were first conditioned with 2 mL of dichloromethane. The cartridges were then equilibrated by passing 2 mL of HPLC grade methanol followed by 10 mL of HPLC grade water through the cartridge. Throughout the equilibration step and onward, care was taken not to allow the cartridges to dry during solvent exchange and sample loading. For extraction, 18 mL of each aqueous solution spiked with the targeted analytes was loaded onto the SPE cartridge. Any water residues were removed from the cartridge by purging it with high purity argon gas for 3

minutes until dryness. A 2 mL volumetric vial was used for collection of the eluate. Elution of the analytes was performed with the addition of dichloromethane to the cartridge. During this step, dichloromethane was initially used to condition the SPE cartridge for 1 min. Elution then proceeded in a dropwise fashion into a volumetric flask. Additional dichloromethane was added to the cartridge until the eluted volume in the vial was 1.5 mL. To eliminate residual water in the eluate, 0.4 g of anhydrous sodium sulfate was added to each vial. The samples were sealed and then stored in the refrigerator at 4 ^{o}C until GC-MS analysis.

2.2.3 SPME Protocol

The extraction efficiency of 5 commercially available SPME fibers, Carboxen®/polydimethylsiloxane (Car/PDMS), divinylbenzene/Carboxen®/polydimethylsiloxane (DVB/Car/PDMS), divinylbenzene/polydimethylsiloxane (DVB/PDMS), polyacrylate (PA), and polydimethylsiloxane (PDMS), were assessed using a 100 µg L^{-1} aqueous solution containing the targeted analytes. pH optimization was performed using both Car/PDMS and DVB/Car/PDMS by adjusting the pH of the 100 µg L^{-1} aqueous solution containing the targeted analytes to pH 4, 6, 8, 10 using disodium hydrogen citrate/sodium dihydrogen citrate/sodium chloride buffer solution at pH 4, trisodium citrate-2-hydrate/disodium hydrogen citrate buffer solution at pH 6, sodium chloride/disodium tetraborate buffer solution at pH 8 and disodium tetraborate/ sodium hydroxide buffer solution at pH 10. The optimized SPME protocol consisted of 1 min incubation followed by 30 min extraction, both performed at 65 °C and 300 rpm agitation speed. Desorption was performed for 10 min in splitless mode at 300 °C for Car/PDMS, 270 °C for DVB/Car/PDMS, 300 °C for

PA, 270 °C for DVB/PDMS and 280 °C for PDMS. The conditions used for desorption prevented the occurrence of carry-over of the analytes on the SPME coatings. Carry-over was tested by re-desorbing the fibers immediately after the first extraction/desorption cycle and verifying the absence of peaks attributable to the targeted analytes in the obtained chromatograms.

2.2.4 TF-SPME Protocol

Samples for TF-SPME method optimization were prepared following the same procedures described for SPE and SPME to ensure direct comparison between extraction methods. During extraction, TF-SPME devices were held in place by stainless steel pins penetrating the vial septum, with the thin-films fully submerged in the sample solution. Samples were placed in a water bath at 65 ^{o}C for 5 min without agitation and subsequently stirred at 900 rpm for 15 min by a magnetic stir bar placed in the vial. After agitation the TF-SPME device was quickly wiped and then placed into a baffled glass desorption liner prior to insertion into the TDU. TDU parameters were first set at 30 °C (held for 0.5 min) to 270 °C (held for 8 min) at a rate of 700 °C min^{-1}, all performed in splitless mode at a 280 °C transfer temperature. Coupled to the TDU was a CIS 4, with an initial temperature of -50 °C to a final temperature of 280 °C (held for 3 min) at 10 °C s^{-1}. Under the desorption conditions used for TF-SPME devices, minimum carry over (<1%) was achieved for the targeted analytes.

2.2.5 Method Validation

The methods developed were validated with respect to linearity, precision, accuracy, and limits of quantitation (LOQs). Calibration curves were obtained for each target by plotting the signal ratio of the analyte and the isotopically labeled internal

standards (A/IS) for various concentration levels (8 for the SPE protocol and 10 for the SPME and TF-SPME protocols) in three independent replicates. Toluene-d8 was used as internal standard for the SPE method, while methylbenzoate-d8 was used for the SPME and TF-SPME methods. Furthermore, three validation points selected within the linear range of each method were analyzed in order to assess precision and accuracy. LOQs were calculated as the lowest calibration point with precision values lower than 20% and accuracy within 70-120%.

2.3 Results and Discussion

2.3.1 SPME optimization

Various parameters affecting SPME were optimized to achieve the most suitable conditions for extraction of the major components of crude MCHM and a metabolite of 4-MCHM, namely MCHCA. At first, we tested the extraction performance of 5 commercially available SPME coatings, PDMS, PA, PDMS/DVB, Car/PDMS and DVB/Car/PDMS in order to select the most suitable extraction phase. Results shown in Figure 2-1 reveal that the best performance were achieved with Car/PDMS and DVB/Car/PDMS. Considering that SPME coating optimization was performed prior optimization of other parameters such as pH, ionic strength of the solution etc., it was not possible to achieve extraction of MCHCA (a carboxylic acid with pKa = 4.89). Consequently, Car/PDMS and DVB/Car/PDMS were both used to perform the optimization of matrix pH with the purpose of determining which of the coatings could best extract MCHCA. Figures 2-2 and 2-3 compare results obtained adjusting the pH of the aqueous solution at 4, 6, 8 and 10 pH units. The results demonstrate that MCHCA is only extracted by the Car/PDMS coating,

which was selected for further optimization and method validation. Moreover, it was also observed that adjusting the pH of the aqueous solution to 4 guaranteed simultaneous extraction of all the analytes targeted in this study. Furthermore, the adjustment of ionic strength was performed by adding opportune concentrations of NaCl to aqueous samples adjusted to pH 4. However, changes in ionic strength also resulted in variations of the final pH of the sample. A similar effect was noticed by changing the type of salt (potassium nitrate and magnesium nitrate) used for ionic strengths adjustments. Therefore, it was decided to perform two separate sample preparations: to extract MCHCA the sample was adjusted to pH 4 with no adjustment of ionic strength and for the remaining analytes the sample was kept at pH 7 adjusting the ionic strength to 20 % with NaCl as per the results obtained in Figure 2-4.

Extraction temperature was also evaluated from 35 °C to 85 °C (Figure 2-5, representative results for 4-MCHM). From the trend obtained the best extraction performances were achieved at 85 °C. However, due to pressure built up in the vial with consequent partial deformation of the vial cap septum, 75 °C was selected as the optimum since no pressure build up occurred in the vial. While performing extraction time profile for MCHM at optimized extraction conditions (pH 7, 20% NaCl content, 75 °C extraction), high variability of the measurements and a decline of the MCHM response over time were observed (Figure 2-6). This indicates that a probable degradation of the analyte occurred under the used experimental conditions. To investigate if the extraction temperature was the main contributing factor to the trend observed, the extraction time profile was repeated at 65 °C, while keeping all the other parameters constant. As can be seen in Figure 2-7, good reproducibility was obtained with an appropriate trend for the equilibration process.

Therefore, 65 °C was considered as the optimum extraction temperature for further testing and validation, the extraction time profile for other analytes demonstrated in Figure 2-8. Moreover, 30 min extraction time was selected as the best compromise between analyte response and analysis throughput. In summary, the extraction conditions used for 4-MCHM, 4MMCH, MMCHC, 1-4CHDM and DM-1-4-CHC were Car/PDMS SPME fiber, 30 min extraction time, 65 °C extraction time with the sample adjusted at pH 7 with 20% (*w:w*) of NaCl. For analysis of MCHM's metabolite MCHCA the optimized extraction conditions were: Car/PDMS SPME fiber, 30 min extraction time, 65 °C extraction time with the sample adjusted at pH 4 with no adjustment of the ionic strength of the solution.

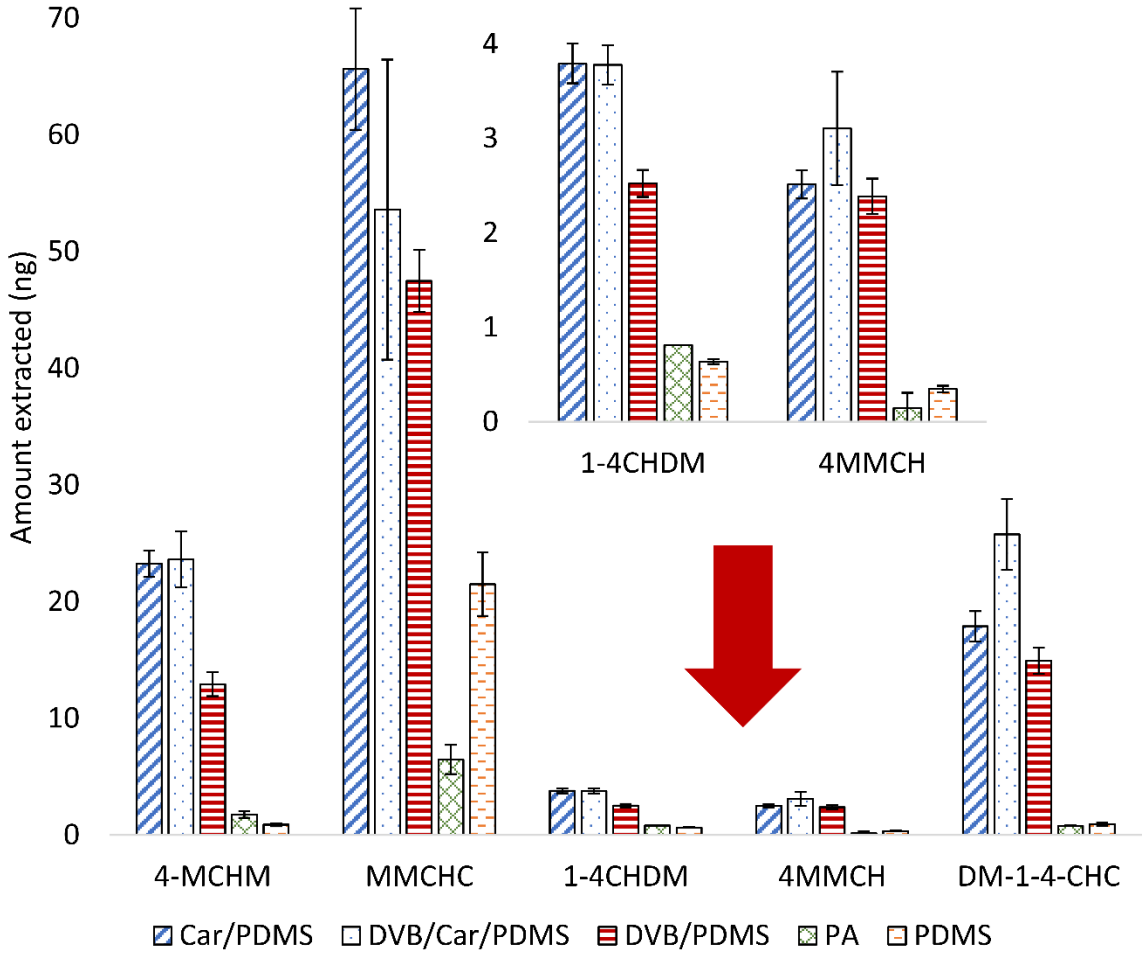

Figure 2-1 Evaluation of SPME fiber extraction phase performance for the studied analytes in water. MCHCA not detected under these conditions.

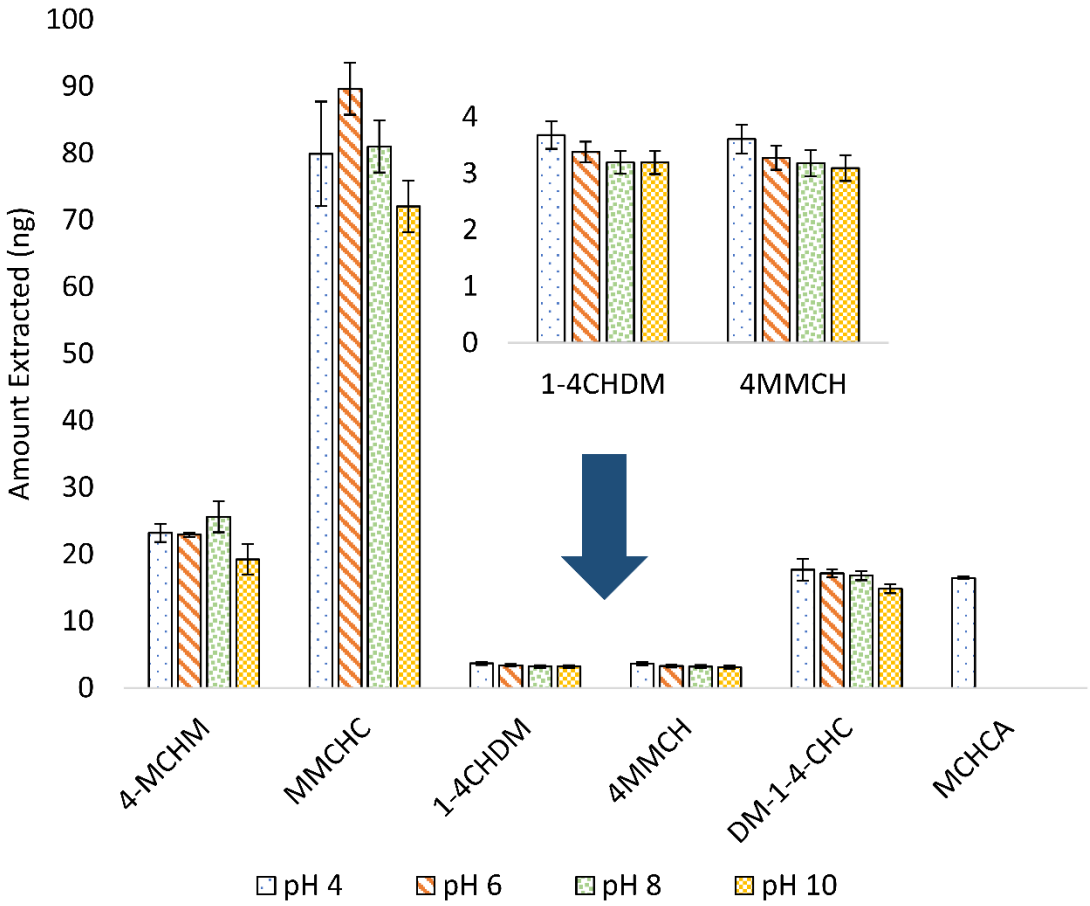

Figure 2-2 pH optimization of aqueous samples utilizing the Car/PDMS extraction phase.

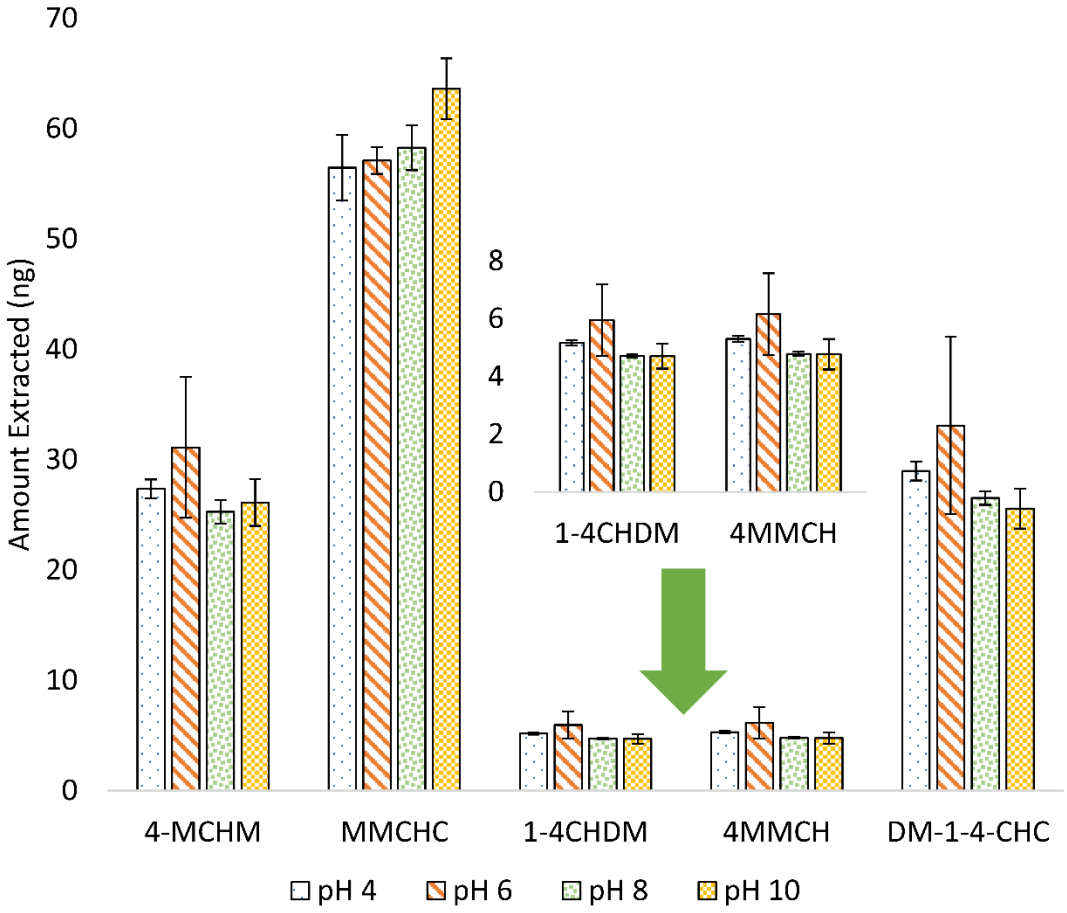

Figure 2-3 pH optimization of aqueous samples utilizing the DVB/Car/PDMS extraction phase. MCHCA not detected under these conditions.

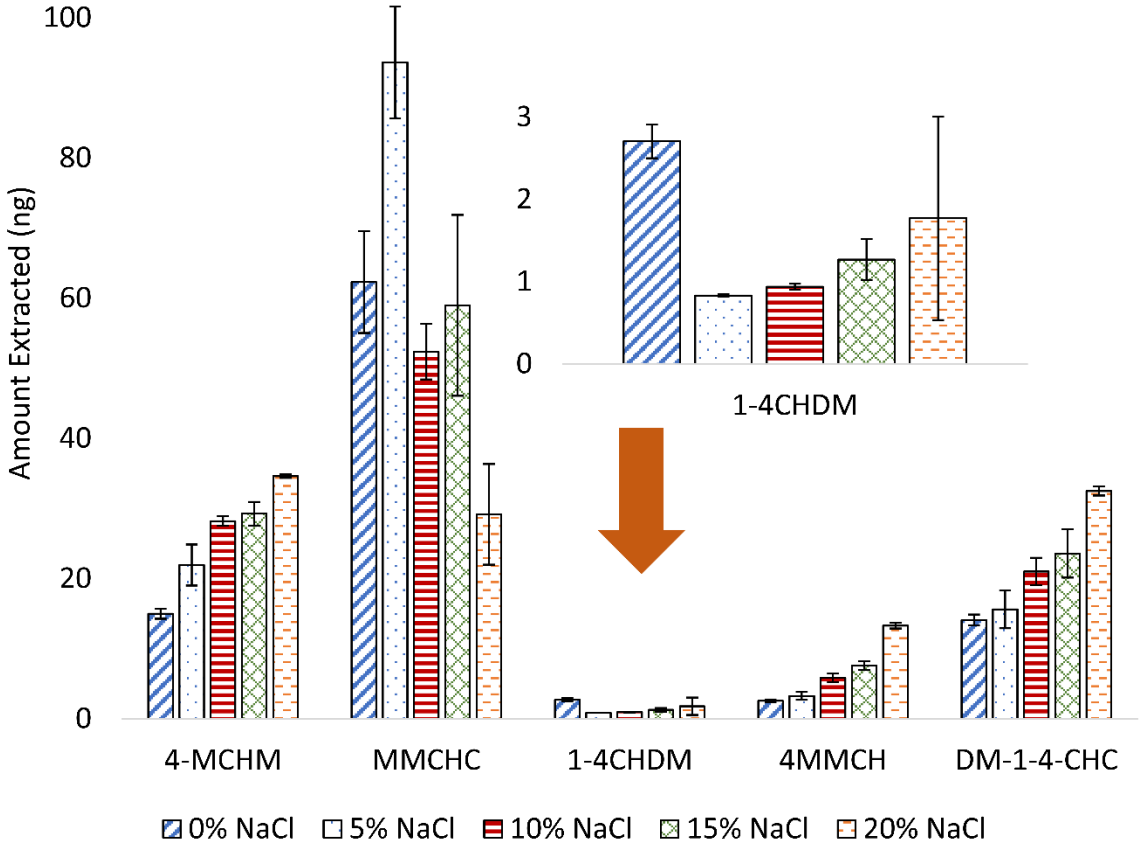

Figure 2-4 Sample ionic strength optimization, evaluated using sodium chloride and Car/PDMS SPME fiber.

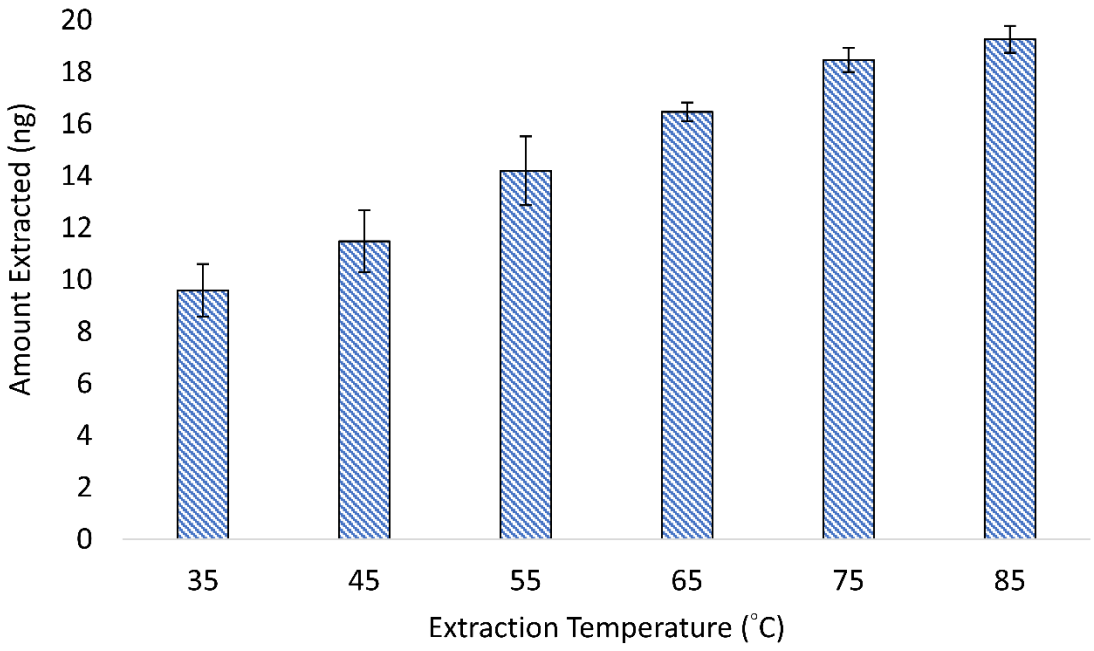

Figure 2-5 Sample temperature optimization for 4-MCHM.

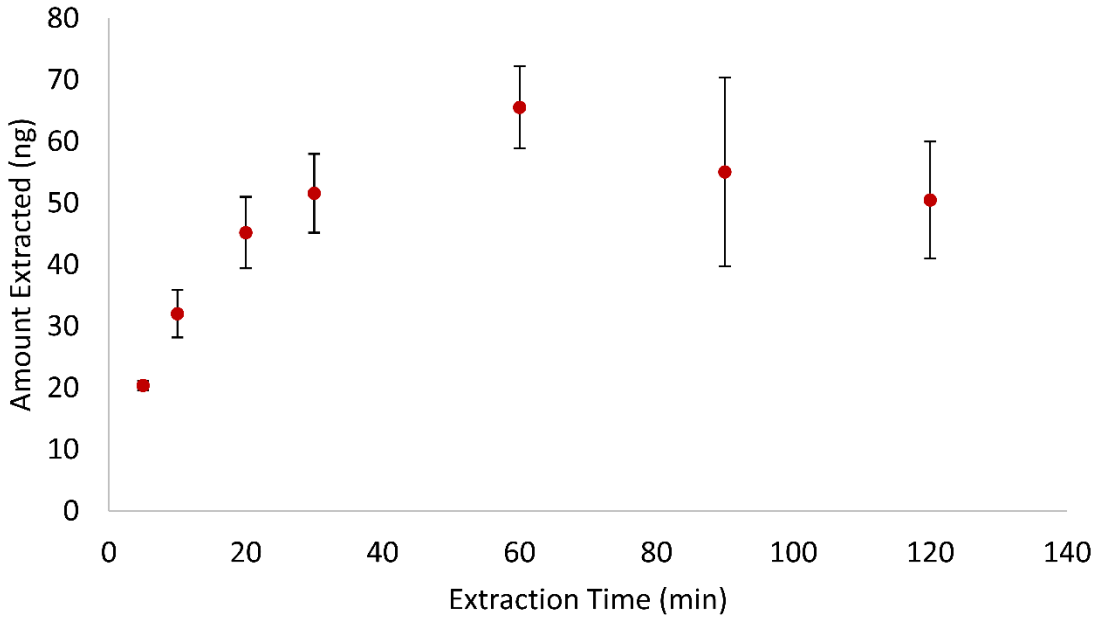

Figure 2-6 Extraction time profile of 4-MCHM at 85 °C.

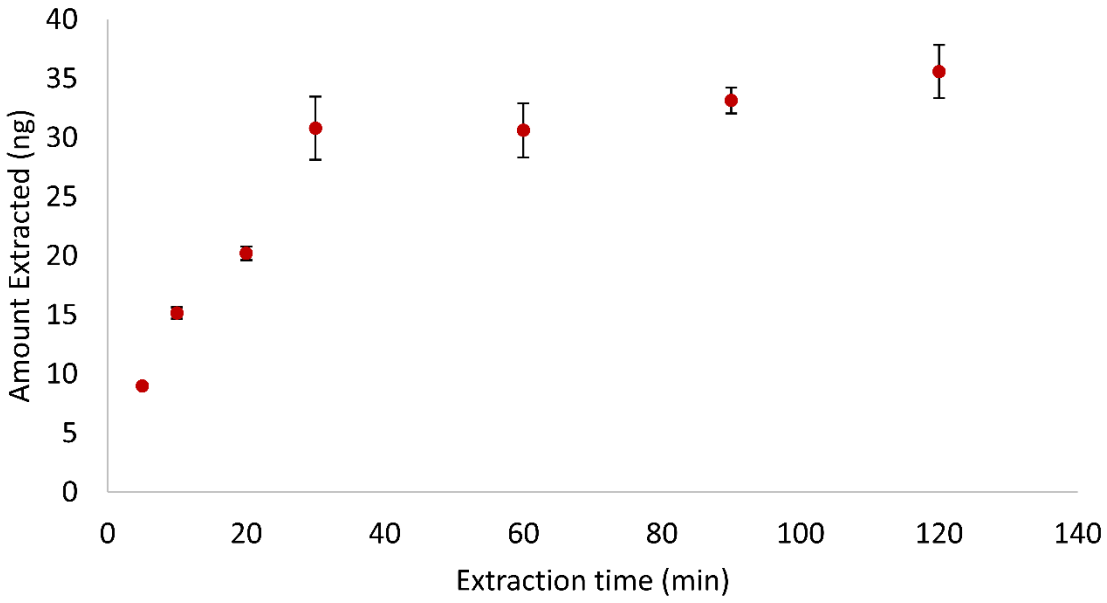

Figure 2-7 Extraction time profile of 4-MCHM at 65 °C.

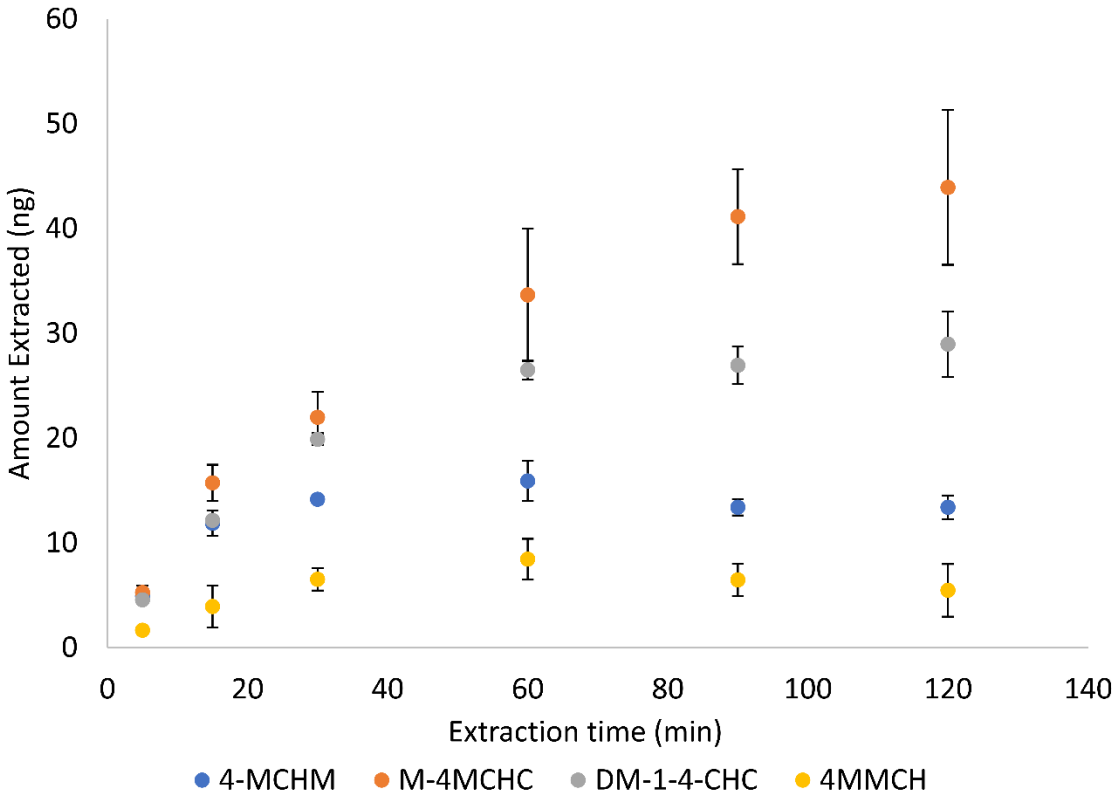

Figure 2-8 Extraction time profile of other crude MCHM constituents at 65 °C.

2.3.2 TF-SPME optimization

During SPME optimization it was determined that the extraction phase Car/PDMS was best suited for analysis of crude MCHM components. Consequently, we used a Car/PDMS TF-SPME device for further method optimization and validation. Some of the optimized operating conditions such as sample ionic strength, pH and extraction temperature are unaffected by the geometry of the microextraction device and thus further optimization of these parameters for the TF-SPME method was unnecessary. However, parameters such as extraction speed and extraction time required further optimization as extraction by TF-SPME devices was not automated (apparatus shown in Figure 2-9). Moreover, the microextraction device geometry as well the agitation method used directly influence the kinetics of the extraction process. Figure 2-10 compares the extraction performance achieved at agitation speeds of 600, 900 and 1200 rpm during extraction, each experiment being performed at optimized conditions. Results show that at 1200 rpm extraction efficiency is the greatest, however, with greater variability compared to the comparably efficient 900 rpm, thus 900 rpm was chosen as the optimal agitation speed. Using this new optimal agitation speed, Figures 2-11 and 2-12 show the extraction time profiles for the analysis of crude MCHM constituents by TF-SPME using all optimized parameters. Obtained results clearly demonstrate that all analytes, with the exception of MMCHC, equilibrate at the optimal 15 min extraction time. MMCHC, equilibrated soon after 15 min, however considering its high affinity for the extraction phase, extraction was carried conveniently at 15 min for all the target analytes.

Figure 2-9 Diagram of the apparatus used for TF-SPME.

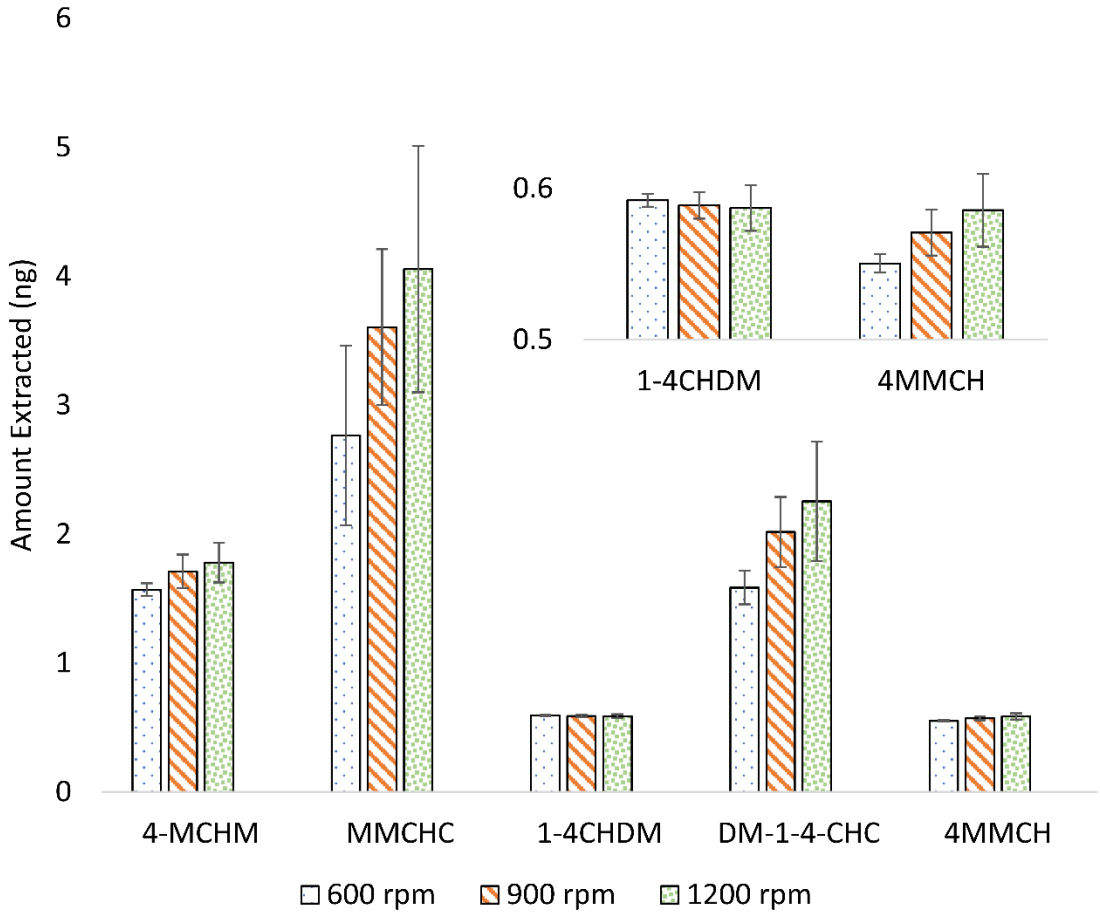

Figure 2-10 Evaluation of agitation/magnetic stir bar speed for TF-SPME.

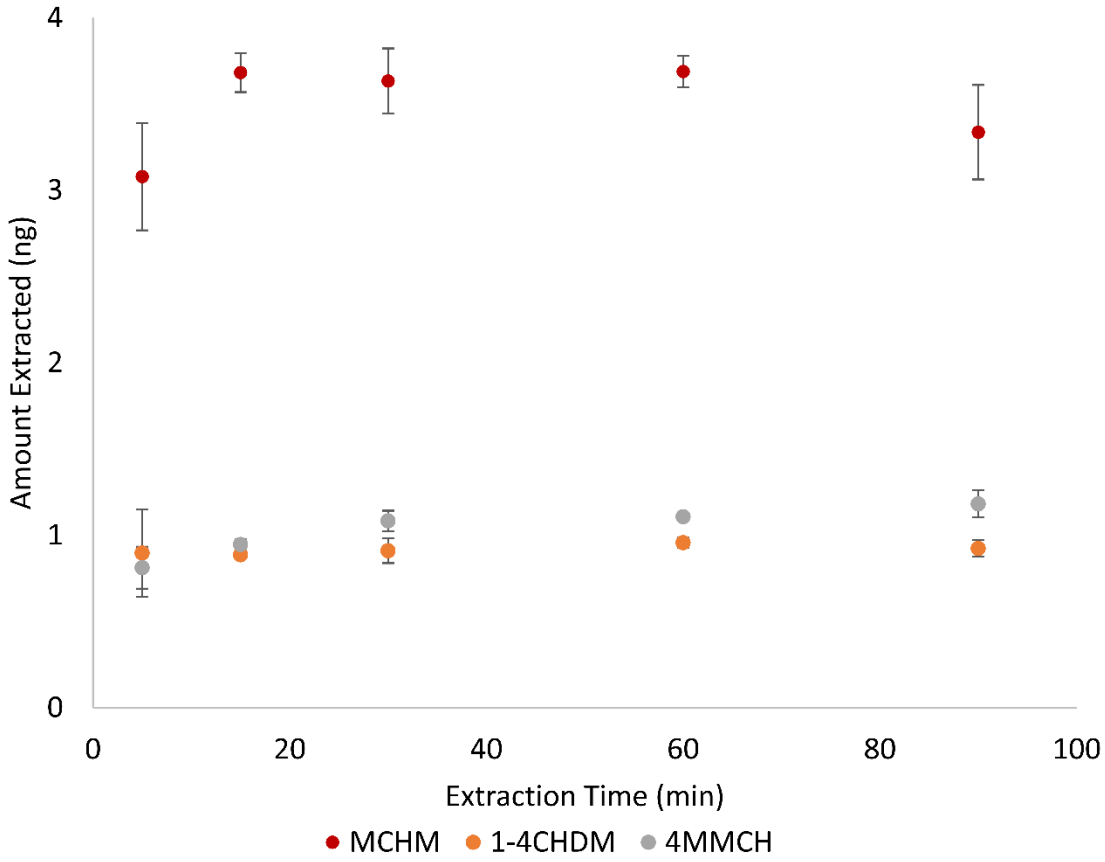

Figure 2-11 Extraction time profile for the analytes MCHM, 1-4CHDM and 4MMCH using TF-SPME.

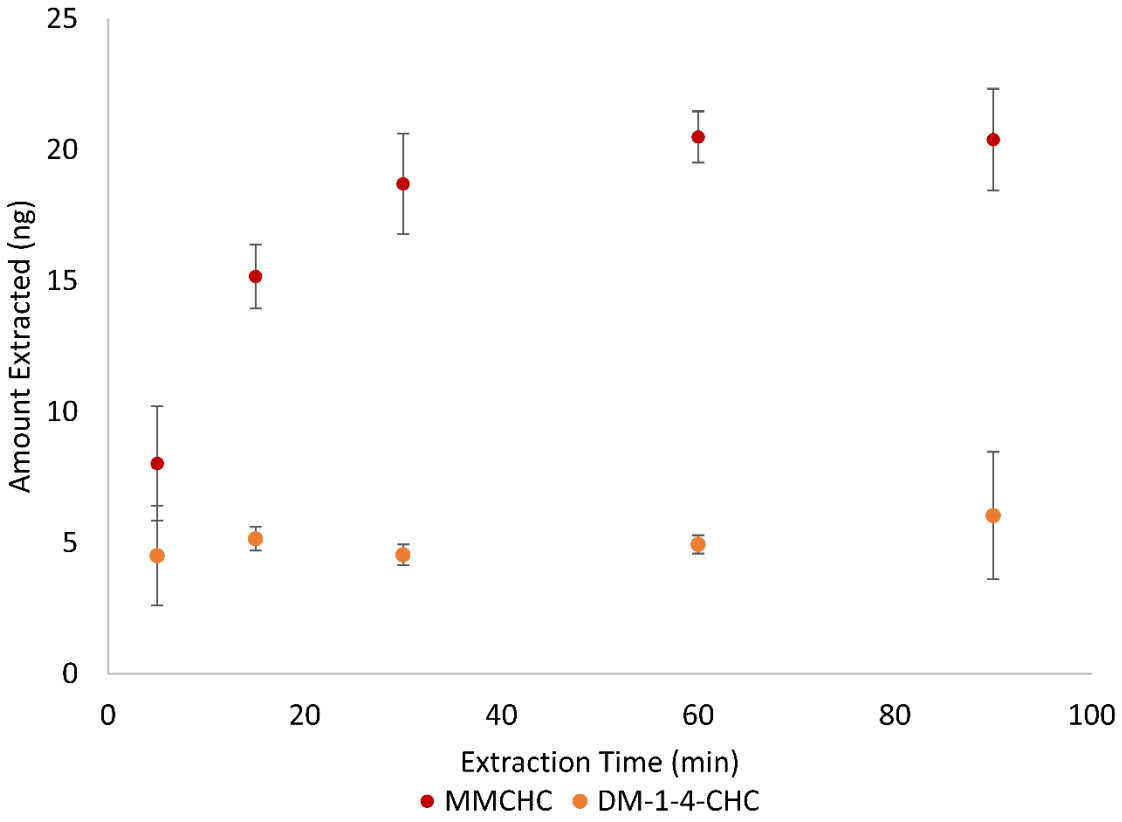

Figure 2-12 Extraction time profile for the analytes MMCHC and DM-1-4-CHC using TF-SPME.

2.3.3 Method Validation and Analysis of Real Samples

A summary of the results obtained from the method validation of the SPE, DI-SPME and DI-TF-SPME methods are presented in Table 2.1. LOQs obtained with the SPE protocol were several orders of magnitude higher than the results of the other two extraction techniques tested, indicating that this technique is not suitable for extraction of crude MCHM constituents at trace level. Linear ranges of most compounds were very narrow, notably for MCHCA, as some ranges spanned only one order of magnitude or less. SPME and TF-SPME both circumvent the caveats of using SPE, with the two microextraction protocols exhibiting similar linear ranges and coefficients of determination, TF-SPME recorded lower limits of quantification than both SPE and SPME for most compounds (Table 2.1) with comparable accuracy, except for the accuracy level at 3.5 ppb (Table 2.2). Figure 2-13 compares the chromatograms obtained by SPME and TF-SPME at 0.25 μg L^{-1}, showing the drastic increase in sensitivity TF-SPME provides. Further comparison with previously published work, Table 2.3, demonstrates that the microextraction methods developed in this study, along with being the first to detect and quantitate simultaneously all known components of crude MCHM, also quantitate 4-MCHM at concentrations lower than any previous published method.

Compared to other extraction techniques in this study, TF-SPME recorded lower limits of quantitation and better throughput as extraction times are shorter than SPME (15 min TF-SPME vs 30 min SPME). Consequently, TF-SPME was chosen as the proper extraction protocol to follow for analyzing real matrices. Tap, river and lake water samples were chosen to compare different possible matrices where 4-MCHM and its constituents might be detected. No detectable amount of the target analytes was discovered in the

samples. Subsequently each sample was fortified with the targeted analytes and tested for accuracy using the TF-SPME method developed and validated as abovementioned. Results in Table 2.4 validate the TF-SPME protocol for analysis of real matrices for the contributing compounds of crude MCHM and one 4-MCHM metabolite, MCHCA.

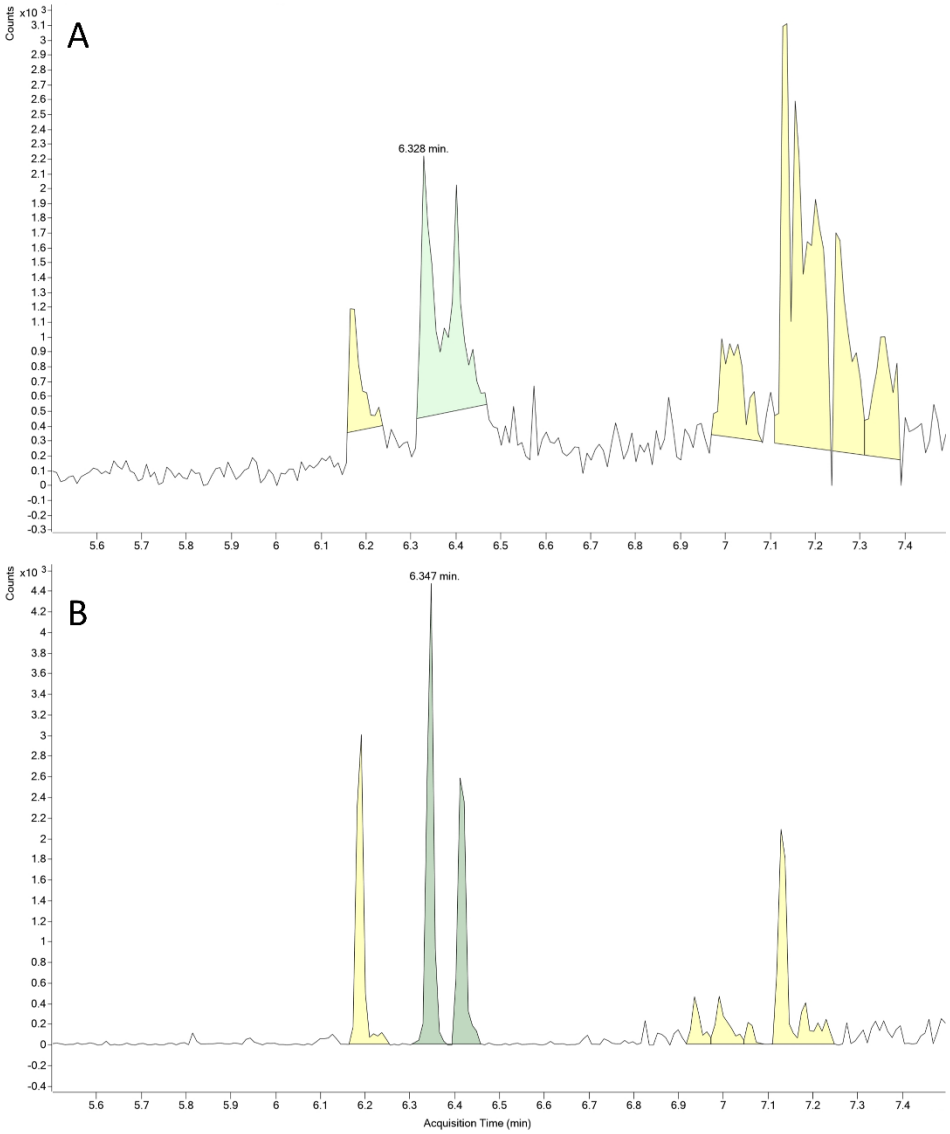

Figure 2-13 Comparison of chromatograms obtained for 4-MCHC spiked at 0.25 µg L^{-1} for A) SPME and B) TF-SPME methods.

Table 2.1 Figures of merit obtained for SPE, SPME, TF-SPME protocols, comparing linear dynamic range, correlation coefficient (R^2), and limits of quantitation (LOQ).

	SPE			SPME			TF-SPME		
	Range ($mg\ L^{-1}$)	R^2	LOQ ($mg\ L^{-1}$)	Range ($\mu g\ L^{-1}$)	R^2	LOQ ($\mu g\ L^{-1}$)	Range ($\mu g\ L^{-1}$)	R^2	LOQ ($\mu g\ L^{-1}$)
MCHM	0.5 - 25	0.983	0.5	1 - 100	0.992	1	0.1 - 75	0.994	0.1
MMCHC	0.25 - 25	0.987	0.25	2.5 - 200	0.992	2.5	0.1 - 100	0.992	0.1
4MMCH	0.5 - 25	0.984	0.5	2.5 - 200	0.991	2.5	1 – 100	0.995	1
1-4CHDM	5 - 25	0.987	5	0.25 - 100	0.985	0.25	0.5 - 75	0.995	0.5
DM-1-4CHC	0.5 - 25	0.987	0.5	0.5 - 100	0.992	0.5	0.1 - 75	0.988	0.1
MCHCA	25 - 50	0.983	25	2.5 - 200	0.992	2.5	2 – 70	0.995	2

Table 2.2 Accuracy values of the validated SPE, SPME, TF-SPME protocols.

	Accuracy % (RSD %)							
	SPE		SPME			TF-SPME		
	7.5 ($mg\ L^{-1}$)	30 ($mg\ L^{-1}$)	3.5 ($\mu g\ L^{-1}$)	35 ($\mu g\ L^{-1}$)	75 ($\mu g\ L^{-1}$)	3.5 ($\mu g\ L^{-1}$)	35 ($\mu g\ L^{-1}$)	50 ($\mu g\ L^{-1}$)
MCHM	95.2	95.3*	92.0	97.7	90.4	137.5	93.2	90.3
	(7.5)	(28.1)	(5.2)	(6.6)	(7.8)	(10.7)	(19.6)	(29.9)
MMCHC	100.0	93.3*	95.6	94.3	97.8	134.6	86.3	95.0
	(9.2)	(20.5)	(11.3)	(21.4)	(16.5)	(11.1)	(3.8)	(23.2)
4MMCH	97.1	102.6*	99.7	104.1	105.7	181.3	93.7	87.7
	(6.3)	(24.7)	(7.9)	(13.0)	(8.9)	(14.6)	(2.3)	(18.9)
1-4CHDM	95.3	98.3*	73.2	86.0	80.7	151.2	107.2	82.0
	(6.3)	(18.7)	(22.2)	(29.7)	(9.2)	(5.7)	(16.2)	(37.9)
DM-1-4CHC	106.8	90.8*	95.4	89.9	85.6	250.8	108.8	95.5
	(7.6)	(28.7)	(15.6)	(28.5)	(16.9)	(15.9)	(9.0)	(19.8)
MCHCA**	-	58.2	104.8	98.8	97.9	92.1[a]	104.1[b]	90.6[c]
	-	(5.5)	(23.9)	(11.8)	(6.2)	(18.5)	(12.2)	(7.4)

*Concentration value above upper limit of quantitation

**Accuracy values for MCHCA were calculated for TF-SPME at:

[a] 7 ($\mu g\ L^{-1}$)

[b] 70 ($\mu g\ L^{-1}$)

[c] 150 ($\mu g\ L^{-1}$)

Table 2.3 Comparison of extraction efficiency between the methods developed in this work and other methods found in the literature.

	LOQ (µg L^{-1})			
	Total 4-MCHM	trans-4-MCHM	cis-4-MCHM	Ref
SPME-GC-MS	1	-	-	This work
TF-SPME-GC-MS	0.1	-	-	This work
LLE-GC-FID	-	[100]	[100]	[63]
LLE-GC-MS	-	[30]	[30]	[64]
HS-GC-FID	5380	-	-	[65]
H-P&T-GC-MS	[0.4]	[0.16]	[0.28]	[59]
HS-SPME-GC-MS	-	[23]	[10]	[66]

[ ] Indicates the value reported as a limit of detection

Table 2.4 Analysis of crude MCHM constituents spiked at 45 µg L^{-1} in different environmental matrices.

	Tap Water		Lake Water		River Water	
	Accuracy %	RSD %	Accuracy %	RSD %	Accuracy %	RSD %
4-MCHM	127.2	13.1	123.6	4.5	141.1	6.3
MMCHC	69.6	5.9	87.4	6.2	78.5	21.4
4MMCH	63.3	6.2	63.9	1.9	63.3	8.0
1-4CHDM	117.5	12.6	115.0	6.0	134.8	13.1
DM-1-4CHC	77.1	13.9	94.6	14.0	88.7	12.2
MCHCA	61.6	20.6	65.8	12.7	88.6	10.0

2.4 Conclusions

For the first time, methods utilizing SPME and TF-SPME were developed and optimized for simultaneous analysis of 4-MCHM and all other known components of crude MCHM. MCHCA, a primary metabolite of 4-MCHM, was also determined independently with only minor modifications to the sample preparation protocol. The performance of these microextraction-based analytical methodologies, were compared to a SPE method also tested in this study. Our results show that the lower limits of quantitation can be achieved with microextraction methods. Relating these results to previously developed methods, both SPME and TF-SPME are competitive in detecting and quantitating 4-MCHM. The TF-SPME-GC-MS recorded a limit of quantitation for 4-MCHM lower than any known method currently, with only 15 min of extraction time needed. To validate this, water samples from various sources were analyzed using TF-SPME and the accuracy of the method was determined. The sensitivity of the TF-SPME method coupled with its increase in analytical throughput put TF-SPME as the optimal extraction approach for 4-MCHM and its constituents found in crude MCHM.

Acknowledgements

This work was supported by funds provided by The University of Toledo. The authors are grateful to GERSTEL USA, particularly to Dr. Robert Collins for enabling the use of GERSTEL TDU unit in our laboratory, to Dr. John Stuff for the useful scientific discussions and for providing the TF-SPME devices used in this work, to Daniel Gatch for the expert technical support with the MPS autosampler and the TDU unit. The authors also thank Prof. Jon Kirchhoff and Daniel Gatch for providing the lake and tap water samples,

respectively. Acknowledgements are also due to Rachel Avina, Elijah Long and Tharuka Ubayasena for their assistance in the early stages of this work.

Chapter 3

Optimization of Thin Film Solid Phase Microextraction and Data Deconvolution methods for accurate characterization of organic compounds in Produced Water

Adapted from a paper published in the *Journal of Separation Science*[69]

Ronald V. Emmons, Tiffany Liden, Kevin A. Schug, Emanuela Gionfriddo

Abstract

The continued rise in the extraction of unconventional oil and gas across the globe poses many questions about how to manage these relatively new waste-streams. Produced water, the primary waste byproduct, contains a diverse number of anthropogenic additives together with the numerous hydrocarbons extracted from the well. Due to potential environmental hazards, it is critical to characterize the chemical composition of this type of waste before proper disposal or remediation/reuse. In this work, a thin film solid phase microextraction approach was developed and optimized to characterize produced water. The thin film device consisted of hydrophilic-lipophilic balance particles embedded in polydimethylsiloxane and immobilized on a carbon mesh surface. These devices were

[69]Reprinted from Journal of Separation Science, 2020, 43, 9-10. Copyright © John Wiley and Sons.

chosen to provide broad extraction coverage and high reusability. Various parameters were evaluated to ensure reproducible results while minimizing analyte loss. This optimized protocol, consisting of a 15 min extraction followed by a short (3 s) rinsing step, enabled the reproducible analysis of produced water without any sample pretreatment. Extraction efficiency was suitable for both produced water additives and hydrocarbons. The developed approach was able to tentatively identify a total of 201 compounds from produced water samples, by using one-dimensional gas chromatography hyphenated to mass spectrometry and data deconvolution.

3.1 Introduction

Unconventional oil and gas, commonly defined as sources of petroleum that are extracted by alternative procedures than the conventional oil well method, have rapidly grown to prominence as a vital energy source in the 21st century.[70] During this process, large amounts of water are intermixed with various additives to aid in oil collection from low porosity shale formations. These additives include biocides, surfactants, proppants, gel breakers and inorganic acids (among others).[71] This solution is injected in the subsurface to fracture the shale, and a portion of it resurfaces with the desired commodity. The resurfaced wastewater is enriched in a variety of different classes of dissolved organic matter (DOM), along with the additives previously mentioned. Wastewater streams from unconventional oil and gas extraction are classified as either flowback water (FW; resurfaced water before significant oil/gas collection) or produced water (PW; water resurfaced concurrently with oil). PW is generally characterized as having higher total dissolved solids (TDS), as a large portion originates from subsurface brines comingled with

the oil/gas. In many cases, FW and PW are disposed by deep well injection of the material, but this practice has been linked to increased seismicity when performed near either shallow or deep fault lines.[72] The approach is meant to completely remove the waste product from the water cycle, a task that is unfortunately not always easy to complete and might have long-lasting ramifications in the future. More recent efforts have progressed toward the filtering and remediation of this waste, allowing the reintroduction of this water into the industrial cycle.[73–77]

It has been proposed by a variety of different sources, academic, industrial and governmental, that the forefront of PW research should focus on the identification of toxicological risks that might be incurred as a result of the various reuse scenarios that have been proposed.[72,78,79] In light of these goals, a comprehensive understanding of the multitude of constituents in these matrices is critical to 1) better inform toxicological research and 2) scrutinize the eligibility of different PW reuse scenarios. The potential of bioaccumulation of these unknown constituents, along with their persistence in soil and water supplies, endangers several of these reuse scenarios that have been proposed. As some of these scenarios involve agriculture and land use, it is imperative to identify the multitude of chemical constituents in PW to better grasp the potential of downstream human toxicity. The accomplishment of these goals, however, is quite challenging as the analysis and characterization of PW are met with various difficulties due to the complexity of its matrix, varying greatly between site locations and the chemical constituents present. Being a mixture of shale oil, native brine and chemical additives, there is a wide range of unknown compounds with different physicochemical properties. These properties in many cases disallow a single analytical method to properly analyze the entire range of analytes,

the matrix itself being often corrosive and hypersaline, which, in turn, makes it challenging to introduce to analytical instrumentation without extensive sample preparation.[78] The majority of organic analysis on PW has been so far non-specific, being driven by techniques such as total organic carbon (TOC) analysis and gravimetric analysis for both dissolved organic matter (DOM) and total suspended solids (TSS).[80] These techniques are important for longitudinal studies of waste-streams and for the comparison of PW site-to-site; however, they are unable to elucidate the potential toxicity and long-term environmental effects PW and similar wastes might have. To this end, there have been various studies aimed to identify organic compounds in PW matrices, most often using gas chromatography hyphenated with either a flame ionization detector (FID)[81–83] or mass spectrometry (MS)[81,84], and few examples of liquid chromatography (LC) hyphenated with MS[83,85] to analyze selected classes of compounds in PW. Many of these procedures have relied on some form of two-dimensional chromatography to manage the incredibly complex matrices that are PW and FW.[81,86] At the present time, sample preparation methodologies are underdeveloped for the extraction and cleanup of diverse organic compounds from oil-rich matrices such as PW and FW. The goal of any analysis is to obtain accurate information representative of the actual composition of any given sample; however, the simultaneous extraction of both polar and nonpolar compounds is often a challenge for traditional techniques,[87] especially with respect to complex matrices.[7,12] Currently, sample preparation for PW has been performed by liquid-liquid extraction (LLE)[83,88], solvent dilution[89], solid-phase extraction (SPE)[89] and stir bar sorptive extraction (SBSE)[86], most of which do not allow effective simultaneous extraction of both polar and non-polar compounds. Most of the reported methods for analysis of PW also include a

filtering step as a sample pre-treatment prior to extraction.[83,85,89,90] This procedure can potentially result in a major loss of certain classes of compounds that limits and biases the characterization of the matrix. This bias is also extended into experimental design. Many attempts to characterize PW have targeted only selected compounds reported by the industry as additives (e.g. www.fracfocus.org).[82,85] To aid the characterization, several examples in the literature apply data deconvolution approaches for analysis of PW, complex environmental[91], and biological matrices.[92] The majority of these used the Automated Mass Spectral Deconvolution and Identification System (AMDIS, NIST).[93,94] These methods have proven to accurately detect and quantitate large ranges of compounds; however, the distinction between close-eluting isomers is still a problem.[91]

In this work, the characterization of PW is facilitated by the development of a comprehensive solid phase microextraction (SPME) approach. SPME, a solvent-less extraction method that has widely been adopted for convenient and green sampling and cleanup, benefits from its geometry, as it allows the direct extraction of compounds from complex matrices without prior filtration.[21] Thin film solid phase microextraction (TF-SPME), an alternative geometry of SPME that allows ultra trace-level analysis, has widely been adopted as the method of choice for environmental samples.[15,53,95–97] To ensure the comprehensive extraction of the various constituents of PW, an extraction phase consisting of hydrophilic-lipophilic balance (HLB) particles embedded in polydimethylsiloxane (PDMS) was used[30], both for the extraction of PW headspace (HS) and for direct immersion (DI). The extraction procedure was optimized by implementing a strategy to load deuterium labeled internal standards prior to extraction and a rinsing step after DI analysis to clean up the TF-SPME device prior to introduction into the thermal desorption

unit for desorption. Analyses were performed by GC-MS, with data being analyzed through deconvolution methods and additional criteria developed.

3.2 Experimental

3.2.1 Chemical and Materials

All PW samples (referred to as samples PW 1, PW 2 and PW 3) were collected from a saltwater disposal (SWD) well from the Permian Basin located in Midland County, Texas. The samples were maintained at temperature between 1-4 °C during transportation and storage. Moreover, the samples were collected in opaque high-density polyethylene (HDPE) containers without headspace to prevent sample exposure to light and potential analytes' losses due to partition into the gas phase. As quality control (QC) standards, methyl benzoate-d_8 (CDN isotopes, Pointe-Claire, Quebec, Canada) and toluene-d_8 (Supelco, Bellefonte, PA, US) were used. The HLB-PDMS TF-SPME devices were kindly provided by Gerstel US (Gerstel, Inc., Linthicum, MD, USA). The TF-SPME devices used were constituted of 2 cm x 0.5 cm carbon mesh support coated with 40 ± 5 µm HLB/PDMS per side.[29]

3.2.2 Instrumentation

Analysis were performed on an Agilent 7890 B gas chromatograph hyphenated to a 5977 B single quadrupole mass spectrometer (Agilent Technologies, Santa Clara, CA, USA). A Rtx®-5MS column (30 m x 250 µm x 0.25 µm, Restek Corporation, Bellefonte, PA, USA) was used in conjunction with a 10 m Integra-Guard Column (Restek Corporation, Bellefonte, PA, USA). The TF-SPME device was desorbed by use of a thermal desorption unit, TDU, (Gerstel, Inc., Linthicum, MD, USA) and a cooled injection

system, CIS 4, (Gerstel, Inc., Linthicum, MD, USA). The desorption process was semi-automated using a Multipurpose Sampler, MPS, (Gerstel, Inc., Linthicum, MD, USA). Ultrapure helium (99.999%) was the carrier gas at a constant flow rate of 1.5 mL/min. The GC oven program was as follows: 40 °C for 5 min, followed by a 5 °C/min ramp to 300 °C which was then held for 5 min, with a total run time of 62 min. The solvent delay was set at 1.5 min, with the MS scanning from 40 to 450 m/z. The MS source was set at 230 °C, the quadrupole was set at 150 °C and the MSD transfer line being 250 °C. Desorption was performed at 250 °C for 5 min in the TDU with the transfer line set at 280 °C, these parameters being optimized to avoid the occurrence of carryover. Under these desorption conditions, carryover experiments did not reveal the presence of the analytes detected in produced water samples. The CIS was initially set to -50 °C, which was then quickly ramped to 300 °C at 10 °C/s and then held for 3 min in a solvent-venting mode. Inter-sample conditioning was performed with the same TDU and CIS settings used for analysis. All data analysis was performed with Agilent Unknowns Analysis software (Agilent Technologies, Santa Clara, CA, USA) and subsequently filtered using Excel 2016 (Microsoft Corporation, USA). Under the optimized conditions, blank analyses –including instrumental blank, TF-SPME device blank and extraction blanks in ultrapure water with and without deuterium-labeled QC standards loading – were performed to demonstrate the selectivity of the method, representative chromatograms are shown in Appendix A, Figure A-1.

3.2.3 Sample Preparation

Aliquots of PW were distributed between 100 mL opaque HDPE bottles (no headspace) and stored at 4 °C prior to analysis. HDPE sample bottles were first agitated at

least 8 h prior to extraction at room temperature to ensure homogeneity. Immediately prior to PW extraction, the TF-SPME device was exposed to a 500 μg L^{-1} mixture of deuterium-labeled QC standards in 9 mL of ultra-pure water for 5 min. The extraction was performed at room temperature, while the sample was agitated at 600 rpm with a magnetic stirbar. After the QC compounds were loaded on to the TF-SPME device, the device was wiped clean of water and then placed into the PW sample vial. The sample vial was a 10 mL amber glass vial containing 2 mL PW for HS extraction and 9 mL for DI extraction. All PW extractions were performed at room temperature. The gap between the vial cap and the vial neck was further sealed with Parafilm® and a thick rubber septum was placed between the vial and stirring plate. The extraction of PW was performed for 15 min with a 600 rpm agitation speed using a magnetic stirbar. After PW extraction, the TF-SPME device was immediately rinsed in agitated (900 rpm) ultra-pure water for 3 s, then wiped free of moisture and placed in the desorption liner prior to thermal desorption and analysis.

3.2.4 Data Processing

Compound identification was carried out using Unknowns Analysis (Agilent Technologies, Santa Clara, CA, USA). Deconvolution parameters included a 0.3 left m/z delta and 0.7 right m/z delta extraction window using integer m/z values. All data were referenced to the NIST library using retention time (RT) matching with a max 50 penalty, this penalty being multiplicative and based on a Gaussian penalty function with a window of 6 seconds. RT window sizes were based on increments of 25, 50, 100 and 200 s. Retention Index (RI) matching was accomplished through a calibration file obtained from the analysis of an alkane mixture (C_7-C_{30}, Sigma Aldrich, St. Louis, MO, USA). All compounds evaluated were those with a 70% or greater match factor, which is an aggregate

of each compounds' likeness to the NIST library using both its RI and deconvoluted mass spectra. After compound identification, all data were then processed in excel to ensure the reproducibility of compound identification between each triplicate run. This reproducibility was also verified between analyses using different extraction modes (HS and DI). Any compound remaining that exceeded a 100 RI discrepancy from its NIST library value was then discarded. Finally, all presented data was cutoff at any compound that met all these criteria and scored an aggregate match factor of at least 80%, the only exceptions being a compound that was 75% or greater in a single sample but was found at 80% or greater in the other two samples. This strategy reduced the bias resulting from a strict cutoff while ensuring that the data provided an accurate chemical snapshot of the samples.

3.3 Results and Discussion

3.3.1 Sample Preparation Optimization

As previously mentioned, PW samples are a diverse range of matrices that differ in their physicochemical properties; the location of the samples studied (Midland-PW) being demonstrated to have TDS as high as 180,000 mg/L with a TOC of 1032 mg/L.[74] In this respect, PW as a whole is hard to encapsulate as only a single matrix, challenging any analytical protocol with the objective to extract, clean up and analyze organic constituents. In light of this, any developed method must strive to limit the chemical biases associated with different techniques and ensure that the procedure is effective for different PW matrices.

Preliminary sample preparation optimization was focused on limiting the number of steps for the user while still achieving the widest range of analyte extraction possible. To achieve this, a polydimethylsiloxane (PDMS) TF-SPME device loaded with HLB particles was used to ensure rapid extraction while still minimizing the number of steps involved. HLB was chosen as the ideal extraction phase as it has been shown to extract a wide range of compounds.[30,98,99] This is critical for a matrix such as PW due to its content of hydrocarbons and both polar and nonpolar additives, further being complicated by potential metabolites and degradation products. To ensure that the scope of the analysis was truly comprehensive, extractions were carried out both in HS and DI modes, in triplicate. The importance of this dual-extraction mode is highlighted in Figure 3-1. HS extraction is essential for the analysis of high-volatile and low molecular weight compounds (additives and degradation products), while DI is more amenable for the analysis of higher molecular weight compounds (native hydrocarbons and petroleum distillates).

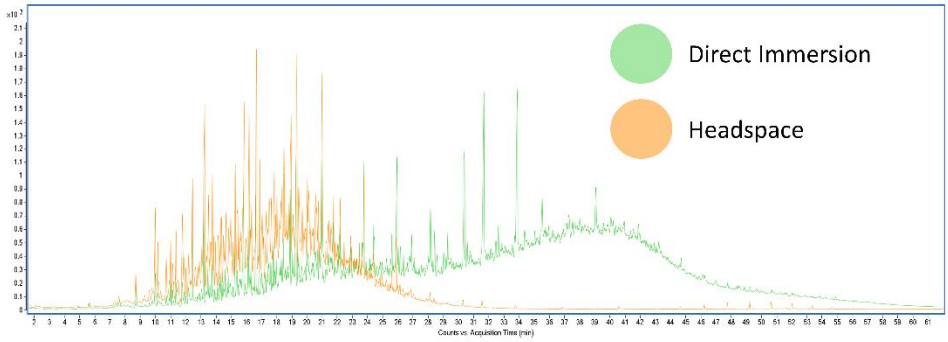

Figure 3-1 Overlaid chromatograms of both headspace and direct immersion extraction.

As the initial goal was to simplify, as much as possible, the extraction protocol while maximizing reproducibility, extractions were first carried out by simply extracting PW in one step (using the same extraction time and desorption parameters described for the final PW extraction procedure, Section 2.3) with the intention of reducing errors and achieving higher throughput. This procedure was carried out for each sample; however, initial findings demonstrated unacceptable variability for all samples due to the complexity of the matrices. This variability was attributed to a variety of factors, most notably potential gas leaks from the sampling vial during HS extraction or the formation of an oily layer on the TF-SPME device during DI extractions. To reliably and reproducibly extract the multitude of constituents from PW, the final developed method utilized Parafilm® to seal the metal screw cap of the vial and minimize highly volatile analyte losses and a thick rubber septum was placed between the sample vial and the stirring plate to reduce heat transfer from the stir plate to the vial, potentially generated by the continuous stirring activity: this would create irreproducible temperature gradient in the sample vial with consequent bias during extraction. To confirm that the use of Parafilm® did not introduce any additional plasticizer contaminant to our sample we applied our TF-SPME protocol to ultrapure water samples in vials with and without Parafilm® sealing. It was determined that the use of Parafilm® did not introduce plasticizer contamination in the samples. In the case of DI, a rapid rinsing step (3 s) in ultrapure water was added after extraction to remove excess matrix components from the TF-SPME device ensuring efficient and reproducible desorption and minimizing instrumental contamination. For the rinsing step, it is critical to ensure a high agitation rate, enough to form a vortex, as this mechanical force is needed to sheer off the oils from the TF-SPME device. Finally, to ensure the extraction efficiency of

the TF-SPME device was constant throughout all experiments, two internal standards (methyl benzoate-d_8, toluene-d_8) were loaded onto the extraction device, prior to PW extraction, by a 5 min DI extraction of an aqueous solution fortified at 500 µg/L with the internal standards. Methyl benzoate-d_8 proved to be the most suitable, in terms of reproducible loading onto the TF-SPME for both inter and intra-sample analysis and thus was further used for the optimized protocol (Appendix A, Figure A-2). The resulting optimized approach is described in Figure 3-2. The final procedure provided satisfactory reproducibility and only took 20 min to fully prepare the sample reliably and efficiently, only 5 min more than the initial irreproducible method (Figure 3-3). During initial method optimization it was observed that certain PW matrices (in particular PW 3) required inter-sample thermal conditioning of the TF-SPME device.

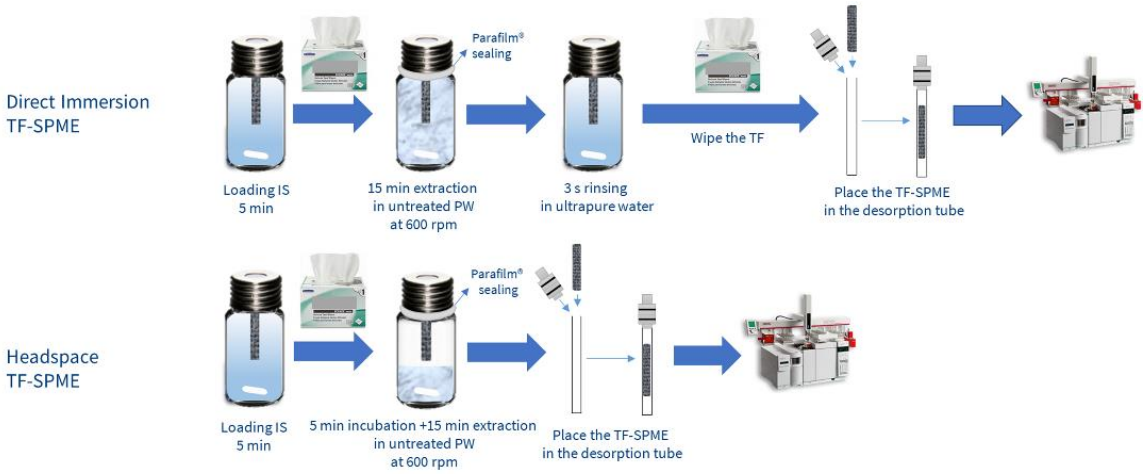

Figure 3-2 Optimized TF-SPME workflow for PW extraction and analysis.

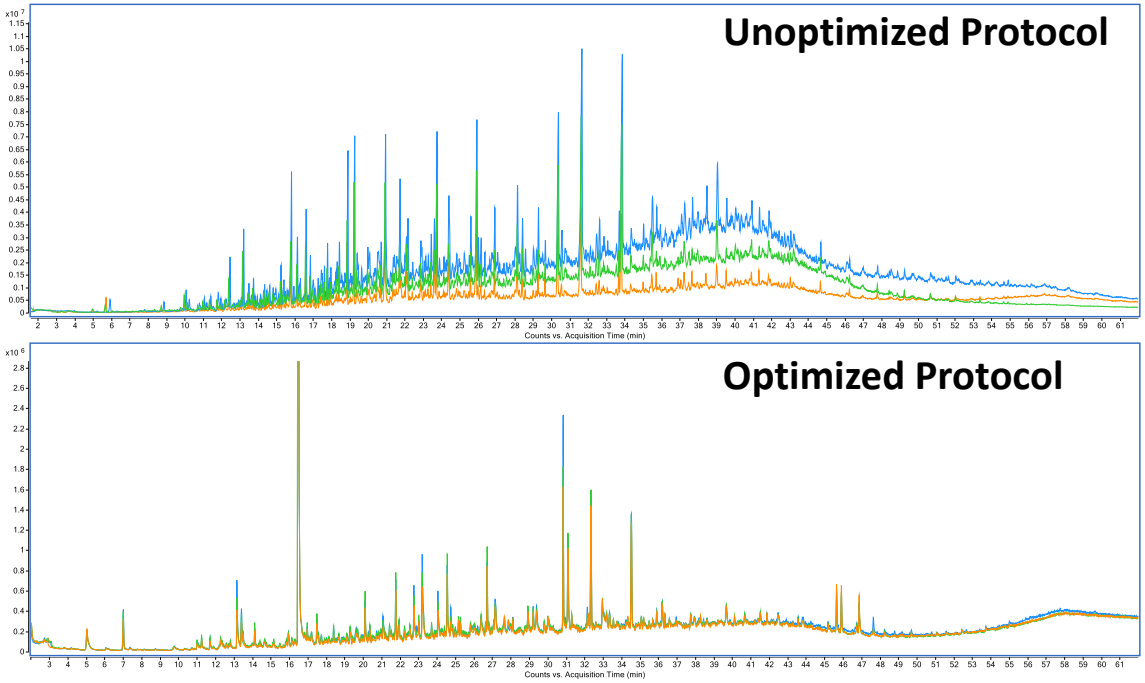

Figure 3-3 Representative chromatograms obtained with the initial unoptimized extraction procedure and the final optimized extraction procedure for PW samples.

3.3.2 Data Processing Method Development

As baseline separation of complex matrices, such as PW, is unfeasible, even in the case of two dimensional GC,[86] advanced data analysis tools must be implemented to better describe the collected data. Previous reports have used AMDIS and similar deconvolution approaches to unravel such complex MS spectra. The results were promising and can be considered semi-quantitative when appropriate internal standards or ionization efficiency correction is used.[86,88,100] In spite of this, great care must be taken when selecting a data approach to ensure optimal results. The interpretation of this data is perhaps more critical due to the possibility of misidentification and false positives. This data processing permits the identification of multiple compounds in the same chromatographic space. As confirmed

by prior data deconvolution methods applied to the GC-MS analysis of complex mixtures,[91] single quadrupole mass spectrometry is fast enough to produce the data density required of deconvolution algorithms. For this reason, these methods allow more accessible instrumentation to perform analysis of complex matrices compared to the more sophisticated instruments, such as two dimensional GC[81] and time-of-flight (TOF)-MS[81] that are often utilized in the analysis of such complex matrices. Deconvolution parameters were set with the goal of having a reasonable window of error prior to further data-filtering. This was to ensure that any compound that only marginally fails in one sample, with respect to match factor, could still be considered if the compound passed in the other replicates. After these compounds were determined, further stipulations were considered when the data was processed in Excel. All compounds recorded must have been determined in at least 2 of the three replicates to ensure no erroneous identification. The results were then compared between HS and DI methods to ensure compound identification was consistent throughout. At this step, the data showed consistent results; afterward, any compound that could be found outside of a 100 RI window of its NIST library value was removed and the final data set was obtained. It should be noted that while deconvolution - followed by spectral search and RI matching - is a powerful tool, in the case of isomeric mixtures, compound identification is far more challenging.[86] Notably, isomers found within 100 RI cannot in most cases be confidently discerned from another, meaning any isomeric information that reaches that criteria presented here should only be considered tentative. As others have suggested, summing the areas of these components would give a more holistic description of the matrix studied.[91] Nonetheless, automated deconvolution

followed by user verification allows confident compound identification in complex matrices with less prohibitive equipment compared to other methods.

3.3.3 Data Deconvolution Fundamentals

The extraction of "pure" or single-component mass spectra from multi-component spectra has long been studied and developed, much of this work being developed for GC-MS data. Early as 1974, Biller and Biemaan developed a data method which extracted a spectrum only composed of mass peaks which simultaneously maximized.[101] More computationally advanced techniques soon were developed into what is referred to as the "model peak" method by Dromey et. al.[102] This peak deconvolution process is able to find all ions that follow the same trend, in a chromatographic sense all ions that "rise and fall" together, and attempt to identify these matching ions as a single component. In this way, the position of each peak maxima is determined not by the scan with the maximized ion, but by a parabolic least squares interpolation using the top 5 points for the maximized major ion. This is expressed in Equation 3-1:

$$t = \frac{7(2Y_{-2}+Y_{-1}-Y_1-2Y_2)}{10(2Y_{-2}-Y_{-1}-2Y_0-Y_1+2Y_2)} \qquad \textbf{(Equation 3-1)}$$

Where t is equal to the time coordinate of the peak maxima and the series Y_{-2} to Y_2 denote the 5 highest points for the ion. An interesting feature to this method is that time coordinates are measured to one-third of the scan speed. Because a spectral scan measures from low to high mass, it is possible to categorize low mass ions as occurring in the first third of the spectral scan, medium mass ions the second third, and high mass ions the last third of the scan. This approach allows narrow chromatographic peaks with only 1.5 to 2 full spectral scans to be accurately deconvoluted. In addition, conventional background

subtraction and peak shape methods are also employed. In the event where peaks are coeluting with an ion of the same *m/z*, or ion intensity is affected by the coeluting elutants, the contribution of each is modeled by minimization of an error function as shown in Equation 3-2:

$$E = \sum(Y_t - pP_t - qQ_t - _{...} - c - dt)^2 \qquad \textbf{(Equation 3-2)}$$

Where E is the error, Y_t is the fragmentation pattern at a given time, P_t is the is the amplitude of elutant 1 at that time, p is the amplitude of elutant 1 above background, Q_t is the is the amplitude of elutant 2 at that time, q is the amplitude of elutant 2 above background, c is the background offset, d is slope and t is time. This equation can be further expanded for each possible coeluting component. In the case of two coelutants, error minimization would consist of 4 linear equations between p, q, c and d. There are various other modifying factors (e.g., detector saturation, triplet case approximation) that have also been leveraged. Modern peak deconvolution methods use much of the same characteristics of the method developed by Dromey et. al. with minor modifications.[102] In the case of the Automated Mass spectral Deconvolution and Identification System (AMDIS) developed by the National Institute of Standards and Technology (NIST), ion abundance is treated as signal-to-noise values to better distinguish weaker signals from background.[93] Proprietary software, such as Agilent Unknowns Analysis (Agilent Technologies, Santa Clara, CA, USA) do not outline their exact methods, however, the "model peak" method is still standard. Modifications of noise analysis or the exact workings on spectral deconvolution may be adapted from software to software. Nonetheless, the acquired deconvoluted spectra

are assigned to separate components then referenced to compound data bases such as the NIST mass spectral library.

3.3.4 Produced Water Characterization

All characterized compounds in samples PW 1, 2, and 3 are listed in Appendix A, Tables A.1, A.2 and A.3, respectively. Data are presented by their extraction type, demonstrating the need for both HS and DI sampling to ensure a comprehensive chemical snapshot of the matrix analyzed. The majority of compounds identified are long-chain hydrocarbons with varying levels of alkylation and length, followed by cyclic hydrocarbons and then potential additives and degradation products. Of these hydrocarbons are a number of polycyclic aromatic hydrocarbons (PAHs), the most abundant being phenanthrenes, anthracenes, and naphthalenes which have been previously described in other work.[103] A pesticide, atrazine, was also found in a single sample (PW 3), albeit at low levels which corroborates the idea that pesticides in PW are at ultra-trace levels and are rarely found in samples.[82,104] Many of these compounds, which given the abundance found in the samples analyzed, pose major environmental concerns due to their toxicity and persistence in the environment, most of which are supported by other works in the literature.[83,103,104] Most notably is the constituent 1,4-dioxane, a previously discovered PW component that is associated with human cancer[82,90] and has been shown to be challenging to remove from the waste-stream.[90]

More polar compounds, such as diiodomethane or the various alcohols found throughout the samples are most likely additives added by the various oil production companies during the collection of oil. The extraction of these additives, being far more polar and less abundant than their hydrophobic counterparts, was enabled by the dual

extraction mode provided by the HLB TF-SPME device. Some compounds of particular interest, iodinated organics, were persistently detected in sample PW 3. Iodinated compounds have been detected in previous studies with the assumption that they are unreported additives.[89] As can be seen in Figure 3-4, these compounds slowly degraded with a sharp molecular iodine peak forming during later analysis. This is most likely due to the well-known photosensitivity of iodinated compounds, the sample slowly becoming a darker shade of brown during the procedure. The formation of free iodide poses another environmental concern. It readily reacts with various chemical species to form potentially toxic compounds. The formation of halogenated species in PW has been previously demonstrated,[89] and other transformation byproducts from additives have also been discovered.[81] More nonpolar additives identified, such as naphthalene derivatives, were found in a variety of samples. Other compounds, such as cholesterin acetate and 4-octen-3-one, may be microbial metabolites.[84,86,105]

In total, across all three PW samples and the two different extraction modes, there were a total of 201 compound hits that were validated, with numerous analytes being exclusive to one extraction mode. These compounds comprise approximately only ~ 5% of the total compound hits from data deconvolution, as most compounds could not meet the stringent data post-processing described in this study. This is to be expected, as previous reports have shown that compound identification, even with the use of GCxGC-TOF-MS, only accounts for approximately 25% of the total compounds in the mixture.[71,86] It should be noted that a comparison between these values is ambiguous as the data verification and post-processing methods follow different approaches; however, one would suspect better structural elucidation using both 2D chromatography and TOF-MS. To

mitigate this oversight, unbiased sample preparation techniques that comprehensively extract compounds from these matrices must be practiced before any separation. In order to verify the accuracy of our method in terms of compound identification, various analytes detected in the PW sample were selected for further targeted analysis, namely atrazine, toluene, benzonitrile and pyridine. Standard solutions of the selected analytes were directly injected for retention index calculation and mass spectrum comparison with PW samples. Moreover, the same analytes were spiked in ultra-pure water at 25 µg L^{-1} and extracted using the optimized DI-TF-SPME-GC-MS workflow described for PW analysis. The results indicated that all the retention indexes of the targeted analytes were comparable to those calculated for the PW analysis (ΔRI= +/- 22), and the mass spectra presented a good match with references obtained from the NIST library and analysis of PW (Figure 3-5). Moreover, the S/N values obtained by TF-SPME-GC-MS analysis of the targeted analytes spiked at 25 µg L^{-1} in ultra-pure water indicate that our method can be potentially feasible for detection of PW constituents at low part per billion levels (Figure 3-6).

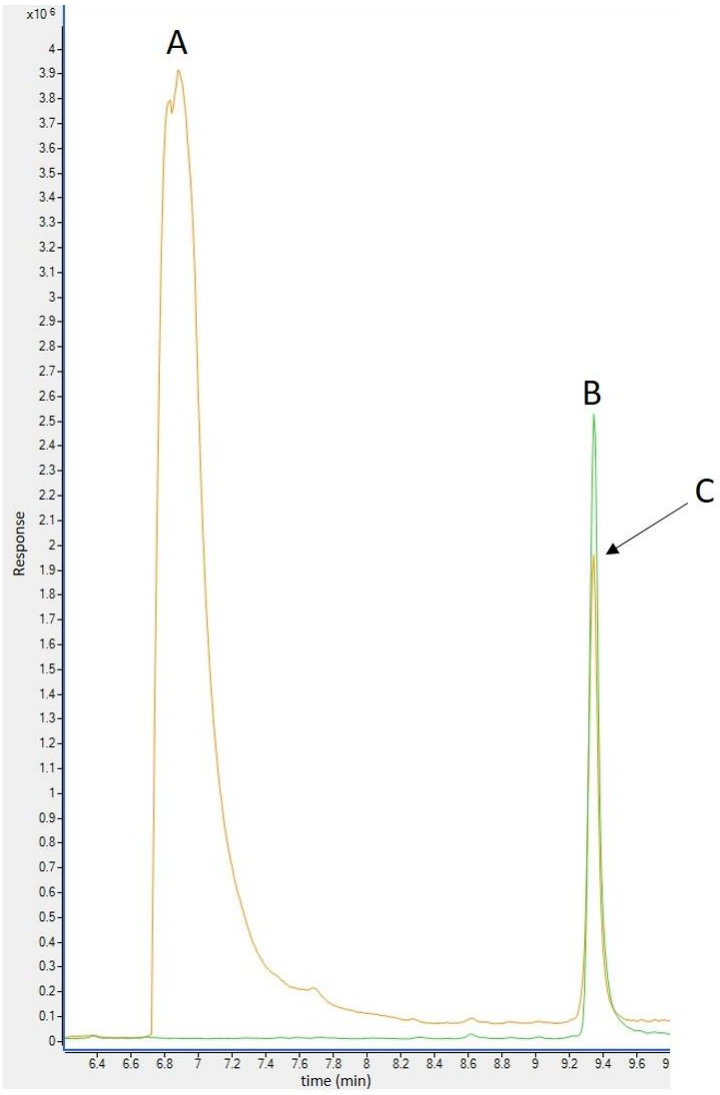

Figure 3-4 Representative chromatograms demonstrating interconversion of molecular iodine formation (peak A) in diiodomethane (peak B). The chromatogram displaying peak A and C were acquired after 24 hours of opening the sample bottle. The chromatogram displaying peak B was acquired directly after opening the sample bottle.

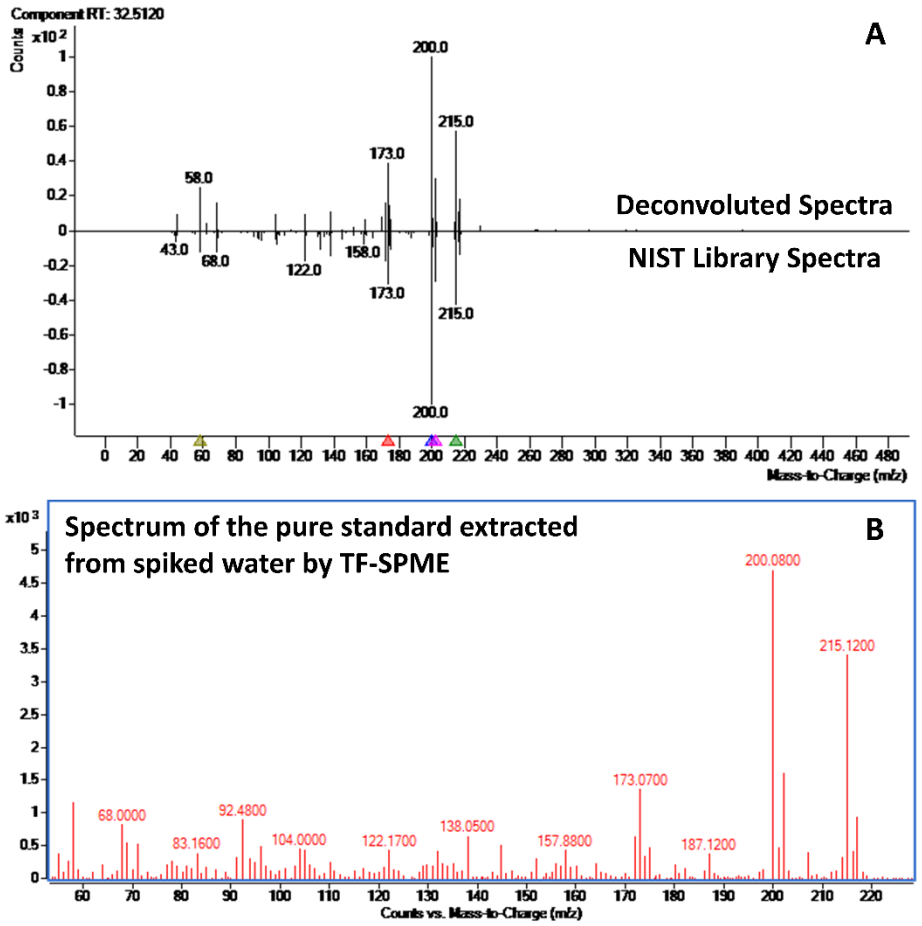

Figure 3-5 Characteristic mass spectra of atrazine obtained from a) deconvolution of PW sample and NIST17 library, b) TF-SPME of atrazine spiked at 100 µg L^{-1} in ultra-pure water.

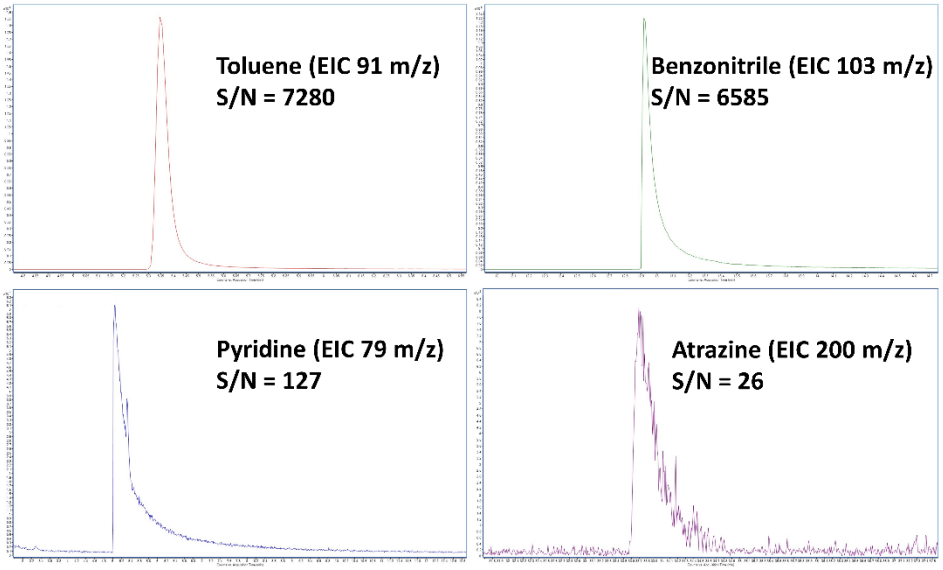

Figure 3-6 Extracted ion chromatograms (EIC) of selected standards extracted from ultra-pure water spiked at 25 µg L-1, extraction conditions were the same as the optimized PW extraction approach described in Section 2.3 of the main manuscript. A) toluene (S/N = 7280), B) benzonitrile (S/N = 6585), C) pyridine (S/N = 127) and d) atrazine (S/N = 26). The results indicated that all the retention indexes of the targeted analytes were comparable to those calculated for the PW analysis (ΔRI= +/- 5)

3.3.5 Method Comparison

As with other methods that have been developed to cleanup these complicated matrices, various steps are necessary to ensure quantitative extraction and a rigorous cleanup prior to analysis. PW, a matrix that often contains suspended solids, dissolved solids, and a partially separated organic layer, requires filtration or emulsification before extraction of the sample. Given that any filtering material potentially has affinity for compounds in such a complex matrix, any sample cleanup procedures utilizing glass, cellulose, or polymer-based filters for untargeted analysis risks the loss of analyte to these materials, especially critical when the method is untargeted. Unlike SPE or other similar methods that have been used for PW or FW in the literature,[89,90] we demonstrated that TF-SPME does not require any filtering step when a proper extraction protocol is optimized. Its geometry allows it to extract compounds of interest without the risk of clogging the extraction device or injecting particulate into the analytical instrument. To evaluate the loss of analytes due to the use of filtering in the developed method, nylon filters were used to filter PW samples prior to extraction with our TF-SPME method. Demonstrated in Figure 3-7**,** a critical loss in analyte is observed when adding this filtering step. This result is expected, as the incredibly wide range of compounds found in PW exhibit diverse chemical properties, many of which cause these different chemical classes to adhere to the filtering material. In doing so, any untargeted chemical classification of such complex matrices would not be comprehensive. Figure 3-8 demonstrates the loss of analyte between the two methods. Only 22 compounds were detected after filtering sample PW 1 (a 72% reduction in identifiable constituents).

This filtering method is usually performed in conjunction with LLE, SPE, or some form of column chromatography; however, sometimes the eluate is simply diluted with solvent and injected into the instrument. This solvent-dilution approach has increased throughput but does not pre-concentrate or cleanup the sample. As the organic additives in PW are more dilute than in FW, pre-concentration is critical for trace components and thus, "dilute and shoot" methods are especially poor for PW.[71] When extracting and pre-concentrating the constituents of PW, the large amounts of oil and salt in these matrices required larger volumes of solvent than most, with the use of 240 mL of dichloromethane[83] being used and 100 mL of chloroform[88] for LLE. SPE methods must also use large volumes for these matrices, with as much as 10 cartridge volumes (30 mL total for a standard 3 mL cartridge) for percent recoveries as low as 0.04%.[89] Many of these studies have also used column chromatography before introduction into the instrument, risking again the significant loss of various classes of compounds. Through the use of HLB as an extraction phase, a far wider and more comprehensive extraction is achieved. Both polar and nonpolar compounds can be extracted and pre-concentrated in one step. This is exemplified by the extraction of molecular iodine from the sample PW 3, a compound that not only would be sparingly extracted by other methods but also would be lost during the long sample preparation workflows that have been previously developed.

There is one instance of an SPME technique being applied to PW samples, although the goal of the study was not a comprehensive compound-specific characterization of the samples.[86] Stir bar sorptive extraction (SBSE) was utilized with an unfiltered diluted sample (20-fold dilution). The method included a 1 h extraction with a monophasic PDMS extraction phase. PDMS would only allow the hydrophobic (mostly native hydrocarbons)

to be extracted, with the dilution prohibiting the detection of any trace constituents. It should be noted that this study, while utilizing a GCxGC-TOF-MS system, was still only able to discriminate approximately 75% of compounds based on their isomeric group.[86] In contrast, the HLB/PDMS TF-SPME device used in this work not only allowed for extraction of a wide range of analytes, it was also incredibly robust and reusable. The efficiency of the TF-SPME device was verified by its QC (methyl benzoate-d_8) to be acceptable for at least 200 extraction and desorption cycles.

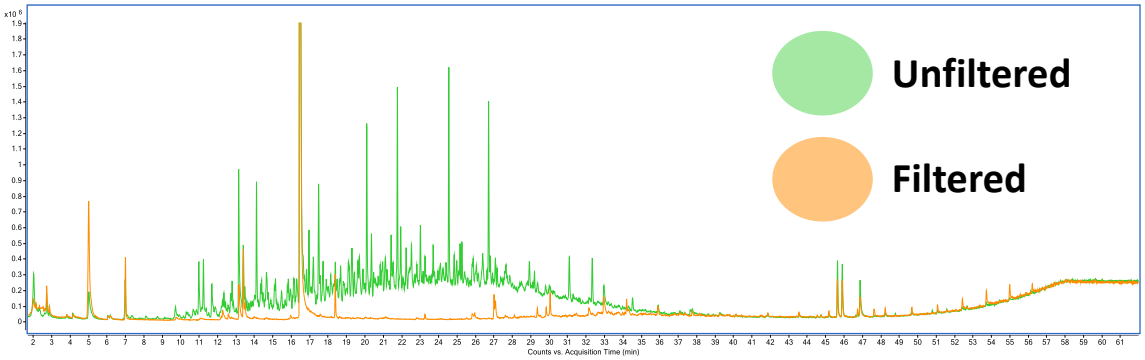

Figure 3-7 Comparison of chromatograms obtained for unfiltered and filtered PW 1 sample.

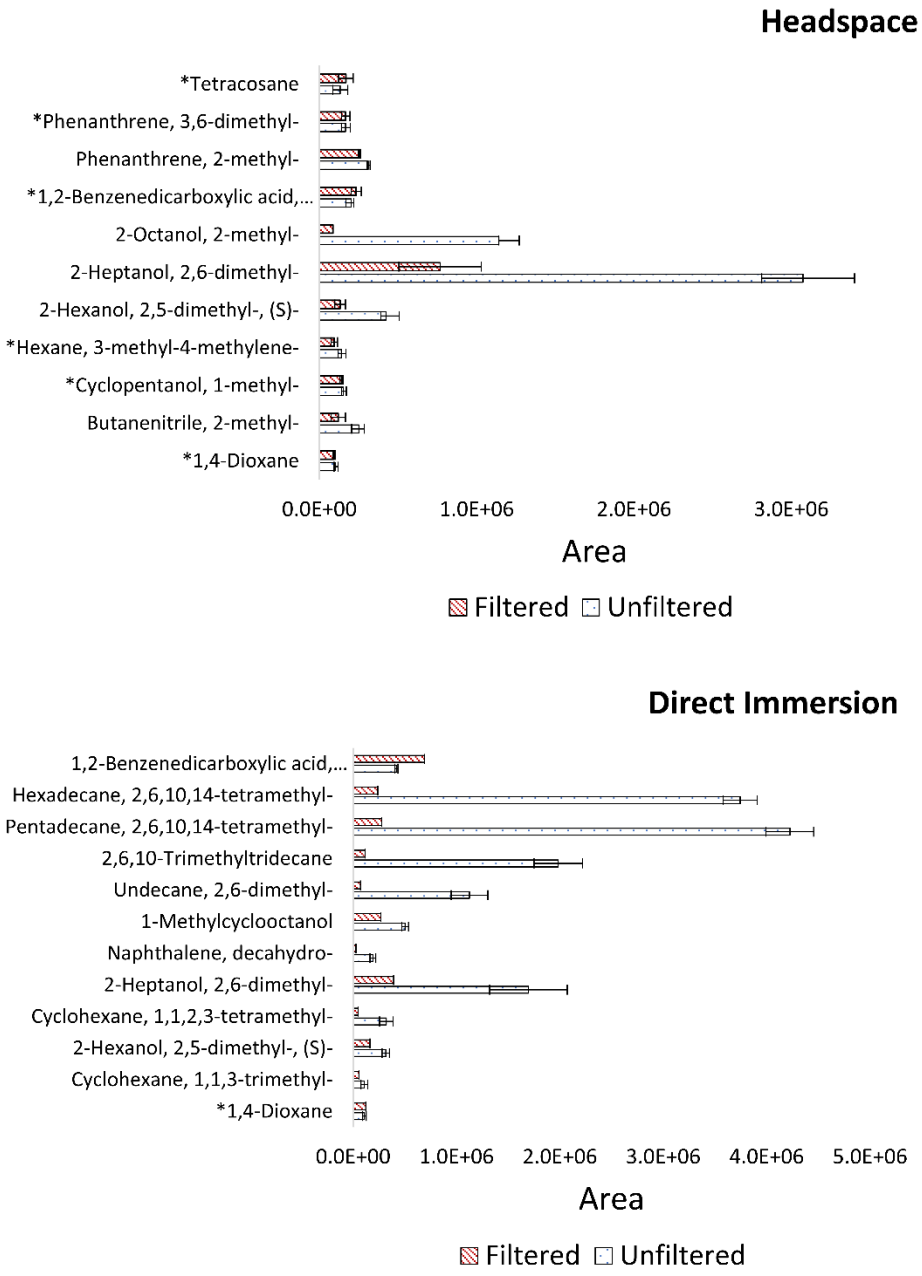

Figure 3-8 Effect of filtering on responses of all conserved analytes for headspace and direct immersion extraction. For compounds marked with (*), t-test analysis showed no significant difference between the response obtained for filtered and unfiltered samples.

3.4 Conclusions

This work demonstrates the critical need for the proper development of sample preparation technologies for the analysis of complex environmental matrices. PW is considered one of the most complex environmental matrices known. The broad range of compounds able to be extracted by HLB, along with the convenient geometry and workflow of TF-SPME, was proven to allow comprehensive and convenient extraction of PW with minimal loss of analyte compared to other methods. This method allows a large reduction of solvent, especially in comparison to other reports using large amounts of solvent to dilute PW.[83,88,89] In spite of the hypersaline, oily and corrosive properties of PW, the HLB TF-SPME device proved to be robust throughout many extractions, retaining its extraction efficiency throughout the entire study. In efforts to meet the goals outlined by various agencies[72,78,79], future efforts should focus on the coupling of comprehensive sampling techniques to more extensive instrumentation such as GCxGC hyphenated to high-resolution mass spectrometry, a strategy already being exploited for oil analysis[106] and a handful of PW reports.[86,89] While liquid chromatography (LC) has been utilized for the analysis of PW[85,107], there is, however, no reports at this time for the analysis of PW using 2D LC hyphenated to MS. These technologies enable more confident and comprehensive compound identification compared to the ones used in this study; however, without proper sample preparation, the results may be unrepresentative. Furthermore, these methods could also be adapted for the analysis of similar waste-streams, such as FW and landfill leachate.

Acknowledgements

The authors thank the University of Toledo for funding and supporting this work. The authors are also grateful to GERSTEL Inc. USA, in particular to Dr. Robert Collins for enabling the use of Gerstel TDU unit in our laboratory, to Dr. John Stuff for the useful scientific discussions and for providing the TF-SPME devices used in this work, and to Daniel Gatch for the expert technical support with the MPS autosampler and the TDU unit. Kevin A. Schug and Tiffany Liden would like to thank industrial collaborators from UT-Arlington CLEAR for providing samples and background information.

.

Chapter 4

Unraveling the Complex Composition of Produced Water by Specialized Extraction Methodologies

Adapted from a paper published in *Environmental Science and Technology*[108]

Ronald V. Emmons, Govind Sharma Shyam Sunder, Tiffany Liden, Kevin A. Schug, Timnit Yosef Asfaha, Joseph G. Lawrence, Jon R. Kirchhoff, Emanuela Gionfriddo

Abstract

Produced water (PW), a waste byproduct of oil and gas extraction, is a complex mixture containing numerous organic solubles and elemental species; these originate from the injected hydraulic fracturing solution and the geological formation. PW has been shown to contain petroleum distillates, polycyclic aromatic hydrocarbons (PAHs), and organic fracturing additives, along with dissolved salts, heavy metals, and naturally-occurring radioactive materials (NORMs). Identification of these compounds is critical to develop future reuse and disposal protocols to minimize environmental contamination and potential health risks. In this study, versatile extraction methodologies were investigated for the untargeted analysis of PW. Thin-film solid-phase microextraction (TF-SPME) with hydrophilic-lipophilic balance particles (HLB) was utilized for the extraction of organic

[108]Reprinted from Environmental Science and Technology, 2022, 56, 4. Copyright © American Chemical Society.

solubles from eight PW samples from the Permian Basin and Eagle Ford formation in Texas. Gas chromatography – mass spectrometry (GC-MS) analysis found a total of 266 different organic constituents including 1,4-dioxane, atrazine, pyridine, PAHs, and substituted alkyl chained hydrocarbons. The elemental composition of PW was evaluated using dispersive solid-phase extraction (D-SPE) followed by inductively coupled plasma – mass spectrometry (ICP-MS), utilizing a new coordinating sorbent, poly(pyrrole-1-carboxylic acid). ICP-MS analysis confirmed the presence of 29 elements including major (Mg, Mn, Zn, Se, Ag, Ba) and trace rare earth elements, as well as hazardous metals, such as Cr, Cd, Pb, and U. Utilizing chemometric analysis, both approaches facilitated the discrimination of each PW sample based on their geochemical origin with a prediction accuracy above 90% using partial least squares-discriminant analysis (PLS-DA), paving the way for PW origin tracing in the environment.

4.1 Introduction

Unconventional oil and gas production has become a major global energy resource as the technology behind hydraulic fracturing matures. However, this rapid growth has produced large volumes of wastewater associated with drilling operations.[109] These operations are often performed by the injection of treated water into the subsurface that contains various publicly undisclosed additives to assist in the drilling process.[70] Additives include surfactants, biocides, petroleum distillates, gel breakers, and various types of acids.[71,104,110] The injected water mixes with groundwater and then resurfaces as waste byproduct containing contaminants both from the drilling site and the additives used. The wastewater is described as either flowback water (FW), the initial waste produced in the

first several weeks of the well, or produced water (PW), the waste produced after FW.[73,111,112] Because PW contains a larger fraction of subsurface water and endogenous constituents unique to the drilling site compared to FW[113], its composition has a high degree of salinity with various inorganic anions and cations, ranging from heavy metals to radioactive species as well as large amounts of dissolved organic matter (DOM).[114] In addition, PW also contains various oils, suspended solids (e.g., silts, sands, precipitated solids), and biological species.[115,116]

From an environmental and human health perspective, many contaminants present in PW are potentially toxic, carcinogenic[112,117] and can act as endocrine disruptors[104,118]. Moreover, PW has also been reported to potentially result in the contamination of nearby water supplies.[119–124] Several reports have suggested that the primary goal of PW research is to understand the environmental implications of reusing or disposing PW, necessitating the identification of hazardous constituents and the associated risks.[78,80,109] Information on the specific constituents of PW is critical for regulatory compliance, understanding environmental impacts, and for the development of proper disposal or recycling applications.[73,125] This aim has been accomplished in part by 1) development of selective screening methodologies for suspected contaminants[126,127] and 2) measurement of total dissolved solids (TDS) and associated alkali earth metal content found in PW.[114] However, limited research has been performed on the combined characterization of organic solubles and the elemental composition due to the complexity of the matrix, which poses significant challenges for analysis.[84,104,110]

Analysis of organic solubles often uses gas chromatography-mass spectrometry (GC-MS).[104,107,113] Time of flight (GCxGC-TOF-MS) is commonly used, as is

conventional single quadrupole mass spectrometric analysis.[69,114,128,129] In 2016, Hoelzer et al. characterized FW and PW utilizing GCxGC-TOF-MS, demonstrating the presence of various chemical classes such as n-alkanes, aromatics, alcohols, and acids.[29] High resolution mass spectrometry (HRMS) has also been widely used in the characterization of hydrocarbons and halogenated compounds found in these wastes.[89,114,130] The advantage of mass spectrometry is it allows structural elucidation of compounds and untargeted analysis.[114] However, these techniques can be sensitive to matrix effects and interferences found in complex matrices such as PW. While electron impact (EI) GC-MS is not as sensitive to matrix effects as, for example, electrospray ionization (ESI) liquid chromatography–mass spectrometry (LC-MS),[85,131–133] it is still critical that appropriate sample preparation steps are utilized to better capture the entire chemical profile and ensure reliable and reproducible results.

Prior attempts to analyze organic solubles in PW have required sample filtration to remove insoluble particulates prior to further sample preparation.[134] Methods for sample preparation commonly used are liquid-liquid extraction (LLE)[135], dilute-and-shoot[83] and solid phase extraction (SPE)[114]. Several reports demonstrated the importance to include an optimal pre-concentration step in the analytical method. For example, SPE with hydrophilic-lipophilic balance (HLB) particles has been shown to be suitable for the trace determination of target additives and to desalt samples prior to analysis with an initial filtration step as SPE is a flow-through technique.[71,118,127,136] Bulk sampling techniques, such as thin film solid phase microextraction (TF-SPME), have recently been demonstrated to permit extraction of PW without prior filtration or dilution.[12,15] Our laboratory has shown that removing the filtration step is critical as many of the organic solubles in PW are

associated with insoluble material and lost in the filtration process.[69] In that work, HLB/polydimethylsiloxane (PDMS) TF-SPME was effectively used to pre-concentrate a wide range of organic solubles from the bulk sample without manipulating the sample.[69] Almaraz et al.[126] and Silva et al.[137] also corroborated that other geometries of SPME can be used for PW analysis. A more comprehensive characterization of organic solubles in PW is thus possible.

In addition to the presence of complex organic solubles, PW also contains a wide range of dissolved inorganic compounds including cations, anions, heavy metals, and radioactive elements. Cations such as Na^+, K^+, Ca^{2+}, Mg^{2+}, Ba^{2+}, Fe^{2+}, and anions such as Cl^-, SO_4^{2-}, CO_3^{2-}, and HCO_3^-, are often found in PW and are known to affect both salinity and scale potential [138]. Salinity of PW is mainly due to the presence of dissolved Na and Cl, while Ca, Mg and K only have a minor contribution.[138] In 2002, Neff et al. reviewed PW samples from different parts of the world and found that the concentrations of metals such as Ba, Fe, Mn, Hg and Zn in PW were about 10^2-10^3 times the amount found in surrounding seawater.[139] Hg, Pb and metalloids (e.g., As) also have been reported in different concentrations depending on location and age of the well.[138] Most studies on the elemental characterization of PW have focused on Mg, Ba, Cd, Cr, Pb, Hg, Mn, Ni, Fe, Se and Zn.[140–148] Fewer reports have investigated the presence of rare earth (REEs) and radioactive elements.[149–154] Comprehensive analysis of both major and trace elements are limited due to the complex nature of PW samples and the wide range of concentrations of the elemental species present.[113,114,155]

A majority of the studies investigating the elemental composition of PW have utilized techniques such as precipitation, co-precipitation or preconcentration by water

evaporation.[143,146–149,156,157] These methods often lead to precipitation of salts or a solution with a high content of TDS, leading to spectral interferences or blockage of the sampling cone and nebulizer in inductively coupled plasma mass spectrometry (ICP-MS) with salt deposits, which require additional time-consuming steps to remove potential interferences.[156–161] Moreover, higher amounts of common ions (Na, Mg, and Fe), TDS, and hydrocarbons further complicate the evaluation of trace levels of less common elements, leading to the potential of analyte masking effects. Therefore, to address these challenges, provide higher sensitivity, and remove potential interfering species, a preconcentration step is often effective.[162] Several studies have utilized solid-phase extraction (SPE) for preconcentration and recovery prior to trace level elemental analysis in complex sample matrices.[162–168] Recently, our collaborators developed a novel sorbent material (poly(pyrrole-1-carboxylic acid); PPy-CO_2) for the preconcentration and determination of REEs, Th, and heavy metals (Cr, Fe, Cd, and Pb) using ultrasound assisted dispersive solid-phase extraction (D-SPE) followed by ICP-MS.[169,170] The selectivity of PPy-CO_2 for these elements is ideal for extracting trace level metals from complex matrices containing alkali and alkaline earths.

In this study, PW samples obtained from various sources (i.e., Permian Basin and Eagle Ford formation in Texas) were characterized for organic solubles using TF-SPME-GC-MS and for elemental species using PPy-CO_2 for the extraction and preconcentration of trace level metals by ultrasound assisted D-SPE, followed by ICP-MS analysis. In consideration of the challenges associated with the sample preparation of PW, the goals of this study were to characterize PW using complementary untargeted methods and to

evaluate the efficacy of both organic and inorganic untargeted profiling to discriminate different PW sources geographically using chemometric tools.

4.2 Experimental

4.2.1 Sample Collection

PW samples were sourced from saltwater disposal wells located in the Permian Basin and the Eagle Ford formation in Texas and stored in opaque high-density polyethylene (HDPE) bottles with no headspace before analysis. A total of eight samples from different locations were collected and stored at 4 °C without treatment or additives present, labeled PW1-8. However, PW5 was filtered and treated onsite by undisclosed methods from the same waste-stream as PW4. As such, PW5 was not included in subsequent statistical modelling.

4.2.2 Organic Solubles Analysis

For the analysis of organic solubles, the HLB/PDMS thin film solid phase microextraction (TF-SPME) devices used in this study were kindly provided by Gerstel US (Gerstel, Inc., Linthicum, MD, USA). A C7-C30 alkane mixture was purchased from Sigma Aldrich (St. Louis, MO, USA). Methyl benzoate-*d*8 was purchased from CDN isotopes (Pointe-Claire, Quebec, Canada). An Agilent 7890 B gas chromatograph coupled to a 5977 B single quadrupole mass spectrometer (Agilent Technologies, Santa Clara, CA, USA) was used for volatile and semi-volatile identification. The gas chromatograph was outfitted with a Rtx-5MS capillary column (30 m x 0.25 mm x 0.25 µm) and a 10 m Integra-Guard column from Restek (Bellefonte, PA, USA). Ultrapure helium (99.999%) was used as the carrier gas in all experiments. A thermal desorption unit (Gerstel, Linthicum, MD,

USA) and a cooled injection system (CIS 4; Gerstel, Linthicum, MD, USA) were used for sample introduction. Sample extraction and subsequent analysis were both previously described by our previously described work in Chapter 3.[69] In short, a HLB/PDMS TF-SPME device was exposed to the internal standard for 5 min prior to extraction of the untreated PW sample by direct immersion (9 mL of sample) or headspace (2 mL of sample) mode for 15 min. A 3 s rinsing step in water was applied afterward to remove particulates from the TF-SPME device. The total sample preparation time was approximately 20 min. The sample was then thermally desorbed and analyzed by GC-MS using the aforementioned protocol.

Data processing utilized Unknowns Analysis (Agilent Technologies, Santa Clara, CA, USA) for deconvolution and integration with extraction windows of 0.3 and 0.7 m/z delta [69]. Deconvoluted mass spectra were then referenced to the NIST 2017 library in conjunction with retention index (RI) matching. RI values were calculated by the analysis of a standard C7-C30 alkane mixture. Retention time windows were based on incremental windows of 25, 50, 100 and 200 s. A Gaussian penalty function of 6 s was also used, allowing a maximum 50-point penalty to the overall match factor from retention index alone. In this way, the match factor was calculated using both mass spectra and retention index equally. To ensure reproducibility and accuracy of the characterized compounds, only compounds with a composite match score equal to or greater than 80 and found in at least 2 of the 3 replicates were further processed.

4.2.3 Inorganic Analysis

For the analysis of inorganic elements, PPy-CO_2 was synthesized according to our collaborators' previous reports.[169] The extraction protocol followed the procedure described by Rohanifar et al.[171] and used the optimized conditions for preconcentration and determination of rare-earth elements (REEs) with poly(pyrrole-1-carboxylic acid (PPy-CO_2) [169]. All samples were analyzed for elemental composition by a Thermo Scientific XSeries 2 inductively coupled plasma mass spectrometer (San Jose, CA) equipped with a slurry nebulizer. Further details on the sample preparation of PW samples for elemental analysis and subsequent analysis are outlined in the published manuscript of this chapter.[108]

4.2.4 Data Processing and Statistical Analysis

The data sets for organic solubles and inorganics were first compiled in Microsoft Excel (2013). Each sample's data was comprised of the characterized molecular or elemental species along with the response (organic solubles) or calculated concentration (inorganics). In the case of organic solubles, only the data obtained from the direct immersion extractions were used as headspace extractions proved to not be statistically significant for sample discrimination (an example of these data used for discrimination can be found in Appendix B, Figure B-1). For inorganics, elemental concentrations for the selected metals were determined from ICP-MS analysis of the filtrate and desorption solution and were summed to represent the bulk PW sample concentrations of the elements. Statistical analysis was performed using Metaboanalyst.[172] Data treatments were optimized by performing principal components analysis (PCA) and partial least squares-discriminant analysis (PLS-DA) on each data set with different data parameters. The optimal parameters giving the greatest separation during data visualization and the best agreement between

PCA and PLS-DA were applied. Normalization of values based on their median, log transformation, and range scaling were found to yield the best results with no data filtering. The combination of data sets was first visualized using PCA and then PLS-DA with no class-ordering. Cross validation was performed using the leave-one-out cross-validation (LOOCV) method[173], showing the method was capable of predicting the sample classifications at 7 components (Figure 4-1). Non-parametric analysis of variance (ANOVA) was performed with a cutoff of $p < 0.05$ using a Fisher's LSD post-hoc analysis.

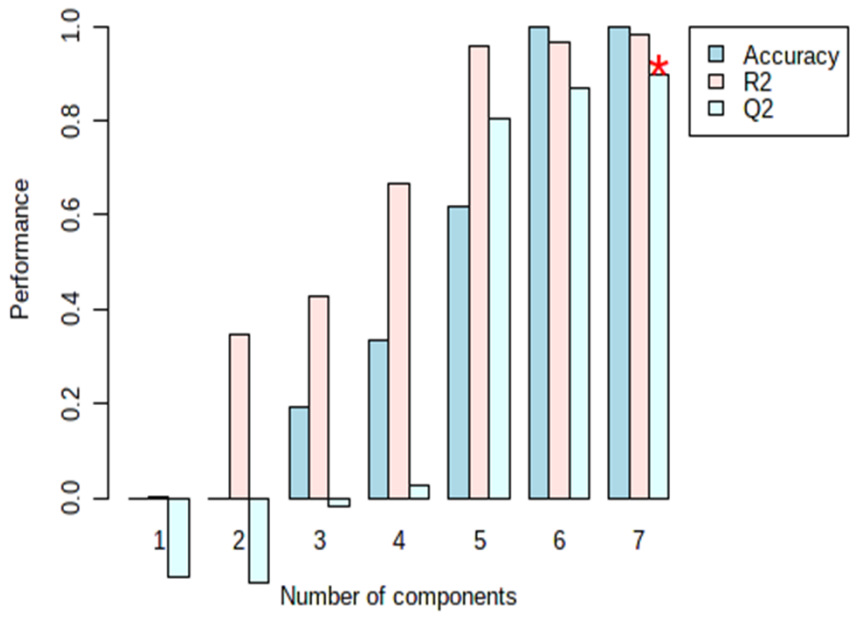

Figure 4-1 Cross validation using the leave-one-out cross-validation (LOOCV) method, demonstrating the need for 5+ components for proper sample discrimination.

4.3 Results and Discussion

4.3.1 Organic Solubles Characterization

HLB-based extraction phases were previously found to extract a wide range of compounds of differing physicochemical properties from hydraulic fracturing wastes, and therefore HLB/PDMS was used for the extraction of organic solubles in this study.[71,118,127] As the scope of this work was the untargeted screening of organics with minimal sample preparation, quantitation was not considered. A broad range of organic molecules was observed in the PW samples, in agreement with previous reports.[104,126,174] The combination of headspace and direct immersion extraction experiments provide complementary environmentally relevant data for PW samples.[69] In total, 266 organic constituents were characterized between all analyzed samples. However, statistically significant data were not obtained between PW samples when headspace extraction was included. This is possibly due to the wider range of compounds accessible using extraction by direct immersion, the headspace fraction not containing enough key compounds to discriminate PW sources. Thus, headspace data were not included in further data processing or discussion. A list of all organic solubles found to be statistically significant for PW source discrimination (84 compounds) is found in Table B.1 with relevant p-values, which demonstrate the discriminatory power of each analyte in the statistical model described in the chemometric analysis section in results and discussion.

Large amounts of n-alkanes and substituted hydrocarbons, and minimal amounts of smaller, more polar compounds were found in all samples. Organic composition was dominated by branched alkyl chained molecules, which were previously reported in high abundance and originating from both the shale formation and also added during hydraulic

stimulation.[130,134] Various aromatics and low-molecular weight polycyclic aromatic hydrocarbons (PAHs) were also found[103], which are environmental contaminants of concern by the World Health Organization.[175] More polar constituents, such as alcohols (e.g., 2-methyl-2-pentanol, 1-methyl-cyclopentanol) and ketones (e.g., cyclopentanone, 2-pentanone) were also detected in all samples. These classes of organics are often used as solvents or corrosion inhibitors.[110] Pyridine, a suspected manufacturing precursor to some of the additives used in hydraulic fracturing, was present in several of the samples (PW4, PW5 and PW7). The presence of pyridine or other basic N-containing molecules has been found to complicate the desulfurization and refinement of shale oil.[106,176] In addition, elemental S (octasulfur) was found in only one sample (PW3), indicating anoxia of its source environment. Other noteworthy molecules found in the PW samples were diiodo-methane (samples PW3 and PW7), a suspected biocide or biocide byproduct[89], and 1,4-dioxane (samples PW1 and PW2), a human carcinogen[90] that cannot be sufficiently removed by traditional reverse-osmosis water treatment.

4.3.2 Chemometric Analysis: Source Discrimination and Insights

Considering the significant amount of chemical information obtained by the untargeted extraction of both soluble organics and elemental species, statistical methods can shine light into the unique compounds found in each sample. This approach allows a more robust comparison between samples, resulting in the ability to discriminate PW samples based on their characterized components and to provide a better understanding of the correlation between the samples and their constituents. The classification methods used in this study were PCA and PLS-DA, which permit the user to classify and discriminate samples based on any recorded data such as the constituents characterized in PW. Prior

reports have utilized these same methods for the discrimination of food sources from different geographical origin, there also being a study utilizing PCA to investigate PW without PLS-DA.[177–179]

Both PCA and PLS-DA are multi-variate statistical evaluations. PCA is an unsupervised technique that models orthogonally the variation of the data set and principle components (PC), where PC represents the maximum amount of variance described in the model. Prior to classification or data visualization using either PCA or PLS-DA, data sets were normalized, scaled and transformed to yield reliable results. Combining data on both organic solubles and elemental species, PCA classification allowed separation with PC1 and PC2 explaining 31.8 % and 18.8 % of the data variance, respectively with a 3rd PC of 14.9 %. These same values were also true for PLS-DA. Furthermore, data sets were processed using PLS-DA, a supervised pattern recognition method that allows complementary results to PCA. This multivariate projection technique is ideal when the number of variables exceeds the amount of objects or samples, which is the case in this study.[180] Through maximizing the correlation between the independent and dependent variables, PLS-DA is able to apply weighting to these variations, the less informative or noisy variations being weighed less.[177] Thus, a classification scheme is made based on the dependent variables (e.g., PW source). Moreover, as the independent variables used in the model (e.g., organic composition, elemental composition) are weighted, the ability of individual organic solubles and elements to discriminate between different PW sources can be found. Due to the amount of variables far outweighing the amount of samples, it is observed in this study that PCA and PLS-DA have the same level of discrimination. This

meaning the between-group variance already was maximized in the unsupervised PCA model.

Visualized statistical discrimination is demonstrated in plots (Figure 4-2) with each axis representing the amount of variance explained in the model. Comparing the abundance of each characterized constituent found in the PW samples allowed the discrimination of PW sources and identification of the unique chemical features of each sample location. Each individual replicate can be found clustered with its respective sample grouping (Figure 4-2), indicating that PW samples were successfully discriminated based on their organic soluble and elemental composition. The greater the separation of each cluster from another in Figure 4-2, the bigger the difference in chemical composition between samples. For example, samples PW6 and PW8 are more similar in chemical composition compared to the other PW samples, indicating that either the subsurface chemistry or the hydraulic fracturing process was comparable between these two locations.

Some of the most significant constituents for discrimination are shown in Table 4.1 with their responses normalized to the highest response. Ag, octasulfur, and diiodo-methane are three of the most distinctive compounds in the eight samples. In this way, discrimination between PW drilling sites can be readily demonstrated using specific identifiers. As an example, pyridine allows PW2, PW4, and PW5 to be confidently discriminated from the rest of the drilling site samples. However, discrimination of PW between these three sources based on pyridine alone is not feasible. The inclusion of a second prominent identifier such as elemental Se allows further discrimination between these drilling sites. Not only does this allow the user to determine possible pollution sources, but it would also enable these data to better capture and characterize the important

geogenic information found in the drilled subsurface. Moreover, a one-way ANOVA was applied to better identify constituents of interest to discriminate the PW sources (Figure 4-3). A p value > 0.05 indicates no significant difference in a given analyte's concentration between samples, while a p value < 0.05 demonstrates the constituent is valuable for sample discrimination. In total, the classification model contained 116 constituents; 108 components were identified as significant, while only 8 were deemed insignificant. Tables of these components are found in Table B.1 (organic solubles) and Table B.2 (elements).

Sample PW4 and PW5 were independently compared to discern the effect of on-site filtration and treatment. Utilizing a two-sample t-test, it was demonstrated that out of 75 unique organic and elemental components found, 28 of them are significantly different before and after treatment (Figure 4-4). A wide range of organic solubles is removed in this treatment process, including n-alkanes and more polar analytes such as phenol and pyridine (Table 4.2). However, a significant number of organic solubles remain after filtration and treatment. Filtration and treatment had a smaller effect on the elemental composition between PW4 and PW5 (Table 4.3) with only five elements significantly reduced in the process (Ce, La, Ba, Ga and Mn). While there was only one treated sample in this study, results do indicate that on-site filtration and pretreatment were more effective for removing organic solubles than individual elements. This is in-line with the filtration results in previous studies, elemental species being able to flow freely through a syringe filter and certain organic solubles are unable to pass through.[69,169]

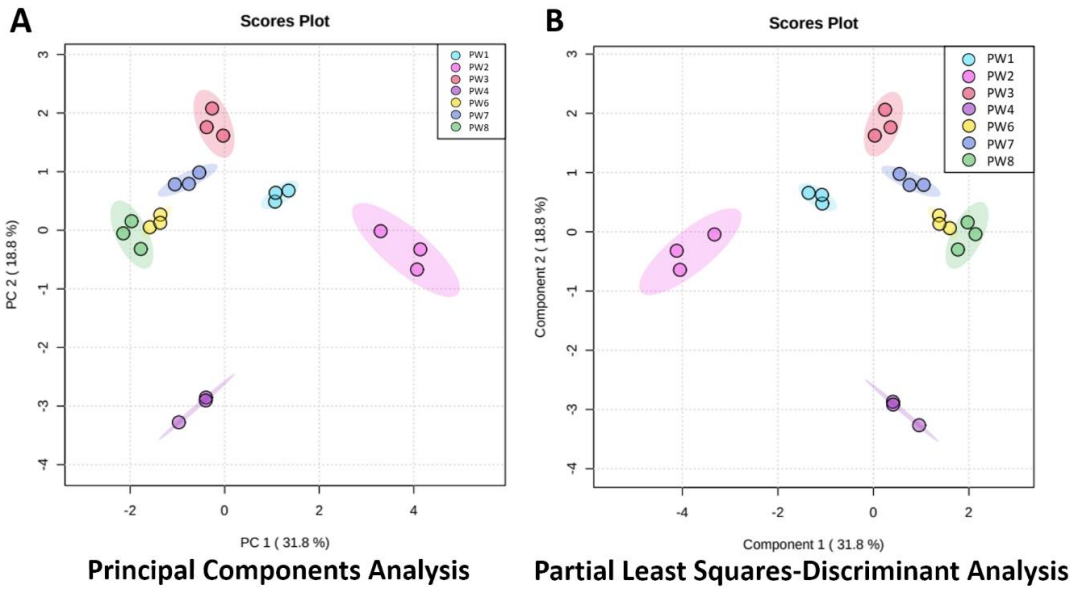

Figure 4-2 Score plots from a) PCA and b) PLS-DA combining data from GC-MS analysis (organic solubles) and ICP-MS analysis (elemental species).

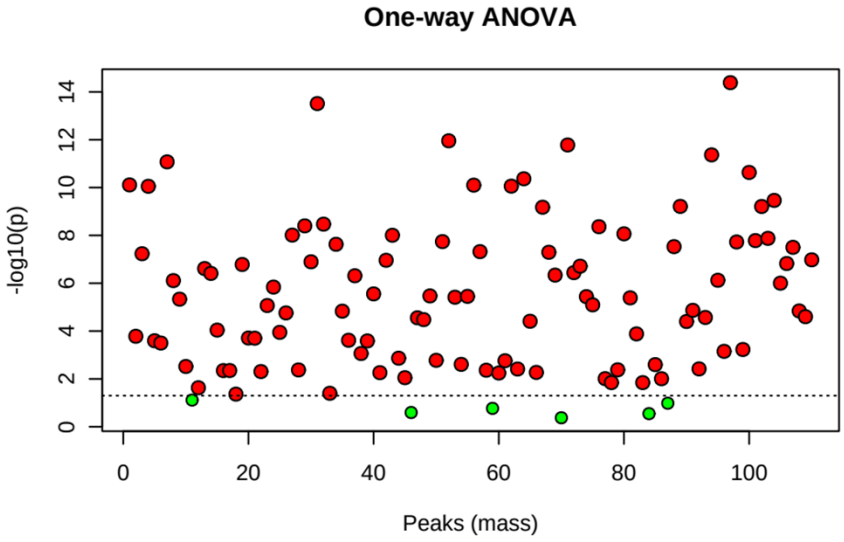

Figure 4-3 One-way ANOVA results illustrating that any constituent above 0.05 (in red) is significant in class discrimination.

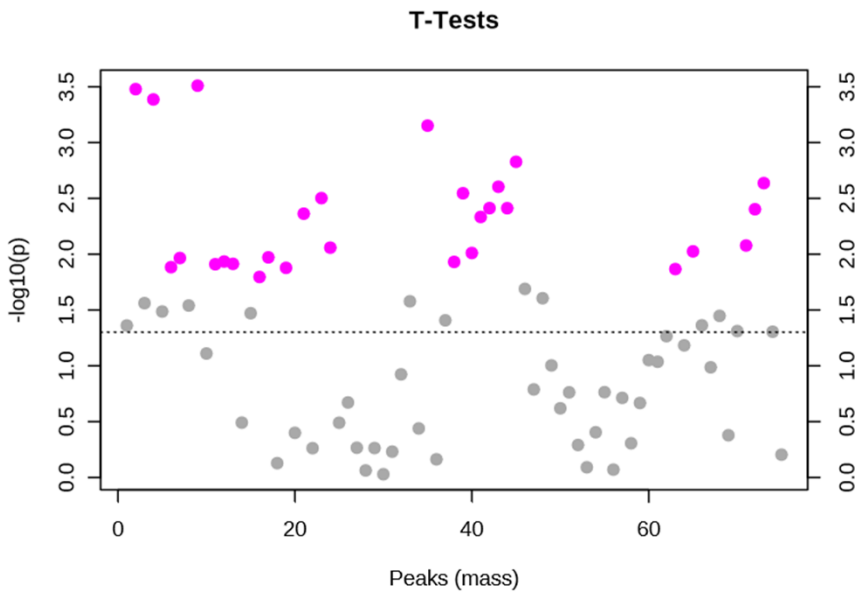

Figure 4-4 Results from a two-sample t-test between samples PW4 and PW5. Grey indicators represent constituents that are not affected significantly by the PW treatment, purple indicators representing constituents that are affected. p-value threshold based on False Discovery Rate (FDR) and not the raw p-value, reducing the chances of false positives.

Table 4.1 Relative response[α] of representative significant compounds from PLS-DA discrimination analysis for each analytical method.

Type	Name	PW1	PW2	PW3	PW4	PW5	PW6	PW7
TF-SPME-GC-MS	Pyridine	0	0.75	0	1	0.7	0	0
	2-Pentanone	0	0	0	1	0.8	0	0
	Diiodo-methane	0	0	1	0	0	0	0.07
	2-methyl-hexadecane	0	1	0	0.41	0	0	0
	Octasulfur	0	0	1	0	0	0	0
dSPE-ICP-MS	Mn	0	0	0.02	0.3	0.35	1	0.65
	La	0.09	0.12	0.19	0.05	0.10	0.09	1
	Se	1	0.99	0.95	0.08	0.33	0.92	0.93
	Cd	0	0	0.48	0.23	0.17	0	1
	Ag	0	0	0	0.96	0.99	1	1

[α]Responses are normalized: the value 1 corresponds to the highest response for that analyte among samples.

Table 4.2 Organic solubles removed in the sample filtration process between samples PW4 and PW5. The list contains compounds which demonstrate p-values ($p < 0.05$; $-\log(p) > 0.77$) obtained from a two-sample t-test, as these organic solubles are significantly removed in the filtration process.

Compound	-log(p)
Tridecane, 5-methyl-	3.51
2,2,4-Trimethyl-1,3-pentanediol diisobutyrate	3.48
Heptacosane	3.39
2,4-Di-tert-butylphenol	3.15
Nonadecane, 4-methyl-	2.83
Octadecane, 3-methyl-	2.60
Cyclohexane, 1,1'-methylenebis-	2.55
Decane, 2-methyl-	2.50
Nonane	2.41
1,2-Benzenedicarboxylic acid, bis(2-methylpropyl) ester	2.41
Heptane, 2,3,4-trimethyl-	2.36
Hexadecane, 2-methyl-	2.33
Cyclohexane, hexyl-	2.06
3,5-di-tert-Butyl-4-hydroxybenzaldehyde	2.01
Benzyl chloride	1.97
Tetracosane	1.97
Octane, 3,6-dimethyl-	1.93
Cyclohexane, 20butyl-1,1,3-trimethyl-	1.93
Pyridine	1.91
Phenol, 3-methyl-	1.91
Phenol	1.88
1-Hexanol, 2-ethyl-	1.88
Phenol, 3,4-dimethyl-	1.80

Table 4.3 Elements removed during the filtration process between samples PW4 and PW5. Metals listed were determined to be statistically significant ($p < 0.05$; $-\log(p) > 0.77$) by use of a two-sample t-test.

Element	-log(p)
Ce	2.64
La	2.4
Ba	2.08
Ga	2.03
Mn	1.87

4.4 Conclusions

The extraction methods outlined in this study represent an innovative strategy for the evaluation of the composition of PW. Sample characterization was achieved with minimal pretreatment and enhanced pre-concentration of trace constituents. Exploiting the unique properties of microextraction methodology and sorbent chemistry allowed the challenges posed by the complex composition of PW to be minimized. The characterization of organic solubles revealed a wide-range of compounds (e.g., octasulfur, n-alkanes, atrazine, diiodomethane). Many of these compounds are known to be harmful to human health and can cause deleterious effects to organisms and the surrounding environment, such as 1,4-dioxane.[181] Moreover, the elemental composition of PW exhibited a wide range of transition metals and REEs, both being unlikely additives to the hydraulic fracturing process.[182] Therefore, it is reasonable that these elements are indicative of the drilled geologic formation or well type.[117,155] Furthermore, hazardous elements such as Se were present at high concentrations; there were also trace amounts of Cr, Pb, Cd, and U. The discovery of these potentially hazardous materials in PW suggests greater monitoring and remediation efforts are needed.

Chemometric analysis of the characterized constituents permitted chemical fingerprinting of each sample location and an investigation of the similarities and statistically significant differences between well-site locations. As previous reports have suggested[129], the statistical discrimination of the contents of each sample not only can shed insight into the processes taking place during hydraulic fracturing, but also the nature of the geologic formation of each well site. While there are certainly anthropogenic contaminants to consider in PW, much of the chemical data represents geogenic chemical

species, both organic and elemental, which could further the understanding of the subsurface features.[104,129,183,184] Furthermore, the successful characterization and statistical discrimination of PW samples demonstrated by this study supports the use and capability of more accessible instrumentation (i.e., single quadrupole GC-MS) in the analysis of this complex matrix compared to more expensive workflows involving high resolution mass spectrometry (HRMS). To move forward, comprehensive characterization of PW is essential for proper reuse or disposal since many of the identified species are listed as chemicals of significant human health concern by the World Health Organization (WHO). In future work, these extraction methodologies if combined with chromatographic strategies and HRMS hold significant promise for even further detailed analysis of the complex composition of PW.

Acknowledgements

The authors would like to thank The University of Toledo for funding and supporting this project. We would also like to thank GERSTEL Inc. USA and Dr. Robert Collins for enabling the use of the Gerstel TDU in this work, Daniel Gatch for his support with the Gerstel TDU and MPS autosampler, and Dr. John Stuff for providing TF-SPME devices and helpful scientific discussions. We acknowledge the National Science Foundation for providing funds for the scanning electron microscope (CHE-0840474) and renovation of Bowman-Oddy Laboratory to create the Center for Biosphere Restoration and Research (ARI-0963345). Kevin A. Schug and Tiffany Liden would like to thank industrial collaborators from UT Arlington CLEAR for providing samples and background information.

Chapter 5

Minimizing Transient Microenvironment-Associated Variability for Analysis of Environmental Anthropogenic Contaminants via Ambient Ionization

Adapted from a paper published in *Science of the Total Environment*[185]

Ronald V. Emmons, Emanuela Gionfriddo

Abstract

The rapid and quantitative analysis of anthropogenic contaminants in environmental matrices is crucial for regulatory testing and to elucidate the environmental fate of these pollutants. Direct ambient mass spectrometry (AMS) methodologies significantly increase sample throughput, can be adapted for onsite analysis and are often regarded as semi-quantitative by most developed protocols. One of the limitations of AMS, especially for onsite analysis applications, is the irreproducibility of the measurements related to the occurrence of transient microenvironments (TME) and variable background interferences. In this work, we report an effective strategy to minimize these effects by hyphenating, for the first time, arrow solid phase microextraction (Arrow-SPME) to mass spectrometry via a thermal desorption unit (TDU) and Direct Analysis in Real Time

[185]Reprinted from Science of the Total Environment, 2021, 775, 145789. Copyright © Elsevier.

(DART) source.

The developed method was optimized for extracting and analyzing pesticides and pharmaceuticals from surface water. It was demonstrated that the hyphenation of the SPME and TDU-DART resulted in reduced background contamination, indicating the suitability of the method for onsite analysis even in variable and non-ideal environments. Model analytes were quantified in the low µg/L range with a total analysis time of less than 5 min, linear dynamic ranges (LDR), and interday reproducibility for most compounds being 2.5 – 500 µg/L and 10 %, respectively. The developed approach provides an excellent analytical tool that can be applied for the onsite high-throughput analysis of water samples as well as air and aerosols. Considering the tunability of our extraction process, time-resolved environmental monitoring can be achieved onsite within minutes.

5.1 Introduction

Environmental monitoring has long been dependent on rapid pre-screening methods prior to confirmation by quantitative analytical approaches, which involve both separation (e.g., liquid chromatography, LC; gas chromatography, GC; capillary electrophoresis, CE) and detection (e.g., mass spectrometry, MS; ultraviolet detection, UV).[186] Pre-screening effectively minimizes the number of samples that are ultimately evaluated by the more time-consuming protocols used to establish compliance, these techniques often being a form of bio-assay (as is the case in ELISA).[187] In terms of portability, there have been great strides in performing pre-screening analysis onsite, reducing the cost of sample transport and ultimately minimizing the amount of time it takes for a sample to be affirmed as compliant or not. Recent efforts have aimed to develop

smartphone-based instruments, optical or electrochemical[186], that while both fast and convenient, present limitations in detecting food and environmental contaminants at regulated levels.[188] Through the miniaturization and simplification of more robust instrumentation such as mass spectrometry, onsite analyses which were once only thought to be suitable for pre-screening have gained the potential to become confirmatory.[189,190]

A great complement to the development of portable mass spectrometry has been demonstrated by the application of ambient mass spectrometry (AMS) in environmental, food and bio-clinical contexts.[48,191–193] AMS not only reduces the footprint of the instrument but it allows direct coupling of samples to MS with minimal or no sample pretreatment, increasing throughput far higher than techniques that require separation or extensive sample preparation. Since its inception, there have been several ambient ionization methods developed, including direct analysis in real time (DART)[49], desorption electrospray ionization (DESI)[194] and dielectric barrier discharge ionization (DBDI)[195,196]. In the case of DART, a stream of heated helium is electrically discharged in an open-air environment, permitting the ionization of compounds from a variety of matrices be they in a solid, liquid or gas form. This allows near-instantaneous analysis of both target and untargeted compounds with minimal or, in some cases, no sample preparation. Typically, DART analysis are viewed as qualitative or semi-quantitative, as most applications have demonstrated high variability in signal intensities, mitigated by the use of autosamplers or internal standard correction.[197]

Much of the signal variability of DART and AMS, in general, is commonly attributed to the positioning of the source and the heterogeneity of the sample. Plasma-based AMS sources in particular have been shown to be susceptible to matrix effects.[198] It

has been demonstrated that variances in both the matrix composition and the environment surrounding the DART source can produce large variations in signal intensity and in-source fragmentation in DART-MS, environmental humidity playing a large role in these phenomena.[199,200] Furthermore, a transient microenvironment mechanism (TME) has been proposed for DART-MS, demonstrating that the inclusion of matrix constituents or environmental contamination can potentially cause these compounds to be directly ionized instead of target analytes.[201] As the then ionized matrix/environmental constituents would be responsible for the ionization of target analytes, it is reasonable to suggest that the variability of these two sources of contamination must be reduced for proper quantitation and reasonable interday reproducibility of a method, especially for onsite applications where environmental contamination is variable.

As the main advantages of AMS techniques are their simplicity and incredibly high throughput, any associated sample preparation protocol must also meet these same demands. The combination of sampling, sample clean-up and pre-concentration SPME provides[193,202,203] makes it a suitable candidate for AMS hyphenation, along with its geometry that permits direct introduction of the sampling device to AMS[98,204,205]. These qualities are especially critical for AMS techniques, as the analysis of a bulk sample without any sample pretreatment suffers from matrix effects and is often challenged by the heterogeneity of the sample. For these reasons, SPME is an ideal candidate for direct coupling to DART-MS, proven already in a variety of applications.[193,206] To date, the majority of SPME-DART-MS analysis has been performed entirely in the open-air environment; consequently, allowing airborne interferences and potential loss of analyte to the sample's surroundings. There have been recent developments in enclosed DART-MS

desorption using SPME or other sampling devices, these methods either being qualitative or evaluated for their quantitative capabilities using a single analyte.[206–208]

To enable more accurate and rugged analysis of pesticides and pharmaceuticals in environmental matrices, this work modified a thermal desorption unit (TDU) to enable easy introduction for SPME-Arrow, permitting convenient enclosed desorption and ionization using a DART source. SPME-Arrow, a geometry of SPME with enhanced mechanical robustness and a larger volume of extraction phase than conventional fiber SPME[209,210], allows higher analyte capacity[211]. With its introduction to this modified interface, exhaustive desorption of all analyte was achieved quickly and performed in a partially-closed system, which allowed a drastic reduction in background signal and minimized variability related to non-ideal or variable environments. Representative compounds were selected from different classes of drugs and pesticides commonly found to contaminate environmental waters, to ascertain the method's real-world onsite capabilities for targeted matrices. Quantitation was performed utilizing sonication-assisted extraction to assess the method's sensitivity, reproducibility and linear dynamic range (LDR). Sonication-assisted extraction has previously been utilized for SPME geometries such as rod and hollow fiber SPME, but has not yet been tested for SPME-Arrow.[202,212] River water was screened for the model analytes. The observed reduced background and rapid analysis enabled by the developed method could be exploited for the onsite analysis of environmental contamination sites, providing further elucidation on contaminant transport and an ideal solution for unstable contaminants analysis.

5.2 Experimental

5.2.1 Materials

The SPME-Arrow devices used in this study, 100 µm coating thickness 20 mm long polydimethylsiloxane (PDMS), 250 µm coating thickness 20 mm long PDMS, 100 µm coating thickness 5 mm long PDMS, 120 µm coating thickness 20 mm long divinylbenzene/carbon wide-range/polydimethylsiloxane (DVB/CWR/PDMS) and Topaz 1.8 mm ID Straight/SPME inlet liner were kindly provided by Restek Corporation (Bellefonte, PA, USA) along with the associated arrow manual SPME holder. Sonication was performed using an ultrasonic cleaner (Electromation Components Corporation, Hauppauge, NY). All analyses were performed on a DART-SVP (IonSense, Saugus, MA, USA) with a modified DART-SVP thermal desorption module (IonSense, Saugus, MA, USA), all coupled to an LTQ XL ion trap MS (Thermo Scientific, San Jose, CA, USA). Methadone, morphine, amphetamine, diazepam, methadone-D_3, amphetamine-D_{11}, diphenylamine and 2-phenylphenol were purchased from Sigma Aldrich (St. Louis, MO, USA). Diphenylamine-d_{10} was purchased from Toronto Research Chemicals (Toronto, ON, Canada). Cocaine hydrochloride was purchased from Supelco (Bellefonte, PA, USA). River water was collected from the surface of Ottawa River located in Toledo, Ohio on the day of analysis.

5.2.2 Procedure and Parameters

Initial TDU-DART optimization was performed with a +350 V electric grid, the MS scanning from 100-600 m/z with a 10 ms maximum injection time and 1 microscan, the scan speed set at “normal” settings. Optimal conditions used were a mass range of 100 – 550 m/z, 1 microscan and a maximum injection time of 10 ms. Confirmatory MS^2

experiments were performed with a maximum injection time of 20 ms. For quantitation, ions selected for each analyte were: methadone, 310.2 m/z; diphenylamine, 170.1 m/z; 2-phenylphenol, 171.1 m/z; diazepam, 285.1 m/z; dimethachlor, 256.0 m/z; amphetamine, 136.1 m/z; morphine, 286.1 m/z; and cocaine, 304.3 m/z. Each ion was monitored with a mass window of 1 m/z. The optimal conditions for TDU-DART coupled with a DVB/CWR/PDMS SPME arrow were found to be 300 °C TDU, 450 °C heated plasma, +50 V electric grid, Vapur interface pump set to 2 and a TDU position being set to 0. Extraction conditions were found to be optimal at 3 min using sonication for agitation, desorption taking place for only 30 s. The response in this 30 s interval was then integrated using Xcalibur software (Thermo Scientific, San Jose, CA, USA) for each model analyte, from baseline to baseline.

5.2.3 Apparatus Development and Experimental Conditions

Model analytes selected for the study are presented in Table 5.1, each chosen for their disparity in physicochemical properties and relevance to anthropogenic environmental contamination. As shown in Figure 5-1, sample introduction was performed by a modification of the commercial TDU-DART interface. To facilitate this, a Topaz liner (Restek Corporation,Bellefonte, PA, USA) was cut to a total length of 32 mm to keep the SPME arrow device stable during exposure to the TDU and minimize the introduction of interferences from the surrounding environment. This glass liner was then adhered to the inside of a ¼” brass Swagelok nut (Swagelok Company, Solon, OH), the nut then being screwed into a native TDU port for analysis. Sample-to-sample signal irreproducibility is often considered high for even automated sample introduction to DART-MS, making reproducible manual introduction of the sampling device even more critical. To provide

further ease-of-use in the handling of samples, small magnetic washers were glued to the nut and the end of the SPME-Arrow holder to allow the user to operate the apparatus hands-free (Figure 5-1). A large fabric washer was adhered to the nut as well to keep the two magnets separated, ensuring a smooth withdrawal of the SPME arrow device from the TDU after desorption.

Optimization of apparatus positioning, electricgrid voltage and the Vapur interface pump were performed by spiking a 100 µm PDMS arrow with 1 µL of a 10 mg/L methanol solution of model analytes and desorbing for 30 s. Spiking was performed by dispensing 1 µL of the methanol solution with a micro-syringe along the surface of the SPME device and allowing enough time for the solvent to evaporate and the analytes being sorbed into the extraction phase. Apparatus positioning was optimized with respect to both the positioning of the TDU-DART apparatus and the plasma temperature. Three positions were tested based on practical distances between the Vapur interface and the DART source; position 1 having complete contact, position 2 being 5 mm away from the interface and position 3 being 10 mm away. During the optimization of these positions, the DART source was always positioned at the same distance from the TDU (2 mm). Experiments were performed in triplicate for each position across a range of different plasma temperatures; 300 °C, 350 °C and 450 °C. The temperature of the TDU was set at a conservative 270 °C for these experiments (Figure 5-2). Electric grid voltage was studied in increments of +50 V, from +50 V to +350 V using the same parameters described in apparatus positioning optimization. Vapur interface pump optimization was carried out using the previously found optimal parameters. As the conventional pumping rate was set to 0 on the needle valve during DART installation, values of -2, 0, 2 and 4 were chosen for optimization.

Desorption parameters were optimized by first extracting the model analytes from ultra-pure water at a concentration of 50 µg/L, the previously optimized apparatus conditions used. Extraction was for 10 min at room temperature in a 3.5 mL volume agitated at 900 rpm with a stirbar. The SPME arrow was then subsequently desorbed for 2 min in the TDU to ensure exhaustive desorption of all analytes. TDU temperature optimization was performed within a temperature range known to effectively desorb the SPME extraction phases: 270 °C, 280 °C, 290 °C, and 300 °C. Coating thickness was evaluated using 100 µm/20 mm, 250 µm/20 mm, and 100 µm/5 mm PDMS SPME arrows. PDMS extraction phases were used in this experiment as other extraction phases are currently not available in different thicknesses. Sample volume optimization was performed in ultra-pure water spiked with model analytes, evaluating volumes of 3.8 and 9.8 mL. These volumes were chosen to completely submerge the arrow's extraction phase in their respective vials. Sonication experiments were performed at room temperature at extraction times of 1, 3, 5 and 10 min.

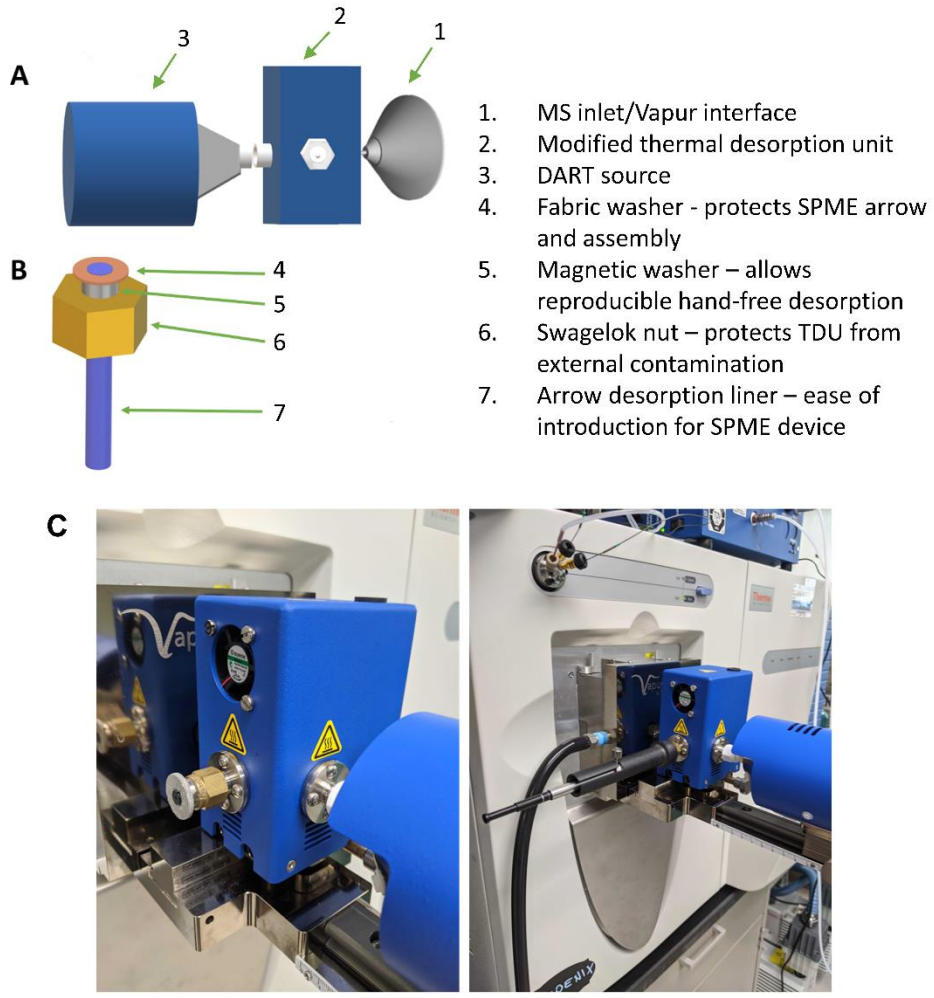

Figure 5-1 A) TDU-DART interface, b) modified 1/4" brass Swagelok nut for controlled introduction of the SPME-Arrow device to the TDU and c) final assembly of apparatus with and without SPME-Arrow holder.

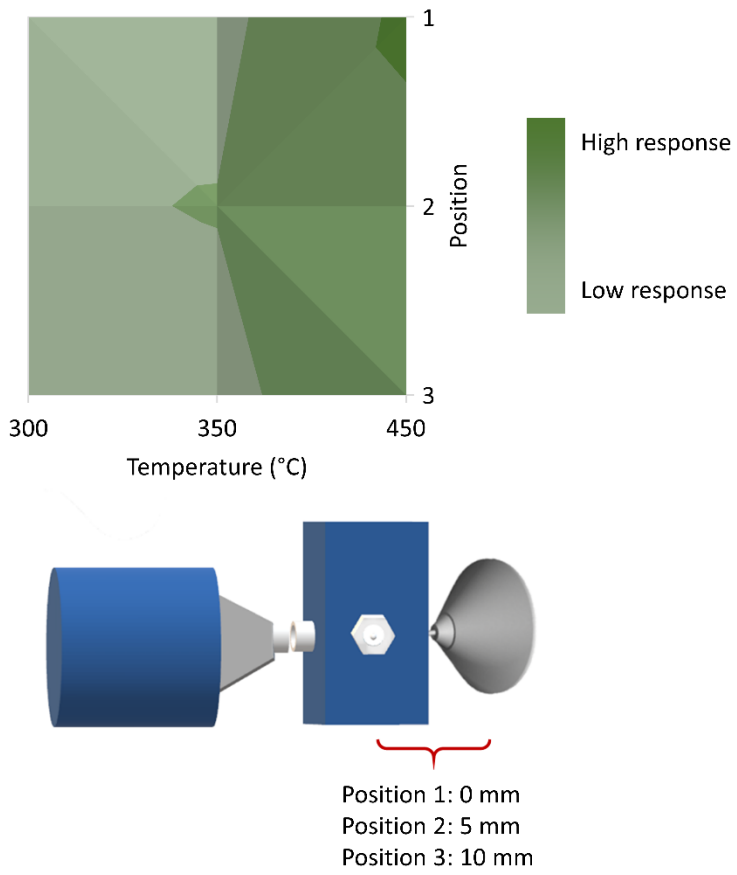

Figure 5-2 Evaluation of DART positioning and plasma heater temperature on signal intensity. The stage was moved 5 mm between each position, each position and temperature combination being evaluated in triplicate. Arrow was held in front of DART source in the same position it would with the TDU interface.

Table 5.1 Model analytes and their physicochemical properties.

Compound	M.W (g/mol)	LogP
Methadone	309.4	3.9
Diphenylamine	169.2	3.5
2-phenylphenol	170.2	3.1
Diazepam	284.7	3.0
Dimethachlor	255.7	2.3
Amphetamine	135.2	1.8
Morphine	285.3	0.8
Cocaine	303.4	2.3

5.3 Results and Discussion

5.3.1 Apparatus Optimization

The various parameters that contribute to ion formation and transmission in DART-MS have already broadly been discussed in the literature.[213] The effects these parameters have on signal intensity are recognized as being consequences in altering fluid dynamics, heat transfer and electrostatics. Positioning of the DART and sample, the temperature and flow of the plasma, and the electric grid voltage are common parameters that can be optimized to tune the sensitivity and reproducibility of the method. As the positioning of the DART-MS potentially has consequences on other parameters[213], initial experiments served to optimize the positioning of the DART and TDU. During the course of apparatus optimization, amphetamine was not consistently detected until electric grid voltage optimization. Malathion exhibited subpar extraction by the SPME arrow and thus was not further studied during extraction optimization, instead being replaced with the analyte cocaine.

To first establish the impact that enclosed analysis had on the desorption and ionization of analytes from the SPME arrow, experiments were performed comparing open-air desorption (as conventionally done in most DART-MS analyses) and enclosed desorption without an external heating supply. Representative ion chronograms, comparing the results of open-air desorption and confined unheated desorption are displayed in Figure 5-3. From the data obtained it is evident how enclosed desorption analysis exhibits a lower background and more efficient transfer of analytes from the SPME device to the MS. This is thought to have occurred due to the unheated TDU focusing the plasma stream onto the SPME device, producing a more stable response and also protecting the ionization region

from airborne interferences as it is partially enclosed These results demonstrate a greater transfer of analyte to the MS the closer the positioning of the TD-DART apparatus is to the Vapur interface, with higher plasma temperature enhancing sensitivity. Subsequent desorption-influenced parameters were optimized employing a DVB/CWR/PDMS SPME arrow. As the model analytes in this study demonstrate disparate polarities and physicochemical properties, this extraction phase was chosen as its two different sorbents (DVB and CWR) allow it to extract a wide-range of analytes.[214]

To ensure there was no carryover on the SPME extraction phase at the lower desorption temperatures evaluated, thermal conditioning was performed with a 2 min blank between each sample at the nominal TDU temperature followed by a 2 min blank at 300 °C. Results shown in Figure 5-4 demonstrate the desorption profiles produced by this newly developed TDU method, with the analytes being desorbed within 30 s. The ion chronograms' desorption profiles for the model analytes differ based on their chemical functionality. This may suggest that ion chronograms' profiles are affected by both analyte's desorption behavior from the extraction phase and any subsequent interaction the analyte has with the TDU surfaces. As the shape of the desorption profile has a considerable effect on the ability to discriminate the analyte signal from noise, it is expected that deactivation of the TDU inner surface could permit better S/N. A TDU temperature of 300 °C was determined to be optimal, offering the greatest desorption efficiency, while 270 °C showed poor reproducibility most likely due to its ineffective desorption (Figure 5-5). The desorption of SPME devices facilitated by heated TDU not only allows rapid introduction of the analyte to the MS but also avoids use of solvent, as previous reports suggest that a volatile matrix (such as methanol) is necessary when plasma desorption is not enough to

desorb less volatile analytes.[215] It was found that at higher temperatures results were more reproducible, possibly owing to a more efficient desorption, 450 °C chosen for further studies (Figure 5-6). The electric grid, a component of the DART source, is responsible for ion-ion recombination and acting as an ion repeller, has been theorized to affect the dominant ionization mechanism[50] and the speed of ion transmission[213]. The two main competing mechanisms are Penning ionization and charge transfer, the former being responsible for $[M + H]^+$ formation and the latter $M^{+\bullet}$. As the study of polar and semi-polar compounds is predominated by $[M + H]^+$ formation, conditions that favor Penning ionization are better suited for this work. That is, low electric grid voltage and an apparatus that allows the inclusion of water vapor.[50] As previous reports indicated this parameter to have little influence on response[216], many studies often do not optimize electric grid voltage and using a conservative value ranging from +200 V to +350 V, at times the value of the electric grid voltage not being discussed.[215,217] However, other reports in the literature have described electric grid voltage as having a significant impact on sensitivity in some cases.[191,213,218–220] As a result, in many DART-MS methods only the desorptive parameters are fully optimized and not the parameters that affect ion formation and transmission. As can be seen in Figure 5-7**,** voltage played a major role in the sensitivity of the method. The majority of studied analytes exhibited substantial increases in sensitivity at lower voltages. These results are in line with previous studies on the interplay between ion velocity and DART-MS positioning.[213] At high ion velocities (high electric grid voltage) ion trajectory is not focused, the movement being greatly influenced by the electrostatic repulsion generated from the electric grid. As a result, a low electric grid voltage of +50 V was found to be the optimal voltage in this study. While the distance between the DART and TDU is

small (2 mm), we suggest that as the TDU is not perfectly enclosed, the overall distance between the MS inlet and DART is sufficient for efficient Penning ionization to take place.

Vapur interface pump rate was found to have minimal effect on the observed sensitivity and reproducibility of the method (Figure 5-8). A flow rate corresponding to a needle valve position of 2 was chosen as the optimal flow rate as it showed marginal signal improvements for the model analyte diazepam.

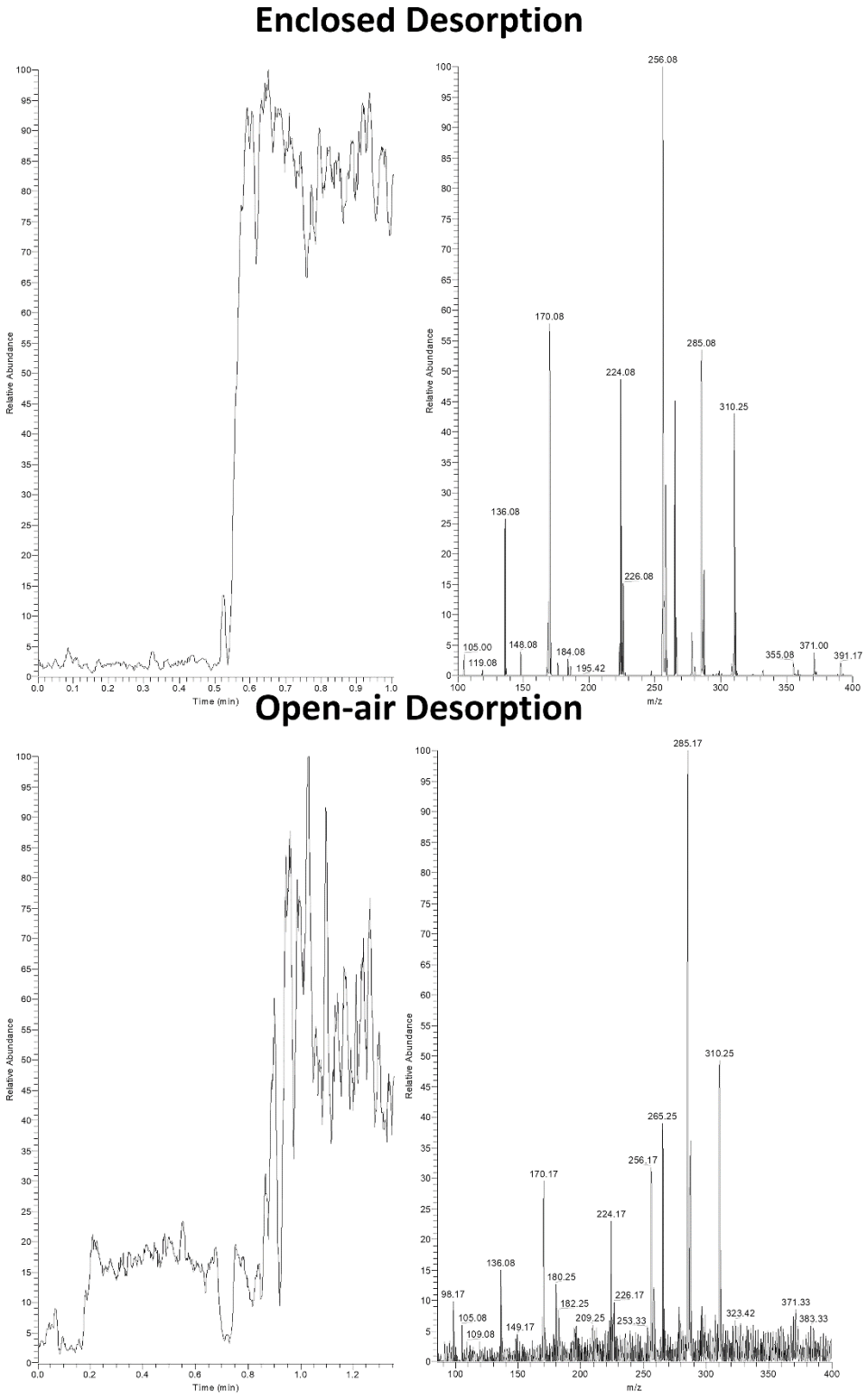

Figure 5-3 Full scan ion chronograms and related mass spectra demonstrating differences in background and analyte response between unheated TDU analysis and open-air desorption of an SPME-Arrow loaded with model analytes.

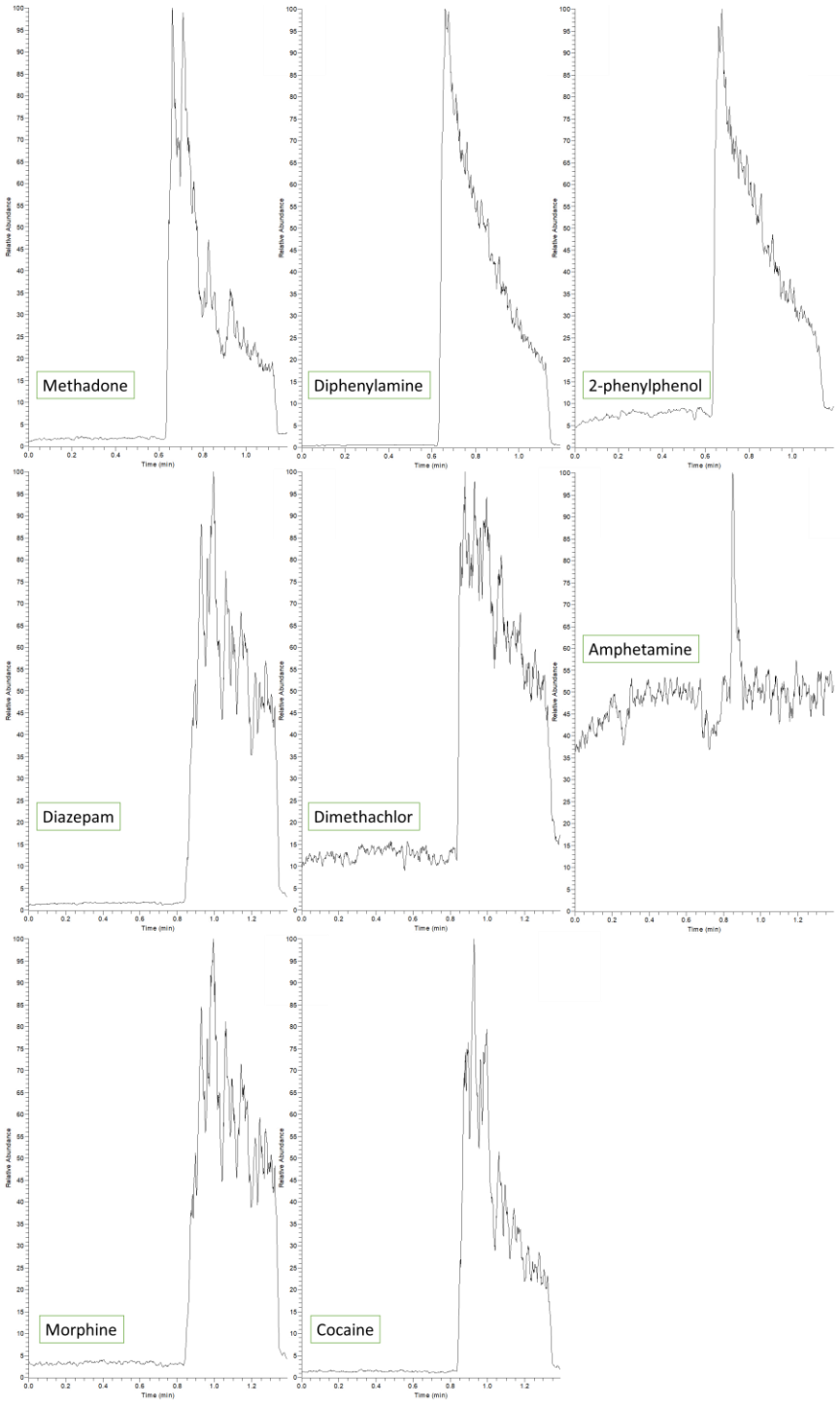

Figure 5-4 Desorption profiles of each model analyte using the optimized method, concentration of analytes being 25 μg L^{-1} in ultra-pure water. Profile width 30 s for each model analyte except amphetamine.

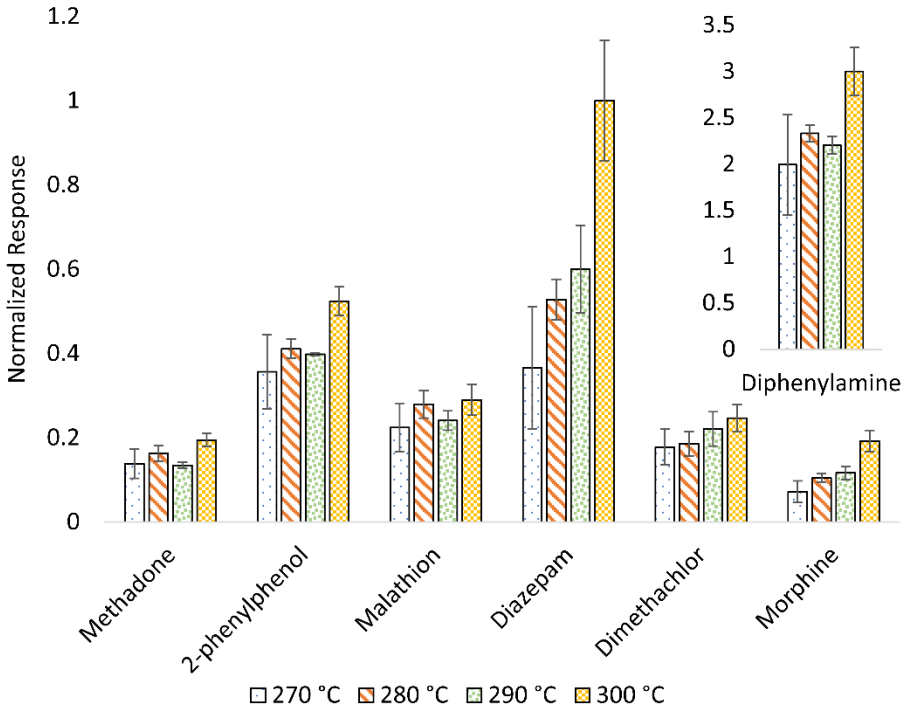

Figure 5-5 Evaluation of TDU temperature on the desorption of the DVB/C-WR/PDMS SPME-Arrow.

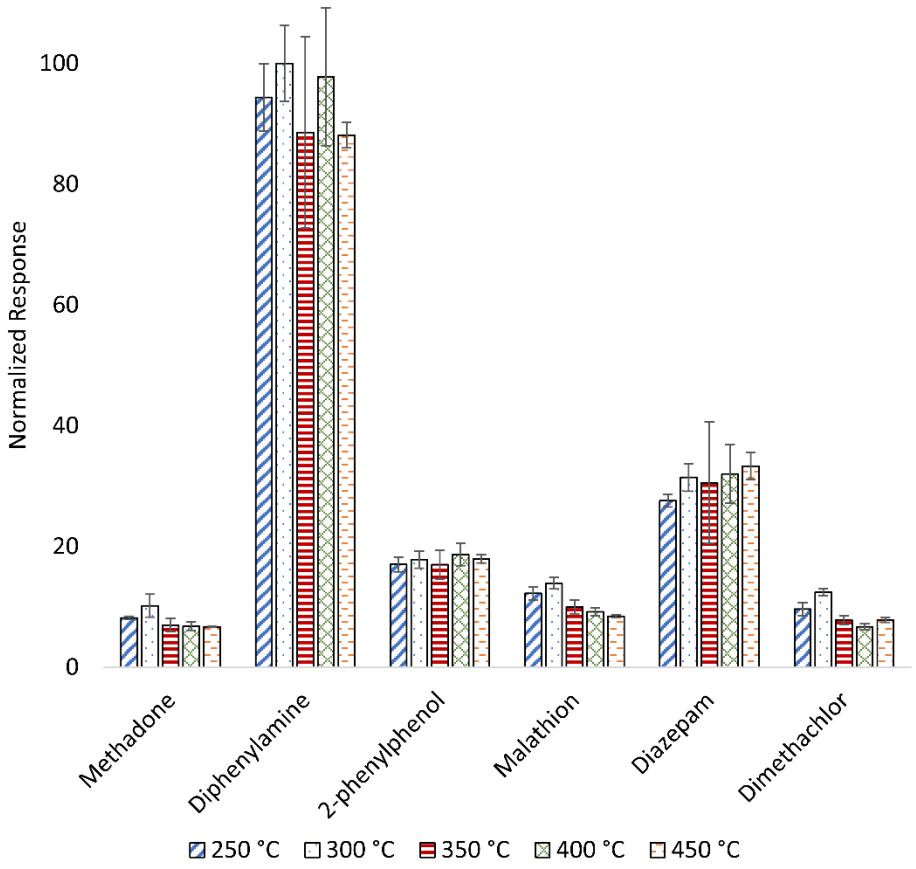

Figure 5-6 Plasma heater temperature optimization demonstrating higher reproducibility at higher temperatures.

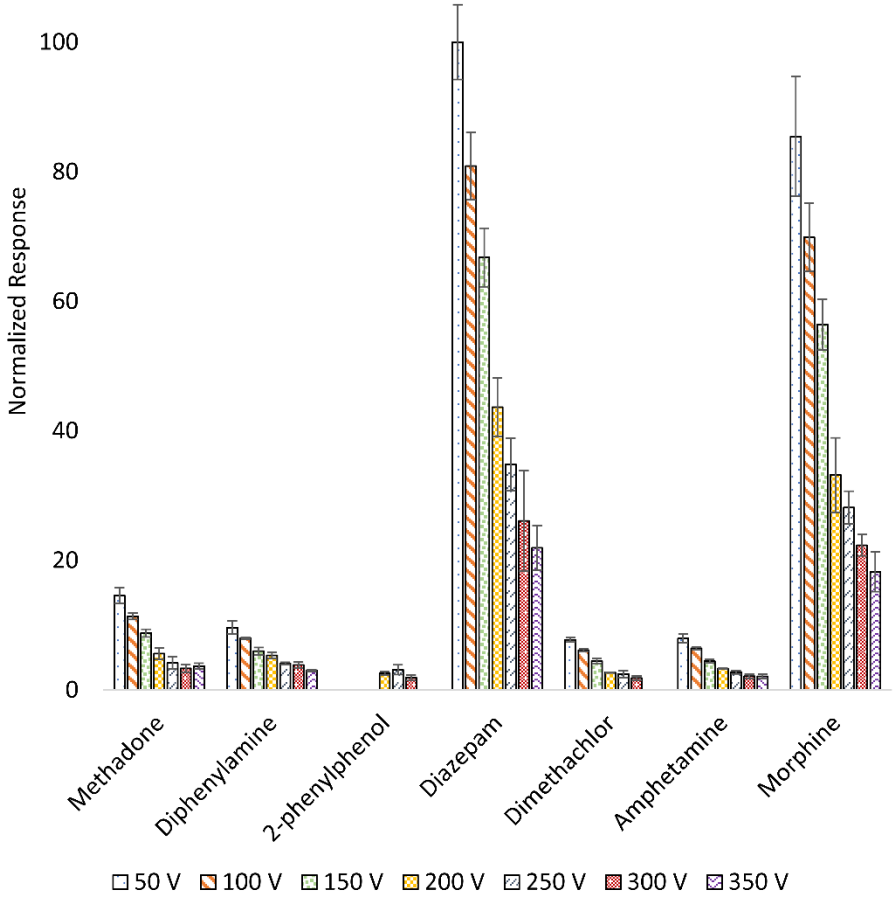

Figure 5-7 DART electric grid voltage optimization for the targeted analytes. Results are normalized to the highest response.

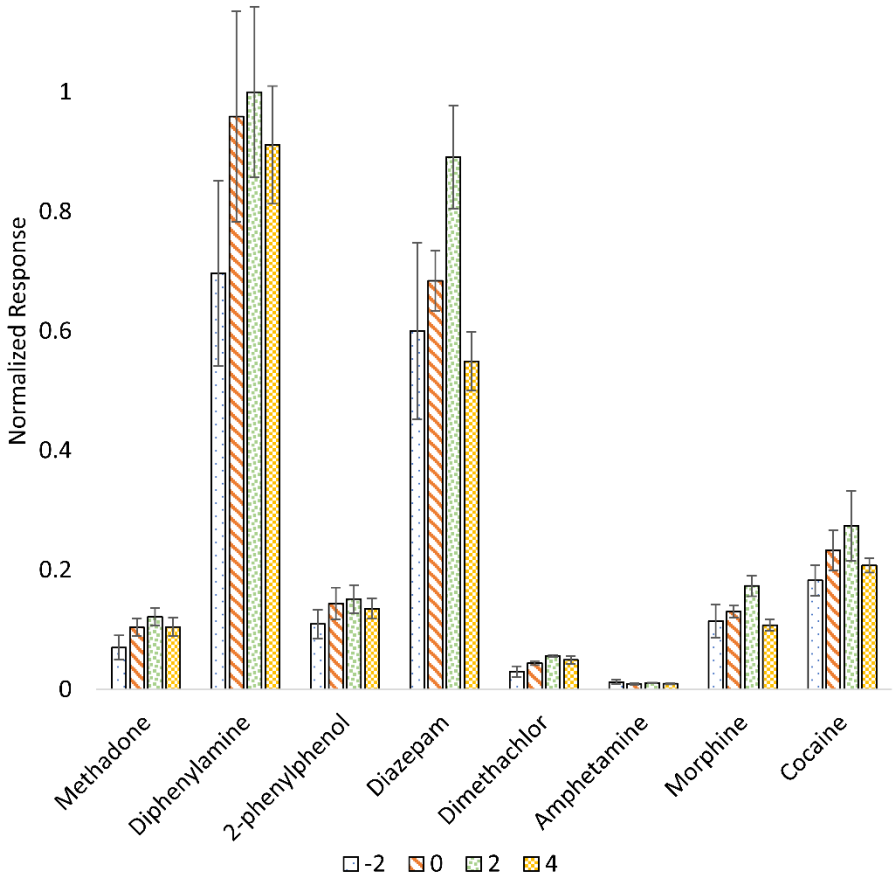

Figure 5-8 Pump speed optimization (ranging from -2 to 4 strength) for Vapur interface.

5.3.2 Extraction and Desorption Conditions

In the context of MS analysis, a "peak-based" signal allows enhanced sensitivity as all analyte is introduced to the MS and detector in a short amount of time.[221] The more analyte detected at a point time the greater the observed signal-to-noise, meaning lower achieved LOQs. As the majority of direct-AMS applications forgo chromatography, the time it takes for the analyte to desorb and ionize from the sample (or from the extraction devices) decides the "peak width" and is a critical factor in direct-AMS method development. In the context of SPME-MS, the desorption kinetics, governed by factors such as desorption temperature and extraction phase thickness, need to be carefully optimized to allow fast and efficient desorption. To assess the influence that arrow-SPME coating thickness has on desorption, devices of the same extraction phase but different phase thickness and length were compared. Results shown in Figure 5-9 demonstrate that greater coating thickness resulted in longer desorption times, reducing the amount of analyte detected per unit of time and in lowering S/N at low concentrations. The 5 mm PDMS arrow-SPME device showed a reduction in extraction capacity due to its smaller extraction phase volume, however, it also provided sharper desorption profiles compared to the 20 mm long SPME-Arrow lengths. 5 mm SPME-Arrow devices with different extraction phases could be exploited in this way for enhanced discrimination of analyte's signal from noise.

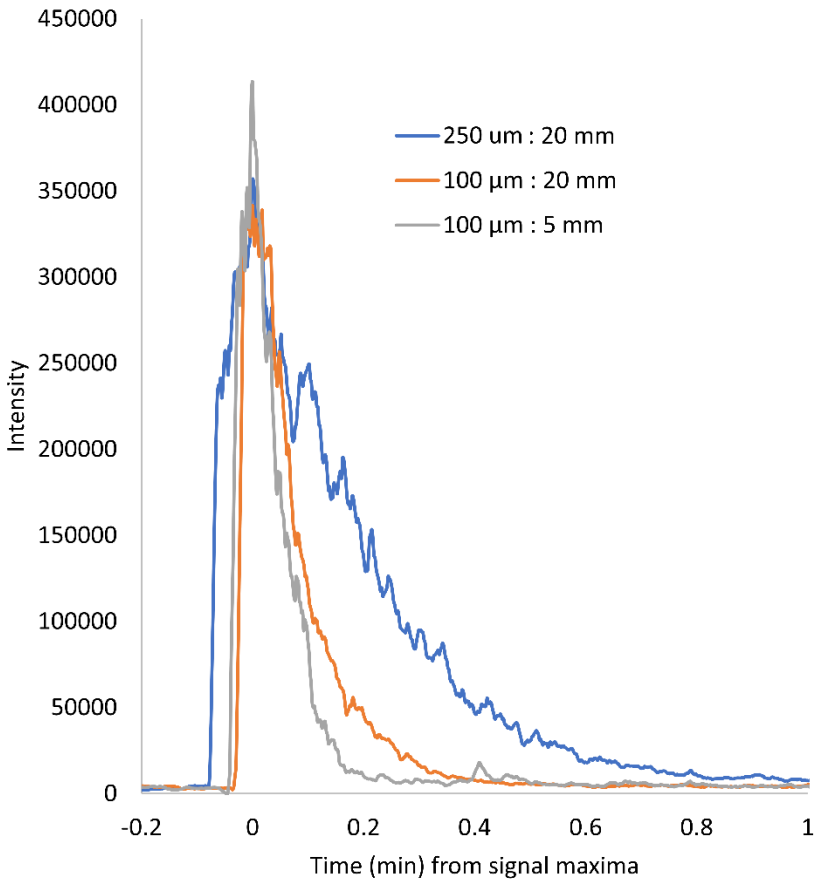

Figure 5-9 Overlapped ion chronograms obtained with PDMS SPME Arrows with different coating thicknesses.

All other SPME parameters were optimized with the DVB/CWR/PDMS SPME arrow to better extract the model compounds with disparate polarities. Results demonstrated that for the majority of analytes, no significant difference between the amount extracted was observed for different sample volumes (Figure 5-10). This is due to SPME being a non-exhaustive technique, therefore, if the sample volume is significantly larger than the volume of the extraction phase, the amount of analyte extracted becomes independent from the volume of the sample.[211] As a result, 3.8 mL was chosen for further optimization.

During SPME, typical agitation modes for aqueous samples utilize either a magnetic stirbar in the sample volume or vortex-assisted agitation. The more vigorous the agitation the more likely damage to the coating or support can occur.[222] As the support of SPME arrow consists of a stainless-steel rod, in this work we evaluated the performance of stirbar agitation and sonication-assisted agitation. Results in Figure 5-11 show that sonication-assisted extraction greatly outperformed stirbar extraction and enabled equilibration in only 10 min for most analytes vs stirbar extraction. Amphetamine, an analyte that could not be extracted in previous optimization experiments performed using stirbar agitation, was extracted and detected only by sonication-assisted extraction. The chosen extraction time of 3 min with sonication allowed approximately 4-8 times higher signal for all analytes compared to the same time with stirbar agitation, several of the analytes unable to be detected at this time point altogether.

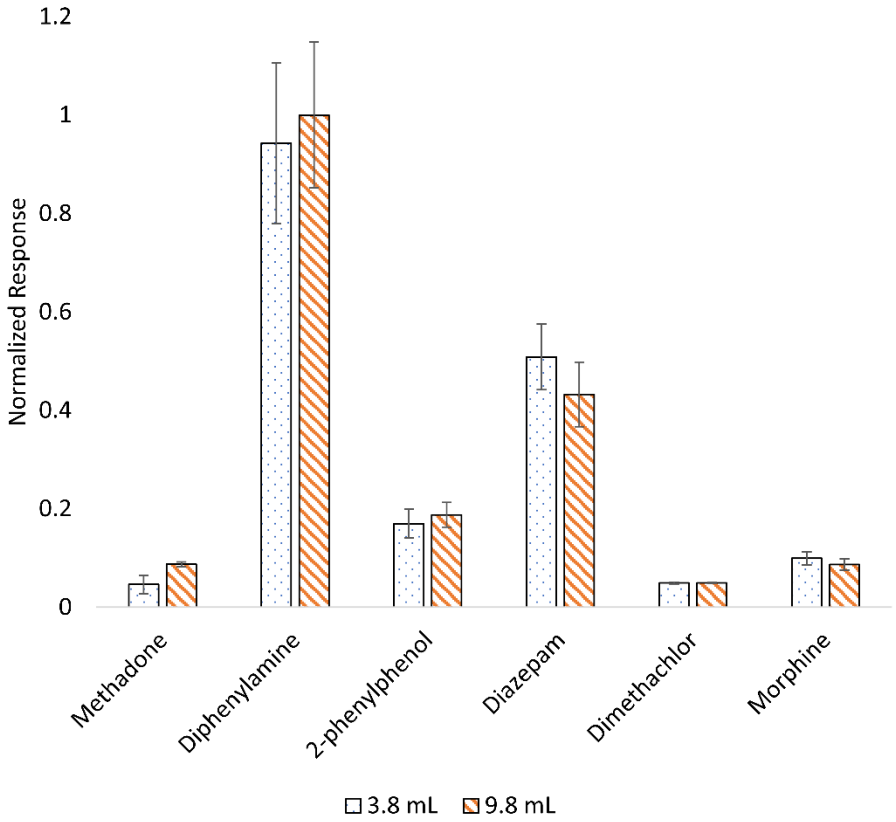

Figure 5-10 Sample volume optimization for SPME arrow extraction

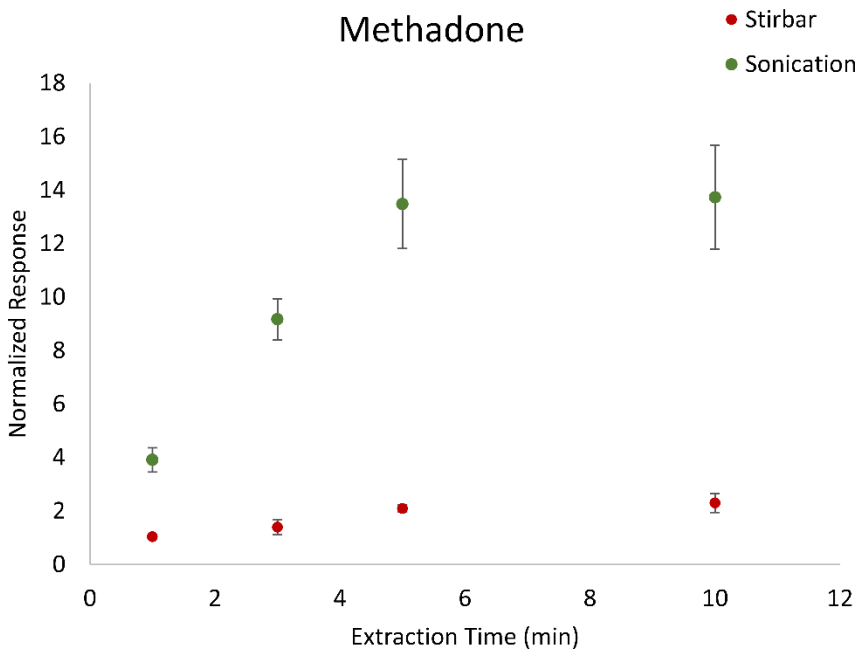
Methadone
Stirbar
Sonication
Normalized Response
Extraction Time (min)
0
2
4
6
8
10
12
14
16
18
0
2
4
6
8
10
12

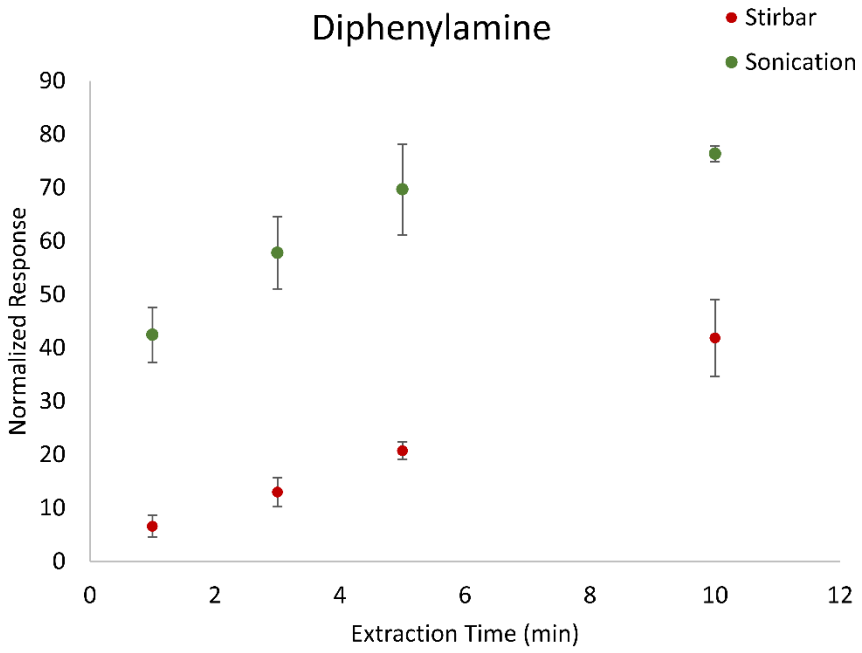
Diphenylamine
Stirbar
Sonication
Normalized Response
Extraction Time (min)
0
10
20
30
40
50
60
70
80
90
0
2
4
6
8
10
12

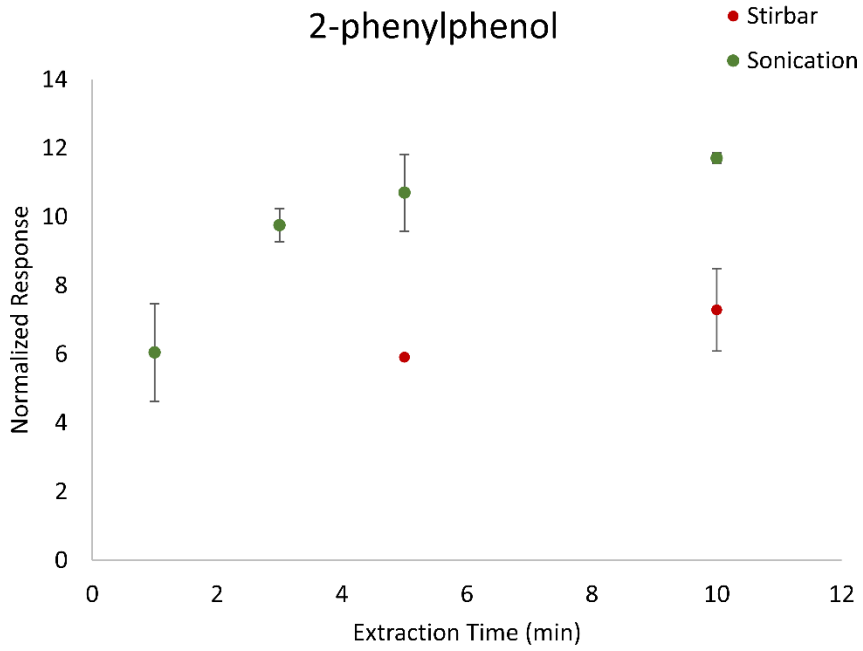
2-phenylphenol
Stirbar
Sonication
Normalized Response
Extraction Time (min)
0
2
4
6
8
10
12
14

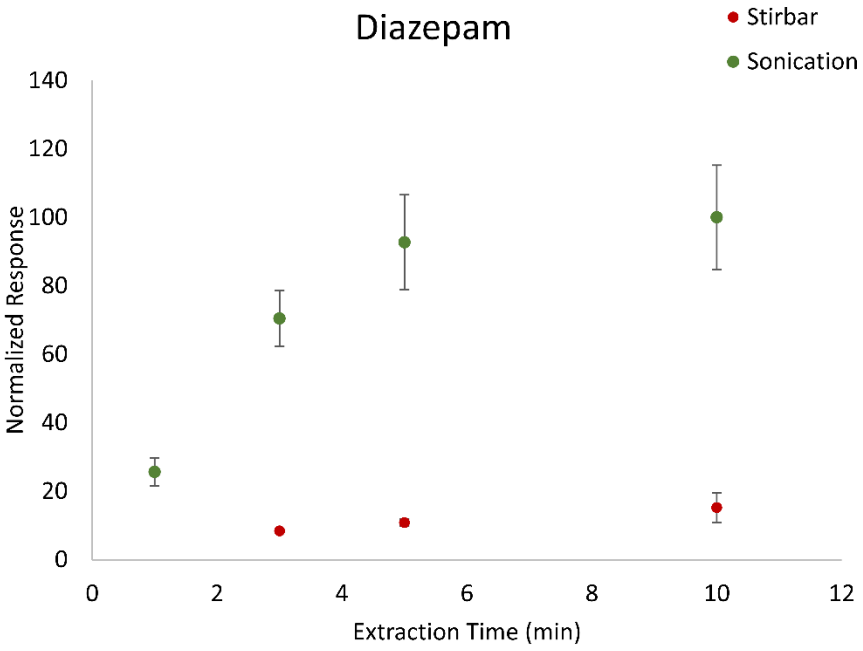
Diazepam
Stirbar
Sonication
Normalized Response
Extraction Time (min)
0
20
40
60
80
100
120
140

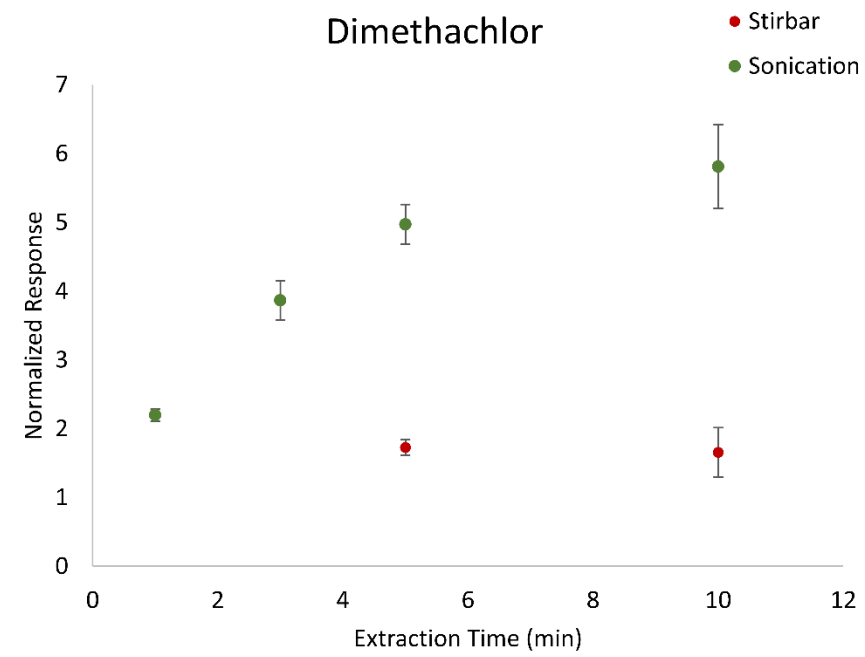
Dimethachlor
Stirbar
Sonication
Normalized Response
Extraction Time (min)
0
1
2
3
4
5
6
7
0
2
4
6
8
10
12

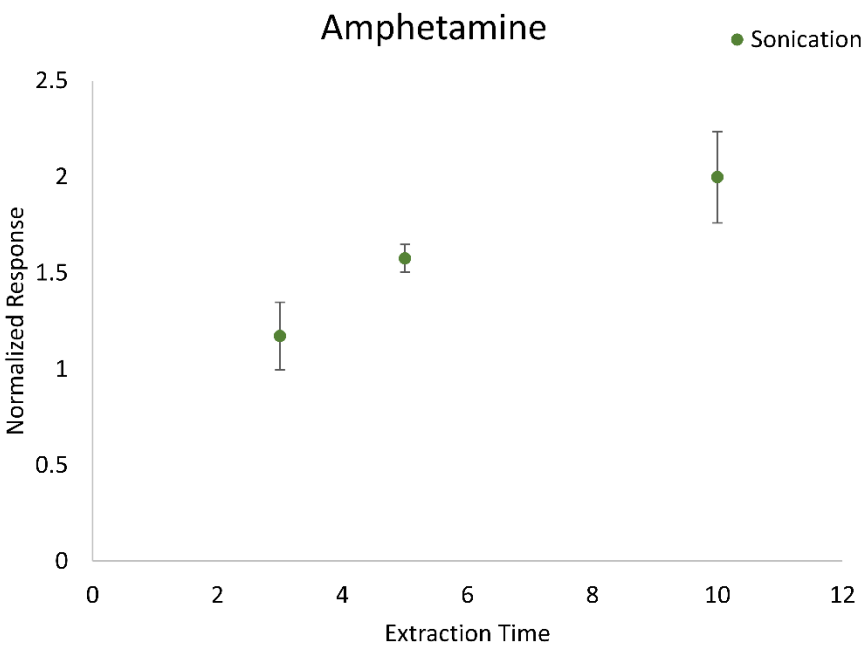
Amphetamine
Sonication
Normalized Response
Extraction Time
0
0.5
1
1.5
2
2.5
0
2
4
6
8
10
12

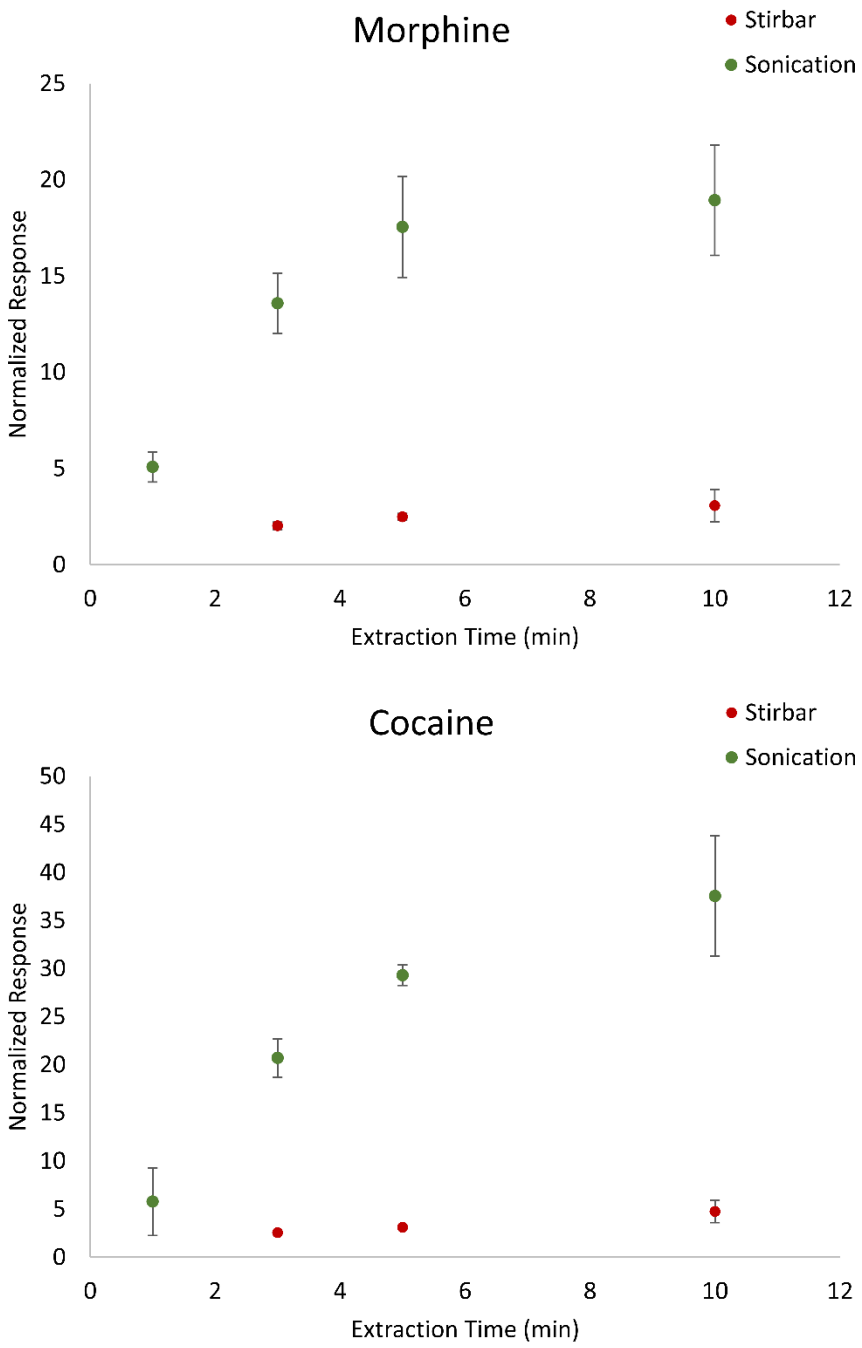

Figure 5-11 Extraction time profiles for each analyte comparing stirbar and sonication-mediated agitation, all responses normalized to the highest response obtained in the experiment (diazepam).

5.3.3 Method Validation

Throughout parameter optimization it was observed that high TDU temperatures allowed rapid and complete desorption of all analytes, characterized by a distinctive profile that provides ease of integration and discrimination from noise. This semi-enclosed apparatus also resulted in lower background signal compared to open-air applications, therefore contributing to the greater sensitivity accomplished through this method. Method validation and calibration were performed with the same DVB/CWR/PDMS SPME arrow used previously using the optimized parameters in this study. Extractions were performed in ultra-pure water spiked with model analytes for 3 min with sonication at room temperature. It should be noted that during initial experiments it was determined that the mass spectrometer in this study was unable to achieve MS^2 of all model analytes and their internal standards simultaneously due to its acquisition speed. Nonetheless, the mass spectrometer running in full scan was able to achieve satisfactory LOQs for the majority of analytes (Table 5.2), calibration levels being prepared between 1 and 500 µg/L for each analyte. Internal standards were spiked in solution at 50 µg/L, with the exception of Amphetamine-d_{11} at 100 µg/L due to its poor response. After analysis, internal standards were chosen for each compound based on the efficacy of their correction not only toward intraday reproducibility but also interday. The majority of the model compounds were reliably quantified in the low µg/L range with only 3 min of extraction. All calibration curves are demonstrated in Figure 5-12. It should be noted that comparable LC-MS/MS methods for the determination of pesticides and pharmaceuticals in water typically have sensitivity in the mid ng/L range, lower than the method developed in this study.[223,224] LC-MS/MS methods, however, are not easily adaptable for *in situ* analysis and their throughput

is greatly diminished compared to AMS, chromatography being as short as 5 min[225] and at times longer than 30 min.[226]

AMS-based methods are rarely evaluated for their interday reproducibility, with some exceptions[191,192,227,228], as the reproducibility across different experiments is often expected to be unsatisfactory due to multiple factors. With optimal DART parameters, the largest factors for method reproducibility are sample introduction, matrix effects and fluctuating ambient conditions.[48] Hyphenating SPME-Arrow with DART affords the ability of preconcentrating analyte from the matrix and allows a reproducible method to introduce the sample to AMS. The enclosed TDU interface permits desorption and ionization to take place protected from ambient conditions, providing better AMS stability than found with methods that are susceptible to ambient fluctuations. The initial unoptimized conditions in this work demonstrated relatively good intraday reproducibility (less than 20 % RSD for most analytes) without internal standard correction, optimal parameters being less than 15 % RSD. These parameters allowed excellent interday reproducibility to be achieved for the majority of analytes (Table 5.3). It should be noted that while intraday reproducibility was below 20 % without internal standard correction for the majority of the analytes, internal standard correction was necessary when comparing interday results. Accuracy values within 100 ±20 % and precision values < 15 % were observed for the majority of analytes. Other reports have also shown good intraday reproducibility without internal standard correction when coupling SPME to DART-MS[204], however, to the best of our knowledge, a comparison between interday reproducibility with and without internal standards for DART-MS has not been published in the literature. S/N was also calculated for each model analyte at their observed LOQ (Table 5.4).

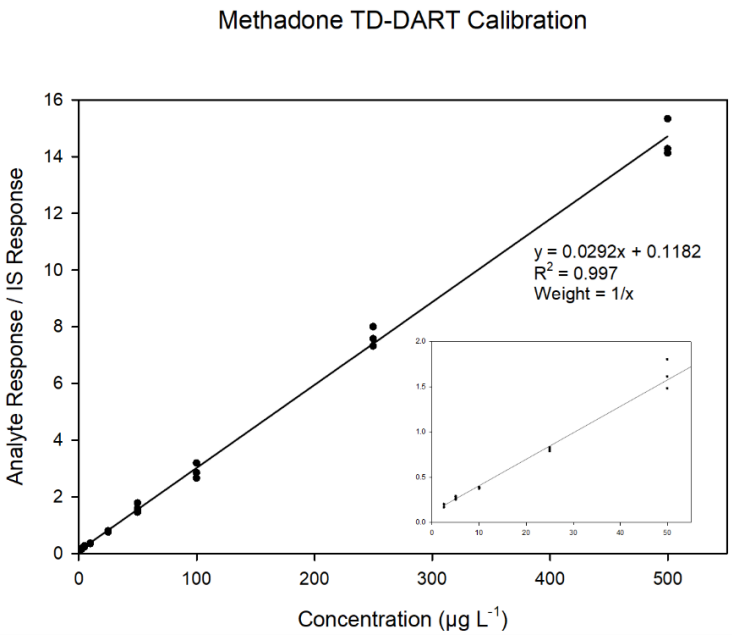

µg L^{-1}	% Accuracy
2.5	90.2
2.5	107.7
2.5	105.0
5	98.1
5	104.1
5	111.0
10	95.9
10	95.4
10	92.2
25	97.9
25	93.2
25	95.6
50	114.5
50	102.4
50	94.1
100	105.8
100	94.8
100	88.3
250	102.4
250	98.9
250	108.1
500	97.1
500	96.0
500	104.2

Calibration Points	
µg L^{-1}	RSD %
2.5	9.3
5	6.2
10	2.1
25	2.5
50	9.9
100	9.2
250	8.3
500	4.5

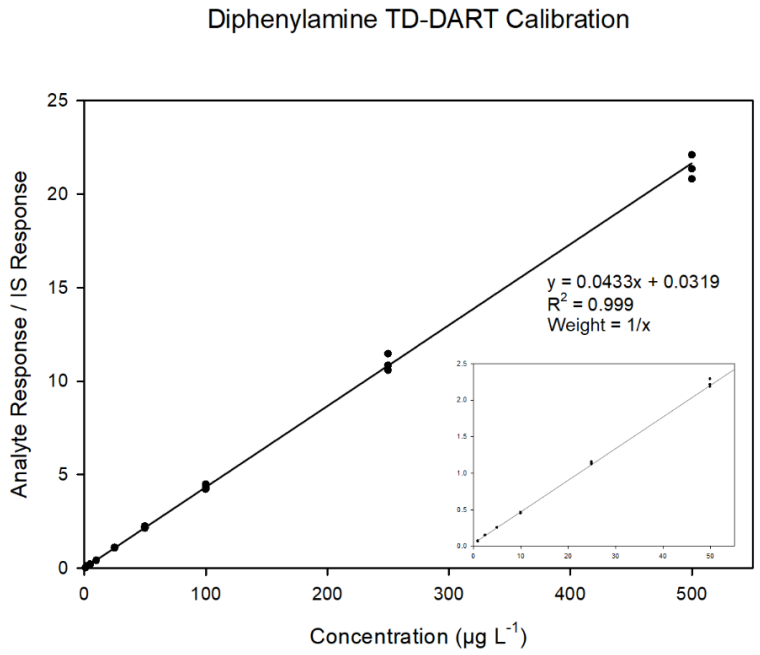

µg L^{-1}	% Accuracy
1	100.3
1	87.2
1	86.1
2.5	107.5
2.5	108.0
2.5	107.1
5	103.5
5	103.5
5	102.6
10	99.3
10	98.7
10	96.9
25	100.8
25	101.2
25	103.4
50	104.0
50	100.6
50	99.2
100	103.5
100	99.4
100	97.5
250	105.7
250	100.0
250	97.5
500	101.8
500	95.8
500	98.3

Calibration Points	
µg L^{-1}	RSD %
1	8.6
2.5	0.4
5	0.5
10	1.3
25	1.4
50	2.4
100	3.1
250	4.1
500	3.0

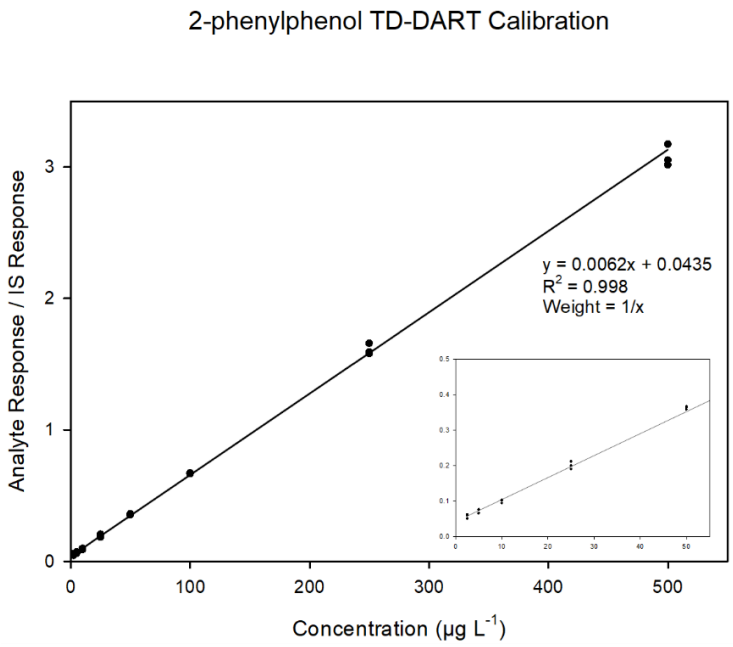

µg L^{-1}	% Accuracy
2.5	88.2
2.5	107.9
2.5	104.1
5	90.2
5	103.8
5	104.3
10	90.7
10	97.5
10	99.1
25	96.5
25	101.3
25	107.4
50	102.0
50	103.6
50	104.2
100	102.5
100	101.6
100	102.1
250	104.7
250	100.5
250	99.8
500	101.4
500	96.3
500	97.5

Calibration Points	
µg L^{-1}	RSD %
2.5	10.5
5	8.0
10	4.7
25	5.4
50	1.1
100	0.5
250	2.6
500	2.7

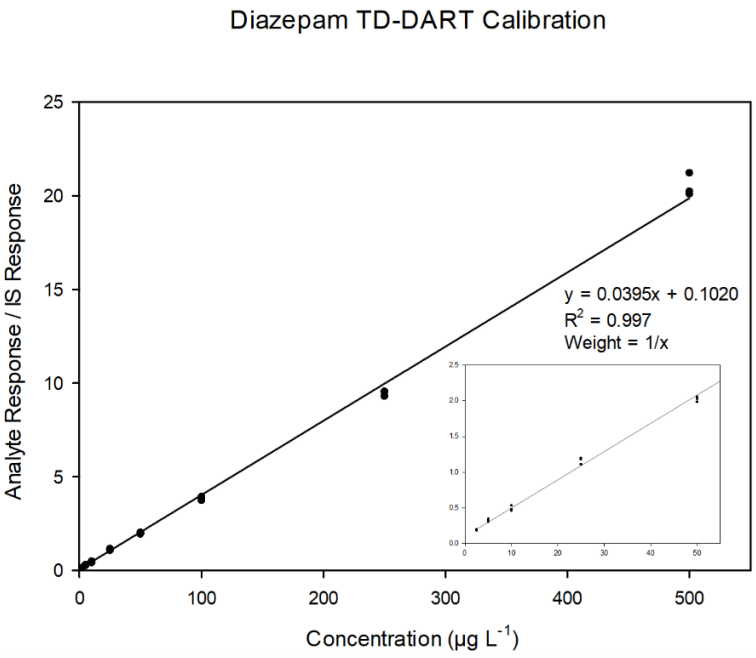

µg L^{-1}	% Accuracy
2.5	98.6
2.5	93.6
2.5	92.6
5	107.8
5	102.4
5	116.1
10	96.3
10	107.5
10	93.0
25	102.1
25	108.5
25	110.1
50	95.5
50	97.6
50	99.1
100	93.0
100	95.2
100	97.6
250	93.5
250	95.8
250	95.9
500	101.9
500	101.2
500	106.8

Calibration Points	
µg L^{-1}	RSD %
2.5	3.4
5	6.3
10	7.7
25	4.0
50	1.8
100	2.4
250	1.4
500	3.0

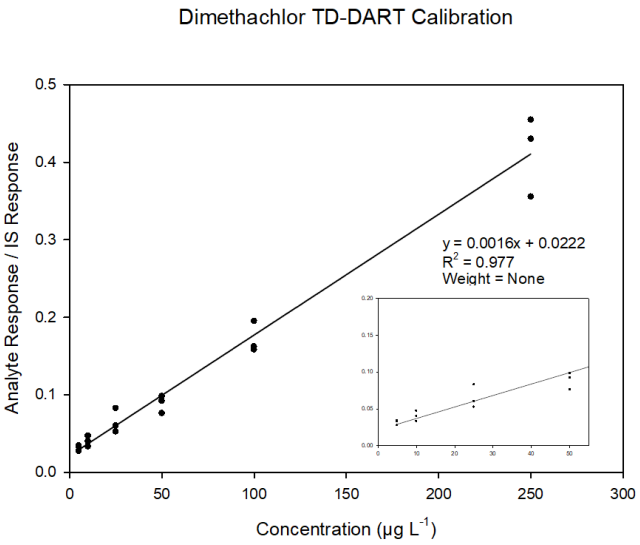

µg L^{-1}	% Accuracy
5	96.1
5	113.5
5	118.2
10	127.9
10	91.2
10	109.3
25	88.0
25	100.6
25	137.3
50	77.4
50	99.5
50	93.3
100	89.6
100	91.9
100	110.3
250	104.8
250	110.8
250	86.7

Calibration Points	
µg L^{-1}	RSD %
5	10.7
10	16.7
25	23.6
50	12.7
100	11.7
250	12.4

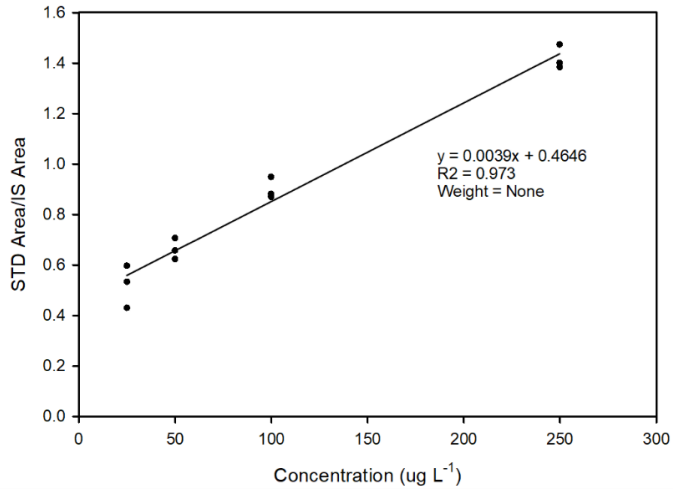

µg L^{-1}	% Accuracy
25	77.2
25	106.7
25	95.5
50	107.7
50	95.0
50	100.2
100	111.4
100	103.6
100	102.2
250	102.5
250	96.4
250	97.5

Calibration Points	
µg L^{-1}	RSD %
25	4.8
50	3.1
100	3.4
250	2.6

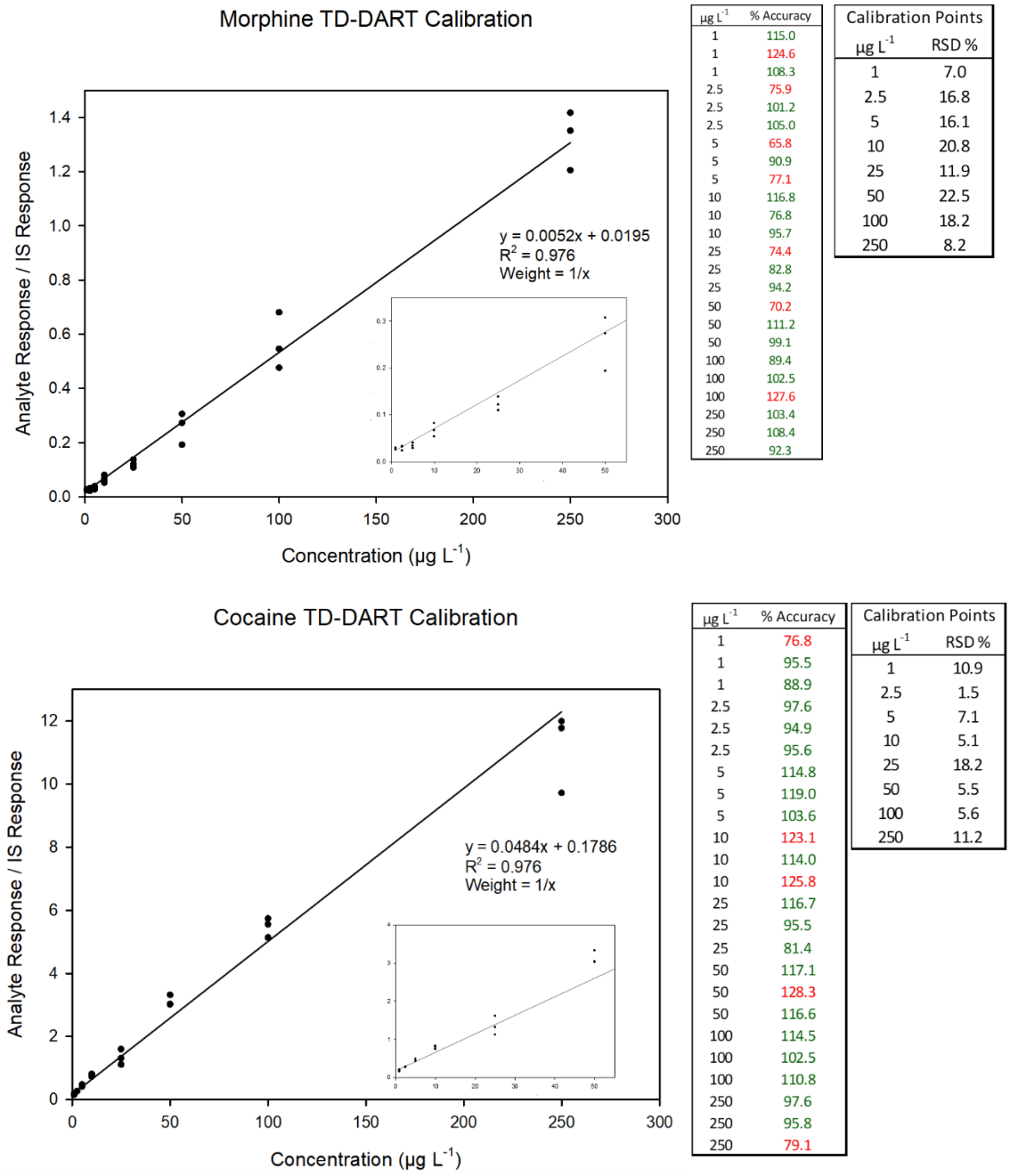

Figure 5-12 Calibration curves for all model analytes with their respective calibration point accuracies and reproducibility.

Table 5.2 Model analytes and figures of merit.

Model Analyte	logP	M.W. (g/mol)	*LOQ (µg/L)	**LDR (µg/L)	R^2	35 (µg/L)		75 (µg/L)		200 (µg/L)	
						Intraday (RSD %)	Interday (RSD %)	Intraday (RSD %)	Interday (RSD %)	Intraday (RSD %)	Interday (RSD %)
Methadone	3.9	309.4	2.5	2.5 - 500	0.997	7.0	4.5	6.1	9.9	4.2	6.0
Diphenylamine	3.5	169.2	1	1 - 500	0.999	2.2	3.0	3.1	7.7	4.6	6.1
2-phenylphenol	3.1	170.2	2.5	2.5 - 500	0.998	1.7	5.4	1.1	3.9	2.6	3.3
Diazepam	3.0	284.7	2.5	2.5 - 500	0.997	2.8	6.9	2.2	2.9	1.6	10.8
Dimethachlor	2.3	255.7	5	5 - 250	0.977	8.8	20.4	7.1	16.5	11.5	20.7
Amphetamine	1.8	135.2	25	25 - 250	0.973	9.3	7.8	6.9	1.2	7.4	4.5
Morphine	0.8	285.3	1	1 - 250	0.976	8.7	29.4	13.1	19.3	15.2	4.9
Cocaine	2.3	303.4	1	1 – 250	0.976	10.9	18.2	9.4	4.3	6.0	17.0

*LOQ, limit of quantitation; calculated as being between 75 and 125 % accuracy and with a relative standard deviation (RSD) % less than 15 %.

**LDR, linear dynamic range; concentration range which is included in the linear calibration curve – satisfactorily achieving high accuracy and precision.

Table 5-3 Intra- and interday reproducibility for each model analyte at their respective accuracy point, inadequate values highlighted in red and underlined.

		Day 1		Day 2		Day 3		Interday	
	Compound	Accuracy%	RSD%	Accuracy%	RSD%	Accuracy%	RSD%	Accuracy%	RSD%
35 ppb	Methadone	110.6	2.2	105.7	12.4	100.1	6.4	105.5	4.5
	Diphenylamine	113.4	0.7	115.3	3.7	108.7	2.0	112.5	3.0
	2-phenylphenol	122.8	1.3	130.4	1.8	114.9	1.9	122.7	5.4
	Diazepam	112.6	1.1	120.8	4.2	105.1	3.2	112.8	6.9
	Dimethachlor	128.4	4.5	93.7	7.9	72.6	13.9	98.2	20.4
	Amphetamine	73.2	9.7	79.7	9.6	135.1	8.6	96.0	7.8
	Morphine	116.7	3.3	95.4	10.9	58.2	12.0	90.1	29.4
	Cocaine	94.8	3.4	81.1	17.2	62.2	12.2	79.4	18.2
75 ppb	Methadone	111.1	5.3	93.7	10.1	114.4	2.9	106.4	9.9
	Diphenylamine	108.2	1.0	99.4	7.7	116.2	0.7	107.9	7.7
	2-phenylphenol	112.2	0.4	112.2	1.5	120.5	1.2	115.0	3.9
	Diazepam	101.0	1.8	101.6	1.5	106.5	3.4	103.1	2.9
	Dimethachlor	118.6	11.9	87.2	2.5	84.2	6.8	96.7	16.5
	Amphetamine	127.6	4.5	131.1	11.2	134.5	5.0	131.1	1.2
	Morphine	111.8	20.3	91.3	13.3	74.3	5.7	92.5	19.3
	Cocaine	75.1	15.9	70.4	10.3	68.7	2.0	71.4	4.3
200 ppb	Methadone	105.7	2.0	97.6	7.1	110.1	3.6	104.5	6.0
	Diphenylamine	104.3	8.1	101.2	4.6	113.7	1.2	106.0	6.1
	2-phenylphenol	108.2	4.5	106.9	2.6	113.9	0.7	109.6	3.3
	Diazepam	98.6	1.8	115.9	1.4	94.9	1.6	103.2	10.8
	Dimethachlor	132.2	21.7	96.7	2.7	88.4	10.1	105.7	20.7
	Amphetamine	120.8	1.1	108.4	7.1	106.6	14.1	111.9	4.5
	Morphine	96.5	24.6	90.8	10.3	87.5	10.7	91.6	4.9
	Cocaine	45.6	0.5	61.9	10.7	65.8	6.8	57.7	17.0

Table 5-4 Signal-to-noise (S/N) at each analyte's calculated limit of quantitation (LOQ).

Compound	LOQ (µg L^{-1})	S/N
Methadone	2.5	9
Diphenylamine	1	15
2-phenylphenol	2.5	6
Diazepam	2.5	16
Dimethachlor	5	8
Amphetamine	25	4
Morphine	1	6
Cocaine	1	6

5.3.4 Application to Environmental Samples

Two samples, river water and apple, were selected as a real matrix to evaluate the capabilities of the developed SPME Arrow-TD-DART-MS method. For river water, extraction and quantitation were performed in the same manner as the method validation, the water being spiked with the method's internal standards prior to extraction. Target analytes found consisted of methadone and cocaine, methadone being detected at 6.2 µg/L and cocaine being found below the method LOQ. Target analytes discovered were all verified by a subsequent MS^2 experiment (Figure 5-13). To extract from apple, the SPME arrow was inserted into the fruit and the extraction phase exposed for 10 min (Figure 5-14). Quantitation was not attempted as static-extraction from a food sample would require a different calibration approach than the one optimized in this work. Results indicate a response for the pesticide diphenylamine, a common pesticide used in apple production (Figure 5-13).[229]

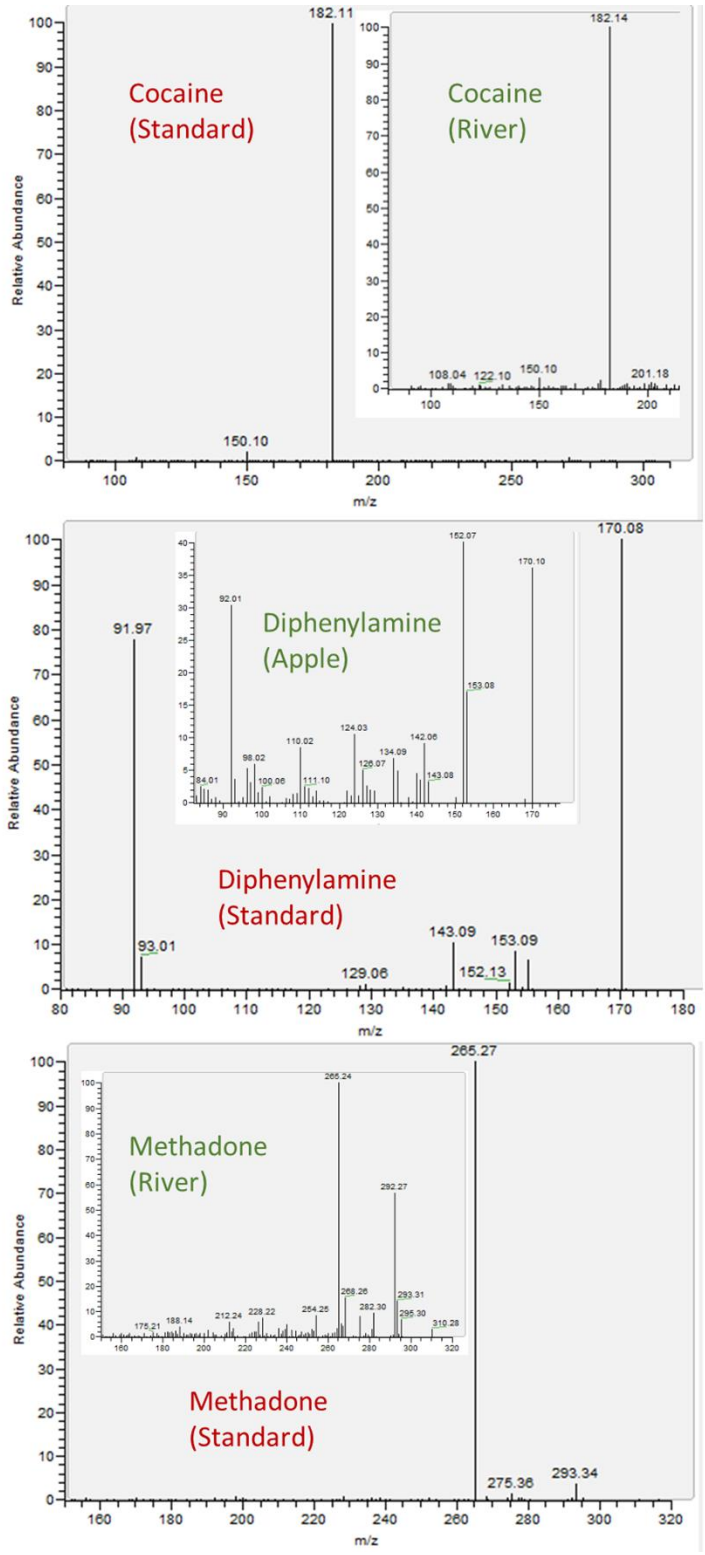

Figure 5-13 MS^2 of each detected analyte by both its analytical standard and the sample it was detected in.

Figure 5-14 Static extraction of an apple using an SPME Arrow device.

5.4 Conclusions

This study developed and accessed an SPME introduction method to DART-MS for rapid analysis of environmental contaminants. The results outlined in this work will allow further expansion of direct-AMS onsite analysis into even more complex samples and sub-optimal environments, its partially enclosed nature shielding the apparatus from potential contamination and TME effects. Application to onsite analysis can be achieved since the TDU-DART apparatus can be easily hyphenated to portable mass spectrometry instrumentation. Quick and reliable quantitation onsite would provide further insight into time-resolved environmental studies, encouraging the study of process and transportation studies of organic compounds *in situ*. Moreover, the sensitivity of the method can be further enhanced by increasing extraction time or by the hyphenating of this method to a mass spectrometer with faster scan speeds, such as a triple quadrupole, as this would allow MS/MS data to be collected. High resolution mass spectrometry would also permit better structural elucidation and discrimination from background, allowing for rapid untargeted analysis. The inclusion of ion mobility spectrometry would allow isobaric compounds to be analyzed at the same time[230–232], however, this would pose challenges for onsite analysis. Selective derivatization could also be an appropriate approach to distinguish isomers, as in the case of the epoxidation of lipids.[233] Further studies into the optimization of SPME arrow for the extraction of contaminants from biological tissues, aerosols and humic substances would allow the rapid onsite analysis of these matrices with minimal background interferences, permitting reliable quantitation in the field.

Acknowledgements

This work was funded by the National Oceanic and Atmospheric Administration (NOAA), award # NA18OAR4170100 (Ohio Sea Grant College Program R/PS-056 subaward # 60074859) and supported by Restek Corporation through the Restek Academic Support Program. The authors are grateful to Dr. Brian Musselman for enabling the use of the TDU-DART in our laboratory and Dr. Gary Stidsen for the development of customized SPME arrows with different coating thicknesses and lengths. The authors are also grateful to Dr. German Gomez and Dr. David Bell for the encouragement in pursuing this project and the useful scientific discussions.

Chapter 6

Rapid Screening and Quantification of PFAS Enabled Through SPME-DART-MS

Manuscript Under Review

Ronald V. Emmons, William Fatigante, Aghogho A. Olomukoro,

Brian Musselman, Emanuela Gionfriddo

Abstract

Per- and polyfluoroalkyl substances (PFAS), an emerging class of toxic anthropogenic chemicals persistent in the environment, are currently regulated at the low part-per-trillion level worldwide in drinking water. Quantification and screening of these compounds currently rely primarily on liquid chromatography hyphenated to mass spectrometry. The growing need for quicker and more robust analysis in routine monitoring has been, in many ways, spearheaded by the advent of direct ambient mass spectrometry (AMS) technologies. Direct analysis in real time (DART), a plasma-based ambient ionization technique that permits rapid automated analysis, effectively ionizes a broad range of compounds, including the negative ionization of PFAS. This work evaluates the performance of DART-MS for the screening and quantification of PFAS of different chemical classes, employing a central composite design (CCD) to better understand the

interactions of DART parameters on their ionization. Furthermore, in-source fragmentation of the model PFAS was evaluated based on the evaluated DART parameters. Preconcentration of PFAS from water samples was achieved by solid phase microextraction (SPME) and extracts were analyzed using the optimized DART-MS conditions, which allowed obtaining linear dynamic ranges (LDR) between 10 and 5000 ng/L and LOQs of 10, 25 and 50 ng/L for all analytes. Instrumental analysis was achieved in less than 20 s per sample.

6.1 Introduction

The analysis of per- and polyfluoroalkyl substances (PFAS) has become critical for routine environmental monitoring, as their presence in drinking water, seafood and other sources has been repeatedly documented throughout the world.[234] Used in various industrial and consumer products such as firefighting foam, non-adhesive cookware and stain-resistant materials,[235–237] these compounds are highly persistent in the environment due to their remarkable chemical stability. Studies have shown these chemicals to contribute toward various human health risks such as diabetes and high blood pressure,[238–241] since then many agencies have proposed increasingly lower drinking water limits for these chemicals. The World Health Organization (WHO) has recommended limits of 100 part-per-trillion (ng/L) for perfluorooctanoic acid (PFOA) and perfluorooctane sulfonic acid (PFOS), two commonly detected legacy PFAS.[242] The US Environmental Protection Agency (EPA) set limits of 70 ng/L for these compounds in 2016, the interim health advisory set at even lower concentrations of 0.004 ng/L for PFOA and 0.02 ng/L for PFOS

in 2022.[243] In addition, this health advisory also set limits of 10 ng/L for hexafluoropropylene oxide dimer acid (GenX) and 2000 ng/L for (perfluoro-1-butanesulfonate) PFBS. In response to the ever-increasing need for ultra-trace analysis of PFAS, highly sensitive techniques must be developed with increasing focus on higher sample throughput for both screening and quantification of these contaminants.

The chemical structure of PFAS varies across different classes, the hydrophobic fluorinated alkyl chain attached to different hydrophilic groups. Most commonly this polar group is a carboxylic acid or sulfonic acid moiety, more recently developed PFAS also containing ether linkages to promote environmental degradation.[244,245] As such, analytical approaches must take these major classes into account. Conventionally, analysis is performed utilizing LC-MS/MS techniques.[241,246–248] While these methods are highly sensitive and allow effective separation of isomeric species, alternative techniques such as direct ambient mass spectrometry (AMS) can enable higher sample throughput, ideal for screening purposes.[249] The plasma-based AMS technique Direct Analysis in Real Time (DART) enables high throughput screening and quantification of various classes of molecules for both positively and negatively ionized species.[231,250–254] Furthermore, there has been recent interest in the DART analysis of PFAS, results from Cody and Maleknia demonstrating robust ng/L-level quantification of PFOA and the screening of various other PFAS such as PFOS, using coated glass capillaries (CGCs) with octadecylamine as an extraction device for PFAS.[255] In fact, many developed AMS methods benefit from analyte preconcentration prior to instrumental analysis.[256,257] Previous work from our research group has demonstrated the use of solid phase microextraction (SPME) devices composed of hydrophilic-lipophilic balance – weak anion exchange particles embedded in

polyacrylonitrile (HLB-WAX/PAN) as an ideal candidate for the preconcentration of multiple classes of PFAS , allowing sub-ng/L detection when coupled with LC-MS/MS.[248,258]

To the authors' knowledge, there has been few studies coupling SPME and DART for the quantitative analysis of PFAS.[255] Furthermore, no exploration of the effects of the various DART parameters on the ionization and detection of PFAS across multiple classes or the chemistry of the sample solution has been performed. This work investigates the effect of various DART parameters with a multi-variate experimental design, central composite design (CCD), to better understand the interactions and roles of each parameter involved in PFAS ionization mechanisms. Four model analytes, PFOA, PFOS, GenX, and PFBS were investigated due to their varying physicochemical properties and relevance in current regulatory efforts.

6.2 Materials and Methods

6.2.1 Chemicals

PFAS standards (PFOA, PFOS, PFBS and GenX) were purchased from AccuStandard (New Haven, CT, USA). Physicochemical data and structures can be found in Table 6.1 and Figure 6-1, respectively. Isotopically labelled internal standards ($^{13}C_8$-PFOA, $^{13}C_8$-PFOS, $^{13}C_3$-GenX) were purchased from Wellington (Ontario, Canada). Ammonium formate was obtained from Fisher Scientific (Waltham, MA, USA). HLB-WAX particles were purchased from Waters Corporation (Milford, MA) and PAN from Millipore Sigma (Bellefonte, PA, USA). N,N-dimethylformamide was obtained from Acros Organics (Pittsburgh, PA, USA). Nitinol wire was purchased from Component Supply Company (Sparta, TN) and stainless-steel blades from Yarder Manufacturing

Company (Toledo, OH). HLB-WAX/PAN SPME devices were developed according the methods outlined in previous works.[248,258] Ultra-pure water was collected from a Nanopure Infinity System (Barnstead, Thermo Fisher Scientific).

Table 6.1 Physicochemical properties of the model analytes.

Compound	Molecular weight (g/mol)	Log P
Perfluoro-n-octanoic acid (PFOA)	414	5.11
Hexafluoropropylene oxide dimer acid (GenX)	330	3.66
Perfluoro-1-butanesulfonate (PFBS)	300	2.63
Perfluoro-1-octanesulfonate (PFOS)	500	5.43

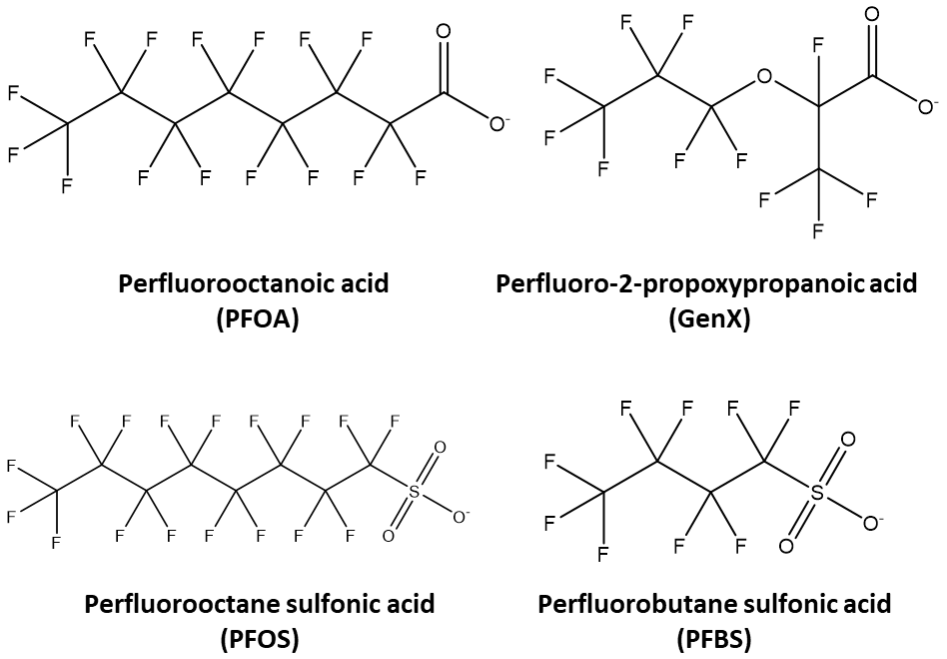

Figure 6-1 Structures of model analytes in their ionic form.

6.2.2 Instrumentation

Method optimization, fragmentation studies and CCD experimentation were all performed on a DART-SVP (Bruker Scientific LLC, Billerica, MA, USA) hyphenated to a LTQ XL ion trap MS (Thermo Fisher Scientific, San Jose, CA, USA). MS parameters include a scan of 80 to 520 m/z with a 10 ms maximum injection time and 1 µscan, the MS set to a "normal" speed setting. Quantification was performed on a DART-SVP hyphenated to a Bruker EVOQ Elite (Bruker Scientific LLC, Billerica, MA, USA). MS/MS conditions are described in Table 6.2.

Table 6.2 Mass spectrometer parameters for the Bruker EVOQ Elite.

Compound	Q1 mass	Q2 mass	Internal Std.	CE (V)
PFOA	413.0	369.0	$^{13}C_8$ PFOA	5
GenX	285.0	185.0	$^{13}C_3$ GenX	15
PFBS	299.1	80.0	$^{13}C_3$ GenX	50
PFOS	498.8	98.8	$^{13}C_8$ PFOS	40
PFOS	498.8	80.0	$^{13}C_8$ PFOS	40
$^{13}C_8$ PFOA	421.0	376.0	-	5
$^{13}C_3$ GenX	287.0	185.0	-	15
$^{13}C_8$ PFOS	507.0	80.0	-	40

6.2.3 Sample Preparation

The sample preparation procedure and development of SPME devices was adapted from Olomukoro et al.[248,258] SPME devices (fibers and blades) consisting of hydrophilic-lipophilic balance particles embedded in polyacrylonitrile (HLB-WAX/PAN) were used (Figure 6-2). The extraction procedure was carried out in 2 mL glass vials with a PTFE cap, the volume of sample 1 mL and agitation of 1000 rpm (vortex agitation) for 30 min. Subsequently, the device was desorbed for 20 min in a 500 µL plastic vial containing 150 µL of 80:20 methanol:water desorption solution with 0.5 % (w:w) ammonium formate for the SPME fiber procedure. For SPME blades, desorption was in 250 µL of methanol:water desorption solution with 2 % (w:w) ammonium formate. All calibration levels were performed in triplicate.

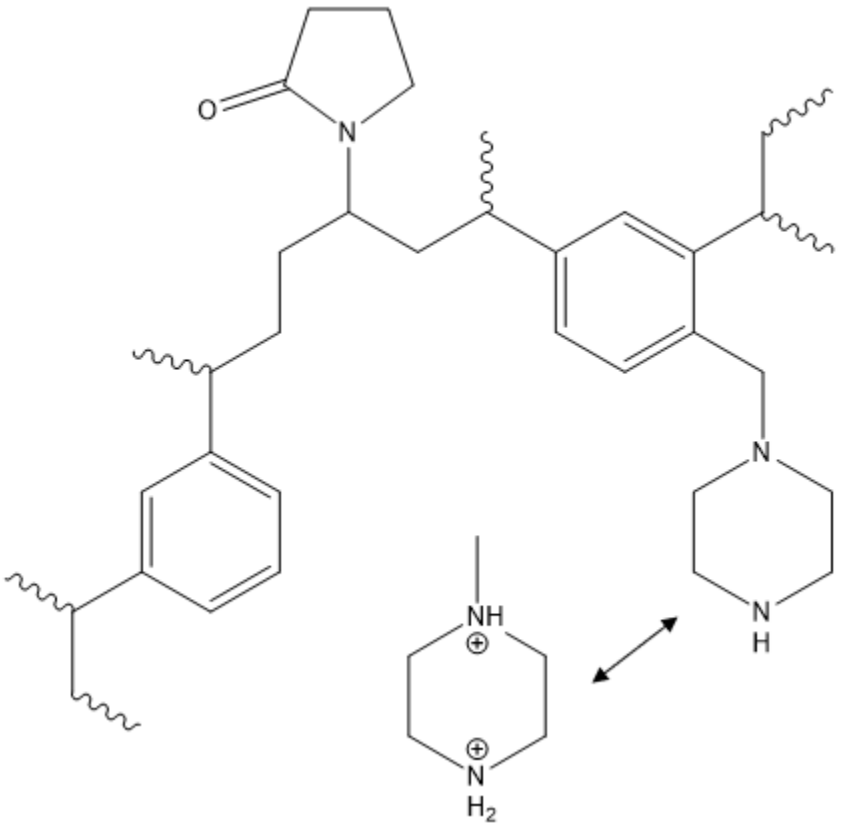

Figure 6-2 Hydrophilic-lipophilic balance/weak anion exchange structure.

6.2.4 Direct Analysis in Real Time

Unless otherwise noted, all DART optimization consisted of spiking 5 µL of a 1 ppm solution of PFAS in methanol onto a QuickStrip (Figure 6-3) in triplicate. A circumscribed central composite design (CCD) was performed with 3 major variables (e.g. electric grid voltage, plasma heater temperature, interface pressure).[259–261] Optimal DART parameters were found to be -50 V for the electric grid and 897 mbar for the interface pressure. Plasma heater values were optimized separately for carboxylic and sulfonic acid-containing PFAS, optimal temperatures being 250 °C and 400 °C for carboxylic and sulfonic acids, respectively (Table 6.3). For each parameter investigated, lower and upper levels of the design were chosen based on the operable conditions of

the DART system, the design of the CCD being described in Table 6.4. Each level of the experiment was performed randomized in triplicate.

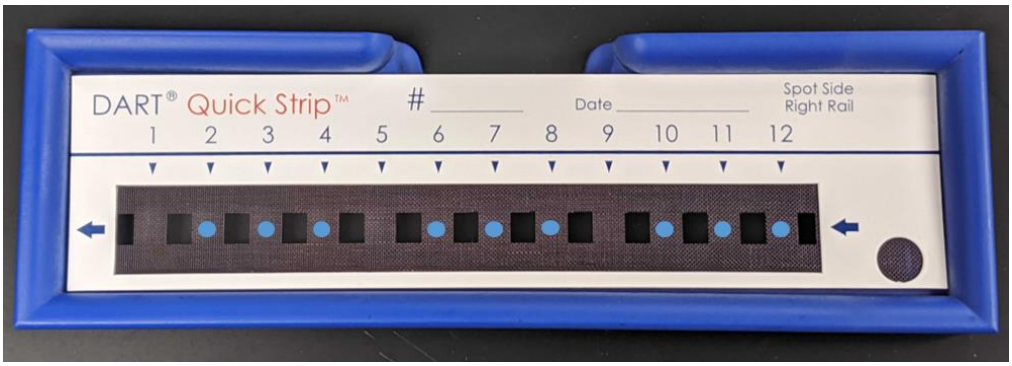

Figure 6-3 Example of sample loading on the QuickStrip, blue dots denoting sample spots with unspiked stainless-steel mesh between each triplicate.

Table 6.3 Optimal DART parameters for each PFAS class.

	PFAS Class	
Parameter	**Carboxylic**	**Sulfonic**
Plasma Temperature	250 °C	400 °C
Voltage	-50 V	-50 V
Pump	897 mbar	897 mbar

Table 6.4 Experimental values used for the DART central composite design (CCD) experiment.

Parameter	Level			Star Points (α = 1.68)	
	Low (-)	Central (0)	High (+)	-α	+α
Electric Grid Voltage (V)	-100	-200	-300	-33	-367
Plasma Temperature (°C)	175	275	375	107*	442*
Interface Pressure (mbar)	897	914	931	884	945

*Due to practical limitations on the temperature controller, the plasma temperature star points were experimentally values of 100 °C and 450 °C in lieu of their calculated values (107 and 442 °C)

6.2.5 Data Analysis

Data obtained for optimization and evaluation of DART and sample composition parameters were obtained and integrated using Xcalibur software (Thermo Fisher Scientific, San Jose, CA, USA) and processed using Excel 2016 (Microsoft Corporation, Albuquerque, NM, USA). The circumscribed CCD model was developed, visualized and evaluated using STATISTICA 12.0 (StatSoft, Tulsa, USA). Prism 5 (Graphpad Software, La Jolla, CA, USA) was used to present calibration curves.

6.3 Results and Discussion

6.3.1 In-source Fragmentation

There are multiple parameters that influence DART ionization of analytes, primarily plasma temperature, plasma makeup (typically helium or nitrogen gas), electric grid voltage and the interface pressure of the DART-MS interface. To study these effects, the four model PFAS were chosen due to their physicochemical diversity. PFOS and PFBS both have terminal sulfonic acid moieties but contain different carbon-chain lengths (PFOS: $C_8HF_{17}O_3S$, PFBS: $C_4HF_9O_3S$), while PFOA has a terminal carboxylic acid group ($C_8HF_{15}O_2$) and GenX has both a terminal carboxylic acid moiety and an internal ether linkage ($C_6HF_{11}O_3$). Initial findings demonstrated a strong degree of in-source fragmentation for these analytes (Figure 6-4). The degree of in-source fragmentation is minor for the sulfonic acids, while the fragmentation of the carboxylic acids was pronounced enough to remove up to four CF_2 subunits with PFOA. This phenomenon is not entirely unexpected as PFAS fragmentation is thought to "unzip"[262] or continuously fragment due to rapid fluorine shifts[263] following initial decarboxylation or loss of SO_3. This results in a series of fragments with the removal of CF_2, C_2F_4, C_3F_6, etc. along a linear chain, with branches also being fragmented (in the case of GenX, a loss of CF_3-CF_1 is observed). While there have been attempts to minimize this characteristic fragmentation pattern[264], loss in sensitivity of the $[M\text{-}H]^-$ is primarily associated with the perfluoroethercarboxylic acids. This is exacerbated by heat in the ion source, in fact decarboxylation can occur at standard operating temperatures of both electrospray ionization and DART. Because of this, most developed methods opt to forgo monitoring the $[M\text{-}H]^-$ ion of perfluoroethercarboxylic acids such as GenX and instead choose its more

prominent $[M\text{-}H\text{-}CO_2]^-$ ion.[248] This phenomenon has been demonstrated to be beneficial in DART-TOF-MS analysis, the fragmentation of PFOA being able to be accurately identified by its unique kendrick mass defect.[255] In this work, all model analytes exhibited in-source fragmentation as a result of removal of the CO_2 or SO_3 group by the heated plasma stream with the exception of PFOS. While sulfonic acid containing PFAS demonstrated better relative $[M\text{-}H]^-$ stability, carboxylic acid containing PFAS demonstrated a larger degree of this fragmentation at higher plasma temperatures. For these reasons, optimization experiments were carried out monitoring $[M\text{-}H]^-$ as the quantitative ion for PFOS, PFBS and PFOA and $[M\text{-}H\text{-}CO_2]^-$ for GenX.

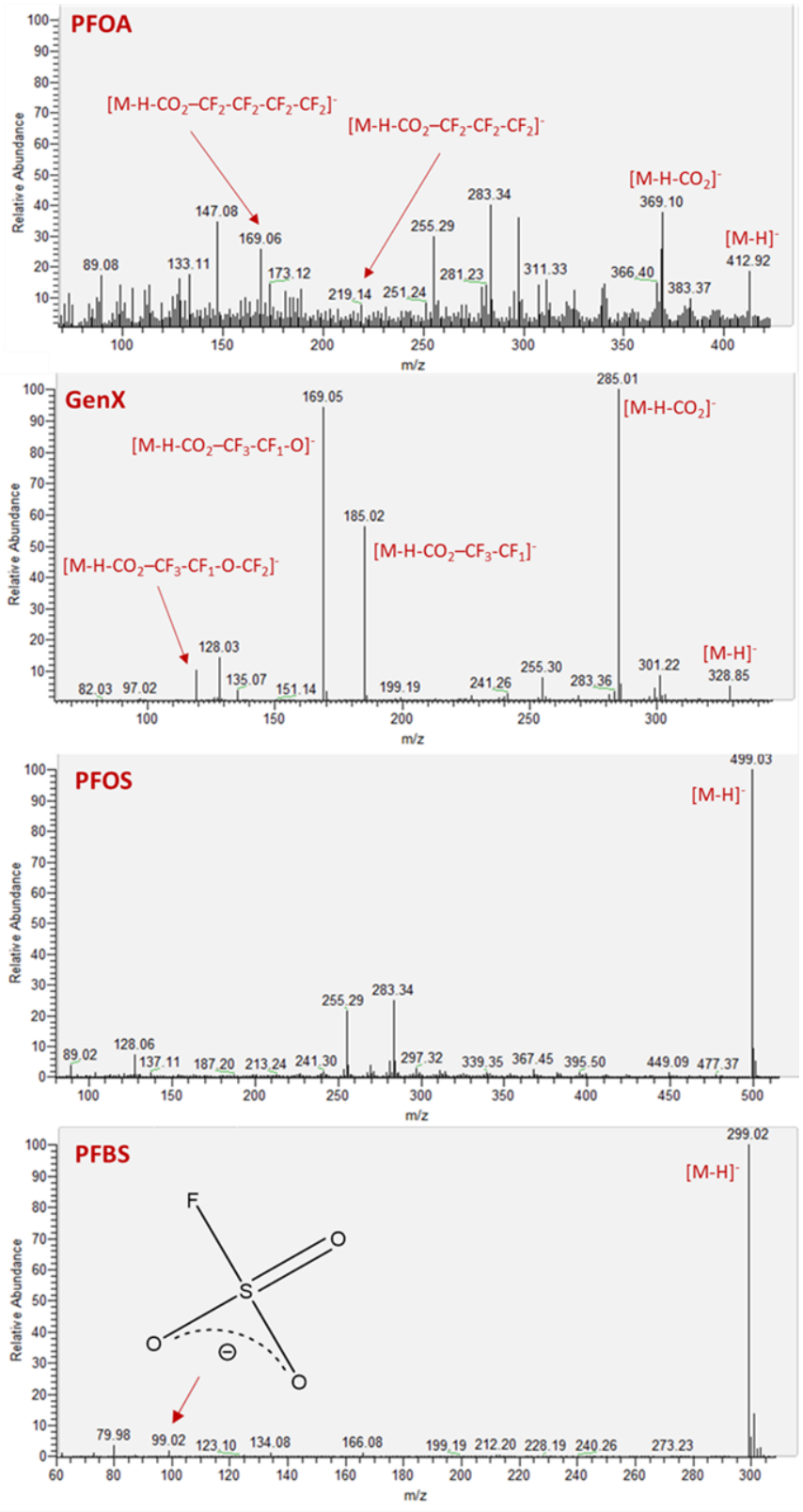

Figure 6-4 Mass spectra of in-source fragmentation of PFAS at 400 °C.

6.3.2 Central Composite Design

Due to the initial observation of in-source fragmentation for all studied model PFAS, a multi-parameter approach that accounts for the selected quantitative ions across all targeted compounds is critical. To accomplish this, a CCD experiment was performed to evaluate DART parameters. CCD is a type of a formal design of experiments (DoE), which allows efficient multivariate modeling of all selected independent variables enabling not only the response optimum to be found but also the interactions between those variables.[261] The basis of CCD is that the measured response is dependent on several factors or independent variables which can be controlled in their operable conditions.[260,265] In our experimental design, we chose three variables (plasma temperature, electric grid voltage and interface interface pressure) with 3 levels. These levels include 2 endpoints near the end of the operable DART conditions and a centerpoint, which can be visualized as -1, 0 and +1 (or in the case of electric grid voltage, -100, -200 and -300 V). To ensure the integrity of the design along the entire studied region, it is important to ensure rotability, meaning the prediction error will be the same for two points that are the same distance from the center point. This is accomplished through proper introduction of axial or "star" points. For a 3-factor circumscribed CCD, this is calculated as $\alpha = \sqrt[4]{8} = 1.68$. This value, also tested in both the positive and negative space, is then tested for each variable. In the case of electric grid voltage, the values tested are -33 and -367 V. The experimental design is described in Table 6.4. All variables tested in the CCD are in Table 6.5 totaling 8 experiments evaluated at each chosen level, 6 experiments for axial points, and 6 central point values (0,0,0). These 20 experiments were performed in triplicate, two independent CCDs were performed using helium and nitrogen plasma. As helium was found to permit

higher sensitivity, initial discussion on the CCD results highlight the interactions associated with helium. Results for GenX and PFOS ionization in helium plasma are demonstrated in Figure 6-5, with the Vapur interface pressure set at 897 mbar. Pressure was measured at the interface capillary, results from pressure optimization vs plasma temperature for GenX found in Figure 6-6. Response was found to be greater with increasingly stronger vacuum, almost doubling with pressure changes as small as 17 mbar.

Table 6.5 Central composite design of DART conditions with three factors and three levels.

Experiment	Label	Electric Grid Voltage (V)	Plasma Heater Temperature (°C)	Interface Pressure (mbar)
15	Factorial	-100	175	897
1	Factorial	-100	375	931
3	Factorial	-300	175	931
2	Factorial	-300	375	897
14	Factorial	-100	175	931
18	Factorial	-100	375	897
17	Factorial	-300	175	897
6	Factorial	-300	375	931
20	Axial	-33	275	914
8	Axial	-367	275	914
16	Axial	-200	100	914
12	Axial	-200	450	914
7	Axial	-200	275	884
11	Axial	-200	275	945
19	Center	-200	275	914
5	Center	-200	275	914
13	Center	-200	275	914
10	Center	-200	275	914
9	Center	-200	275	914
4	Center	-200	275	914

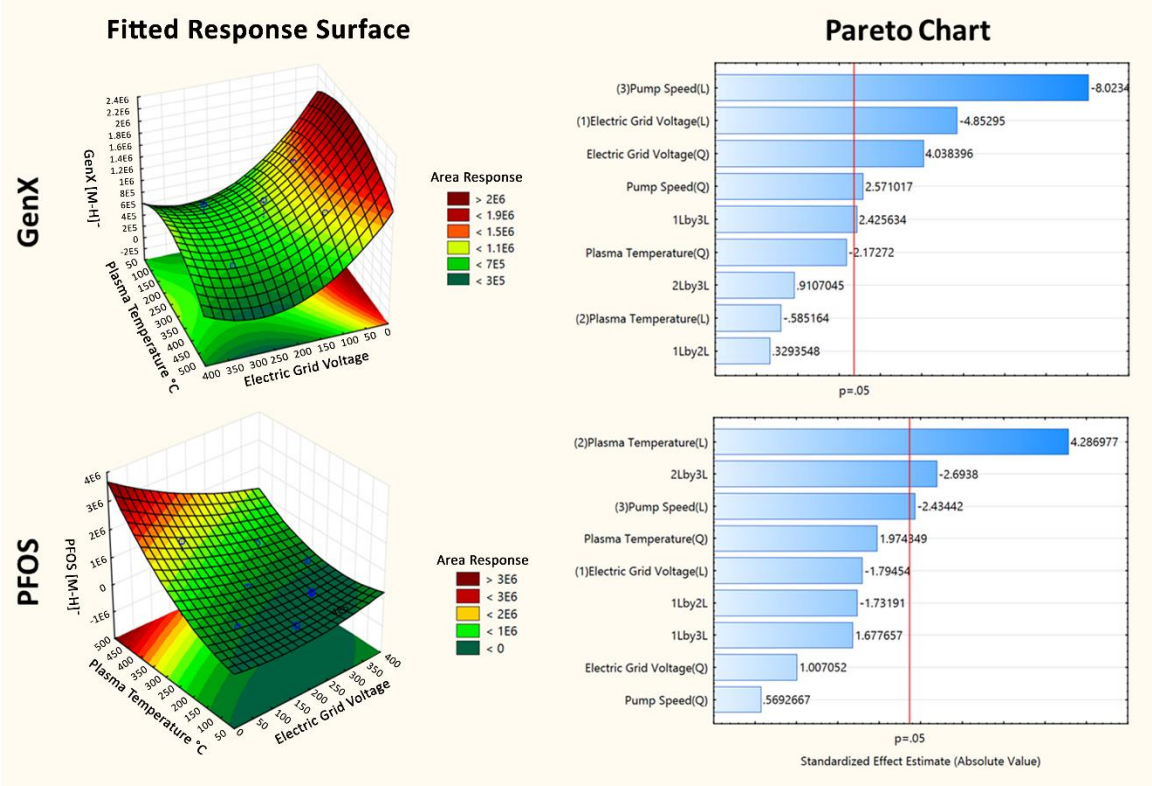

Figure 6-5 Central composite design of GenX and PFOS using helium plasma, with interface pressure kept constant (897 mbar).

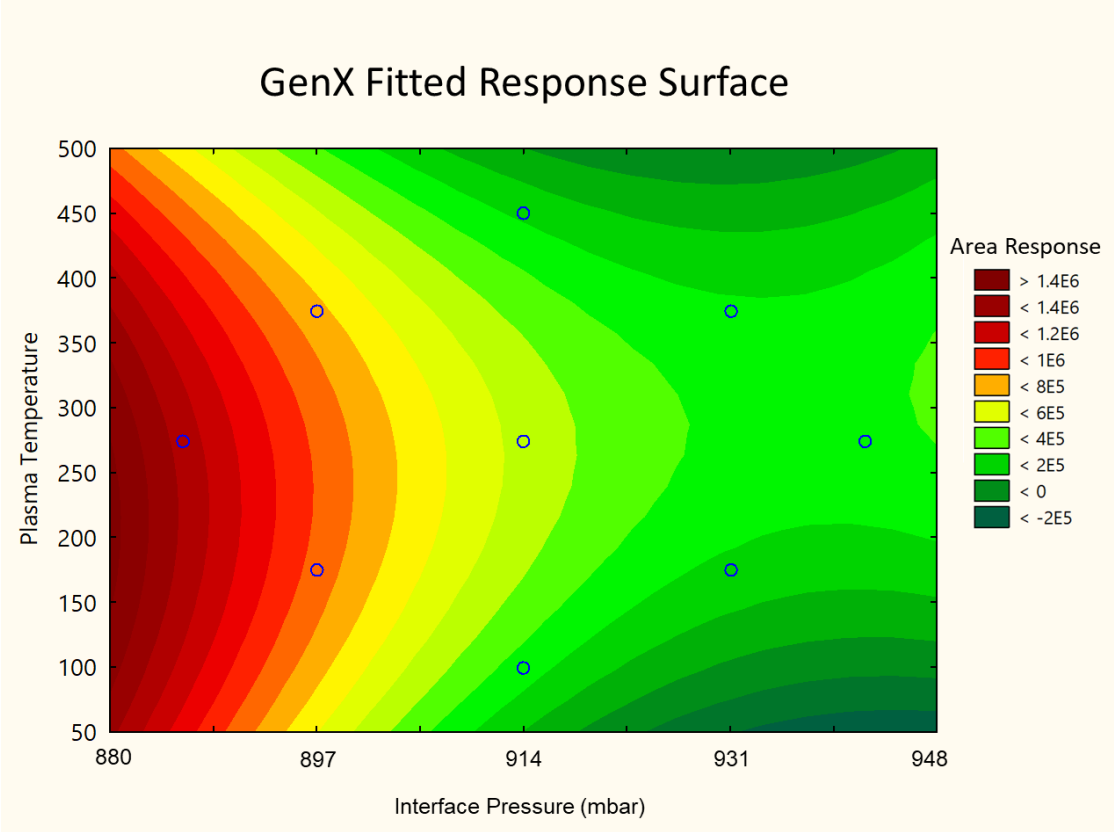

Figure 6-6 Two-dimensional fitted response surface comparing the effects of plasma temperature and interface pressure on the parent ion of GenX. Electric grid is held at a constant value of -50 V in this figure.

The fitted response surface of GenX in Figure 6-6, along with PFOA in Figure 6-7, demonstrate that the response of carboxylic acid PFAS is highly dependent on the voltage of the DART electric grid. The lower the electric grid, the greater the response is obtained. This can also be observed in their Pareto charts (Figures 6-6 and Figure 6-7, respectively), each parameter above $p = 0.05$ being a significant factor in the response of the model analyte. These electric grid voltage values are significantly lower than conventional voltages of -300-400 V, a parameter seldomly optimized in literature. This trend has also been observed in the DART-MS analysis of positive ion species as well,[185] it being posited that the voltage applied to the electric grid could be negatively affecting the transmission of ions to the MS inlet. Comparing the mass spectra obtained between the

two end points at -100 and -300 V (Figure 6-8), the $[M-H]^-$ species of GenX is unable to be discriminated from noise at -300 V (m/z = 329) but is readily apparent at -100 V. This voltage played a very minor role in the response of sulfonic acids (Figures 6-6 and Figure 6-9), higher response values were obtained with lower voltage but were not statistically significant in the CCD. An optimal electric grid voltage of -50 V was chosen for all model analytes.

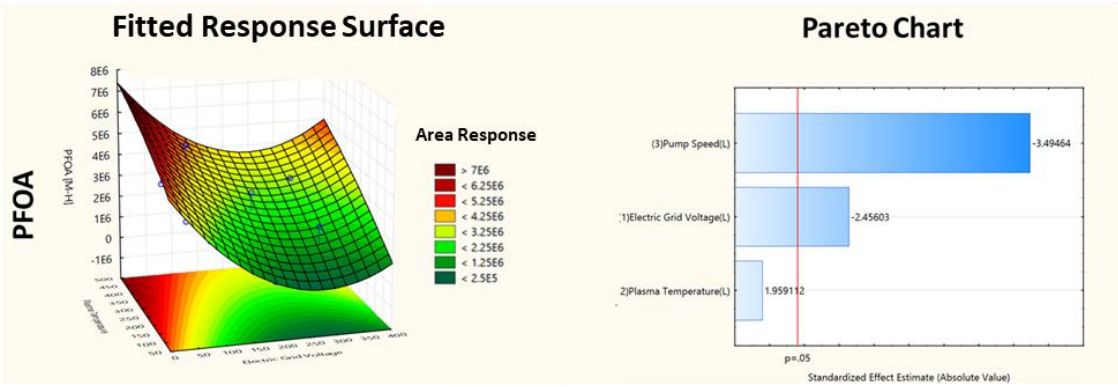

Figure 6-7 Three-dimensional fitted response surface of PFOA ionized with helium plasma. The Pareto chart indicates a low interface pressure and smaller electric grid voltage is significant in increasing the response of PFOA.

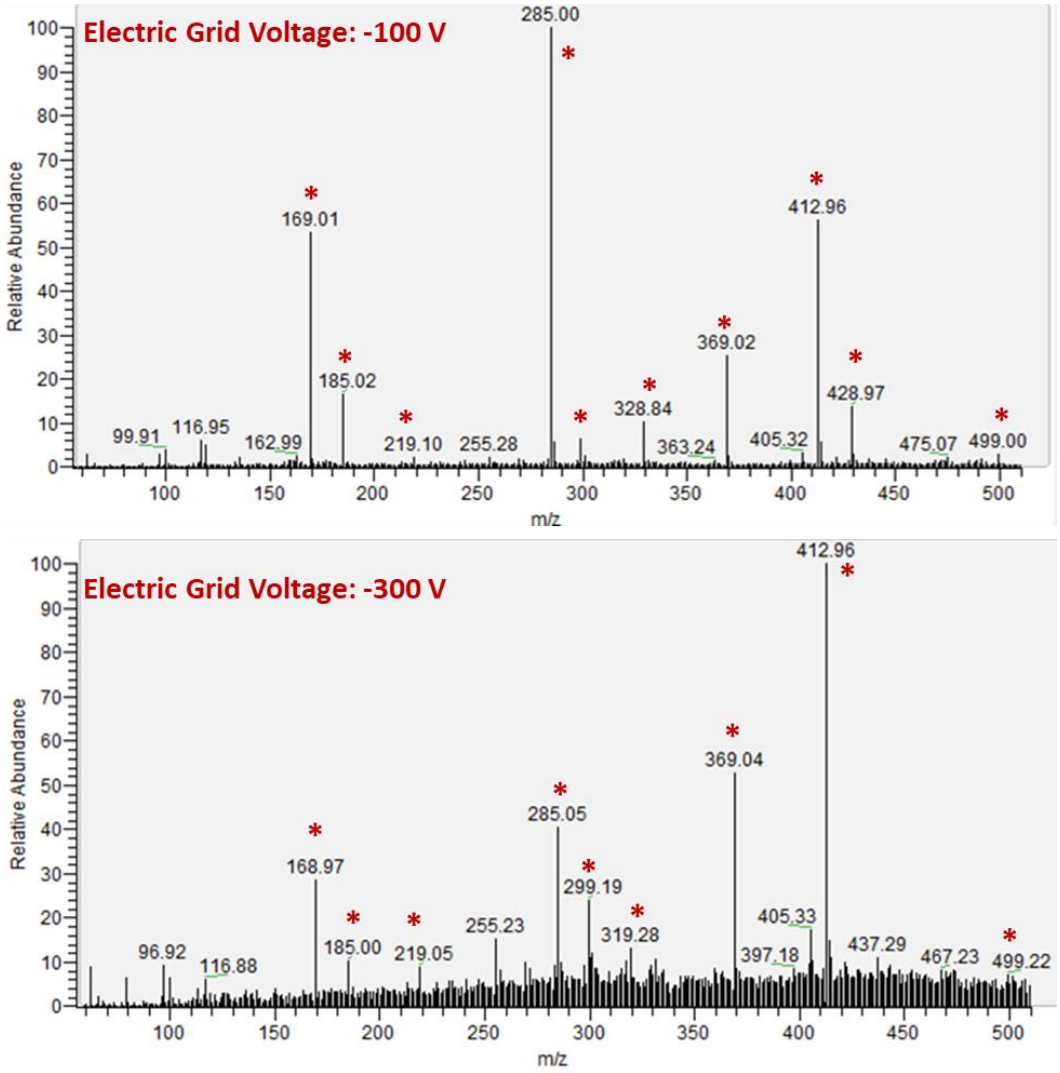

Figure 6-8 Mass spectra of all model analytes at -100 and -300 V applied to the electric grid, both performed at 375 °C plasma heater temperature with helium. Asterisks denote major PFAS ions.

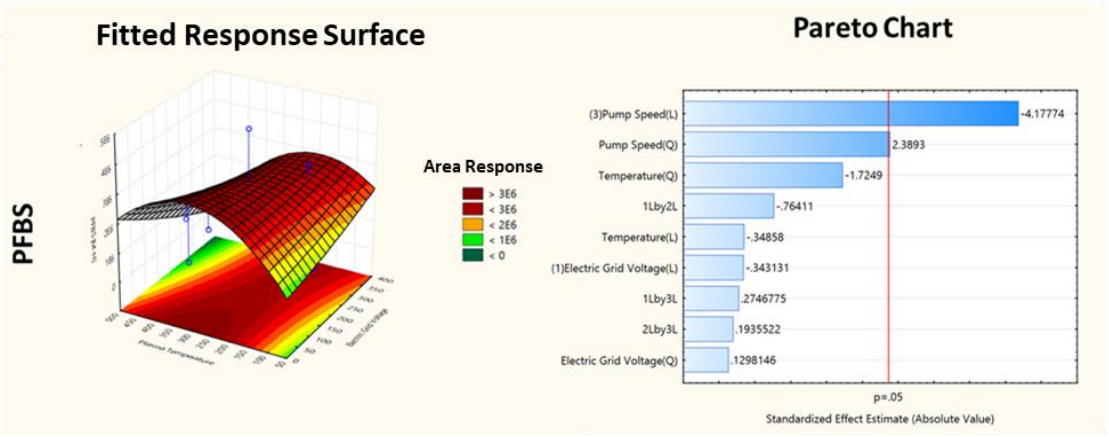

Figure 6-9 Three-dimensional fitted response surface for PFBS using helium plasma. The Pareto chart indicates low interface pressure is the major influence on PFBS response.

For plasma heater temperature, it should be mentioned that the nominal temperature recorded is the temperature of the DART ceramic heater, not the plasma stream. Measured at sample position, the temperature of the helium plasma is 122 °C with the temperature set at 200 °C. To achieve a similar temperature with nitrogen, a plasma heater temperature value of 400 °C is necessary to achieve a 127 °C plasma stream, due to nitrogen's lower heat capacity. The plasma heater temperature was found to be quite significant in response for PFOS, with no significant response on the quantitative ion of the other model analytes. In contrast to other compounds, it appears that both the sulfonic acid functionality and the length of the carbon chain of PFOS are reliant on a high plasma temperature to properly ionize. Moreover, the profile of the ion chronogram of PFOS negatively impacted by lower temperatures due to improper desorption into the ionizing gas (Figure 6-10). At the higher tested plasma temperatures, the response of GenX and PFOA are slightly reduced, most likely due to their proclivity for decarboxylation and subsequent fragmentation. This is line with past literature describing that plasma heater temperatures up to 380 °C were not

detrimental to the $[M-H]^-$ response of PFOA but resulted in an increased response of the fragment $[M-HCF_2O]^-$.[255] Most likely, $[M-H]^-$ response is able to be preserved even with more fragmentation due to the increased ionization efficiency of the heated plasma stream. In light of these results, it was decided that optimal values for plasma heater temperature for the carboxylic acids and sulfonic acids were 250 and 400 °C, respectively.

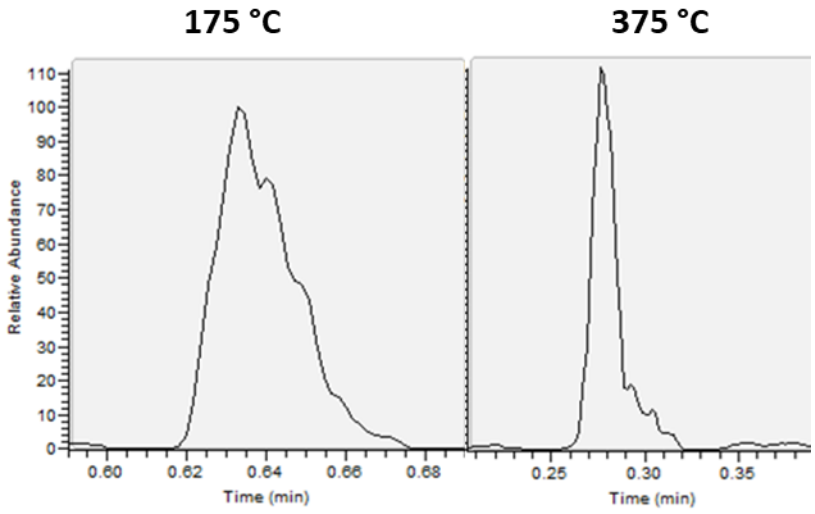

Figure 6-10 The effect of plasma heater temperature on the ion chronogram of PFOS.

The space between the DART and MS inlet in many cases requires a negative pressure interface to better direct the plasma stream and limit the amount of gas into the MS. This is operated by a membrane pump, creating a negative pressure in the interface. Pump settings were optimized between 897 and 931 mbar to evaluate the importance of analyte transmittivity in the plasma stream and ensure if there were any interactions between it and the other parameters studied. Interface pressure was found to play a significant role in response for all analytes, most interestingly for GenX and PFOS. As can be seen in the Pareto chart of Figure 6-5, interface pressure is the most significant influence on the response of GenX. However, there is also a statistically significant positive interaction between interface pressure and electric grid voltage (denoted by 1Lby3L in the Pareto chart). This implies that the influence of the electric grid voltage on GenX is not only the

ionization of the sample but also its transmittivity in the plasma stream. Likewise for PFOS, which exhibited a strong preference for high plasma temperature, there is an interaction between interface pressure and plasma temperature (denoted by 2Lby3L on the Pareto chart). This again suggests that plasma temperature plays a major role in the transmittivity of the analyte from the sample to the MS inlet. Optimal conditions for all model analytes were found to be at 897 mbar.

Nitrogen as an ionizing gas is commonly used as a much cheaper and greener alternative to helium; however, its excited state's ionization energy is significantly lower than helium's at 19.8 electron volts.[49] This can often result in lower ionization efficiency of analytes, thus lower response. Conversely, the lower ionization energy is also beneficial as it can reduce the amount of background interferences that can be ionized. The CCD performed with nitrogen plasma (Figure 6-11) demonstrated lower response for all model analytes, however, the amount of background interferences was also reduced (Figure 6-12). Moreover, the relative intensity of the $[M-H]^-$ of PFOA (413 m/z) and $[M-H-CO_2]^-$ of GenX (285 m/z) were increased compared to their fragments, indicating a softer ionization. Comparing this CCD to that of helium, low electric grid voltage plays a statistically significant role in all model analytes. Surprisingly, GenX demonstrated a strong negative correlation with higher plasma temperature. This could be due to the increased prevalence of the $[M-H]^-$ and $[M-H-CO_2]^-$ species when using nitrogen, these ions then being quickly fragmented at high plasma temperatures. Plasma heater temperature was not statistically significant for PFOS response; however, a positive trend is still demonstrated in Figure 6-10. Most likely this is due to the heat capacity of nitrogen, as the highest tested plasma heater temperature is unable to sufficiently heat nitrogen for proper PFOS desorption. Due to the reduced background, nitrogen is an ideal alternative as an ionizing gas for carboxylic

acids, however, ionization efficiency could be poor for the more temperature-dependent sulfonic acids.

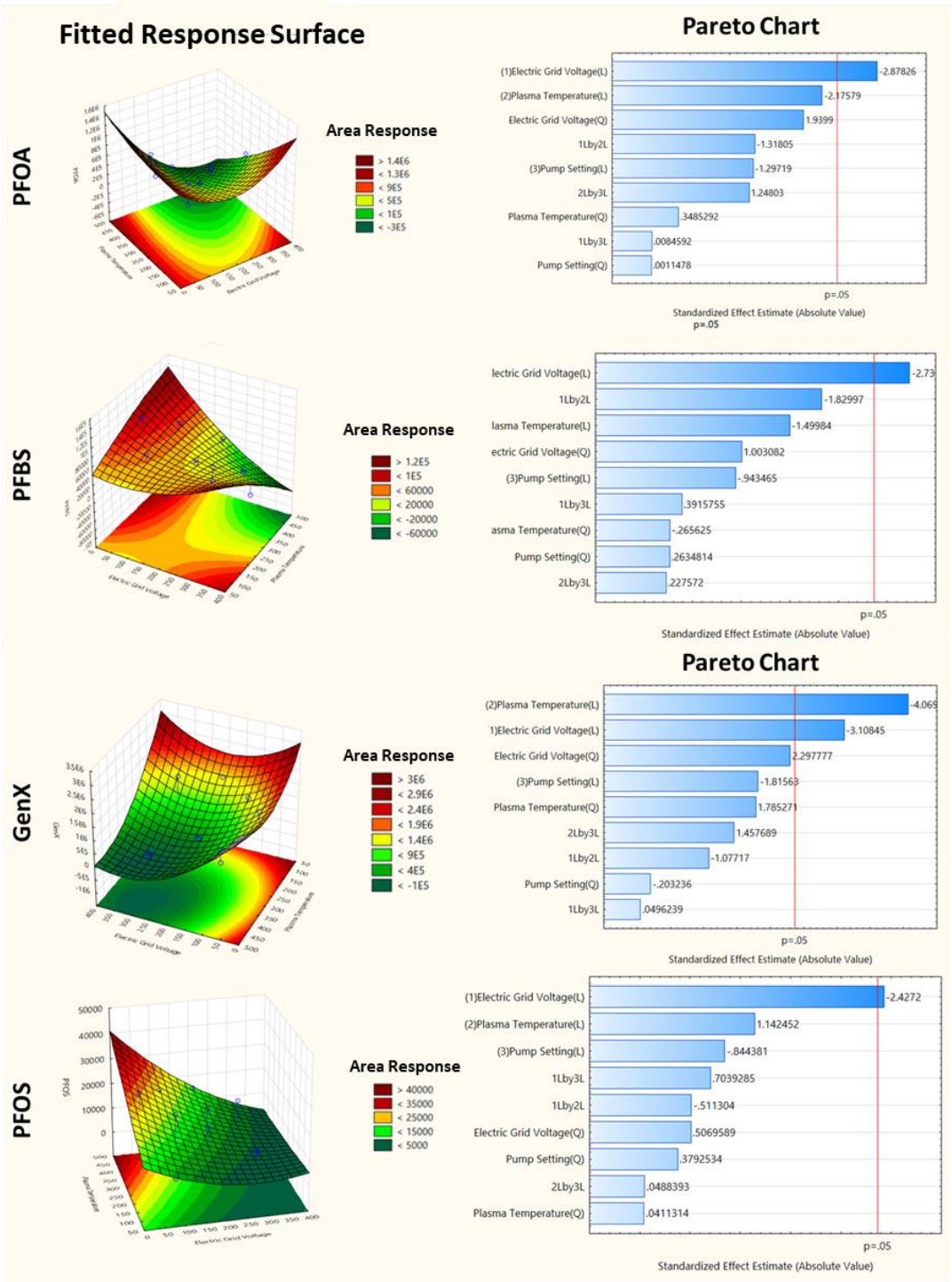

Figure 6-11 Fitted response surfaces for model analytes obtained utilizing nitrogen plasma for ionization.

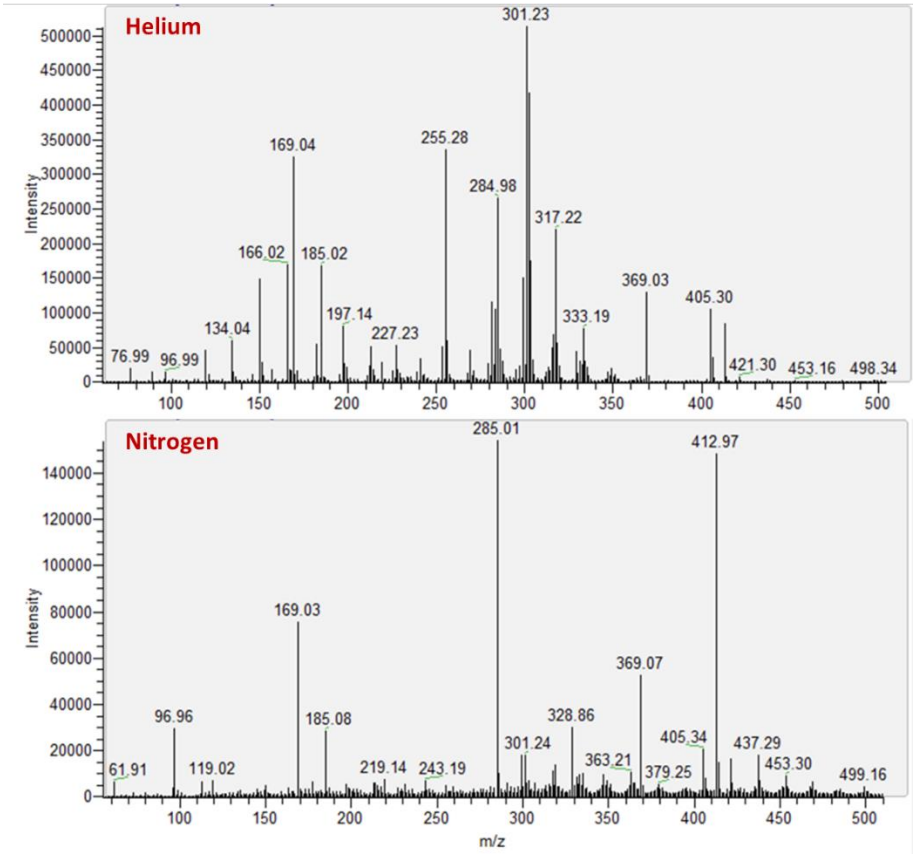

Figure 6-12 Mass spectra obtained for a mixture of model analytes using helium and nitrogen as the ionizing plasma. Experiment performed at 450 °C and -50 V.

6.3.3 Sample Preparation

Previous work in our laboratory has demonstrated that HLB-WAX/PAN SPME devices are ideal for the preconcentration of PFAS prior to instrumental analysis.[248,258] This work utilized SPME blades as they have been demonstrated to provide better sensitivity than SPME fibers for PFAS.[258] Initial findings showed no desorption of PFAS from SPME devices into DART directly, as the plasma stream was unable to disrupt the ion-exchange interaction of the analyte on the device's extraction phase. Desorption from SPME devices into DART plasma has been demonstrated in other works, utilizing neutral extraction phases.[185,206,266,267] Therefore, a liquid desorption step was added before DART analysis.

While ammonium hydroxide was optimized as the best additive for SPME desorption for the model analytes when analyzed through LC-MS/MS,[248] ammonium formate has also been demonstrated to be effective as a desorption additive when analyzing a larger scope of PFAS.[258] Demonstrated in Figure 6-13, results indicate that the presence of these additives increase response substantially for sulfonic acids, particularly with the addition of ammonium formate. As negative DART ionization is believed to be initiated by thermal electrons in ambient conditions, the addition of dopants such as different solvents or salts can play a major role in method sensitivity.[216]

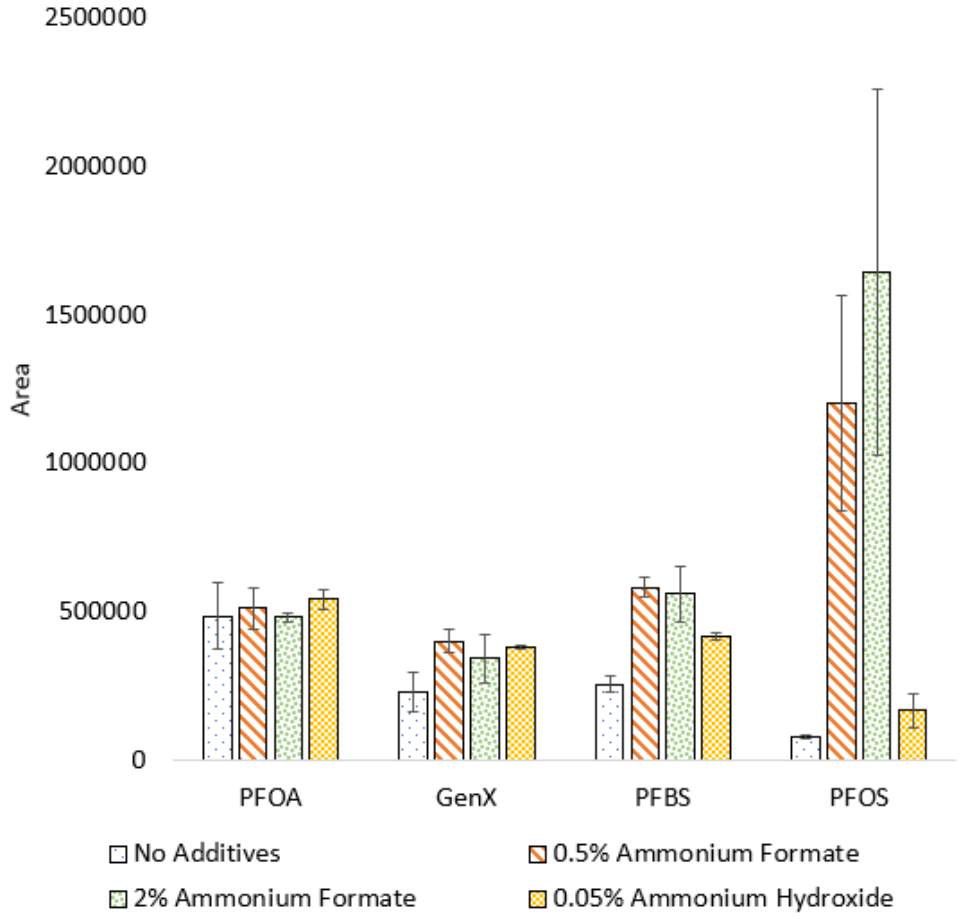

Figure 6-13 Additive effects on the ionization of PFAS in the desorption solution, results obtained using the optimized DART conditions.

6.3.4 Method Performance

Calibrations using SPME extractions from ultra-pure water were performed on a triple quadrupole, Bruker EVOQ Elite, for enhanced sensitivity in tandem mass spectrometry conditions. Calibration levels at concentrations of 5, 10, 25, 50, 150, 500, 1000, 2500, and 5000 ng/L were analyzed in triplicate with accuracy points at concentrations of 30, 300 and 3000 ng/L. Three isotopically labelled PFAS internal standards were spiked at 250 ng/L for each concentration level. Results indicate excellent linearity for all model analytes, with linear dynamic ranges of the carboxylic acids being broader than the sulfonic acids (PFOA: 10–5000, GenX: 50–5000, PFOS: 50–2500, PFBS: 25-2500 ng/L. Reproducibility is also less than 10 % relative standard deviation for the majority of points with the exception of the calibration PFBS. An example of an ion chronogram obtained is in Figure 6-14 for PFOA between 50 and 500 ng/L. While each sample spotting on the quick strip exhibited great profile shape and discrimination from noise, it should be noted that the variability seen, in particular the spotting for 150 ng/L, is easily corrected for by correct internal standard selection. As PFBS was the only analyte without an isotopically labelled analogue, other internal standards were tested. Results demonstrate poor signal correction, with the internal standard $^{13}C_3$-GenX correcting PFBS better than $^{13}C_8$-PFOS due to its shorter chain length. Ionization variability can greatly differ with molecules of different physicochemical properties, in this case each model analyte requiring a different internal standard for robust quantitation. Calibrations for each analyte are presented in Figure 6-15, limit of quantitation (LOQ) values were all calculated as the lowest point of the calibration curve which exhibited signal-to-noise (S/N) values above 10 (Table 6.6). Moreover, the accuracy and reproducibility were evaluated for each

accuracy point within the calibration range. With the exception of PFBS, all analytes demonstrated accuracy between 80 – 120 % and reproducibility less than 20 % relative standard deviation (Table 6.7). While the $^{13}C_3$ GenX was able to correct for most of the variability of PFBS within the calibration curve experiment, it was unable to correct for the analyzed accuracy points. This further illustrates not only the importance of internal standard selection but also the unique ionization chemistry of each PFAS.

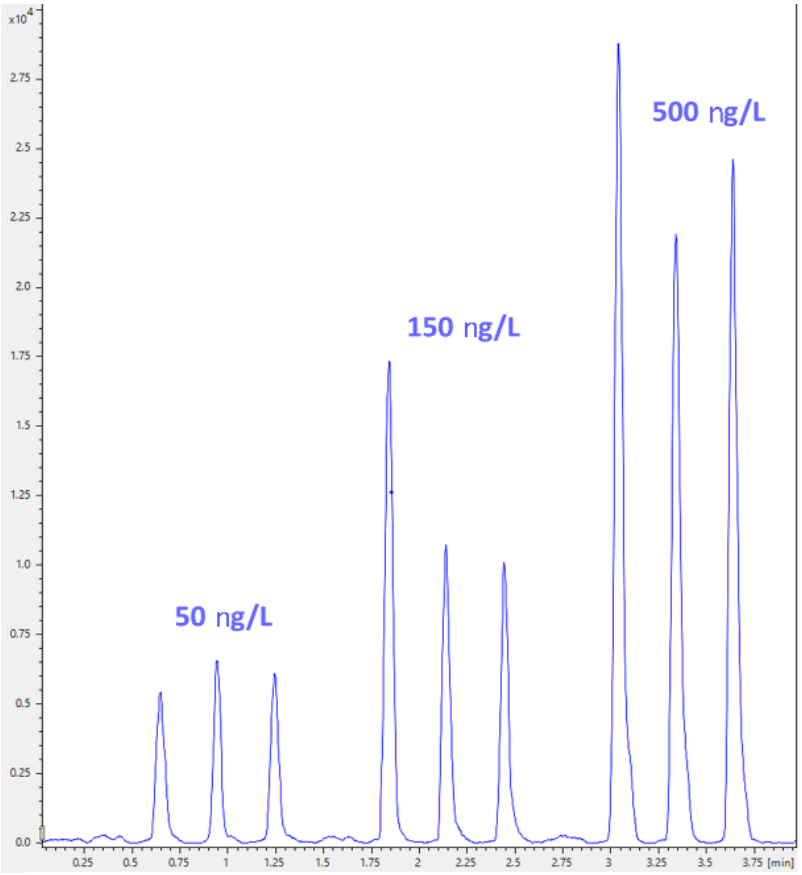

Figure 6-14 Ion chronogram of PFOA for the concentration range of 50 – 500 ng/L, in triplicate with a blank QuickStrip spot between each concentration level. Variability in response is corrected by the internal standard C^{13}-PFOA.

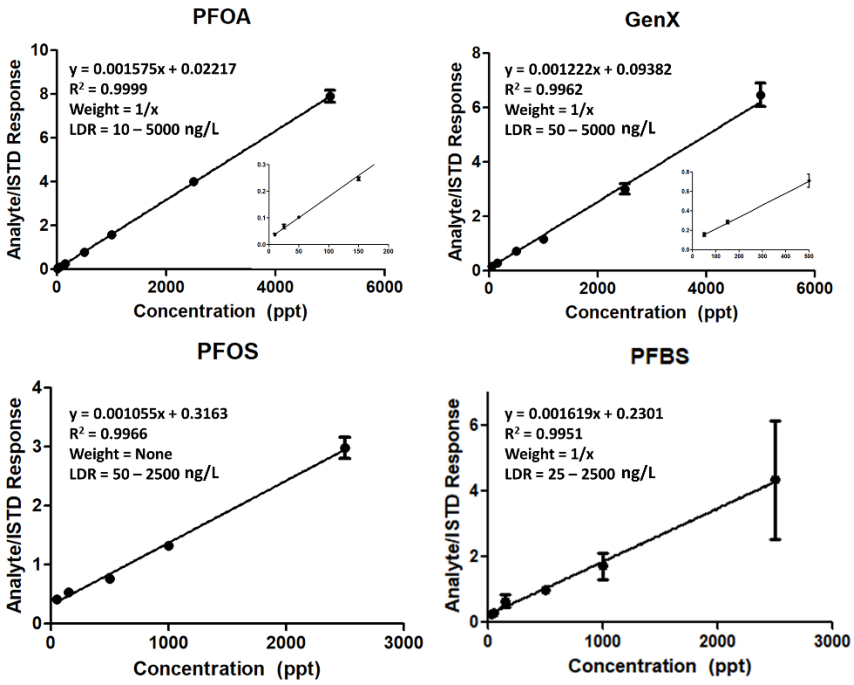

Figure 6-15 Calibration curves of all analytes using the developed SPME-DART-MS approach.

Table 6.6 Method performance of the SPME blade calibration utilizing helium plasma.

Model Analyte	LDR (ng/L)	R^2	LOQ (ng/L)	S/N*	Weight
PFOA	10 – 5000	0.999	10	12.0	1/x
GenX	50 – 5000	0.996	50	10.1	1/x
PFOS	50 – 2500	0.997	50	13.9	-
PFBS[ɣ]	25 – 2500	0.995	25	18.2	-

* Signal-to-noise (S/N) calculated at LOQ of each calibration using the ASTM method.

[ɣ] Accuracy points inadequate to verify robustness of calibration curve.

Table 6.7 Accuracy points for the SPME blade calibration performed with helium plasma.

Model Analyte	30 ppt	300 ppt	3000 ppt
PFOA	100.9 (19.7)	97.2 (1.1)	94.2 (1.9)
GenX	-	93.7 (4.4)	94.2 (1.7)
PFOS	-	84.5 (17.3)	-
PFBS	-78.7 (25.8)	94.9 (40.2)	-

*Data represented in accuracy percent followed by relative standard deviation in parenthesis

6.4 Conclusions

This study evaluated the robustness of SPME-DART-MS/MS for the quantitation of multi-class PFAS by using a multi-variate approach, enabling a better understanding of the parameters which effect PFAS ionization and introduction to the MS inlet. All model analytes studied exhibited different behavior and variable interactions in the developed CCD due to their differing physicochemical properties. These results indicate the need for parameter optimization of multi-class analytes when developing these methods, as small differences in chemical structure can influence variable interactions. The developed method allows robust quantitation of PFAS enabled through SPME coupled to DART-MS; however, it was discovered that the selection of isotopically labelled internal standards is especially critical as even a small change in physiochemical properties can create unique variability in the ionization process. Moving forward, the hyphenation of DART to high resolution mass spectrometry would allow better sensitivity and screening potential, the use of Kendrick mass defect being essential in this effort.

Acknowledgements

This project was funded in part by the National Oceanic and Atmospheric Administration (NOAA), award # NA18OAR4170100 (Ohio Sea Grant College Program R/PS-056 subaward # 60074859), the NSF CAREER grant #2144591, and further supported by the American Chemical Society Division of Analytical Chemistry Graduate Fellowship Program sponsored by PittCon.

Chapter 7

Leveraging Multi-mode Microextraction and Liquid Chromatography Stationary Phases for Quantitative Analysis of Neurotoxin β-N-methylamino-L-alanine and other non-proteinogenic amino acids

Adapted from a paper published in *Journal of Chromatography A*[16]

Ronald V. Emmons, Endri Karaj, Erasmus Cudjoe, David S. Bell,

L.M. Viranga Tillekeratne, Emanuela Gionfriddo

Abstract

Effective quantitative analysis of BMAA (β-N-methylamino-L-alanine) and its isomers without the need for derivatization has always been an analytical challenge due to their poor retention and separation on various liquid chromatography stationary phases. Previous studies that utilized conventional hydrophilic interaction chromatography (HILIC) demonstrate false negatives compared to reverse-phase workflows with derivatization. This work evaluates the chromatographic behavior of BMAA and its isomers, in their underivatized forms, on selected stationary phases, in particular

[16]Reprinted from Journal of Chromatography A, 2022, 1685, 463636. Copyright © Elsevier

fluorophenyl-based columns, to attain effective retention and separation. Detection and quantification were achieved with an ion-trap mass spectrometer. Extraction and preconcentration were achieved via solid phase microextraction (SPME) by assessing the effectiveness of multiple extraction phases, including hydrophilic-lipophilic balanced (HLB) and mixed-mode (MM). A MM extraction phase consisting of C_8 and benzene sulfonic acid moieties permitted the ideal extraction performance of BMAA and its isomers (2,4-diaminobutyric acid, DABA; N-(2-aminoethyl) glycine, AEG). Chromatographic separation was achieved within 8 min on a fluorophenyl stationary phase, ensuring high throughput without derivatization, and showing exceptional improvement from conventional HILIC methods. Limits of quantification in water for BMAA and AEG were 2.5 µg L^{-1} and DABA was 5 µg L^{-1}, with linear dynamic ranges from 2.5 µg L^{-1} - 200 µg L^{-1} for BMAA and AEG and 5 µg L^{-1} - 200 µg L^{-1} for DABA.

7.1 Introduction

Low-molecular weight cyanobacterial neurotoxins, in particular β-N-methylamino-L-alanine (BMAA) and its structural isomers (2,4-diaminobutyric acid, DABA; N-(2-aminoethyl)glycine, AEG), have been linked to progressive neurodegenerative diseases such as amyotrophic lateral sclerosis (ALS) and Alzheimer's disease (AD).[268–271] These non-proteinogenic amino acids are released from cyanobacteria and readily bioaccumulate at various trophic levels, ranging from the seeds of the cycad tree[272] to blue crab[273]. Currently, the most established theory of their neurotoxicity is incorporation into protein by replacing L-serine, resulting in misfolding and the formation of protein aggregates in the brain.[271] The human health impact of this class of compounds has been readily

demonstrated in the Guam population, their traditional diet consisting of flour and meat containing high levels of BMAA.[272] Consequently, a high incidence of amyotrophic lateral sclerosis-parkinsonian dementia complex (ALS-PDC) can be observed within the Guam population. Reportedly, BMAA has been measured in a variety of different matrices including water samples, cyanobacteria samples, fish tissue, mussels, blue crab, human blood plasma, human cerebrospinal fluid, and human brain.[274] The monitoring of these cyanobacterial neurotoxins in different matrices is essential, however, the complexity of these samples and the challenges associated to amino acid analysis have proven BMAA determination to be challenging and even a source of controversy throughout the literature.[274,275] Furthermore, as different studies employ disparate analytical procedures and techniques for such complex matrices, a consensus on the presence and distribution of these neurotoxins in food and biological specimens has been difficult to attain.[276] One of the major controversies involves the presence of BMAA in the brain of patients with AD: while a study could detect BMAA in patients' brain, subsequent work using an alternative analytical technique proposes that BMAA is not found in that same matrix.[273,274] The major differences in BMAA analysis protocols involve a derivatization step and the mode of chromatography utilized.[277]

Sample preparation of BMAA, while the specifics change depending on the matrix, commonly involves an acid hydrolysis step when analyzing biological tissues. The rationale for this being protein-associated BMAA can be present in biological specimens along with its free form.[278] Typically, acid hydrolysis is performed in 6 M HCl at 110 °C for 24 h.[279] After reconstitution, the analytes are derivatized, in most procedures, and subsequently the sample is cleaned up using solid phase extraction (SPE). Derivatization

allows amenability for reverse-phase liquid chromatography (RPLC), a recent review article reporting that 70% of studies found in the literature use this technique.[280] Another 19% of studies avoid the derivatization step and analyze the amino acids by hydrophilic interaction liquid chromatography (HILIC). Both chromatographic techniques above mentioned are often hyphenated to mass spectrometry, however, differences in detection rate among complex matrices are pronounced possibly due to discrepancies in limits of detection (LOD) or matrix effects between methods.[275] The same systematic review noted that only 57% of HILIC studies detect BMAA, in contrast to RPLC at a detection rate of 92%. Furthermore, these differences can be correlated with matrix-type, cyanobacterial samples, for example, demonstrating a 25% positive detection rate for HILIC compared to 95% when RPLC is used.[280] In light of this, further research is critical to better understand the reasons for these discrepancies and how the analysis of underivatized BMAA and its isomers can be improved further.

The separation of underivatized BMAA from its isomers has so far been accomplished through conventional HILIC chemistry. HILIC is a versatile chromatographic mode that enables the retention and separation of polar compounds, foregoing the need for derivatization. The most accepted theory of conventional HILIC retention relies on the formation of a water layer on the stationary phase, where the polar analytes partition between the aqueous layer and organic-rich mobile phase layer.[281] While HILIC allows the analysis of underivatized polar analytes, this mode often requires longer equilibration times between injections and is prone to poor retention time stability due to inadequate re-equilibration times.[282] Using conventional HILIC, it is common to use gradient programs of 30 min or more for BMAA and its isomers, while RPLC usually

provides much faster separation at around 12 min but requires a derivatization step.[273,283] Despite this, much work is still needed to develop better chromatographic strategies for these analytes. In fact, many studies use the same HILIC methods that have been demonstrated to exhibit false negatives for these analytes in complex matrices.[277] For this reason, it is necessary to consider alternative chromatographic strategies for the separation of polar analytes such as BMAA.

Fluorophenyl stationary phases, a common example being pentafluorophenyl (PFP), have been widely used for RPLC as an alternative to C_{18} when unique selectivity is needed. The versatility of these stationary phases also allows them to retain polar analytes, through what is referred to as a HILIC-like mechanism. However, a significant body of literature suggests that PFP columns behave differently than conventional HILIC, which implies a multi-mode retention mechanism. Early reports from Needham and colleagues[284] proposed that both PFP and cyanopropyl (CN) stationary phases exhibited ion-exchange properties with basic analytes at high organic mobile phase conditions (90%). The selectivity and further elucidation of this mechanism have also been explored in further detail, demonstrating that not only does the PFP ligand contribute toward a wide range of intermolecular interactions (hydrogen bonding, dipole, π-π) but the silica support itself can play a major role in a cation-exchange mechanism.[285,286] Moreover, in a study analyzing neurotransmitters such as glutamate, dopamine and γ-aminobutyric acid, PFP was used to separate these polar analytes in only 5 min including equilibration time, a much faster separation than what is conventionally labeled as HILIC.[287] This was accomplished by starting the separation with high organic mobile phases (90% acetonitrile) and using an aqueous solvent as the eluting force with no buffer system needed. It has been posited that

the retention of basic analytes on PFP could be a result of a hydrophobically-assisted ion-exchange mechanism, the ligand interacting with the small polar analyte while the accessible silanol groups interact with the positive charge (in many cases located on a nitrogen atom).[288] In brief, PFP chemistry can be used as an alternative to conventional HILIC for basic polar analytes with faster equilibration times and different chromatographic strategies.

This work provides an alternative strategy for both the extraction and chromatography of BMAA and its isomers without derivatization, consequently furthering the discussion on how the ultra-trace analysis of amino acids and similar analytes in complex media can be achieved. Solid phase microextraction (SPME), a non-exhaustive sampling technique that combines sampling, extraction and preconcentration in one step, was utilized for the first time in this work for extraction of BMAA and its isomers from water.[12,23] Various column chemistries were investigated and compared for the retention and separation of the targeted non-proteinogenic amino acids, PFP being eventually chosen as the best stationary phase for the analysis. The developed multi-mode approach not only allows the rapid analysis of these constituents with a parallel workflow to what is found in the literature, but also provides a working model for further studies investigating small polar basic compounds from both a sample preparative and chromatographic standpoint. Efficient baseline separation of these isomeric cyanotoxins is critical as they are isobars with similar fragmentation patterns. Furthermore, the developed SPME protocol can facilitate convenient toxicological and biomonitoring studies, leveraging the biocompatibility of the extraction phases used.

7.2 Experimental

7.2.1 Materials and Instrumentation

BMAA hydrochloride was purchased from Sigma-Aldrich (St. Louis, MO, USA). DABA dihydrochloride was purchased from Alfa Aesar (Ward Hill, MA, USA) and AEG was purchased from Toronto Research Chemicals Inc (Toronto, ON, Canada). DL-serine-d_3 as a preliminary isotopically labeled standard was purchased from CDN Isotopes (Pointe-Claire, Quebec, Canada). L-BMAA-HCl-d3 was synthesized as outlined in according the published manuscript of this work.[16] Molecular structures of all analytes can be found in Figure 7-1. LC-MS grade solvents (acetonitrile, methanol and water) were purchased from Birch Biotech (Morgantown, PA, USA). LC columns evaluated in this study were provided by Restek Corporation (Bellefonte, PA, USA): Force FluoroPhenyl (100 mm x 2.1 mm x 1.8 µm), Raptor FluoroPhenyl (100 mm x 2.1 mm x 1.8 µm), Pinnacle DB Cyano (100 mm x 2.1 mm x 5 µm) Pinnacle DB IBD (100 mm x 2.1 mm 1.9 µm) and Raptor Polar X (100 mm x 2.1 mm x 2.7 µm). The hydrophilic-lipophilic balance/polyacrylonitrile (HLB/PAN) and mixed-mode (MM/PAN; silica particles functionalized with benzene sulfonic acid and C_8 moieties, embedded in PAN) SPME fibers were provided by Millipore Sigma (Bellefonte, PA, USA). Hydrophilic-lipophilic balance-weak anion-exchange/polyacrylonitrile (HLB-WAX/PAN) SPME fibers were manufactured by a procedure optimized in our laboratory and described in previous work.[248]

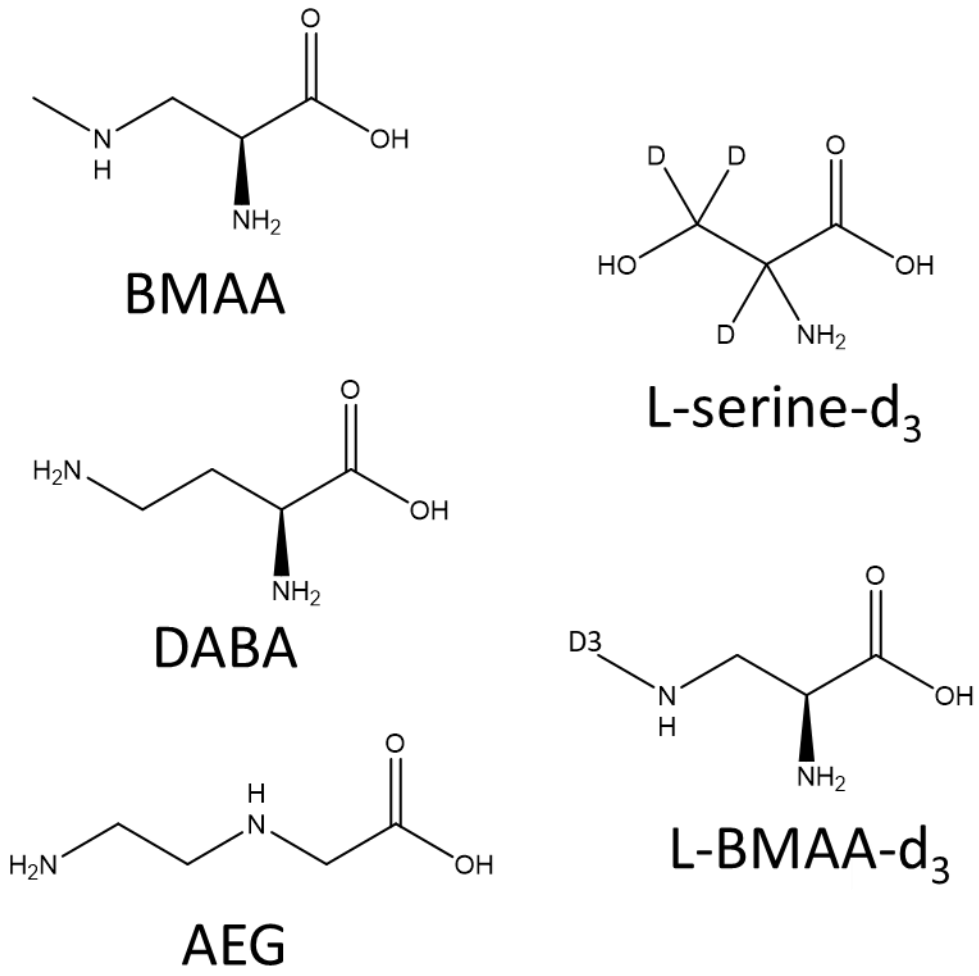

Figure 7-1 Molecular structures of BMAA, DABA, AEG, L-serine-d3 and L-BMAA-d3.

7.2.2 SPME Protocol

Extractions were carried out in a 2 mL glass vial for all optimization and method validation steps. SPME fibers were conditioned in MeOH:Water (1:1) for 30 min before each extraction prior to a brief rinse in ultra-pure water to ensure removal of residual organic phase. Sample volume was 1.5 mL and extraction was performed for 30 min with a vortex agitation rate of 1000 rpm. Fiber desorption was carried out in 150 µL of a 80:20 Water:Acetonitrile solution spiked with 0.1 % formic acid for 30 min at 1000 rpm. At the end of each experiment, SPME fibers were cleaned with 1.5 mL ultra-pure water for 10 min to ensure minimal analyte carryover.

7.2.3 Liquid Chromatography and Mass Spectrometry Conditions

Method optimization and calibration were performed on a Vanquish UHPLC hyphenated to an LTQ XL Linear Ion Trap Mass Spectrometer (Thermo Fisher Scientific, San Jose, CA, USA). After preliminary chromatographic evaluation, two mobile phase compositions and four LC gradients were evaluated for each column at a flow rate of 0.45 mL/min. Mobile phase compositions are listed in Table 7.1, the different LC gradients are presented in Table 7.2. All gradients can be further visualized in Figure 7-2. The best conditions evaluated in this study include gradient 1, mobile phase 2, Force FluoroPhenyl LC column, 40 °C column oven, 50:50 H_2O:ACN syringe wash, 10 µL sample injection. Mass spectrometric conditions are available in Appendix C, Table F.1 representing global parameters and Table F.2 analyte-specific parameters. Ionization of the analytes was performed in positive electrospray ionization (ESI) mode, a stable signal with negative ESI was not obtained. Adduct formation was not observed with these conditions. Mass spectra of all analytes can be found in Figure C-1.

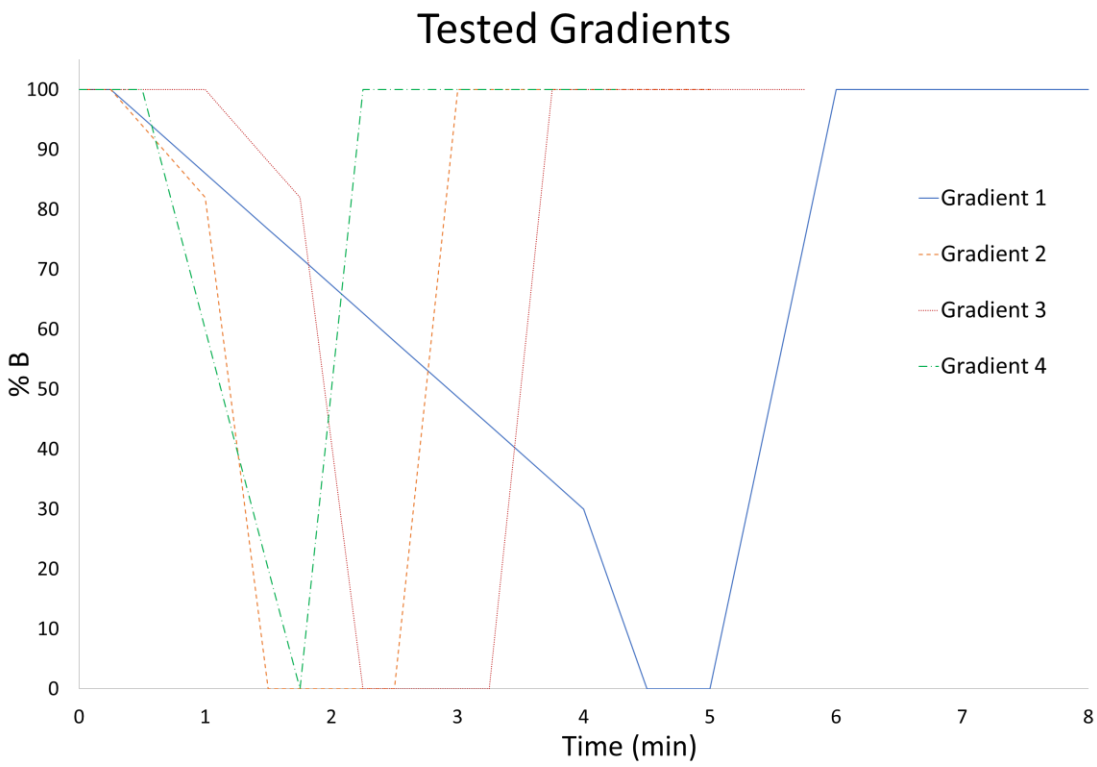

Figure 7-2 Gradients evaluated in this work using mobile phase 1 and 2, gradient 1 being optimal for both the PFP and Cyano columns.

Table 7.1 Composition of the two mobile phases used for chromatographic screening.

Mobile Phase 1	A	80% H_2O	20% MeOH
	B	5% H_2O	95% MeOH
Mobile Phase 2	A	90% H_2O	10% ACN
	B	10% H_2O	90% ACN

*All mobile phases spiked with 0.1% formic acid

Table 7.2 The four mobile phases gradients evaluated in this study.

Gradient 1		Gradient 2		Gradient 3		Gradient 4	
Time (min)	% B	Time (min)	% B	Time (min)	% B	Time (min)	% B
0	100	0	100	0	100	0	100
0.25	100	0.25	100	1	100	0.5	100
4	30	1	82	1.75	82	1.75	0
4.5	0	1.5	0	2.25	0	2.25	100
5	0	2.5	0	3.25	0	4.25	100
6	100	3	100	3.75	100		
8	100	5	100	5.75	100		

7.2.4 Data Analysis and Method Validation

Both data acquisition and processing were performed with Xcalibur® software (Thermo Scientific, San Jose, CA, USA). Data analysis and graphical development of results were performed with Excel 2016 (Microsoft Corporation, Albuquerque, NM, USA). Calibration curves and figures of merit were processed using Prism 5 (GraphPad Software, La Jolla, CA, USA). Each analyte, apart from DABA, was monitored for both a quantifier and qualifier ion. LOQs were determined as the lowest point of the calibration curve that achieves accuracy within ± 20% of the nominal value and precision of less than 20% relative standard deviation.[289] The method's accuracy and precision were evaluated at 3 concentration levels (7.5, 35, and 75 µg L^{-1}) analyzed on different days (1 and 3). The

linear dynamic range of the method includes all concentration levels included in the final calibration curve, including the calculated LOQs.

7.3 Results and Discussion

7.3.1 Development of Chromatographic Conditions for Separation of Underivatized Isomeric Amino Acids

The retention and separation of amino acids is a critical challenge, particularly when performing ultra-trace analysis in different matrices. Moreover, in the case of BMAA, this task is further complicated by the presence of structural isomers. Because they are isobars with very similar mass fragmentation patterns, baseline separation is critical. To overcome the challenges associated with conventional HILIC separation for these compounds, LC columns with diverse chemistries were investigated under different conditions. Four chromatographic gradients were developed, envisioning the application of this method for analysis of complex matrices, each method reaching 100% aqueous solvent composition to better elute any polar constituents from the LC column before subsequent injections. It should be noted that each gradient (shown in Figure 7-2) described already incorporates the equilibration time into the chromatographic run, with the longest run evaluated (8 min) being much shorter than conventional HILIC separation of the targeted analytes. Mobile phase 1 contains methanol, a common LC solvent that typically does not perform well with HILIC due to its higher elution strength and its competitiveness with water on the stationary phase surface.[37] Mobile phase 2, with the organic phase consisting of ACN, was selected as it is amenable to conventional HILIC methods and similar to previous works utilizing PFP with high organic starting conditions.[285,287,288]

A comparison of the gradients and mobile phases was first established by injecting BMAA and DABA in 60:40 ACN:H_2O with 0.1% formic acid. Under all the evaluated conditions, two columns, Pinnacle DB IBD and Raptor Polar X, were not suited for the separation of these two isomers. Pinnacle DB IBD demonstrated no retention (Figure C-2) and Raptor Polar X had retention but no separation (Figure C-3). The Pinnacle DB IBD column is referred to as a "proprietary polar functional embedded alkyl", and while its exact chemistry is unknown publicly, it is listed as a strong hydrogen bonder that allows retention for both acids and bases, particularly acids. What's most interesting about this column is that IBD columns, or "intrinsically base deactivated" columns, contain a polar functional group along the alkyl chain.[290] This design allows a great deal of polar shielding, resulting in little access to any free silanol groups which may be present on the stationary phase surface. Consequently, RPLC of basic compounds will exhibit better peak shape and less tailing due to the diminished secondary interactions of the silica surface. As the alkyl ligand is not sufficient to retain polar analytes such as the ones studied in this work, it is likely that the polar shielding inhibits any ion-exchange interactions these amino acids could establish with the silica surface. The chemistry of the Raptor Polar X column on the other hand allows both a HILIC and ion-exchange mechanism on a single ligand. Moreover, this chemistry has been demonstrated to allow the retention of 21 amino acids with similar conditions of this study in only 10 min.[291] However, the analytes in this study could only be retained, not separated, using the gradients and mobile phases tested with the other LC columns. Furthermore, a different mobile phase consisting of 50 mM ammonium formatted added to mobile phase B (90% ACN, 10% H_2O) was also evaluated, however, no retention of analytes was observed.

Cyanopropylsilane (Cyano) demonstrated sufficient resolution for both these analytes, however, with the addition of the third isomer AEG, efficient separation was not achieved. Cyano is an interesting multi-mode stationary phase used in RPLC, HILIC and NPLC, that is especially suitable for analysis of protonated bases. The retention mechanism of this stationary phase has been long studied, with reports showing that its unique selectivity arises from a combination of unreacted silanol groups contributing to ion exchange along with localization effects on the stationary phase surface.[292] Chromatographic results (Figure C-4) for the Cyano column suggest that methanol is an ideal organic solvent choice for the separation of BMAA and DABA. Mobile phases 1 and 2 display similar retention for these analytes, however, the conditions evaluated in this study demonstrate lower resolution with the use of ACN (Table F.3). The observed chromatographic behavior is particularly interesting as Cyano columns are considered less retentive than other HILIC stationary phases. This factor, along with separation obtained with methanol, suggests multi-mode retention could be possible in these circumstances. However, this column proved to be ineffective in the separation of mixtures containing all three isomers, including AEG. Nevertheless, its promising retention in multi-mode chromatography, used in this work, might be leveraged for other small charged molecules.

Force and Raptor Fluorophenyl columns (PFP) both exhibited great potential for the retention of BMAA and DABA. The major difference between the two columns being the Raptor FluoroPhenyl consists of superficially coated particles. Preliminary experiments suggested substantially greater retention and separation on the Force FluoroPhenyl column, either due to its fully porous particles or a higher amount of accessible free silanol groups. Also in this case, methanol proved efficient as a mobile phase suggesting that the

conventional HILIC mechanism alone is not responsible for the separation achieved with these conditions. While both mobile phases provided efficient separation with Force and Raptor Fluorophenyl columns, mobile phase 2, with acetonitrile as its organic phase, was chosen for its enhanced resolution (Table 7.3) and sensitivity. The best conditions selected for further experiments involved the use of the Force Fluorophenyl LC column, mobile phase 2 **(**Table 7.1**)** with gradient 1 **(**Table 7.2**)**. Chromatographic separation of the three isomers and L-serine-d_3, first intended to be used as an internal standard, is demonstrated in Figure 7-3. It should be noted that Figure 7-3 displays 5 overlaid chromatograms of injected analytes' mixtures at 250 µg L^{-1} in 80:20 H_2O:ACN with 0.1% formic acid. Reproducibility of the method proved to be excellent over a large number of injections, with retention variability less than 0.24% for all analytes over 120 injections. The use of metal passivated or PEEK-lined column hardware may improve the overall efficiency of the method and further reduce any peak tailing resulting from adsorption of analyte onto the column-wall surface. Taking into account this tailing by using the tangential line method, the number of theoretical plates (N) calculated for BMAA, DABA and AEG are 3721, 4679 and 5329, respectively.

The retention order of the analytes on the PFP stationary phase suggests that the terminal secondary amino group on the targeted analytes (Figure 7-1) played a critical role in the interaction with the stationary phase. As the nitrogen becomes more accessible and less sterically hindered, retention increases. Conversely, L-serine-d_3 only contains one amino group that is non-terminal and as such has far less retention. This retention behavior is most likely due to an ion-exchange mechanism between the free silanol groups on the PFP column and the positively charged amino groups on the analytes. As suggested by

earlier accounts, the low dielectric constant of ACN should allow easier access to free silanol groups on the stationary phase surface and greater retention compared to other solvents, such as methanol.[288] Furthermore, as conventional HILIC commonly loses retention with increasing column temperature,[37] column temperature effects on the retention of BMAA and its isomers on PFP were evaluated from 20 to 50 °C. The dependence of retention on column temperature can be described by the van't Hoff equation (Equation 7-1)[293]:

$$\ln k = \ln \beta - \frac{\Delta H^\circ}{RT} + \frac{\Delta S^\circ}{R} \qquad \textbf{(Equation 7-1)}$$

Where k is the retention factor, β is the phase ratio, ΔH° is enthalpy, R is the gas constant, T is temperature and ΔS° is the entropy of transfer. ΔH° describes the transfer of analyte from mobile phase to stationary phase and is calculated by the slope of a van't Hoff plot. While behavior differs for different analytes and chromatographic conditions, in most RPLC and HILIC modes, analytes tend to favor this transfer and, thus are exothermic. In this case, a van't Hoff plot would have a positive slope demonstrating that increased column temperature results in loss of retention. Results in Figure 7-4 indicate that increased column temperature enhances the retention of these analytes with the PFP stationary phase, suggesting again that an ion-exchange mechanism could be present as an endothermic process must be dominant. The relatively low slope of L-serine in this van't Hoff analysis, comparatively to the target analytes, further indicates that the only one charged amino group in the molecule structure severely reduces the ion-exchange interaction between the analyte and stationary phase. The physical behavior of this phenomenon has been described as when solvent temperature increases, the solvent-solute interaction decreases, allowing better access of the positively-charged analytes to the stationary phase.[294,295] Figure 7-5

demonstrates these possible interactions with the stationary phases in the analyte retention order.

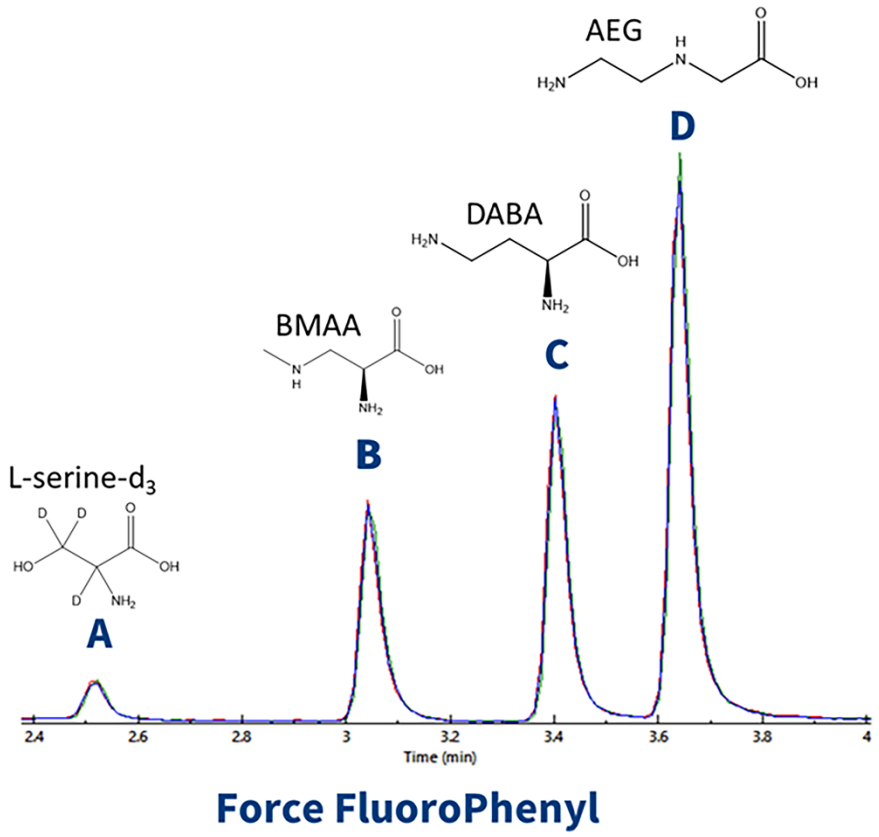

Figure 7-3 5 Overlaid chromatograms depicting the separation of underivatized BMAA and its isomers using the optimal screened conditions for the Force FluoroPhenyl column.

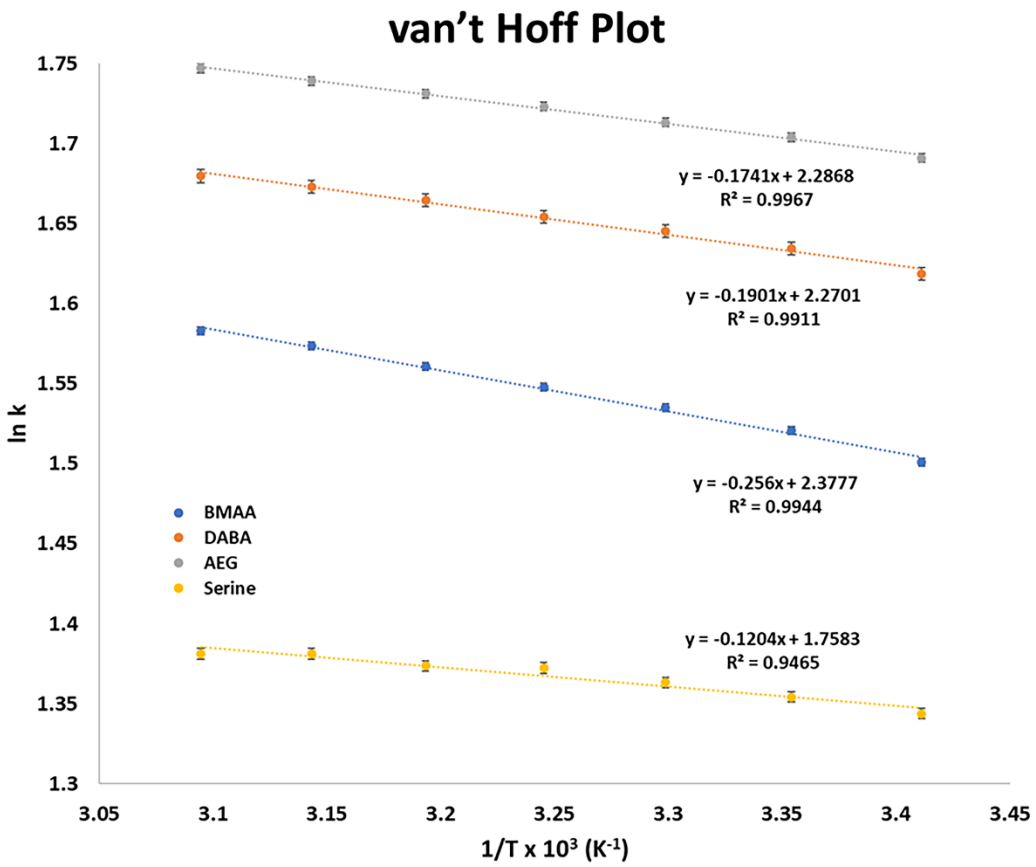

Figure 7-4 van't Hoff Plot for BMAA, DABA and AEG on the Force FluoroPhenyl column. Higher temperatures permit greater analyte retention and substantial decrease in system back pressure.

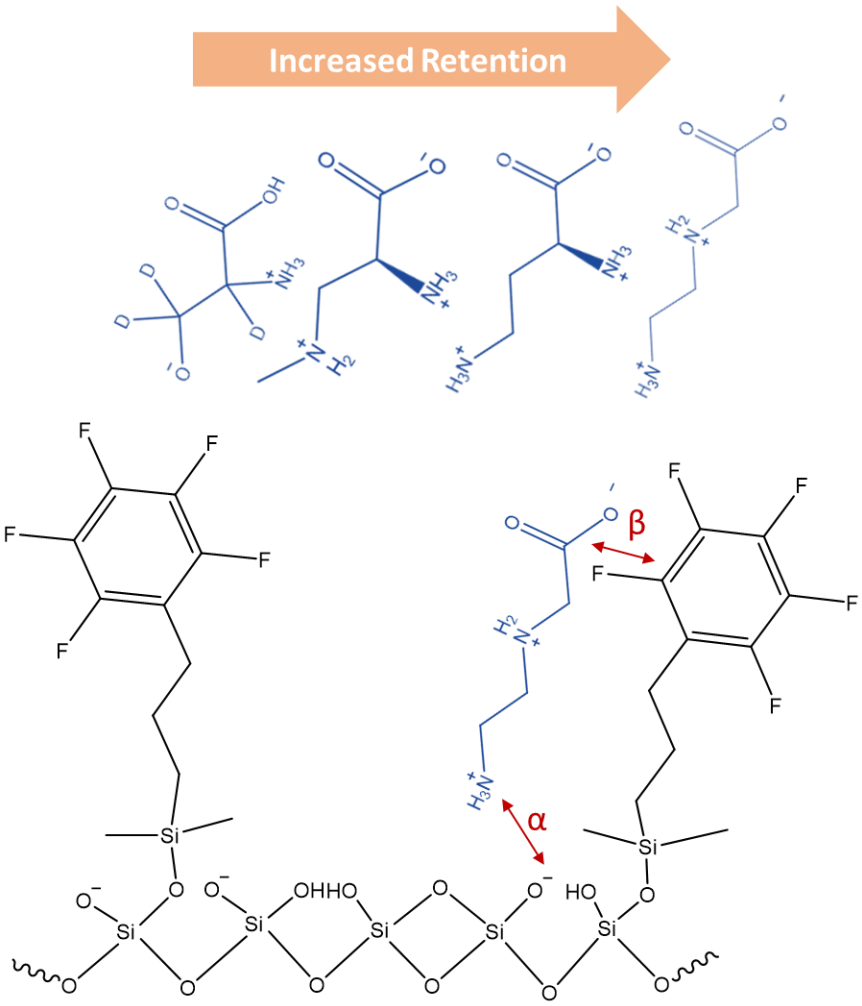

Figure 7-5 PFP stationary phase with analytes in their retention order. Ion-exchange (α) and non-electrostatic interactions (β) contributing toward analyte retention.

Table 7.3 Separation factors and resolutions calculated for the separation of BMAA and DABA using the Force FluoroPhenyl column. Mobile phase 2 (ACN-based) and gradient 1 were used for chromatographic separation.

	Gradient	Separation Factor	Resolution
Mobile Phase 1 (MeOH-based)	1	1.2	4.2
	2	1.1	2.2
	3	1.1	3.0
	4	1.1	2.7
Mobile Phase 2 (ACN-based)	1	1.1	6.0
	2	1.1	2.1
	3	1.1	3.0
	4	1.1	2.6

7.3.2 SPME Optimization

Due to the analytes' small molecular weights (118 g/mol) and high polarity (Log P approximately -4, specific values along with pKa and log D values found in Table 7.4), any efficient extraction method developed for these compounds must either exploit the molecules' polarity or their ionic form. As the compounds are positively charged at most useful chromatographic pH values, pH control is critical in both the extraction and desorption process. The SPME extraction phases evaluated in this study were hydrophilic-lipophilic balance/polyacrylonitrile (HLB/PAN), mixed-mode/polyacrylonitrile (MM/PAN) and hydrophilic-lipophilic balance-weak anion-exchange/polyacrylonitrile (HLB-WAX/PAN). Effect of pH on the extraction recovery was tested in different media extracting at 1000 rpm for 90 min to ensure equilibrium was established. The media tested were ultra-pure water, phosphate-buffered saline (PBS), and 3 buffer solutions at pH 4, 7 and 10. A comparison between ultra-pure water, PBS and pH buffer 7 was investigated to

probe the effect of salt content on extraction efficiency and evaluate coating performance in biologically-relevant media (PBS). As demonstrated in Figure 7-6, the weak anion-exchange interaction of HLB-WAX with the negatively charged carboxylic group of the analytes was not effective in the extraction of BMAA compared to conventional HLB. Both HLB and MM are suited for the extraction of BMAA in different conditions. At neutral pH values, MM/PAN greatly outperforms the other SPME extraction phases as its cation-exchange mechanism readily interacts with the positively charged amino groups of the analytes. Conversely, if the pH is increased to 10, the amino groups become neutral resulting in a higher extraction efficiency by the neutral HLB/PAN extraction phase and a lower recovery for MM/PAN. It is expected that the loss in extraction efficiency between water and PBS is due to the interaction of salts with the coating surface, swamping secondary interactions with HLB and competing with the ion-exchange mechanism of MM.[296] Envisioning the use of this method for analysis of complex environmental samples and biological specimens to better understand the path forward for *in situ* and *in vivo* analysis of free BMAA, we selected optimal conditions that allow for minimum sample modification maintaining neutral pH. Thus, the MM/PAN extraction phase was chosen for its performance in water and PBS.

Initial experiments were performed desorbing SPME fibers in 70:30 ACN:H_2O with 0.1% formic acid, resulting in analyte carryover on the SPME coating to be over 20%. To remedy this, desorption solutions of increasing aqueous content were tested. Demonstrated in Figure 7-7, the amount of analyte desorbed greatly increases when the amount of aqueous content is increased to 80%. However, it was also observed that desorption solutions with an aqueous content above 80% resulted in poor chromatographic

performance due to solvent mismatch with the initial chromatographic conditions. As shown in Figure 7-8, carryover was drastically reduced to less than 5% for these high aqueous desorption solutions, and thus 80% H_2O, 20% ACN with 0.1% formic acid was chosen as the optimal desorption solution. pH values of tested desorption solutions ranged between 2.60 (80% H_2O) and 2.97 (30% H_2O), the difference in pH was not significant enough to induce changes in the major ionic species distribution in solution. Because the high aqueous content of the desorption solution seems to be the only factor needed to significantly lower carryover, it is expected that the high surface tension of water helps displace the analytes from the fiber surface while its relatively high dielectric constant shields the ion-exchange moiety from further interaction.[297] The extraction time profile of these analytes was performed at room temperature with an agitation rate of 1000 rpm (Figure 7-9), indicating that equilibrium of the analytes between the 1.5 mL water sample and the MM/PAN fiber was established at 30 min. This trend is also mirrored in the desorption time profile (Figure 7-10), a desorption time of 30 min also being chosen. The optimized SPME method exhibited absolute extraction recovery from ultrapure water of 4.5 %, 13.1 % and 7.8 % for BMAA, DABA and AEG, respectively.

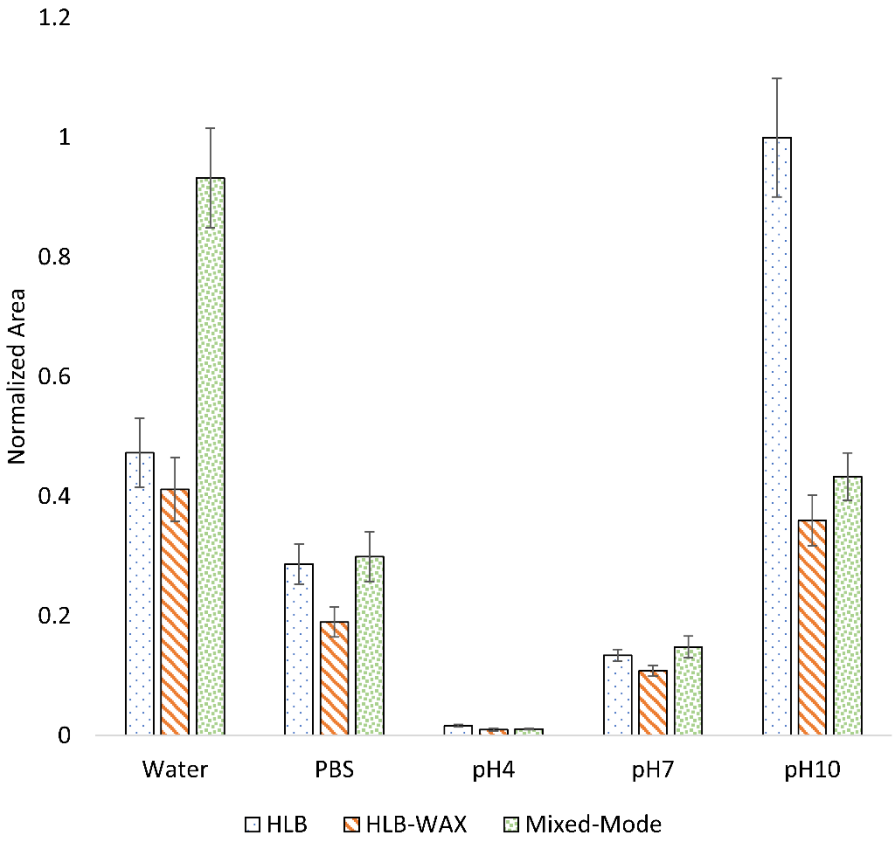

Figure 7-6 SPME coating evaluation comparing the three tested extraction phases in various media including water, phosphate buffered saline (PBS) and three pH buffers of 4, 7 and 10 pH.

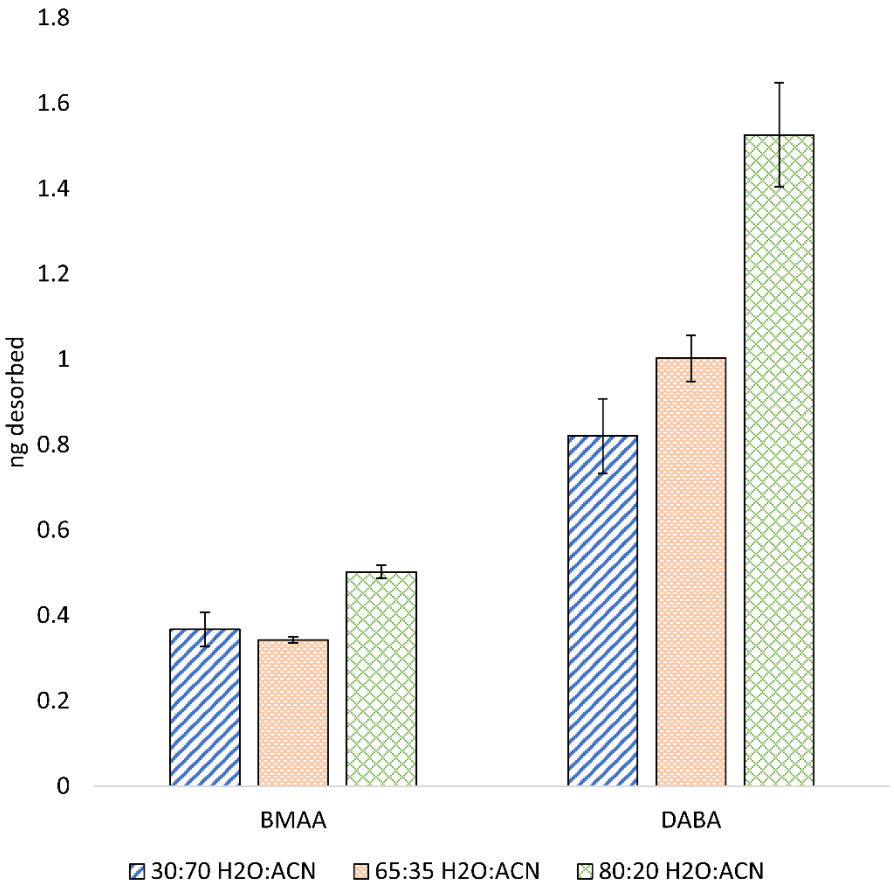

Figure 7-7 Desorption solution evaluation, each solvent composition spiked with 0.1% formic acid.

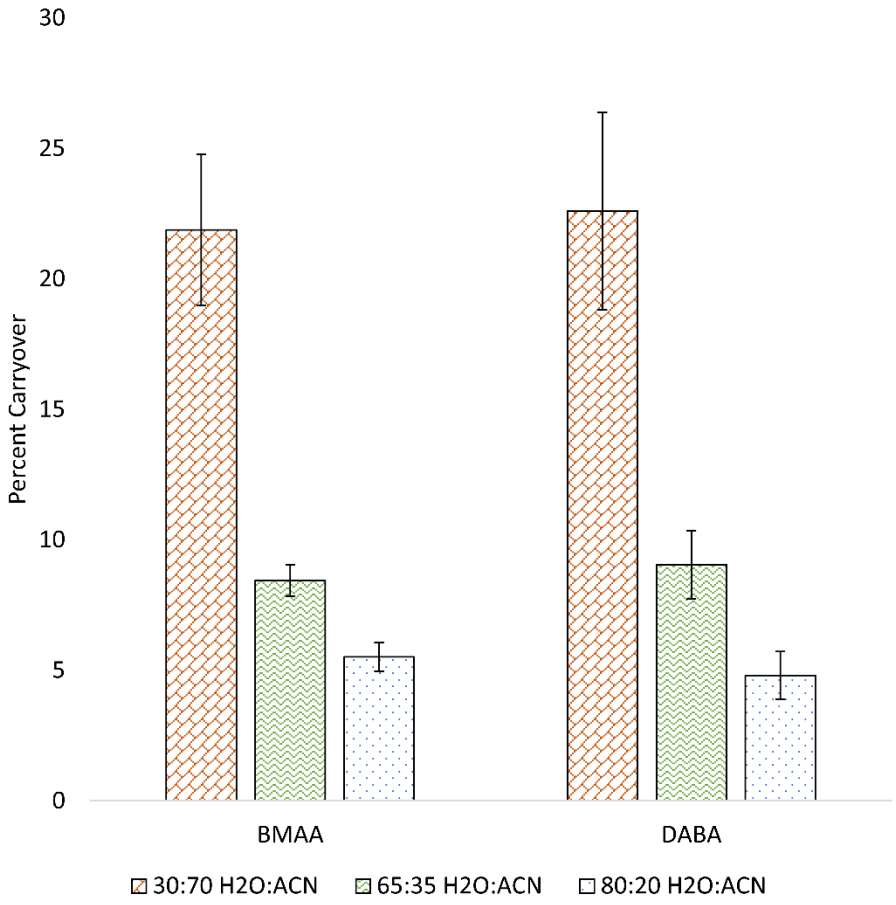

Figure 7-8 Analyte carryover on SPME fiber for the evaluated desorption conditions.

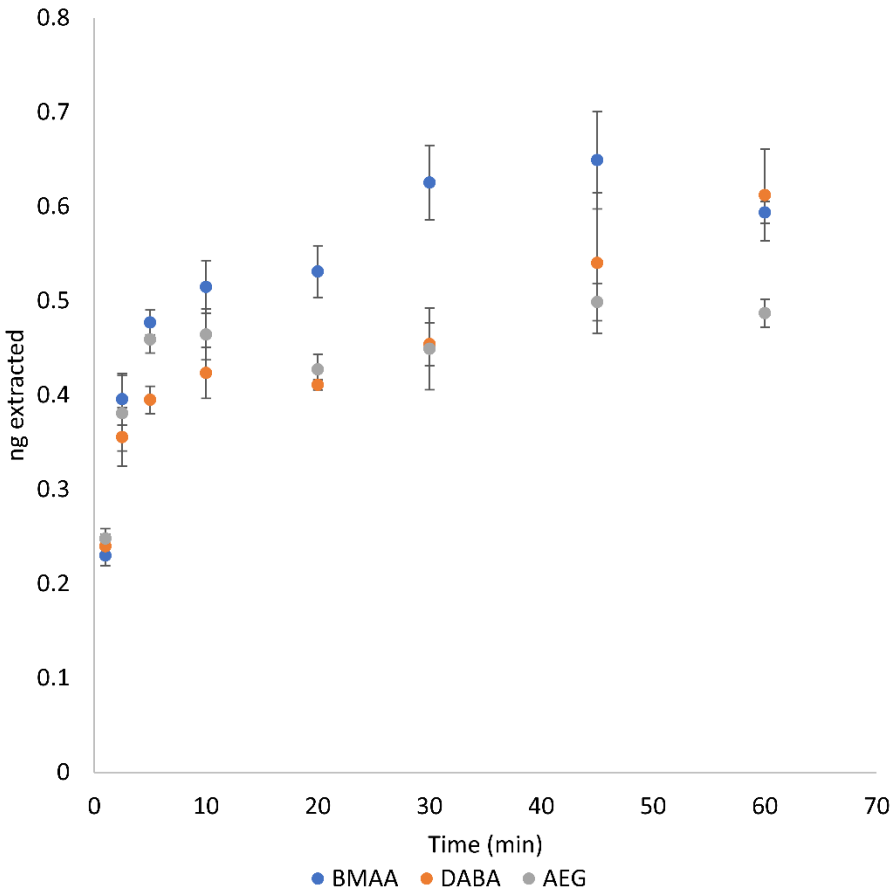

Figure 7-9 Extraction time profile for mixed-mode SPME fiber from ultra-pure water.

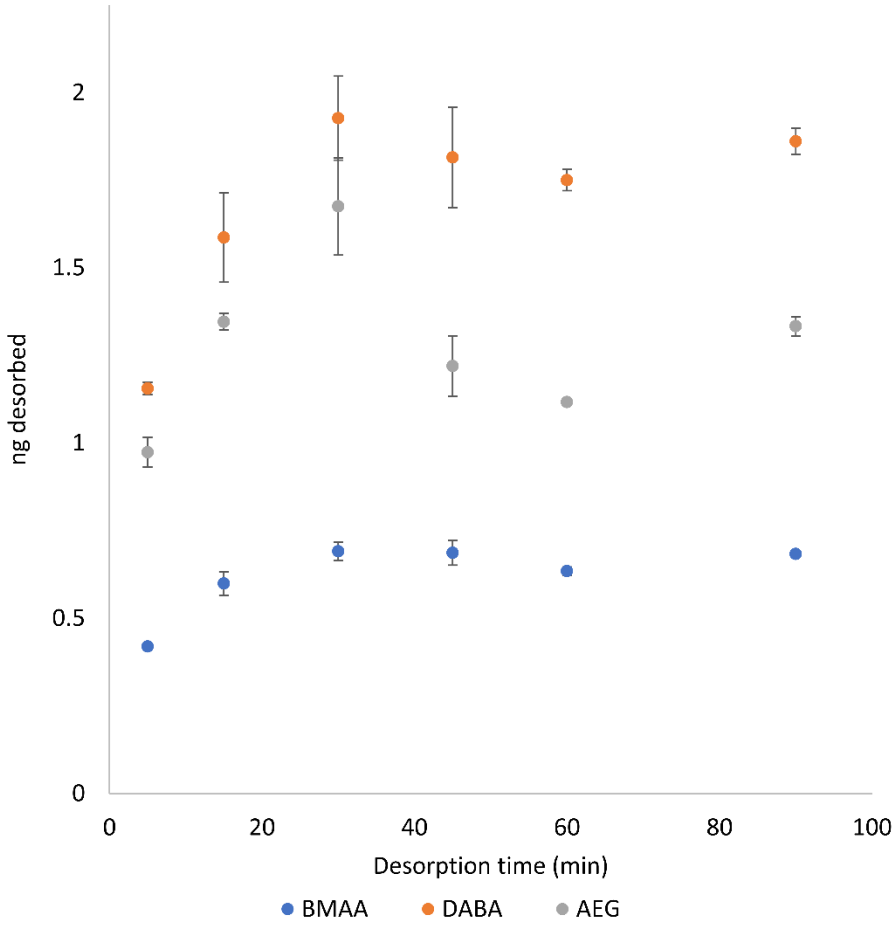

Figure 7-10 Desorption time profile for mixed-mode SPME fiber in 80:20 ACN:H2O with 0.1% formic acid.

Table 7.4 Chemical properties of BMAA and its isomers.

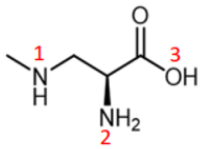

Analyte	pKa[1]	pKa[2]	pKa[3]	logP	logD (pH 1.7)	logD (pH 6.5)
BMAA	9.9	6.6	2.0	-3.8	-7.03	-4.11
DABA	10.0	8.0	2.6	-4	-7.52	-5.4
AEG	7.2	10.1	2.2	-4	-7.39	-4.69

*All values calculated from Chemaxon

7.3.3 Method Performance

As a proof-of-concept, the techniques and methods developed in this study were tested by performing a calibration curve in ultra-pure water, ranging from 2.5 – 200 µg L^{-1}. Preliminary results indicated that L-serine-d_3 is unable to correct for any of the evaluated analytes, suggesting that the lack of a terminal amino group plays a major role in the chemical behavior of these analytes during extraction, detection, and chromatographic separation. Isotopically labeled L-BMAA-d_3 was thus synthesized, providing adequate extraction efficiency and data correction for both BMAA and AEG. Calibration curves are shown in Figure 7-11, demonstrating the linear dynamic range (LDR) and sensitivity of the method. BMAA and AEG exhibited LDR ranges of 2.5 to 200 µg L^{-1} with limits of quantification (LOQ) of 2.5 µg L^{-1}. DABA had a slightly higher LOQ of 5 µg L^{-1}, a LDR of 5 – 200 µg L^{-1}. Accuracy and precision of intermediate calibration levels at 7.5, 35 and 75 µg L^{-1} can be found in Table 7.5. Results demonstrate great accuracy and reproducibility for BMAA and AEG at all tested accuracy points with RSD% values less than 15% and accuracy values between 80-120%. R^2 values are 0.9998 and 0.9977, respectively with a

1/x weighting. DABA demonstrated good reproducibility, however, its accuracy for the point 75 µg L^{-1} was consistently lower than the value calculated by its calibration curve. This suggests that an alternative internal standard to L-BMAA-d_3 for DABA could prove to be more efficient in future protocols. Moreover, an R^2 value of 0.9815 was calculated for DABA with a 1/x weighted calibration curve. Stability of high-aqueous desorption solutions was found to be adequate during this time frame.

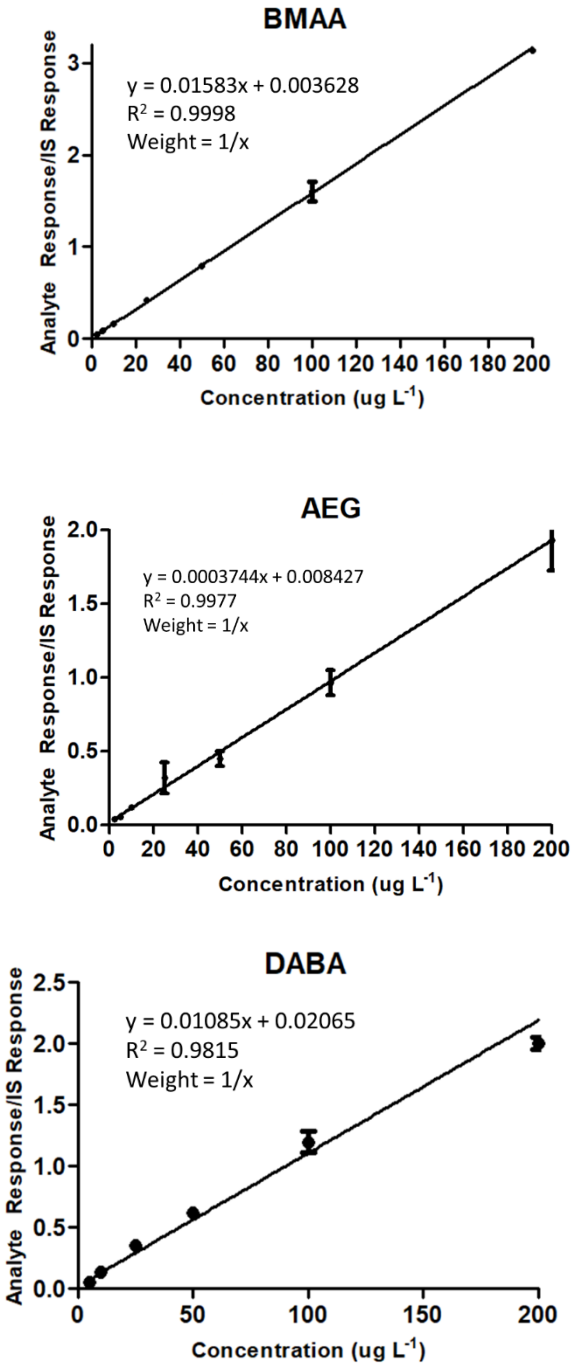

Figure 7-11 Calibration curves for each analyte with L-BMAA-d3 used as an internal standard. Good linearity is observed for BMAA and AEG, however, results indicate that DABA's unique chemistry might necessitate a more adequate internal standard to achieve a wider linear dynamic range.

Table 7.5 Method Performance including the intra- and interday reproducibility for each model analyte at their respective accuracy points.

		7.5 µg L^{-1}		35 µg L^{-1}		75 µg L^{-1}	
	Compound	Accuracy%	RSD%	Accuracy%	RSD%	Accuracy%	RSD%
Day 1	BMAA	98	11	98	5	104	3
	DABA	113	19	105	7	38	11
	AEG	104	18	107	15	86	1
Day 3	BMAA	96	4	99	4	105	2
	DABA	105	6	91	9	45	4
	AEG	114	1	112	15	92	6

7.4 Conclusions

A convenient and fast chromatographic method has been developed for BMAA and its isomers, allowing their separation to be obtained under 8 min without the need for derivatization on a PFP column. This same methodology can be extended further toward other basic polar analytes to avoid the long equilibration times associated with conventional HILIC methods. Furthermore, the established SPME protocol demonstrates the robustness of amino acid sample preparation in water, the composition of the desorption solution proving critical for method development due to the unique chemistry and polarity of these analytes. The obtained LOQs, BMAA: 2.5, DABA: 5, and AEG: 2.5 µg L^{-1}, suggest similar method performance to established HILIC protocols with separation times 3 times faster than the average method. As this work employs a linear ion trap for its quantification, future studies could employ triple-quadrupole mass spectrometry or high-resolution mass spectrometry to further the method's applicability for analysis of BMAA and its isomers at sub ppb levels. As these results suggest, proper screening of LC column chemistry is crucial for method development for small polar molecule analysis.

Furthermore, the developed SPME protocol can facilitate convenient toxicological and biomonitoring studies for unbound BMAA and can be further adapted toward total BMAA determination.

Acknowledgements

This work was supported by the Restek Academic Support Program and the American Chemical Society Division of Analytical Chemistry Graduate Fellowship Program sponsored by PittCon. The authors would like to thank Connor Flannery for his insightful discussion and Dr. Wei Li for his help with the initial synthesis attempts of BMAA-d_3. We also acknowledge Supelco-Millipore Sigma for providing some of the SPME sampling devices used in this study.

Chapter 8

Sample Preparation Strategies for the Analysis of the Cyanoneurotoxin β-N-methylamino-L-alanine and its Isomers from Brain and Blue Crab

Manuscript in Preparation

Ronald V. Emmons, Endri Karaj, Erasmus Cudjoe, David S. Bell,

L.M. Viranga Tillekeratne, Emanuela Gionfriddo

Abstract

Non-proteinogenic cyanoneurotoxins, in particular β-N-methylamino-L-alanine (BMAA) and its isomers, have been demonstrated to bioaccumulate in aquatic fauna such as blue crab. These same toxins have also been detected in the brains of patients with amyotrophic lateral sclerosis (ALS) and dementia. A sample preparation method is developed in this work for the extraction of these toxins in brain and blue crab utilizing solid phase microextraction (SPME) hyphenated to liquid chromatography – mass spectrometry (LC-MS). Through an initial solvent-extraction approach, SPME device fouling and matrix effects were found to be acceptable. Further expansion of this workflow should enable the robust extraction of cyanoneurotoxins from complex matrices with consecutive reuse of the SPME device.

8.1 Introduction

β-N-methylamino-L-alanine (BMAA) and its major isomers have been demonstrated to be associated with neurodegenerative diseases such as Guam disease, amyotrophic lateral sclerosis and Alzheimer's disease.[268–271,298,299] Since its discovery, the primary route of exposure of these cyanoneurotoxins has been found to be dietary.[272,273,300–303] Bioaccumulation has been found to occur in seeds, shellfish and even has been found in the human brain.[304] It is critical to monitor these toxins through potential dietary sources, along with investigating the brains of individuals affected by neurodegenerative diseases to access the exposure level of the general public. These complex matrices pose a major challenge in these efforts, however, many developed analytical methods demonstrates conflicting results.[274–276] A major controversy found throughout the literature is the analysis of human brain and blue crab. Many of these reports detect no BMAA when employing underivatized protocols.[273,274,277] These biological matrices are in particular complex, due to their relatively high lipid and ion concentrations which may induce analyte-matrix binding or matrix effects during ionization.[305–307]

Across the majority of matrices, sample preparation of BMAA is often similar with minor modifications. Sample preparation first consists of acid hydrolysis (6 M HCl at 110 °C for 24 h) followed by reconstitution in solvent such as acetonitrile.[279] For underivatized protocols, this reconstituted sample is filtered then injected directly into a LC-MS system utilizing hydrophilic interaction chromatography (HILIC).[273,277] Derivatization is often performed by reacting the reconstituted sample with 6-aminoquinoly l-N-hydroxysuccinimidyl carbamate (AQC) before injection into LC-MS with a reversed-phase column.[308] Further investigation into sample cleanup strategies is warranted, as not many

developed methods employ other sample preparation approaches such as solid phase extraction (SPE).[309,310] In this way, matrix interference can be reduced, and analyte can be preconcentrated, lowering the method's limit of detection. Previous work done in our lab (Chapter 7) has demonstrated the applicability of solid phase microextraction (SPME) for the preconcentration of underivatized BMAA and two of its isomers, (2,4-diaminobutyric acid, DABA; N-(2- aminoethyl) glycine, AEG), from water and their separation via a multi-mode chromatographic technique.[16] Furthermore, there are already developed SPME methods for the extraction of neurotransmitters from brain. However, as these protocols are *in vivo,* the reusability of the SPME device is not evaluated.[311–314] This work seeks to expand the previously developed SPME and LC-MS protocol for the analysis of BMAA and its isomers from brain and blue crab, investigating the associated matrix effects and device robustness for these complex matrices.

8.2 Experimental

8.2.1 Chemicals and Materials

BMAA hydrochloride was purchased from Sigma-Aldrich (St. Louis, MO, USA). DABA dihydrochloride was purchased from Alfa Aesar (Ward Hill, MA, USA) and AEG was purchased from Toronto Research Chemicals Inc (Toronto, ON, Canada). L-BMAA-HCl-d3 was synthesized according the a previous work without modification.[16] LC-MS grade acetonitrile, water and methanol were purchased from Birch Biotech (Morgantown, PA, USA). The mixed-mode/polyacrylonitrile (MM/PAN) SPME devices were provided by Millipore Sigma (Bellefonte, PA, USA). Lamb brain and blue crab were used as a surrogate matrix for human brain, and were purchased at local markets in Toledo, OH.

Samples were homogenized using a 350 W Spice and Nut Grinder (Laralov, Guandong, Jiangxi, China).

8.2.2 SPME Procedure

SPME extractions were performed in 2 mL glass vials with 1.5 mL sample volume. Fibers were conditioned in MeOH:water (1:1) for 30 min followed by a brief rinse in ultra-pure water. Extractions were performed for 30 min at a vortex agitation rate of 1000 rpm. Subsequently, SPME devices were desorbed for 30 min in 150 µL 80:20 water:acetonitrile solution spiked with 0.1 % formic acid at 1000 rpm. For homogenate samples, after the extraction step, a lint-free tissue was used to remove any residual solids from the device's surface. This was followed by an additional water rinse to ensure the removal of loosely attached matrix components before being wiped again with the tissue. Fibers were washed in ultra-pure water between optimization experiments to ensure there were no carryover of matrix constituents. Solvent-assisted experiments were performed by portioning a single, 5 g tissue sample into separate centrifuge tubes for each solvent composition. This 5 mL of solvent was then portioned into three separate 1.5 mL aliquots and extracted by three separate SPME fibers. Homogenate experiments were performed similarly, however, as the volume of the sample is reduced after dry ice pulverization, only two SPME fiber replicates were performed.

8.2.2.1 Homogenate Preparation

Brain tissue was first collected and homogenized from the entire lamb brain with no discrimination of the different regions. Crab tissue consisted of the muscle found in the crab's legs, claws and thorax. To prepare brain and crab, thawed tissue was first homogenized using a mortar and pestle and approximately 5 g was transferred to a 5 mL

plastic centrifuge tube. Homogenate was then spiked with an analyte mixture at 1 µg/mL and thoroughly mixed with a metal spatula. This tube was then sealed with parafilm and placed into a refrigerator at 4 °C for 6 hours to ensure analyte equilibration. Then the sample was removed and underwent 3 freeze-thaw cycles using liquid nitrogen and a warm water bath, with 2 min freeze and 3 min thaw cycles. After this, 5 g of dry ice was pulverized in an electric grinder before addition of the sample and further pulverization, this mixture placed into separate centrifuge tubes and allowed to degas overnight in a freezer at -20 °C. No individual fragments of tissue were visually observed at this point. In the case of direct homogenate extraction, the sample was equilibrated to room temperature and then separated into three 2 mL glass vials prior to SPME fiber introduction. Extraction was performed for 4 h. In solvent-assisted extraction, the pulverized sample was mixed with 5 mL of different solvent compositions and the tube resealed with parafilm and tape. The sample was then sonicated for 4 h in an ice bath and centrifuged at 15000 rpm for 10 min prior to collection of the supernatant. This supernatant was then pooled and used for the SPME protocol. An outline of this procedure can be found in Figure 8-1.

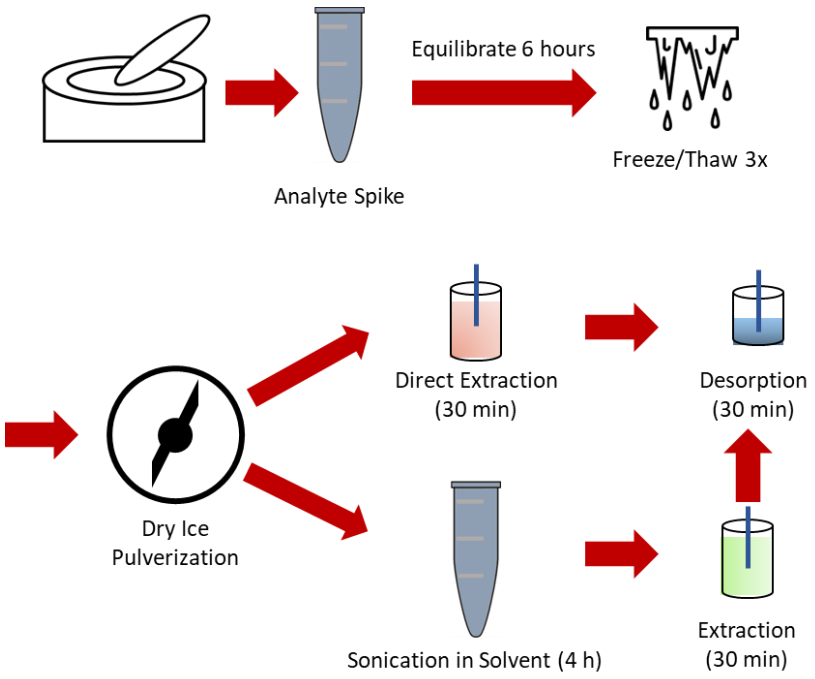

Figure 8-1 Sample preparation procedure for brain and crab.

8.2.3 Liquid Chromatography-Mass Spectrometry Conditions

LC-MS analysis was performed on a Vanquish UHPLC hyphenated to a LTQ XL Linear Ion Trap Mass Spectrometer (Thermo Fisher Scientific, San Jose, CA, USA). A Force FluoroPhenyl (100 mm x 2.1 mm x 1.8 µm; Restek Corporation, Bellefonte, PA, USA) analytical column was used with a flow rate of 0.45 mL/min. Mobile phase A consisted of 90% H_2O and 10% ACN with 0.1% formic acid added, mobile phase B composed of 90% ACN, 10% H_2O with 0.1% formic acid. Gradient elution was performed as the following: 100% mobile phase B was held for 15 seconds, decreased to 30% B at 4 min, then reduced to 0% by 4.5 min. This composition was held until 5 min, followed by an increase to 100% B by 6 min and held until 8 min. The column oven was held at 40 °C, with a 50:50 H_2O:ACN syringe wash with a 10 µL sample injection (partial loop). Mass spectrometric conditions are the same as used in Chapter 7, shown in Appendix C (Tables

C.1 and C.2). Positive ESI was used, with no adduct formatted observed under the optimized conditions.

8.2.4 Data Analysis

All data acquisition and peak integration was performed with Xcalibur® software (Thermo Scientific, San Jose, CA, USA). Data analysis and figures made with Excel 2016 (Microsoft Corporation, Albuquerque, NM, USA).

8.3 Results and Discussion

8.3.1 The Extraction of Tissue Homogenate

Previous works have demonstrated the robust *in vivo* extraction of neurotransmitters from rat brain utilizing SPME with relatively short equilibration times (between 20 and 45 min) in static mode.[311,315] The initial workflow, described in section 8.2.2 for extraction directly from tissue homogenate, was successful in extracting BMAA and its isomers from the bulk matrix. A consequence of this method, however, was fouling of the SPME device after only one extraction. When first introduced to a biological matrix, any foreign device will quickly form a layer of water, proteins and other biomolecules at the device surface. The adhesion of proteins on this surface can limit the diffusion of small molecules into the extraction phase. A wide range of biomedical applications, such as membrane dialysis, has already circumvented this issue by developing polymers that are biocompatible. These polymers, such as polyacrylonitrile (PAN) and polyurethane, develop a hydration layer on their hydrophilic surface preventing the transfer of large biomolecules from the matrix to the polymer.[316] This property of PAN has been used extensively to coat SPME devices to facilitate biocompatibility in complex matrices.[317,318]

Nonetheless, extraction efficiency was found to drastically reduce after direct contact of the SPME device to the bulk matrix (Figure 8-2). Due to the biocompatible properties of the PAN coating, protein adhesion is most likely not the reason for this phenomenon. It is possible that the adhesion of small molecules (e.g., lipids) or interaction with ions (e.g., sodium, magnesium) is interfering with the diffusion or ion-exchange interaction of the SPME device. Furthermore, interaction of these constituents with the analytes is also possible.

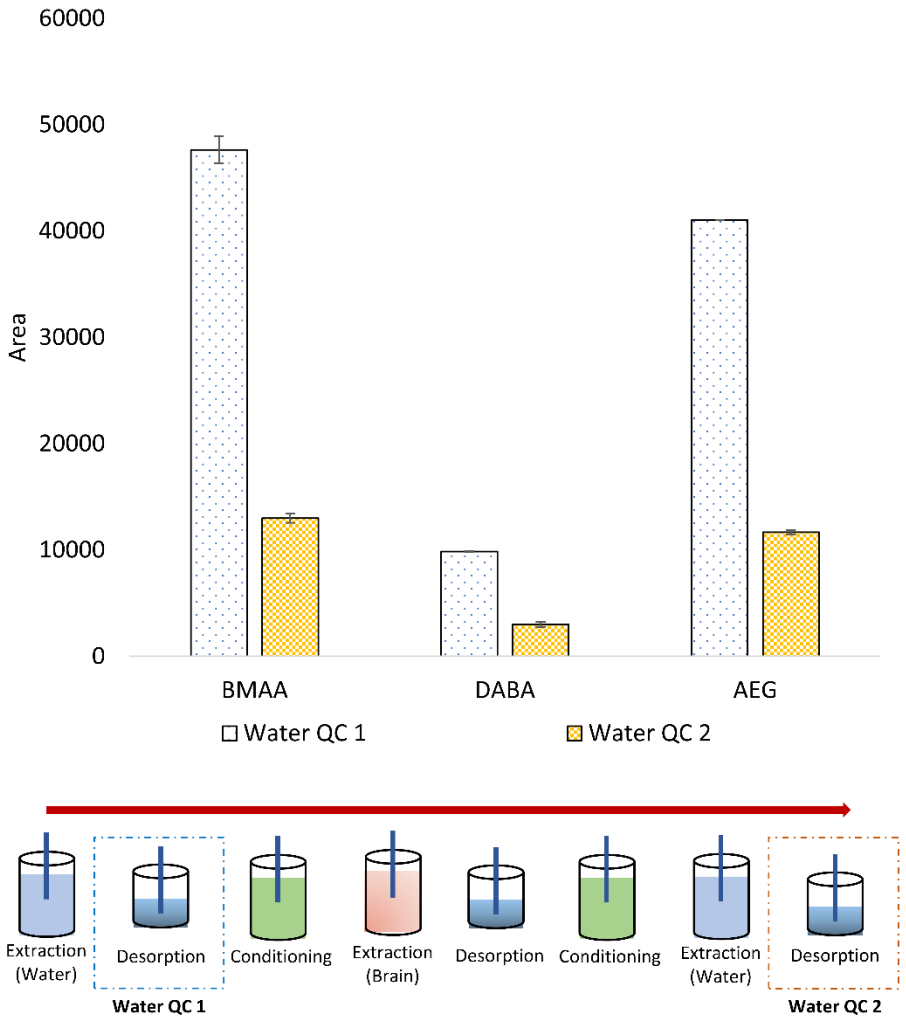

Figure 8-2 Loss in extraction efficiency after one direct extraction from brain homogenate (data obtained from the extraction of spiked water before and after brain analysis). Data averaged, between two SPME fiber replicates.

8.3.2 Solvent-Mediated SPME

In light of the extraction efficiency loss found with direct contact of the SPME device to brain and crab tissues, an alternative approach was developed to limit SPME fiber fouling. Solvent extraction of crab tissue is quite common in literature, facilitating the extraction of multi-class components including amino acids.[319–321] This approach involves homogenization of the sample, addition of solvent and agitation to facilitate transfer of

analyte from the matrix. This agitation can consist of a sonication approach or Homogenization steps can vary, however, due to the consistencies of homogenized crab and brain tissue, subsampling is challenging and the tissue itself demonstrates a degree of inhomogeneity. To remedy this, previous reports have used pulverization with dry ice to form a powder-like consistency for marine matrices.[322,323] Homogenizing and extracting with solvent alone, however, would not facilitate a selective extraction and allow a wide range of matrix interferences to be present in the final sample. By extracting from this solvent with SPME, the target analytes can be preconcentrated and selectively extracted minimizing matrix effects and enhancing method response. Shown in Figure 8-3, extraction efficiency remains relatively stable when extracting from organic solvent, particularly when higher organic compositions are used.

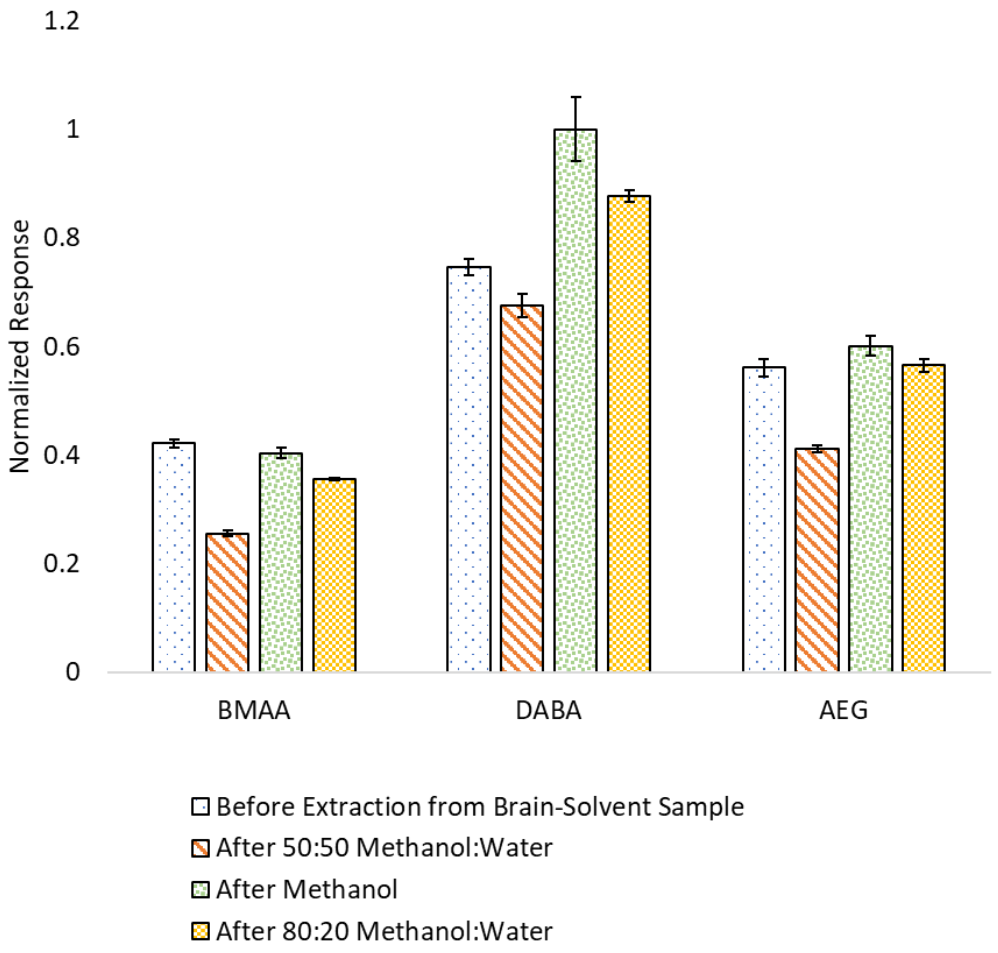

Figure 8-3 Extraction efficiency stabilized by extracting from organic solvent (data obtained from the extraction of spiked water). Results averaged between two SPME replicates and normalized by the highest response observed in the experiment.

8.3.2.1 Solvent Effects on SPME Extraction

PAN coated SPME devices are compatible with organic solvent, however, SPME extraction is conventionally performed in aqueous media with the organic solvent composition being kept under 1%.[12] As SPME is predicated on the equilibria of the analyte between the extraction phase and sample, any changes to the sample's chemical composition can impact this equilibria. In a majority of applications, if organic solvent composition is too high, analytes will preferentially equilibrate toward the organic phase,

reducing extraction efficiency. As far as the authors are aware, there has been no study evaluating the effect of organic solvent composition on the extraction efficiency of SPME fibers with ion-exchange extraction phases. This was investigated by spiking a mixture of analytes in neat solvent compositions and extracting with the optimized method outlined in Chapter 7, section 7.2.2 paragraph 1. Demonstrated in Figure 8-4, with increasing composition of methanol, the partition from the sample to the extraction phase increased considerably. This experiment was also repeated for increasing amounts of acetonitrile (Figure 8-5). These results can most likely be explained in a similar manner as the multi-mode separation developed for these same analytes in Chapter 7.[16] The solvation of these charged analytes is largely affected by the solvents' polarizability and dielectric constants, the lower the dielectric constant the less solvation. Dielectric constants at 298 K for water, methanol and acetonitrile are 78.30, 32.66 and 35.94, respectively.[294] Not only would increasing these organic solvents reduce solubility, but also play a large role in the surface interactions of the extraction phase and the analyte. When solvated in primarily water molecules, the interaction between the positive charge of the analytes and the negative charge of the extraction phase will be partially shielded by water molecules, owing to their high dielectric constant. Acetonitrile will not be as effective as separating these charges or solvating these molecules, allowing faster kinetics and an equilibria more shifted toward the charged extraction phase.[286,288]

A comparison of the extraction of these analytes spiked in pure water, methanol and acetonitrile can be found in Figure 8-6, results indicating far better extraction efficiency with acetonitrile than the other two solvents. The increased interaction between these analytes with an ion-exchange mechanism when in acetonitrile as opposed to

methanol is furthered supported by their observed retention in the separation developed in Chapter 7.[16] When using these solvent systems for the extraction from brain, it is demonstrated (Figure 8-7) that extraction efficiency of acetonitrile and methanol are quite similar. This combined with the previously discussed spiked-solvent experiments suggests that methanol is more efficient than acetonitrile at extracting these analytes from brain, however, results in lower extraction efficiency compared to acetonitrile. Similar behavior can also be found when extracting from crab tissue (Figure 8-8).

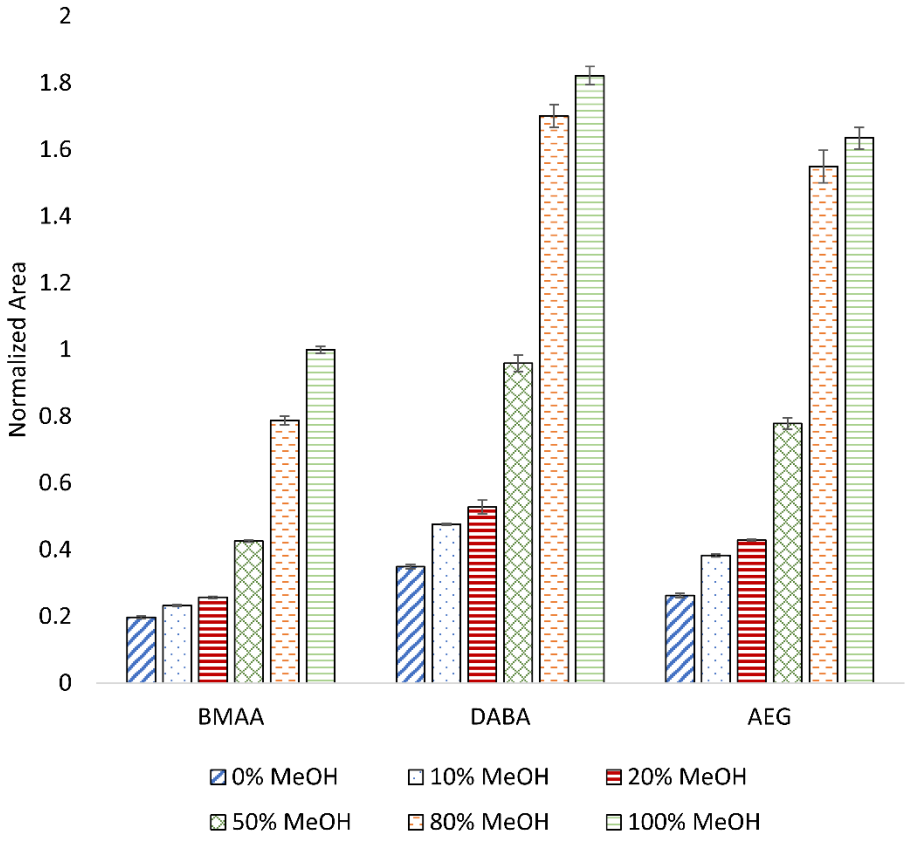

Figure 8-4 Effect of methanol content on the extraction of analyte spiked in pure solvent. Normalized based off the highest response obtained for BMAA.

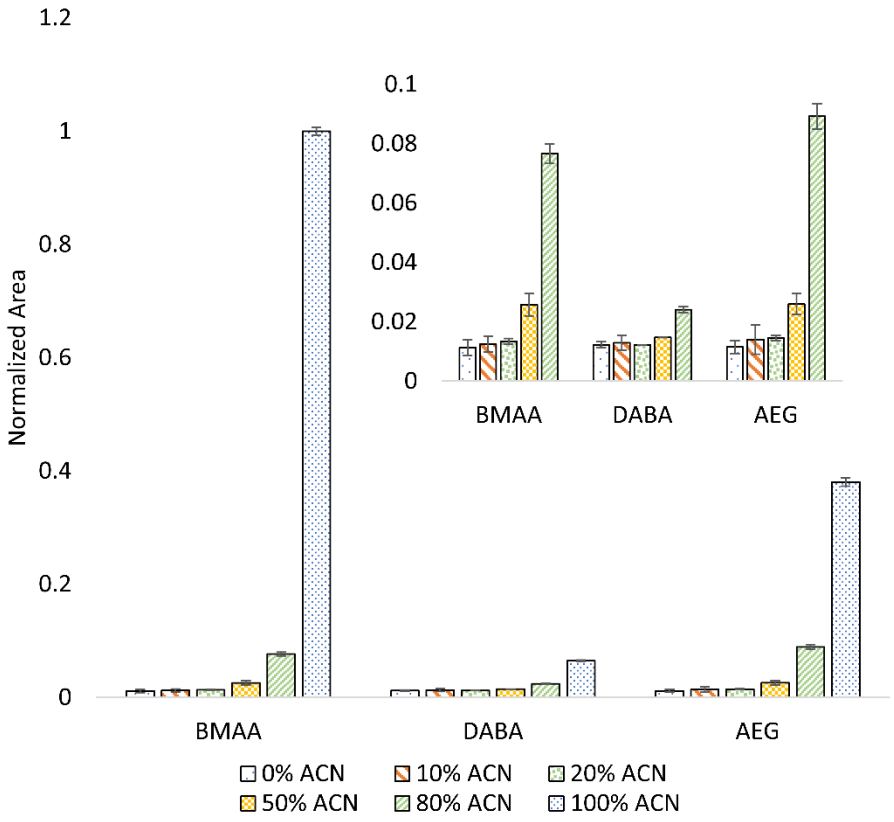

Figure 8-5 Effect of acetonitrile content on the extraction of analyte spiked in pure solvent. The inset figure demonstrates the same data with the 100% ACN values removed for clarity. Data normalized based on the highest response obtained for BMAA.

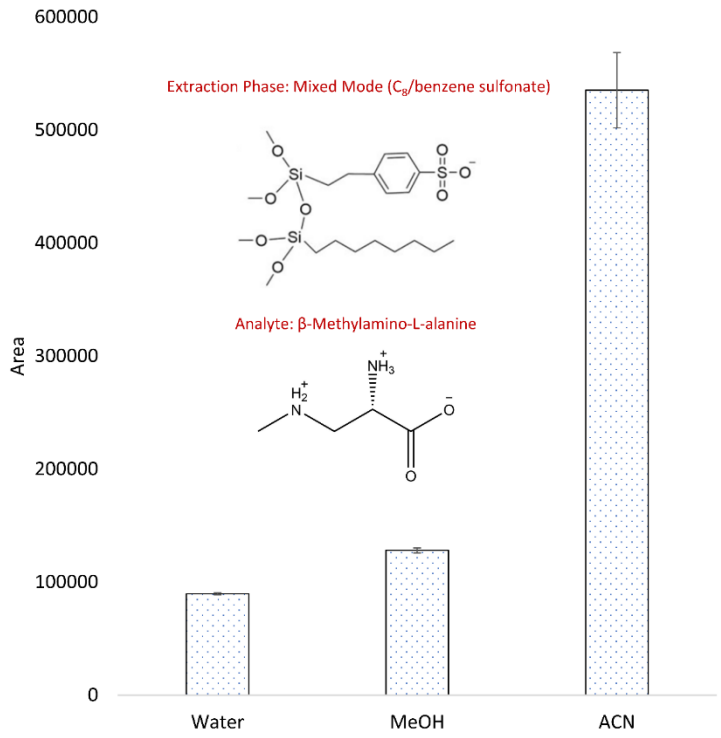

Figure 8-6 Comparison between the extraction of BMAA between water, methanol and acetonitrile solvent.

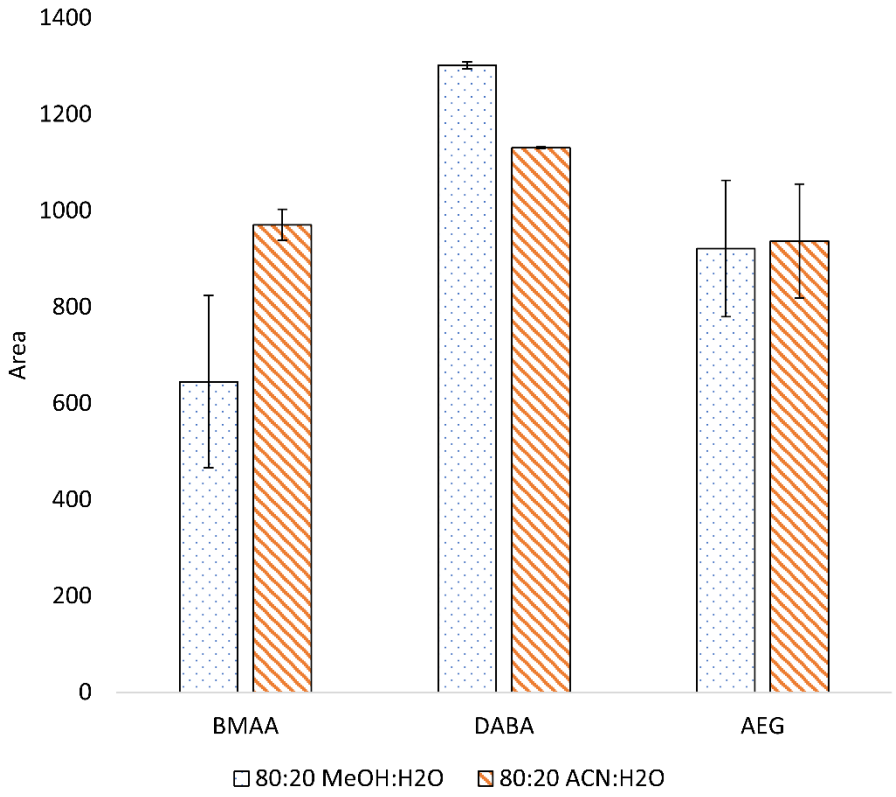

Figure 8-7 The extraction of analytes from the brain-solvent solution spiked with analytes after the sonication process.

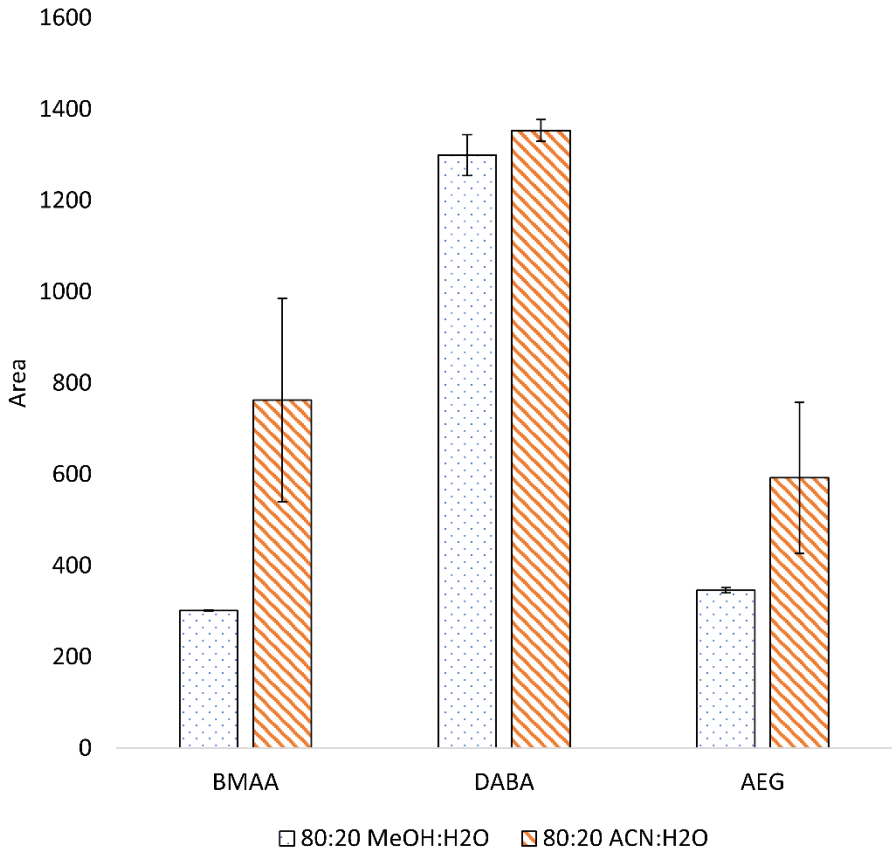

Figure 8-8 The extraction of analytes from the crab-solvent solution spiked with analytes after the sonication process.

8.3.2.2 Matrix Effects

Investigation into the matrix effects associated with this extraction method were then evaluated using the post extraction method.[324] This is performed by comparing the MS response of two samples: one sample (A) is neat desorption solution spiked at a known concentration. The other sample, B, is the same composition and concentration, however, SPME fibers were desorbed in this solution after undergoing the extraction process. In this way, desorption solution B will contain all matrix components extracted in the analytical workflow while desorption solution A will only contain the target analytes in the neat solvent. Shown in equation 8-1:

$$Matrix\ Effect\ \% = \frac{B}{A} \times 100\%$$

A matrix effect of 100% indicates no matrix effect while higher values indicate matrix enhancement and lower values indicate matrix suppression. This evaluation was performed with brain at different compositions of methanol and acetonitrile (Table 8.1) and the same applied for crab (Table 8.2). Results indicate minor matrix effects, with only the analyte DABA demonstrating considerable matrix effects when extracted from brain. A solvent composition of 80:20 acetonitrile:water was chosen as an optimal solvent choice for both matrices.

Table 8.1 Calculated matrix effect % for different solvents used for the extraction of the target analytes from brain.

	50:50 ACN:H_2O	80:20 ACN:H_2O	100 ACN	50:50 MeOH:H_2O	80:20 MeOH:H_2O	100 MeOH
BMAA	112.8	108.6	102.7	111.0	117.3	99.2
DABA	91.1	80.6	83.2	82.7	82.2	79.0
AEG	98.7	94.9	90.5	99.3	99.1	94.4

Table 8.2 Calculated matrix effect % for different solvents used for the extraction of the target analytes from crab.

	50:50 ACN:H_2O	80:20 ACN:H_2O	100 ACN	50:50 MeOH:H_2O	80:20 MeOH:H_2O	100 MeOH
BMAA	107.0	105.4	109.2	102.6	97.8	94.6
DABA	99.6	96.7	96.8	91.8	94.7	87.6
AEG	99.8	99.7	102.4	95.7	92.9	92.1

8.3.2.2 The Effect of Additives on Extraction

BMAA has previously been demonstrated to readily chelate with metals such as zinc, a metal found in high µmol concentration in the brain. An example of this chelation can be found in Figure 8-9.[325] Furthermore, interaction with other divalent cations is possible (e.g., magnesium), alongside the formation of carbamate adducts.[326] In light of this, the addition of metal chelating agents to the sample could disrupt these interactions, facilitating the transfer of analyte more readily into its free form in the solvent mixture. To test this, citric acid and disodium ethylenediaminetetraacetic acid (EDTA) were added to these matrices in opportune amounts (0, 0.1 and 0.5 M). While citric acid demonstrated complete loss of detectable analytes, the addition of 0.1 M EDTA showed a great

enhancement of the extraction of AEG (approximately 70 times larger response area) and a loss of extraction for the other two analytes. Most commercially available EDTA chemicals are not in their free acid form ($[CH_2N(CH_2CO_2H)_2]_2$) but are instead sold as a salt such as disodium EDTA dihydrate. To better probe the phenomena observed with AEG, varying concentrations of free acid EDTA, disodium EDTA dihydrate and sodium chloride were evaluated for their effect on analyte extraction both in neat 80:20 acetonitrile:water and also during the sonication process for brain. Concentration levels tested were 0.001, 0.01, and 0.1 M for free acid EDTA and disodium EDTA. For sodium chloride, 0.002, 0.02, and 0.2 M were used. All additives were added to 80:20 acetonitrile:water for this experiment. It is important to note that at the highest tested concentration level, these additives do not fully solubilize. Precipitate was removed during the centrifugation step.

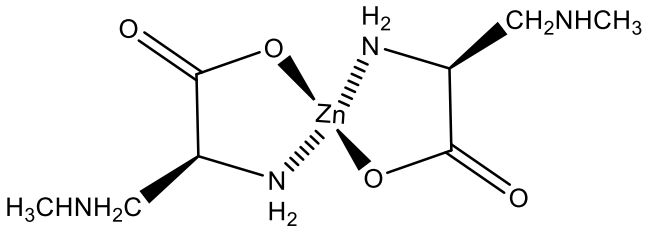

Figure 8-9 BMAA complexation with zinc.

Demonstrated in Figure 8-10, all three additives have effects on analyte extraction even without the presence of matrix, with both BMAA and DABA decreasing greatly at even the smallest concentrations. With increasing levels of both free EDTA and disodium EDTA, extraction efficiency generally reduces for BMAA and DABA but increases for AEG. On the other hand, sodium chloride reduces response for all analytes. When added during the sonication process with brain (Figure 8-11), the impact of additives on extraction efficiency is lessened. Some trends are reversed, such as larger amount of sodium chloride

increasing extraction efficiency when added to brain. Additional experiments were performed by adding 0.1% formic acid to the brain sample and removing the ice from the sonication bath; however, extraction was not enhanced. Curiously, it was demonstrated that the addition of free EDTA to the sample, both brain and pure solvent, increased extraction efficiency greatly for AEG. This behavior in pure solvent suggests it's not a chelating phenomenon but EDTA sequestering AEG away from the solvent mixture. The specificity of this EDTA – AEG interaction is still being investigated. To further probe the effect of different constituents on extraction efficiency, an unspiked sample of brain was sonicated in 80:20 acetonitrile:water. The resulting solution was spiked with a mixture of analytes at the same concentration as Figure 8-10 (200 ppb) and let sit for 30 min to equilibrate. Subsequently, SPME was performed as previously described. Due to the very minor matrix effect of this extraction method as shown in Table 8.1, any difference between the response of this experiment and spiking additive-free neat solution will be a result of analyte-matrix component interactions. Referred to in Figure 8-10 as "Brain-Solvent Sample", extraction efficiency severely reduced when extracting from this spiked sample. These data together suggests that a large portion of analyte is not in its free form, but instead associated with matrix components such as divalent cations. As chelating agents were unable to avoid this phenomenon, it is possible that the addition of competing amino acids (e.g., serine) will displace analyte from matrix components and allow them to be further extracted.

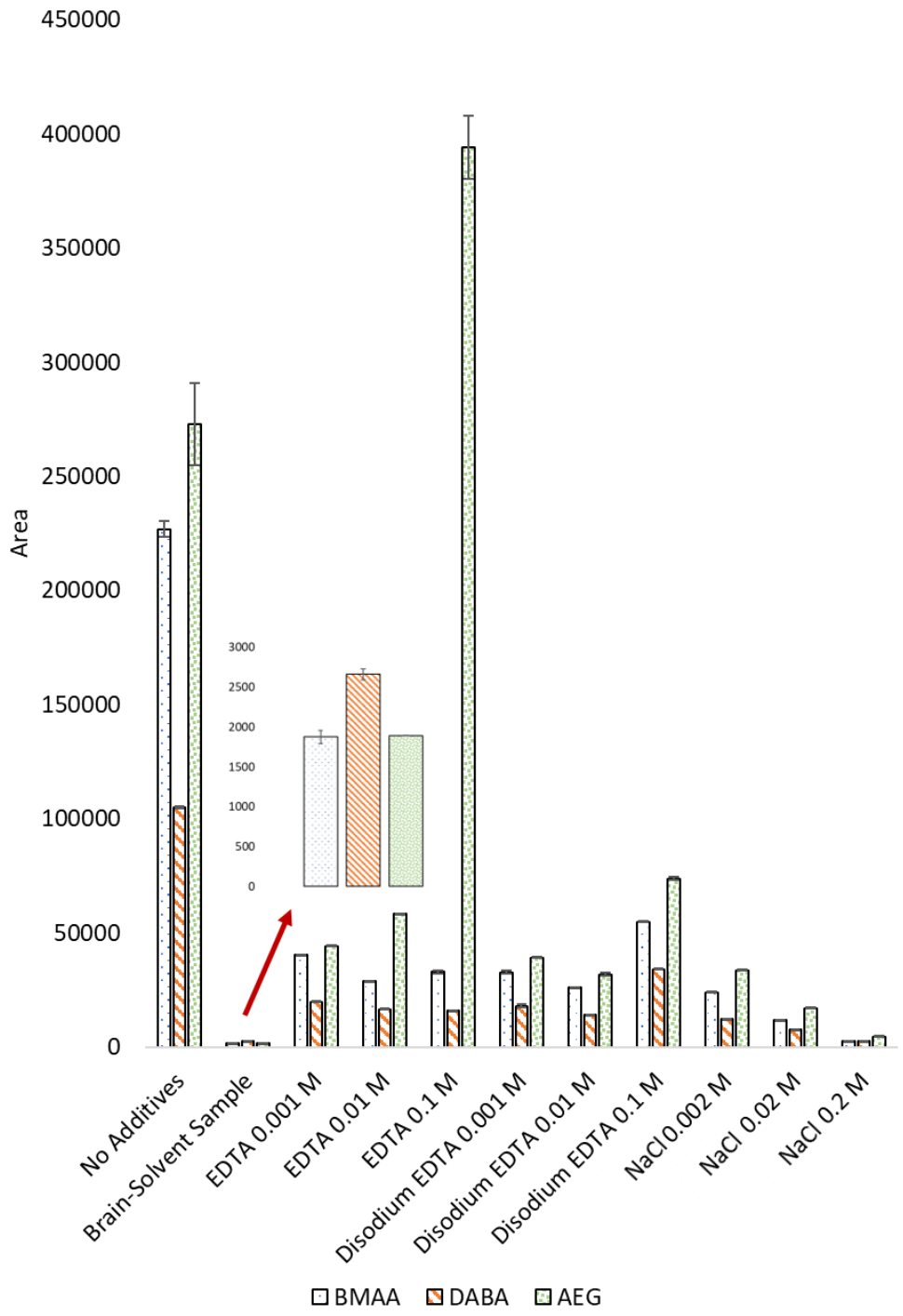

Figure 8-10 Extraction from 80:20 ACN:H_2O with varying levels of additives. Analytes spiked at 200 ppb. For the brain-solvent sample, the 80:20 ACN:H_2O solution was first used to sonicate an unspiked brain sample.

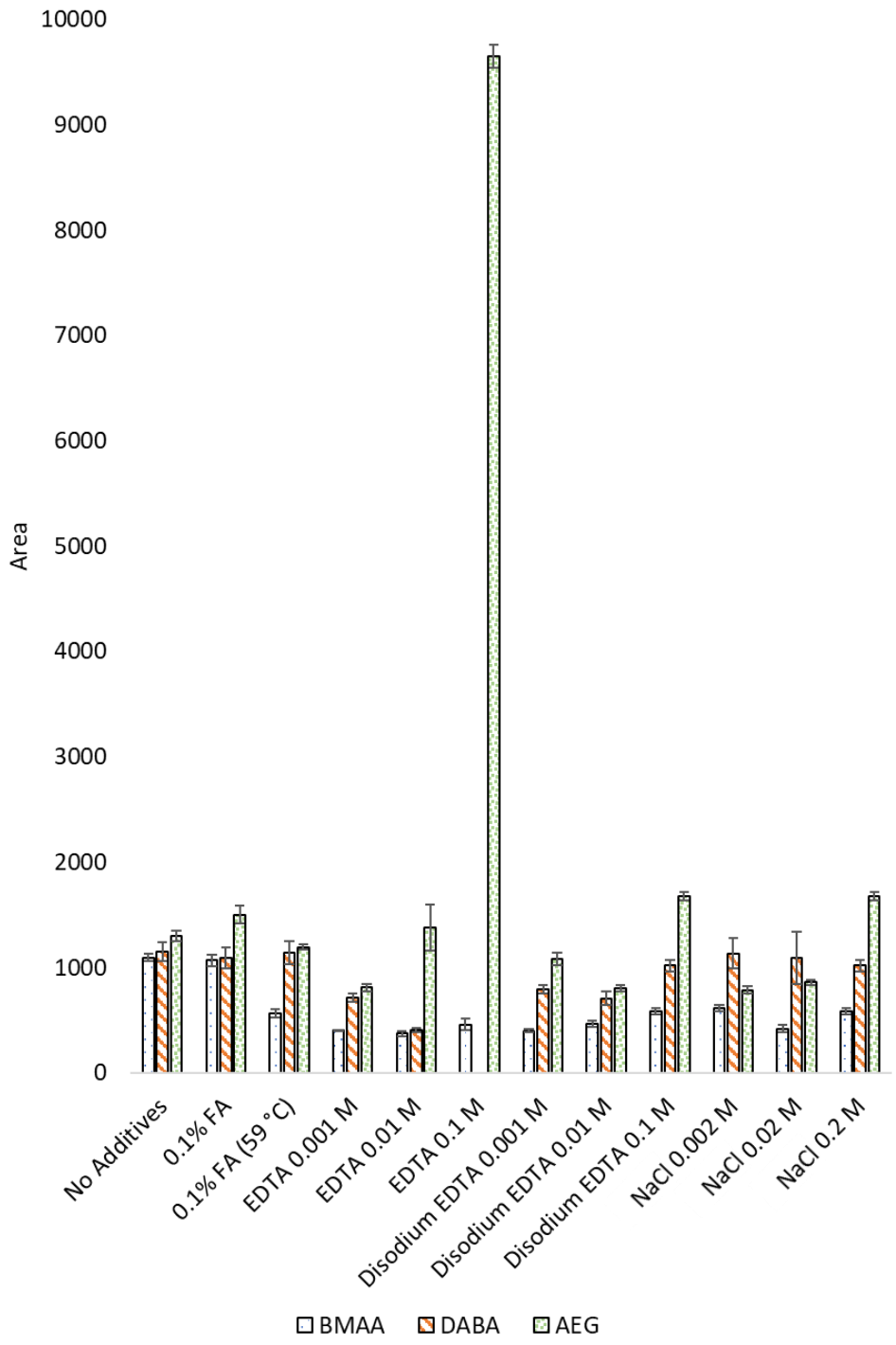

Figure 8-11 Extraction from 80:20 ACN:H_2O used to sonicate brain with different concentrations of additives.

8.3.3 Sample Hydrolysis

Extraction methods for the analysis of BMAA from brain, crab and other matrices often involve hydrolysis in 6 N HCl at elevated temperatures of 110 °C for up to 24 hours. While this should result in complete hydrolysis of the sample, it also removes any information on the difference between the free bioavailable portion of BMAA and BMAA incorporated into proteins or other matrix associations. Preliminary work employed these same conditions, followed by evaporation of the sample to dryness and reconstitution to water. Extractions from this water demonstrated no detectable analyte, possibly due to the sample itself being very acidic and presumably containing matrix components not easily accessed from the other extraction methods. In light of this, milder hydrolysis conditions were investigated including 3 M HCl, formic acid, citric acid and acetic acid. After dry ice homogenization, 1 g of brain was portioned to each vial and suspended in an aqueous solution of the various acids. This mixture was heated at 110 °C for a total of 12 hours and then evaporated to dryness. After reconstitution in 5 mL of a 80:20 acetonitrile:water mixture, 0.25 M of ammonium acetate was added to increase the pH, facilitating SPME extraction. The pH of the acetic acid and formic acid samples were approximately 4.5, with HCl being 3 and citric acid 1 even with additional ammonium acetate to the concentration of 0.75 M. Out of the 4 samples, citric acid was not extracted from due to its low pH and the HCl sample separated into two separate phases, this sample then being centrifuged and the aqueous portion being sampled. Samples can be visualized in Figure 8-12. Analyte response was found to be much lower with this method than solvent-mediated SPME extraction (Figure 8-13).

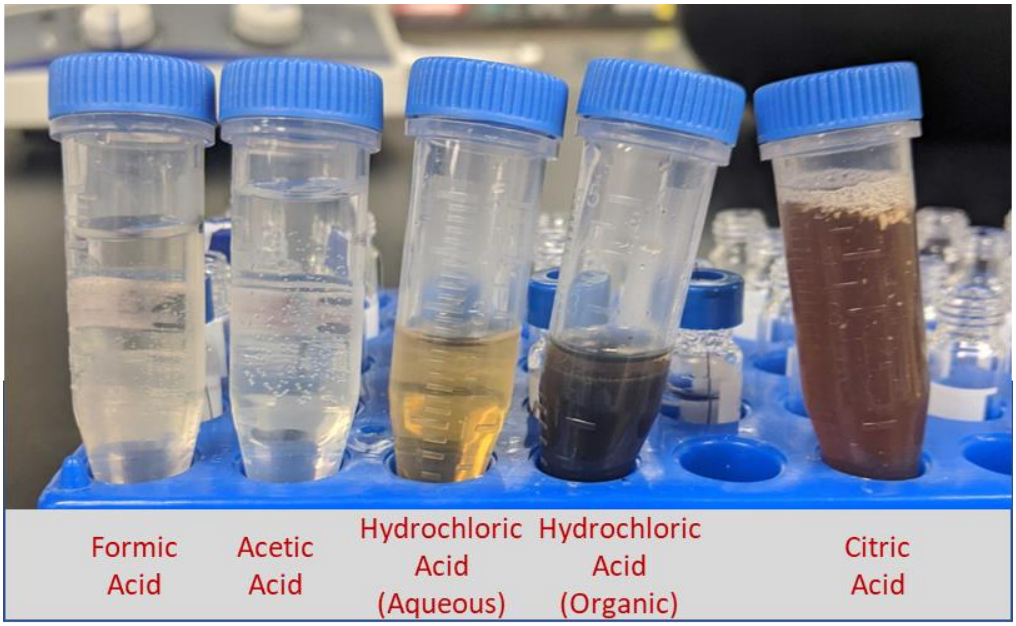

Figure 8-12 Solvent extracts from brain with different acids used in the hydrolysis process.

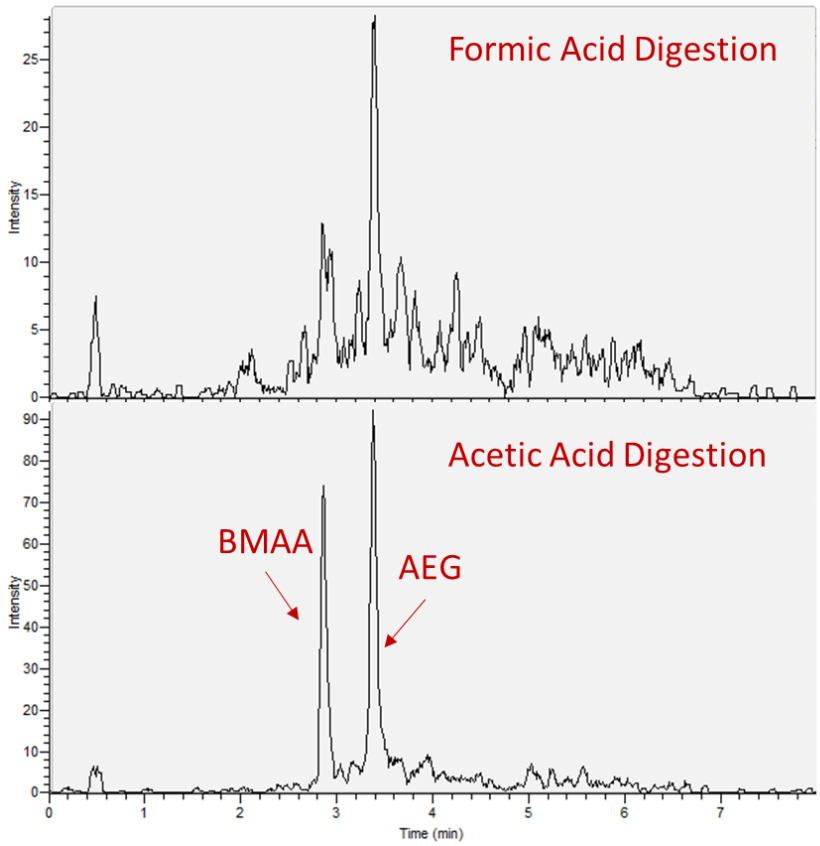

Figure 8-13 Chromatograms obtained for the hydrolysis samples of brain. This was performed using formic and acetic acid, the brain spiked at 1 ppm for the target analytes.

8.4 Conclusions

An extraction approach was developed for the SPME extraction of BMAA and its isomers from brain and blue crab, the developed methodology avoiding fouling of the extraction phase. Furthermore, the effect of common organic solvents was evaluated for their impact on ion-exchange SPME, revealing a strategy to increase extraction efficiency when low-dielectric constant solvents are added to the matrix. Further investigation into sample additives should be explored to improve the extraction of analyte prior to method validation and assessment of the methods limit of detection. Moreover, the evaluation of

alternative methods to free these amino acids from proteins, such as the use of proteinase K, could prove to be a more suitable approach comparatively to acid-hydrolysis.

Acknowledgements

This work was in part supported by the American Chemical Society Division of Analytical Chemistry Graduate Fellowship Program sponsored by PittCon along with the Restek Academic Support Program. We also would like to thank Supelco-Millipore Sigma for providing the MM/PAN SPME devices used.

References

(1) Moldoveanu, S.; David, V. *Sample Preparation In Chromatography*, 1st ed.; Elsevier, 2002.

(2) Chen, Y.; Guo, Z.; Wang, X.; Qiu, C. Sample Preparation. *J. Chromatogr. A* **2008**, *1184* (1–2), 191–219. https://doi.org/10.1016/j.chroma.2007.10.026.

(3) Kim, L.; Lee, D.; Cho, H. K.; Choi, S. D. Review of the QuEChERS Method for the Analysis of Organic Pollutants: Persistent Organic Pollutants, Polycyclic Aromatic Hydrocarbons, and Pharmaceuticals. *Trends Environ. Anal. Chem.* **2019**, *22*. https://doi.org/10.1016/j.teac.2019.e00063.

(4) Kanu, A. B. Recent Developments in Sample Preparation Techniques Combined with High-Performance Liquid Chromatography: A Critical Review. *J. Chromatogr. A* **2021**, *1654*, 462444. https://doi.org/10.1016/j.chroma.2021.462444.

(5) Zhang, L.; Liu, S.; Cui, X.; Pan, C.; Zhang, A.; Chen, F. A Review of Sample Preparation Methods for the Pesticide Residue Analysis in Foods. *Cent. Eur. J. Chem.* **2012**, *10* (3), 900–925. https://doi.org/10.2478/s11532-012-0034-1.

(6) Pawliszyn, J. *Sampling and Sample Preparation for Field and Laboratory: Fundamentals and New Directions in Sample Preparation*; 2002.

(7) Pawliszyn, J. Sample Preparation: Quo Vadis? *Anal. Chem.* **2003**, *75* (11), 2543–

2558. https://doi.org/10.1021/ac034094h.

(8) Wen, Y.; Chen, L.; Li, J.; Liu, D.; Chen, L. Recent Advances in Solid-Phase Sorbents for Sample Preparation Prior to Chromatographic Analysis. *TrAC - Trends Anal. Chem.* **2014**, *59*, 26–41. https://doi.org/10.1016/j.trac.2014.03.011.

(9) Hennion, M. C. Solid-Phase Extraction: Method Development, Sorbents, and Coupling with Liquid Chromatography. *J. Chromatogr. A* **1999**, *856* (1–2), 3–54. https://doi.org/10.1016/S0021-9673(99)00832-8.

(10) Badawy, M. E. I.; El-Nouby, M. A. M.; Kimani, P. K.; Lim, L. W.; Rabea, E. I. *A Review of the Modern Principles and Applications of Solid-Phase Extraction Techniques in Chromatographic Analysis*; Springer Nature Singapore, 2022; Vol. 38. https://doi.org/10.1007/s44211-022-00190-8.

(11) Andrade-Eiroa, A.; Canle, M.; Leroy-Cancellieri, V.; Cerdà, V. Solid-Phase Extraction of Organic Compounds: A Critical Review. Part Ii. *TrAC - Trends Anal. Chem.* **2016**, *80*, 655–667. https://doi.org/10.1016/j.trac.2015.08.014.

(12) Pawliszyn, J. *Handbook of Solid Phase Microextraction*; Chemical Industry Press: Beijing, 2009. https://doi.org/10.1016/C2011-0-04297-7.

(13) Berrueta, L. A.; Gallo, B.; Vicente, F. A Review of Solid Phase Extraction: Basic Principles and New Developments. *Chromatographia*. 1995, pp 474–483. https://doi.org/10.1007/BF02269916.

(14) Arthur, C. L.; Pawliszyn, J. Solid Phase Microextraction with Thermal Desorption Using Fused Silica Optical Fibers. *Anal. Chem.* **1990**, *62* (19), 2145–2148. https://doi.org/10.1021/ac00218a019.

(15) Emmons, R. V; Tajali, R.; Gionfriddo, E. Development, Optimization and

Applications of Thin Film Solid Phase Microextraction (TF-SPME) Devices for Thermal Desorption: A Comprehensive Review. *Separations*. 2019, p 39. https://doi.org/10.3390/separations6030039.

(16) Emmons, R. V.; Karaj, E.; Cudjoe, E.; Bell, D. S.; Tillekeratne, L. M. V.; Gionfriddo, E. Leveraging Multi-Mode Microextraction and Liquid Chromatography Stationary Phases for Quantitative Analysis of Neurotoxin β-N-Methylamino-L-Alanine and Other Non-Proteinogenic Amino Acids. *J. Chromatogr. A* **2022**, *1685*, 463636. https://doi.org/10.1016/j.chroma.2022.463636.

(17) Godage, N. H.; Cudjoe, E.; Neupane, R.; Boddu, S. H.; Bolla, P. K.; Renukuntla, J.; Gionfriddo, E. Biocompatible SPME Fibers for Direct Monitoring of Nicotine and Its Metabolites at Ultra Trace Concentration in Rabbit Plasma Following the Application of Smoking Cessation Formulations. *J. Chromatogr. A* **2020**, *1626*. https://doi.org/10.1016/j.chroma.2020.461333.

(18) Musteata, M. L.; Musteata, F. M.; Pawliszyn, J. Biocompatible Solid-Phase Microextraction Coatings Based on Polyacrylonitrile and Solid-Phase Extraction Phases. *Anal. Chem.* **2007**, *79* (18), 6903–6911. https://doi.org/10.1021/ac070296s.

(19) Reyes-Garcés, N.; Gionfriddo, E.; Gómez-Ríos, G. A.; Alam, M. N.; Boyacı, E.; Bojko, B.; Singh, V.; Grandy, J.; Pawliszyn, J. Advances in Solid Phase Microextraction and Perspective on Future Directions. *Anal. Chem.* **2018**, *90*, 302–360. https://doi.org/10.1021/acs.analchem.7b04502.

(20) Bianchin, J. N.; Nardini, G.; Merib, J.; Dias, A. N.; Martendal, E.; Carasek, E. Screening of Volatile Compounds in Honey Using a New Sampling Strategy

Combining Multiple Extraction Temperatures in a Single Assay by HS-SPME-GC-MS. *Food Chem.* **2014**, *145*, 1061–1065. https://doi.org/10.1016/j.foodchem.2013.08.139.

(21) Reyes-Garcés, N.; Gionfriddo, E.; Gómez-Ríos, G. A.; Alam, M. N.; Boyaci, E.; Bojko, B.; Singh, V.; Grandy, J.; Pawliszyn, J. Advances in Solid Phase Microextraction and Perspective on Future Directions. *Anal. Chem.* **2018**, *90* (1), 302–360. https://doi.org/10.1021/acs.analchem.7b04502.

(22) Alam, M. N.; Pawliszyn, J. Effect of Binding Components in Complex Sample Matrices on Recovery in Direct Immersion Solid-Phase Microextraction: Friends or Foe? *Anal. Chem.* **2018**, *90* (4), 2430–2433. https://doi.org/10.1021/acs.analchem.7b05436.

(23) Emmons, R. V.; Olomukoro, A. A.; Gionfriddo, E. Microextraction-Based Samplers for Liquid and Tissue Analysis. In *Analytical Sample Preparation With Nano- and Other High-Performance Materials*; Elsevier, 2021; pp 131–158. https://doi.org/10.1016/b978-0-12-822139-6.00017-1.

(24) James, A. T.; Martin, A. J. Gas-Liquid Partition Chromatography; the Separation and Micro-Estimation of Volatile Fatty Acids from Formic Acid to Dodecanoic Acid. *Biochem. J.* **1952**, *50* (5), 679–690. https://doi.org/10.1042/bj0500679.

(25) Grob, R. L.; Barry, E. F. *Modern Practice of Gas Chromatography*, 4th ed.; John Wiley & Sons, Inc., 2004; Vol. 29. https://doi.org/10.1002/0471651141.

(26) Sandra, P. *High Resolution Gas Chromatography*, 2nd ed.; Hyver, K. J., Ed.; HEWLETT-PACKARD, 1989.

(27) Snow, N. H. Split , Splitless, and Beyond — Getting the Most from Your Inlet

from Dea to Delivery Simply Solved. *LCGC North Am.* **2018**, *36* (7), 448–455.

(28) Snow, N. H. Split/Splitless Inlets in Gas Chromatography: What's Up with All Those Different Glass Inlet Liners? *LC-GC North Am.* **2022**, *40* (3), 121–124. https://doi.org/10.56530/lcgc.na.wv7676x8.

(29) Grandy, J. J.; Boyaci, E.; Pawliszyn, J. Development of a Carbon Mesh Supported Thin Film Microextraction Membrane As a Means to Lower the Detection Limits of Benchtop and Portable GC/MS Instrumentation. *Anal. Chem.* **2016**, *88* (3), 1760–1767. https://doi.org/10.1021/acs.analchem.5b04008.

(30) Grandy, J. J.; Singh, V.; Lashgari, M.; Gauthier, M.; Pawliszyn, J. Development of a Hydrophilic Lipophilic Balanced Thin Film Solid Phase Microextraction Device for Balanced Determination of Volatile Organic Compounds. *Anal. Chem.* **2018**, *90* (23), 14072–14080. https://doi.org/10.1021/acs.analchem.8b04544.

(31) Hoh, E.; Mastovska, K. Large Volume Injection Techniques in Capillary Gas Chromatography. *J. Chromatogr. A* **2008**, *1186* (1–2), 2–15. https://doi.org/10.1016/j.chroma.2007.12.001.

(32) Hoffman, E. de; Stroobant, V. *Mass Spectrometry: Principles and Applications*, 3rd ed.; John Wiley & Sons, Ltd, 2007.

(33) Maciel, E. V. S.; Pereira dos Santos, N. G.; Vargas Medina, D. A.; Lanças, F. M. Electron Ionization Mass Spectrometry: Quo Vadis? *Electrophoresis* **2022**, *43* (15), 1587–1600. https://doi.org/10.1002/elps.202100392.

(34) Beran, J. A.; Kevan, L. Molecular Electron Ionization Cross Sections at 70 EV. *J. Phys. Chem.* **1969**, *73* (11), 3866–3876. https://doi.org/10.1021/j100845a050.

(35) Snyder, L. R.; Kirkland, J. J.; Dolan, J. W. *Introduction to Modern Liquid*

Chromatography, 3rd ed.; John Wiley & Sons, Inc., 2009. https://doi.org/10.1093/jaoac/58.1.169.

(36) Guo, Y.; Gaiki, S. Retention and Selectivity of Stationary Phases for Hydrophilic Interaction Chromatography. *J. Chromatogr. A* **2011**, *1218* (35), 5920–5938. https://doi.org/10.1016/j.chroma.2011.06.052.

(37) Jandera, P. Stationary and Mobile Phases in Hydrophilic Interaction Chromatography: A Review. *Anal. Chim. Acta* **2011**, *692* (1–2), 1–25. https://doi.org/10.1016/j.aca.2011.02.047.

(38) Valkó, K.; Snyder, L. R.; Glajch, J. L. Retention in Reversed-Phase Liquid Chromatography as a Function of Mobile-Phase Composition. *J. Chromatogr. A* **1993**, *656* (1–2), 501–520. https://doi.org/10.1016/0021-9673(93)80816-Q.

(39) Hemström, P.; Irgum, K. *Hydrophilic Interaction Chromatography*; 2006; Vol. 29. https://doi.org/10.1002/jssc.200600199.

(40) Nawrocki, J. The Silanol Group and Its Role in Liquid Chromatography. *J. Chromatogr. A* **1997**, *779* (1–2), 29–71. https://doi.org/10.1016/S0021-9673(97)00479-2.

(41) Sýkora, D.; Řezanka, P.; Záruba, K.; Král, V. Recent Advances in Mixed-Mode Chromatographic Stationary Phases. *J. Sep. Sci.* **2019**, *42* (1), 89–129. https://doi.org/10.1002/jssc.201801048.

(42) Fenn, J. B.; Mann, M.; Meng, C. K.; Wong, S. F. Electrospray Ionization-Principles and Practice. *Mass Spectrom. Rev.* **1990**, *9*, 37–70.

(43) de la Mora, J. F.; Loscertales, I. G. The Current Emitted by Highly Conducting Taylor Cones. *J. Fluid Mech.* **1994**, *260* (special issue), 155–184.

https://doi.org/10.1017/S0022112094003472.

(44) Konermann, L.; Ahadi, E.; Rodriguez, A. D.; Vahidi, S. Unraveling the Mechanism of Electrospray Ionization. *Anal. Chem.* **2013**, *85* (1), 2–9. https://doi.org/10.1021/ac302789c.

(45) Cech, N. B.; Enke, C. G. Practical Implications of Some Recent Studies in Electrospray Ionization Fundamentals. *Mass Spectrom. Rev.* **2001**, *20* (6), 362–387. https://doi.org/10.1002/mas.10008.

(46) Douglas, D. J.; Frank, A. J.; Mao, D. Linear Ion Traps in Mass Spectrometry. *Mass Spectrom. Rev.* **2005**, *24* (1), 1–29. https://doi.org/10.1002/mas.20004.

(47) Sleno, L.; Volmer, D. A. Ion Activation Methods for Tandem Mass Spectrometry. *J. Mass Spectrom.* **2004**, *39* (10), 1091–1112. https://doi.org/10.1002/jms.703.

(48) Kuo, T. H.; Dutkiewicz, E. P.; Pei, J.; Hsu, C. C. Ambient Ionization Mass Spectrometry Today and Tomorrow: Embracing Challenges and Opportunities. *Anal. Chem.* **2020**, *92* (3), 2353–2363. https://doi.org/10.1021/acs.analchem.9b05454.

(49) Cody, R. B.; Laramée, J. A.; Durst, H. D. Versatile New Ion Source for the Analysis of Materials in Open Air under Ambient Conditions. *Anal. Chem.* **2005**, *77* (8), 2297–2302. https://doi.org/10.1021/ac050162j.

(50) Cody, R. B. Observation of Molecular Ions and Analysis of Nonpolar Compounds with the Direct Analysis in Real Time Ion Source. *Anal. Chem.* **2009**, *81* (3), 1101–1107. https://doi.org/10.1021/ac8022108.

(51) Cody, R. B.; Dane, A. J. Soft Ionization of Saturated Hydrocarbons, Alcohols and Nonpolar Compounds by Negative-Ion Direct Analysis in Real-Time Mass

Spectrometry. *J. Am. Soc. Mass Spectrom.* **2013**, *24* (3), 329–334. https://doi.org/10.1007/s13361-012-0569-6.

(52) Yost, R. A.; Enke, C. G. Triple Quadrupole Mass Spectrometry for Direct Mixture Analysis and Structure Elucidation. *Anal. Chem.* **1979**, *51* (12). https://doi.org/10.1021/ac50048a002.

(53) Emmons, R. V; Devasurendra, A. M.; Godage, N. H.; Gionfriddo, E. Exploring the Efficiency of Various Extraction Approaches for Determination of Crude (4-Methylcyclohexyl)Methanol (MCHM) Constituents in Environmental Samples. *LCGC North Am.* **2019**, *37* (S4), 28–34.

(54) Eastman Chemical Company. Crude MCHM- Safety Data Sheet Version 3.1. **2016**, 1–18.

(55) Ahart, M.; Gallagher, D. L.; Scardina, P.; Dietrich, A. M. Industrial Spills and Water Distribution: Crude MCHM Sorption and Desorption in Polymer Pipes and Linings. *J. Environ. Eng.* **2016**, *142* (10), 04016045. https://doi.org/10.1061/(ASCE)EE.1943-7870.0001116.

(56) West Virginia Division of Homeland Security and Emergency Management. Operation Log 18Jan1800 Initial http://dhsem.wv.gov/Documents/Sampling Results/OPERATION LOG 18JAN1800 Initial.pdf.

(57) West Virginia Division of Homeland Security and Emergency Management. MCHM test results at 2 ppb http://dhsem.wv.gov/Documents/Sampling Results/MCHM Test Results at 2ppb.pdf.

(58) Whelton, A. J.; McMillan, L. K.; Connell, M.; Kelley, K. M.; Gill, J. P.; White, K. D.; Gupta, R.; Dey, R.; Novy, C. Residential Tap Water Contamination Following

the Freedom Industries Chemical Spill: Perceptions, Water Quality, and Health Impacts. *Environ. Sci. Technol.* **2015**, *49* (2), 813–823. https://doi.org/10.1021/es5040969.

(59) Foreman, W. T.; Rose, D. L.; Chambers, D. B.; Crain, A. S.; Murtagh, L. K.; Thakellapalli, H.; Wang, K. K. Determination of (4-Methylcyclohexyl)Methanol Isomers by Heated Purge-and-Trap GC/MS in Water Samples from the 2014 Elk River, West Virginia, Chemical Spill. *Chemosphere* **2015**, *131*, 217–224. https://doi.org/10.1016/j.chemosphere.2014.11.006.

(60) Disaster Response and Recovery Needs of Communities Affected by the Elk River Chemical Spill, West Virginia. U.S. CDC, Nation Center for Environmental Health, Division of Environmental Hazards and Health Effects; Health Studies Branch: Atlanta, GA USA http://dhhr.wv.gov/News/2014/Documents/WVCASPERReport.pdf.

(61) Lan, J.; Hu, M.; Gao, C.; Alshawabkeh, A.; Gu, A. Z. Toxicity Assessment of 4-Methyl-1-Cyclohexanemethanol and Its Metabolites in Response to a Recent Chemical Spill in West Virginia, USA. *Environ. Sci. Technol.* **2015**, *49* (10), 6284–6293. https://doi.org/10.1021/acs.est.5b00371.

(62) Han, A. A.; Fabyanic, E. B.; Miller, J. V.; Prediger, M. S.; Prince, N.; Mouch, J. A.; Boyd, J. In Vitro Cytotoxicity Assessment of a West Virginia Chemical Spill Mixture Involving 4-Methylcyclohexanemethanol and Propylene Glycol Phenyl Ether. *Environ. Monit. Assess.* **2017**, *189* (4), 190. https://doi.org/10.1007/s10661-017-5895-5.

(63) Weidhaas, J.; Lin, L. S.; Buzby, K. A Case Study for Orphaned Chemicals: 4-

Methylcyclohexanemethanol (MCHM) and Propylene Glycol Phenyl Ether (PPH) in Riverine Sediment and Water Treatment Processes. *Sci. Total Environ.* **2017**, *574*, 1396–1404. https://doi.org/10.1016/j.scitotenv.2016.08.063.

(64) Gallagher, D. L.; Phetxumphou, K.; Smiley, E.; Dietrich, A. M. Tale of Two Isomers: Complexities of Human Odor Perception for Cis - And Trans -4-Methylcyclohexane Methanol from the Chemical Spill in West Virginia. *Environ. Sci. Technol.* **2015**, *49* (3), 1319–1327. https://doi.org/10.1021/es5049418.

(65) Jeter, T. S.; Sarver, E. A.; McNair, H. M.; Rezaee, M. 4-MCHM Sorption to and Desorption from Granular Activated Carbon and Raw Coal. *Chemosphere* **2016**, *157*, 160–165. https://doi.org/10.1016/j.chemosphere.2016.04.125.

(66) Cozzarelli, I. M.; Akob, D. M.; Baedecker, M. J.; Spencer, T.; Jaeschke, J.; Dunlap, D. S.; Mumford, A. C.; Poret-Peterson, A. T.; Chambers, D. B. Degradation of Crude 4-MCHM (4-Methylcyclohexanemethanol) in Sediments from Elk River, West Virginia. *Environ. Sci. Technol.* **2017**, *51* (21), 12139–12145. https://doi.org/10.1021/acs.est.7b03142.

(67) Speijers, G.; Renwick, A. WHO Food Additives Series: 50. Alicyclic Primary Alcohols, Aldehydes, Acids, and Related Esters http://www.inchem.org/documents/jecfa/jecmono/v50je10.htm.

(68) Munch, J. W.; Grimmet, P. *Method 522 - Determination of 1,4-Dioxane in Drinking Water by Solid Phase Extraction (SPE) and Gas Chromatography Mass Spectrometry (GC/MS) with Selected Ion Monitoring (SIM)*; 2008.

(69) Emmons, R. V; Liden, T.; Schug, K. A.; Gionfriddo, E. Optimization of Thin Film Solid Phase Microextraction and Data Deconvolution Methods for Accurate

Characterization of Organic Compounds in Produced Water. *J. Sep. Sci.* **2020**, *42* (9–10), 1915–1924. https://doi.org/10.1002/jssc.201901330.

(70) Sun, Y.; Wang, D.; Tsang, D. C. W.; Wang, L.; Ok, Y. S.; Feng, Y. A Critical Review of Risks, Characteristics, and Treatment Strategies for Potentially Toxic Elements in Wastewater from Shale Gas Extraction. *Environ. Int.* **2019**, *125* (October 2018), 452–469. https://doi.org/10.1016/j.envint.2019.02.019.

(71) Ferrer, I.; Thurman, E. M. Chemical Constituents and Analytical Approaches for Hydraulic Fracturing Waters. *Trends Environ. Anal. Chem.* **2015**, *5*, 18–25. https://doi.org/10.1016/j.teac.2015.01.003.

(72) OWRB. Report of the Oklahoma Water for 2060 Produced Water Reuse and Recycling. **2017**.

(73) Liden, T.; Santos, I. C.; Hildenbrand, Z. L.; Schug, K. A. Treatment Modalities for the Reuse of Produced Waste from Oil and Gas Development. *Sci. Total Environ.* **2018**, *643*, 107–118. https://doi.org/10.1016/j.scitotenv.2018.05.386.

(74) Liden, T.; Carlton, D. D.; Miyazaki, S.; Otoyo, T.; Schug, K. A. Forward Osmosis Remediation of High Salinity Permian Basin Produced Water from Unconventional Oil and Gas Development. *Sci. Total Environ.* **2019**, *653*, 82–90. https://doi.org/10.1016/j.scitotenv.2018.10.325.

(75) Liden, T.; Hildenbrand, Z. L.; Schug, K. A. Pretreatment Techniques for Produced Water with Subsequent Forward Osmosis Remediation. *Water* **2019**, *11* (7), 1437. https://doi.org/10.3390/w11071437.

(76) Sosa-Fernandez, P. A.; Post, J. W.; Leermakers, F. A. M.; Rijnaarts, H. H. M.; Bruning, H. Removal of Divalent Ions from Viscous Polymer-Flooding Produced

Water and Seawater via Electrodialysis. *J. Memb. Sci.* **2019**, *589* (July), 117251. https://doi.org/10.1016/j.memsci.2019.117251.

(77) Chang, H.; Li, T.; Liu, B.; Vidic, R. D.; Elimelech, M.; Crittenden, J. C. Potential and Implemented Membrane-Based Technologies for the Treatment and Reuse of Flowback and Produced Water from Shale Gas and Oil Plays: A Review. *Desalination* **2019**, *455* (January), 34–57. https://doi.org/10.1016/j.desal.2019.01.001.

(78) Danforth, C.; McPartland, J.; Blotevogel, J.; Coleman, N.; Devlin, D.; Olsgard, M.; Parkerton, T.; Saunders, N. Alternative Management of Oil and Gas Produced Water Requires More Research on Its Hazards and Risks. *Integr. Environ. Assess. Manag.* **2019**, *15* (5), 677–682. https://doi.org/10.1002/ieam.4160.

(79) Shonkoff, S. Is Reuse of Produced Water Safe? First, Let's Find out What's in It. *Mag. Environ. Manag.* **2017**, No. August.

(80) Hildenbrand, Z. L.; Santos, I. C.; Liden, T.; Carlton, D. D.; Varona-Torres, E.; Martin, M. S.; Reyes, M. L.; Mulla, S. R.; Schug, K. A. Characterizing Variable Biogeochemical Changes during the Treatment of Produced Oilfield Waste. *Sci. Total Environ.* **2018**, *634*, 1519–1529. https://doi.org/10.1016/j.scitotenv.2018.03.388.

(81) Hoelzer, K.; Sumner, A. J.; Karatum, O.; Nelson, R. K.; Drollette, B. D.; O'Connor, M. P.; D'Ambro, E. L.; Getzinger, G. J.; Ferguson, P. L.; Reddy, C. M.; et al. Indications of Transformation Products from Hydraulic Fracturing Additives in Shale-Gas Wastewater. *Environ. Sci. Technol.* **2016**, *50* (15), 8036–8048. https://doi.org/10.1021/acs.est.6b00430.

(82) Thomas, H. Sampling and Analysis of Water Streams Associated with the Development of Marcellus Shale Gas. *Final Rep. Marcellus Shale Coalit.* **2009**, 249 pp.

(83) Orem, W.; Tatu, C.; Varonka, M.; Lerch, H.; Bates, A.; Engle, M.; Crosby, L.; McIntosh, J. Organic Substances in Produced and Formation Water from Unconventional Natural Gas Extraction in Coal and Shale. *Int. J. Coal Geol.* **2014**, *126*, 20–31. https://doi.org/10.1016/j.coal.2014.01.003.

(84) Akob, D. M.; Cozzarelli, I. M.; Dunlap, D. S.; Rowan, E. L.; Lorah, M. M. Organic and Inorganic Composition and Microbiology of Produced Waters from Pennsylvania Shale Gas Wells. *Appl. Geochemistry* **2015**, *60*, 116–125. https://doi.org/10.1016/j.apgeochem.2015.04.011.

(85) Ferrer, I.; Thurman, E. M. Analysis of Hydraulic Fracturing Additives by LC/Q-TOF-MS. *Anal. Bioanal. Chem.* **2015**, *407* (21), 6417–6428. https://doi.org/10.1007/s00216-015-8780-5.

(86) Strong, L. C.; Gould, T.; Kasinkas, L.; Sadowsky, M. J.; Aksan, A.; Wackett, L. P. Biodegradation in Waters from Hydraulic Fracturing: Chemistry, Microbiology, and Engineering. *J. Environ. Eng. (United States)* **2014**, *140* (5), 1–8. https://doi.org/10.1061/(ASCE)EE.1943-7870.0000792.

(87) Mirnaghi, F. S.; Goryński, K.; Rodriguez-Lafuente, A.; Boyaci, E.; Bojko, B.; Pawliszyn, J. Microextraction versus Exhaustive Extraction Approaches for Simultaneous Analysis of Compounds in Wide Range of Polarity. *J. Chromatogr. A* **2013**, *1316*, 37–43. https://doi.org/10.1016/j.chroma.2013.09.084.

(88) Maguire-Boyle, S. J.; Barron, A. R. Organic Compounds in Produced Waters from

Shale Gas Wells. *Environ. Sci. Process. Impacts* **2014**, *16* (10), 2237–2248. https://doi.org/10.1039/c4em00376d.

(89) Luek, J. L.; Schmitt-Kopplin, P.; Mouser, P. J.; Petty, W. T.; Richardson, S. D.; Gonsior, M. Halogenated Organic Compounds Identified in Hydraulic Fracturing Wastewaters Using Ultrahigh Resolution Mass Spectrometry. *Environ. Sci. Technol.* **2017**, *51* (10), 5377–5385. https://doi.org/10.1021/acs.est.6b06213.

(90) Lester, Y.; Ferrer, I.; Thurman, E. M.; Sitterley, K. A.; Korak, J. A.; Aiken, G.; Linden, K. G. Characterization of Hydraulic Fracturing Flowback Water in Colorado: Implications for Water Treatment. *Sci. Total Environ.* **2015**, *512–513*, 637–644. https://doi.org/10.1016/j.scitotenv.2015.01.043.

(91) Bergmann, A. J.; Points, G. L.; Scott, R. P.; Wilson, G.; Anderson, K. A. Development of Quantitative Screen for 1550 Chemicals with GC-MS. *Anal. Bioanal. Chem.* **2018**, *410* (13), 3101–3110. https://doi.org/10.1007/s00216-018-0997-7.

(92) Buszewska-Forajta, M.; Bujak, R.; Yumba-Mpanga, A.; Siluk, D.; Kaliszan, R. GC/MS Technique and AMDIS Software Application in Identification of Hydrophobic Compounds of Grasshoppers' Abdominal Secretion (Chorthippus Spp.). *J. Pharm. Biomed. Anal.* **2015**, *102*, 331–339. https://doi.org/10.1016/j.jpba.2014.09.039.

(93) AMDIS- Automated Mass Deconvolution and Identification System.

(94) Davies, T. The New Automated Mass Spectrometry Deconvolution and Identification System (AMDIS). *Spectrosc. Eur.* **1998**, *10* (3), 24–27.

(95) Piri-Moghadam, H.; Gionfriddo, E.; Rodriguez-Lafuente, A.; Grandy, J. J.; Lord,

H. L.; Obal, T.; Pawliszyn, J. Inter-Laboratory Validation of a Thin Film Microextraction Technique for Determination of Pesticides in Surface Water Samples. *Anal. Chim. Acta* **2017**, *964* (July 2016), 74–84. https://doi.org/10.1016/j.aca.2017.02.014.

(96) Piri-Moghadam, H.; Gionfriddo, E.; Grandy, J. J.; Alam, M. N.; Pawliszyn, J. Development and Validation of Eco-Friendly Strategies Based on Thin Film Microextraction for Water Analysis. *J. Chromatogr. A* **2018**, *1579*, 20–30. https://doi.org/10.1016/j.chroma.2018.10.026.

(97) Jiang, R.; Pawliszyn, J. Preparation of a Particle-Loaded Membrane for Trace Gas Sampling. *Anal. Chem.* **2014**, *86* (1), 403–410. https://doi.org/10.1021/ac4035339.

(98) Gómez-Ríos, G. A.; Gionfriddo, E.; Poole, J.; Pawliszyn, J. Ultrafast Screening and Quantitation of Pesticides in Food and Environmental Matrices by Solid-Phase Microextraction-Transmission Mode (SPME-TM) and Direct Analysis in Real Time (DART). *Anal. Chem.* **2017**, *89* (13), 7240–7248. https://doi.org/10.1021/acs.analchem.7b01553.

(99) Gionfriddo, E.; Boyacl, E.; Pawliszyn, J. New Generation of Solid-Phase Microextraction Coatings for Complementary Separation Approaches: A Step toward Comprehensive Metabolomics and Multiresidue Analyses in Complex Matrices. *Anal. Chem.* **2017**, *89* (7), 4046–4054. https://doi.org/10.1021/acs.analchem.6b04690.

(100) Kruve, A. Semi-Quantitative Non-Target Analysis of Water with Liquid Chromatography/High-Resolution Mass Spectrometry: How Far Are We? *Rapid Commun. Mass Spectrom.* **2019**, *33* (S3), 54–63. https://doi.org/10.1002/rcm.8208.

(101) Biller, J. E.; Biemarm, K. Reconstructed Mass Spectra, A Novel Approach For The Utilization Of Gas Chromatograph—Mass Spectrometer Data. *Anal. Lett.* **1974**, *7* (7), 515–528. https://doi.org/10.1080/00032717408058783.

(102) Hargrove David Rosenthal, W. F.; Cooley, P. C. *Improvement of Algorithm for Peak Detection in Automatic Gas Chromatography-Mass Spectrometry Data Processing*; 1981; Vol. 53.

(103) Orem, W. H.; Tatu, C. A.; Lerch, H. E.; Rice, C. A.; Bartos, T. T.; Bates, A. L.; Tewalt, S.; Corum, M. D. Organic Compounds in Produced Waters from Coalbed Natural Gas Wells in the Powder River Basin, Wyoming, USA. *Appl. Geochemistry* **2007**, *22* (10), 2240–2256. https://doi.org/10.1016/j.apgeochem.2007.04.010.

(104) Luek, J. L.; Gonsior, M. Organic Compounds in Hydraulic Fracturing Fluids and Wastewaters: A Review. *Water Res.* **2017**, *123*, 536–548. https://doi.org/10.1016/j.watres.2017.07.012.

(105) Cluff, M. A.; Hartsock, A.; Macrae, J. D.; Carter, K.; Mouser, P. J. Temporal Changes in Microbial Ecology and Geochemistry in Produced Water from Hydraulically Fractured Marcellus Shale Gas Wells. *Environ. Sci. Technol.* **2014**, *48* (11), 6508–6517. https://doi.org/10.1021/es501173p.

(106) Pollo, B. J.; Alexandrino, G. L.; Augusto, F.; Hantao, L. W. The Impact of Comprehensive Two-Dimensional Gas Chromatography on Oil & Gas Analysis: Recent Advances and Applications in Petroleum Industry. *TrAC - Trends Anal. Chem.* **2018**, *105*, 202–217. https://doi.org/10.1016/j.trac.2018.05.007.

(107) Thacker, J.; Carlton, D.; Hildenbrand, Z.; Kadjo, A.; Schug, K. Chemical Analysis

of Wastewater from Unconventional Drilling Operations. *Water* **2015**, *7* (12), 1568–1579. https://doi.org/10.3390/w7041568.

(108) Emmons, R. V; Sharma, G.; Sunder, S.; Schug, K. A.; Asfaha, T. Y.; Lawrence, J. G.; Kirchho, J. R.; Gionfriddo, E. Unraveling the Complex Composition of Produced Water by Specialized Extraction Methodologies. *Environ. Sci. Technol.* **2022**. https://doi.org/10.1021/acs.est.1c05826.

(109) Scanlon, B. R.; Reedy, R. C.; Xu, P.; Engle, M.; Nicot, J. P.; Yoxtheimer, D.; Yang, Q.; Ikonnikova, S. Can We Beneficially Reuse Produced Water from Oil and Gas Extraction in the U.S.? *Sci. Total Environ.* **2020**, *717* (February), 137085. https://doi.org/10.1016/j.scitotenv.2020.137085.

(110) Elsner, M.; Hoelzer, K. Quantitative Survey and Structural Classification of Hydraulic Fracturing Chemicals Reported in Unconventional Gas Production. *Environ. Sci. Technol.* **2016**, *50* (7), 3290–3314. https://doi.org/10.1021/acs.est.5b02818.

(111) Røe Utvik, T. I. Chemical Characterisation of Produced Water from Four Offshore Oil Production Platforms in the North Sea. *Chemosphere* **1999**, *39* (15), 2593–2606. https://doi.org/10.1016/S0045-6535(99)00171-X.

(112) Veil, J. A.; Puder, M. G.; Elcock, D.; Redweik Jr., R. J. *A White Paper Describing Produced Water from Production of Crude Oil, Natural Gas, and Coal Bed Methane.*; United States, 2004. https://doi.org/10.2172/821666.

(113) Liden, T.; Santos, I. C.; Hildenbrand, Z. L.; Schug, K. A. Chapter 9 - Analytical Methods for the Comprehensive Characterization of Produced Water. In *Separation Science and Technology*; Ahuja, S., Ed.; Academic Press, 2019; Vol.

11, pp 199–217. https://doi.org/10.1016/B978-0-12-815730-5.00009-0.

(114) Jiang, W.; Lin, L.; Xu, X.; Cheng, X.; Zhang, Y.; Hall, R.; Xu, P. A Critical Review of Analytical Methods for Comprehensive Characterization of Produced Water. *Water* **2021**, *13* (2), 183. https://doi.org/https://doi.org/10.3390/w13020183.

(115) Santos, I. C.; Hildenbrand, Z. L.; Schug, K. A. A Review of Analytical Methods for Characterizing the Potential Environmental Impacts of Unconventional Oil and Gas Development. *Anal. Chem.* **2019**, *91* (1), 689–703. https://doi.org/10.1021/acs.analchem.8b04750.

(116) Acharya, S. M.; Chakraborty, R.; Tringe, S. G. Emerging Trends in Biological Treatment of Wastewater From Unconventional Oil and Gas Extraction. *Front. Microbiol.* **2020**, *11* (September). https://doi.org/10.3389/fmicb.2020.569019.

(117) Akstinat, M. Chemical and Physicochemical Properties of Formation Waters of the Oil and Gas Industry. *J. Hydrol.* **2019**, *578*, 124011. https://doi.org/10.1016/j.jhydrol.2019.124011.

(118) Kassotis, C. D.; Tillitt, D. E.; Davis, J. W.; Hormann, A. M.; Nagel, S. C. Estrogen and Androgen Receptor Activities of Hydraulic Fracturing Chemicals and Surface and Ground Water in a Drilling-Dense Region. *Endocrinology* **2014**, *155* (3), 897–907. https://doi.org/10.1210/en.2013-1697.

(119) Vidic, R. D.; Brantley, S. L.; Vandenbossche, J. M.; Yoxtheimer, D.; Abad, J. D. Impact of Shale Gas Development on Regional Water Quality. *Science (80-.).* **2013**, *340*, 1235009. https://doi.org/10.1126/science.1235009.

(120) Warner, N. R.; Christie, C. A.; Jackson, R. B.; Vengosh, A. Impacts of Shale Gas

Wastewater Disposal on Water Quality in Western Pennsylvania. *Environ. Sci. Technol.* **2013**, *47* (20), 11849–11857. https://doi.org/10.1021/es402165b.

(121) Brantley, S. L.; Yoxtheimer, D.; Arjmand, S.; Grieve, P.; Vidic, R.; Pollak, J.; Llewellyn, G. T.; Abad, J.; Simon, C. Water Resource Impacts during Unconventional Shale Gas Development: The Pennsylvania Experience. *Int. J. Coal Geol.* **2014**, *126* (November 2013), 140–156. https://doi.org/10.1016/j.coal.2013.12.017.

(122) Lauer, N. E.; Harkness, J. S.; Vengosh, A. Brine Spills Associated with Unconventional Oil Development in North Dakota. *Environ. Sci. Technol.* **2016**, *50* (10), 5389–5397. https://doi.org/10.1021/acs.est.5b06349.

(123) Darrah, T. H.; Vengosh, A.; Jackson, R. B.; Warner, N. R.; Poreda, R. J. Noble Gases Identify the Mechanisms of Fugitive Gas Contamination in Drinking-Water Wells Overlying the Marcellus and Barnett Shales. *Proc. Natl. Acad. Sci.* **2014**, *111* (39), 14076–14081. https://doi.org/10.1073/pnas.1322107111.

(124) Kondash, A.; Vengosh, A. Water Footprint of Hydraulic Fracturing. *Environ. Sci. Technol. Lett.* **2015**, *2* (10), 276–280. https://doi.org/10.1021/acs.estlett.5b00211.

(125) Khan, N. A.; Engle, M.; Dungan, B.; Holguin, F. O.; Xu, P.; Carroll, K. C. Volatile-Organic Molecular Characterization of Shale-Oil Produced Water from the Permian Basin. *Chemosphere* **2016**, *148*, 126–136. https://doi.org/10.1016/j.chemosphere.2015.12.116.

(126) Almaraz, N.; Regnery, J.; Vanzin, G. F.; Riley, S. M.; Ahoor, D. C.; Cath, T. Y. Emergence and Fate of Volatile Iodinated Organic Compounds during Biological Treatment of Oil and Gas Produced Water. *Sci. Total Environ.* **2020**, *699*, 134202.

https://doi.org/10.1016/j.scitotenv.2019.134202.

(127) Sitterley, K. A.; Linden, K. G.; Ferrer, I.; Thurman, E. M. Desalting and Concentration of Common Hydraulic Fracturing Fluid Additives and Their Metabolites with Solid-Phase Extraction. *J. Chromatogr. A* **2020**, No. May, 461094. https://doi.org/10.1016/j.chroma.2020.461094.

(128) Llewellyn, G. T.; Dorman, F.; Westland, J. L.; Yoxtheimer, D.; Grieve, P.; Sowers, T.; Humston-Fulmer, E.; Brantley, S. L. Evaluating a Groundwater Supply Contamination Incident Attributed to Marcellus Shale Gas Development. *Proc. Natl. Acad. Sci. U. S. A.* **2015**, *112* (20), 6325–6330. https://doi.org/10.1073/pnas.1420279112.

(129) Hoelzer, K.; Sumner, A. J.; Karatum, O.; Nelson, R. K.; Drollette, B. D.; O'Connor, M. P.; D'Ambro, E. L.; Getzinger, G. J.; Ferguson, P. L.; Reddy, C. M.; et al. Indications of Transformation Products from Hydraulic Fracturing Additives in Shale-Gas Wastewater. *Environ. Sci. Technol.* **2016**, *50* (15), 8036–8048. https://doi.org/10.1021/acs.est.6b00430.

(130) Piotrowski, P. K.; Weggler, B. A.; Yoxtheimer, D. A.; Kelly, C. N.; Barth-Naftilan, E.; Saiers, J. E.; Dorman, F. L. Elucidating Environmental Fingerprinting Mechanisms of Unconventional Gas Development through Hydrocarbon Analysis. *Anal. Chem.* **2018**, *90* (8), 5466–5473. https://doi.org/10.1021/acs.analchem.8b00822.

(131) Panuwet, P.; Hunter, R. E.; D'Souza, P. E.; Chen, X.; Radford, S. A.; Cohen, J. R.; Marder, M. E.; Kartavenka, K.; Ryan, P. B.; Barr, D. B. Biological Matrix Effects in Quantitative Tandem Mass Spectrometry-Based Analytical Methods:

Advancing Biomonitoring. *Crit. Rev. Anal. Chem.* **2016**, *46* (2), 93–105. https://doi.org/10.1080/10408347.2014.980775.

(132) Thurman, E. M.; Ferrer, I.; Blotevogel, J.; Borch, T. Analysis of Hydraulic Fracturing Flowback and Produced Waters Using Accurate Mass: Identification of Ethoxylated Surfactants. *Anal. Chem.* **2014**, *86* (19), 9653–9661. https://doi.org/10.1021/ac502163k.

(133) Dearmond, P. D.; Digoregorio, A. L. Characterization of Liquid Chromatography-Tandem Mass Spectrometry Method for the Determination of Acrylamide in Complex Environmental Samples. *Anal. Bioanal. Chem.* **2013**, *405*, 4159–4166. https://doi.org/10.1007/s00216-013-6822-4.

(134) Peers, C. M. G. Characterising Organic and Inorganic Chemical Signatures of Water Associated with Shale Gas Extraction Operations, Imperial College London, 2020.

(135) Klemz, A. C.; Weschenfelder, S. E.; Lima de Carvalho Neto, S.; Pascoal Damas, M. S.; Toledo Viviani, J. C.; Mazur, L. P.; Marinho, B. A.; Pereira, L. dos S.; da Silva, A.; Borges Valle, J. A.; et al. Oilfield Produced Water Treatment by Liquid-Liquid Extraction: A Review. *J. Pet. Sci. Eng.* **2021**, *199* (November 2020). https://doi.org/10.1016/j.petrol.2020.108282.

(136) DeArmond, P. D.; DiGoregorio, A. L. Rapid Liquid Chromatography-Tandem Mass Spectrometry-Based Method for the Analysis of Alcohol Ethoxylates and Alkylphenol Ethoxylates in Environmental Samples. *J. Chromatogr. A* **2013**, *1305*, 154–163. https://doi.org/10.1016/j.chroma.2013.07.017.

(137) Silva, M.; Bjørnstad, T. Determination of Phase-Partitioning Tracer Candidates in

Production Waters from Oilfields Based on Solid-Phase Microextraction Followed by Gas Chromatography-Tandem Mass Spectrometry. *J. Chromatogr. A* **2020**, 461508. https://doi.org/10.1016/j.chroma.2020.461508.

(138) BR, H.; SR, D. Review of Potential Technologies for the Removal of Dissolved Components from Produced Water. *Chem. Eng. Res. Des.* **1994**, *72* (2), 176–188.

(139) Neff, J. M. *Bioaccumulation in Marine Organisms: Effects of Contaminants from Oil Well Produced Water*; Elsevier: Amsterdam, Netherlands, 2002. https://doi.org/10.1016/B978-0-08-043716-3.X5000-3.

(140) Johnson, B. M.; Kanagy, L. E.; Rodgers Jr, J. H.; Castle, J. W. Feasibility of a Pilot-Scale Hybrid Constructed Wetland Treatment System for Simulated Natural Gas Storage Produced Waters. *Environ. Geosci.* **2008**, *15* (3), 91–104. https://doi.org/10.1306/eg.06220707004.

(141) Azetsu-Scott, K.; Yeats, P.; Wohlgeschaffen, G.; Dalziel, J.; Niven, S.; Lee, K. Precipitation of Heavy Metals in Produced Water: Influence on Contaminant Transport and Toxicity. *Mar. Environ. Res.* **2007**, *63* (2), 146–167. https://doi.org/10.1016/j.marenvres.2006.08.001.

(142) Shpiner, R.; Vathi, S.; Stuckey, D. C. Treatment of Oil Well "Produced Water" by Waste Stabilization Ponds: Removal of Heavy Metals. *Water Res.* **2009**, *43* (17), 4258–4268. https://doi.org/10.1016/j.watres.2009.06.004.

(143) Spacil, M. M.; Rodgers, J. H.; Castle, J. W.; Chao, W. Y. Performance of a Pilot-Scale Constructed Wetland Treatment System for Selenium, Arsenic, and Low-Molecular-Weight Organics in Simulated Fresh Produced Water. *Environ. Geosci.* **2011**, *18* (3), 145–156. https://doi.org/10.1306/eg.01281110020.

(144) Neff, J.; Lee, K.; DeBlois, E. M. Produced Water: Overview of Composition, Fates, and Effects. In *Produced Water: Environmental Risks and Advances in Mitigation Technologies*; Lee, K., Neff, J., Eds.; Springer New York: New York, NY, 2011; pp 3–54. https://doi.org/10.1007/978-1-4614-0046-2_1.

(145) Guerra, K.; Dahm, K.; Dundorf, S. Oil and Gas Produced Water Management and Beneficial Use in the Western United States. *U.S. Dep. Inter. Bur. Reclamation, Manag. Water West* **2011**, No. 157, 129.

(146) Xiao, F. Characterization and Treatment of Bakken Oilfield Produced Water as a Potential Source of Value-Added Elements. *Sci. Total Environ.* **2021**, *770*, 145283. https://doi.org/10.1016/j.scitotenv.2021.145283.

(147) Hu, L.; Yu, J.; Luo, H.; Wang, H.; Xu, P.; Zhang, Y. Simultaneous Recovery of Ammonium, Potassium and Magnesium from Produced Water by Struvite Precipitation. *Chem. Eng. J.* **2020**, *382*, 123001. https://doi.org/10.1016/j.cej.2019.123001.

(148) Chen, M.; Shafer-Peltier, K.; Veisi, M.; Randtke, S.; Peltier, E. Complexation and Precipitation of Scale-Forming Cations in Oilfield Produced Water with Polyelectrolytes. *Sep. Purif. Technol.* **2019**, *222*, 1–10. https://doi.org/10.1016/j.seppur.2019.04.014.

(149) Yan, X.-P.; Kerrich, R.; Hendry, M. J. Flow Injection On-Line Group Preconcentration and Separation of (Ultra) Trace Rare Earth Elements in Environmental and Geological Samples by Precipitation Using a Knotted Reactor as a Filterless Collector for Inductively Coupled Plasma Mass Spectrometric. *J. Anal. At. Spectrom.* **1999**, *14* (2), 215–221. https://doi.org/10.1039/A806435K.

(150) Noack, C. W.; Jain, J. C.; Stegmeier, J.; Hakala, J. A.; Karamalidis, A. K. Rare Earth Element Geochemistry of Outcrop and Core Samples from the Marcellus Shale. *Geochem. Trans.* **2015**, *16* (1), 6. https://doi.org/10.1186/s12932-015-0022-4.

(151) Lerat, J. G.; Sterpenich, J.; Mosser-Ruck, R.; Lorgeoux, C.; Bihannic, I.; Fialips, C. I.; Schovsbo, N. H.; Pironon, J.; Gaucher, É. C. Metals and Radionuclides (MaR) in the Alum Shale of Denmark: Identification of MaR-Bearing Phases for the Better Management of Hydraulic Fracturing Waters. *J. Nat. Gas Sci. Eng.* **2018**, *53*, 139–152. https://doi.org/10.1016/j.jngse.2018.02.015.

(152) Tian, L.; Chang, H.; Tang, P.; Li, T.; Zhang, X.; Liu, S.; He, Q.; Wang, T.; Yang, J.; Bai, Y.; et al. Rare Earth Elements Occurrence and Economical Recovery Strategy from Shale Gas Wastewater in the Sichuan Basin, China. *ACS Sustain. Chem. Eng.* **2020**, *8* (32), 11914–11920. https://doi.org/10.1021/acssuschemeng.0c04971.

(153) Hamilton, L. D.; Meinhold, A. F.; Nagy, J. Health Risk Assessment for Radium Discharged in Produced Waters. In *Produced Water*; Springer, 1992; pp 303–314. https://doi.org/10.1007/978-1-4615-2902-6_25.

(154) Zhang, T.; Gregory, K.; Hammack, R. W.; Vidic, R. D. Co-Precipitation of Radium with Barium and Strontium Sulfate and Its Impact on the Fate of Radium during Treatment of Produced Water from Unconventional Gas Extraction. *Environ. Sci. Technol.* **2014**, *48* (8), 4596–4603. https://doi.org/10.1021/es405168b.

(155) Conrad, C. L.; Ben Yin, Y.; Hanna, T.; Atkinson, A. J.; Alvarez, P. J. J.; Tekavec,

T. N.; Reynolds, M. A.; Wong, M. S. Fit-for-Purpose Treatment Goals for Produced Waters in Shale Oil and Gas Fields. *Water Research*. 2020, p 115467. https://doi.org/10.1016/j.watres.2020.115467.

(156) Arslan, Z.; Oymak, T.; White, J. Triethylamine-Assisted Mg(OH)2 Coprecipitation/Preconcentration for Determination of Trace Metals and Rare Earth Elements in Seawater by Inductively Coupled Plasma Mass Spectrometry (ICP-MS). *Anal. Chim. Acta* **2018**, *1008*, 18–28. https://doi.org/10.1016/j.aca.2018.01.017.

(157) Freslon, N.; Bayon, G.; Birot, D.; Bollinger, C.; Barrat, J. A. Determination of Rare Earth Elements and Other Trace Elements (Y, Mn, Co, Cr) in Seawater Using Tm Addition and Mg(OH)2 Co-Precipitation. *Talanta* **2011**, *85* (1), 582–587. https://doi.org/10.1016/j.talanta.2011.04.023.

(158) Chung, C. H.; Brenner, I.; You, C. F. Comparison of Microconcentric and Membrane-Desolvation Sample Introduction Systems for Determination of Low Rare Earth Element Concentrations in Surface and Subsurface Waters Using Sector Field Inductively Coupled Plasma Mass Spectrometry. *Spectrochim. Acta - Part B At. Spectrosc.* **2009**, *64* (9), 849–856. https://doi.org/10.1016/j.sab.2009.06.013.

(159) Dulski, P. Interferences of Oxide, Hydroxide and Chloride Analyte Species in the Determination of Rare Earth Elements in Geological Samples by Inductively Coupled Plasma-Mass Spectrometry. *Fresenius. J. Anal. Chem.* **1994**, *350* (4–5), 194–203. https://doi.org/10.1007/BF00322470.

(160) Cao, S.; Chen, H.; Zeng, X. Determination of Rare Earth Elements in Biological

Samples by Inductively Coupled Plasma Mass Spectrometry. *Fenxi Huaxue* **1999**, *27* (6), 624–625. https://doi.org/10.1021/ac00019a013.

(161) Shaw, T. J.; Duncan, T.; Schnetger, B. A Preconcentration/Matrix Reduction Method for the Analysis of Rare Earth Elements in Seawater and Groundwaters by Isotope Dilution ICPMS. *Anal. Chem.* **2003**, *75* (14), 3396–3403. https://doi.org/10.1021/ac026158e.

(162) Shyam Sunder, G. S.; Adhikari, S.; Rohanifar, A.; Poudel, A.; Kirchhoff, J. R. Evolution of Environmentally Friendly Strategies for Metal Extraction. *Separations*. 2020. https://doi.org/10.3390/separations7010004.

(163) Dimpe, K. M.; Ngila, J. C.; Nomngongo, P. N. Preparation and Application of a Tyre-Based Activated Carbon Solid Phase Extraction of Heavy Metals in Wastewater Samples. *Phys. Chem. Earth* **2018**, *105*, 161–169. https://doi.org/10.1016/j.pce.2018.02.005.

(164) AlSuhaimi, A. O.; AlRadaddi, S. M.; Al-Sheikh Ali, A. K.; Shraim, A. M.; AlRadaddi, T. S. Silica-Based Chelating Resin Bearing Dual 8-Hydroxyquinoline Moieties and Its Applications for Solid Phase Extraction of Trace Metals from Seawater Prior to Their Analysis by ICP-MS. *Arab. J. Chem.* **2019**, *12* (3), 360–369. https://doi.org/10.1016/j.arabjc.2017.10.006.

(165) Duval, B.; Gredilla, A.; Fdez-Ortiz de Vallejuelo, S.; Tessier, E.; Amouroux, D.; de Diego, A. A Simple Determination of Trace Mercury Concentrations in Natural Waters Using Dispersive Micro-Solid Phase Extraction Preconcentration Based on Functionalized Graphene Nanosheets. *Microchem. J.* **2020**, *154*, 104549. https://doi.org/10.1016/j.microc.2019.104549.

(166) Heidari, M.; Ghanemi, K.; Nikpour, Y. Applying Al2O3@Ag@trithiocyanuric Acid as an Efficient Metal Ion Scavenger for the Selective Extraction of Iron (III) and Lead (II) from Environmental Waters. *Ecotoxicol. Environ. Saf.* **2020**, *203*, 110995. https://doi.org/10.1016/j.ecoenv.2020.110995.

(167) Pyrzynska, K.; Kubiak, A.; Wysocka, I. Application of Solid Phase Extraction Procedures for Rare Earth Elements Determination in Environmental Samples. *Talanta*. 2016, pp 15–22. https://doi.org/10.1016/j.talanta.2016.03.022.

(168) García-Mesa, J. C.; Montoro Leal, P.; López Guerrero, M. M.; Vereda Alonso, E. I. Simultaneous Determination of Noble Metals, Sb and Hg by Magnetic Solid Phase Extraction on Line ICP OES Based on a New Functionalized Magnetic Graphene Oxide. *Microchem. J.* **2019**, *150*, 104141. https://doi.org/10.1016/j.microc.2019.104141.

(169) Shyam Sunder, G. S.; Rohanifar, A.; Alipourasiabi, N.; Lawrence, J. G.; Kirchhoff, J. R. Synthesis and Characterization of Poly(Pyrrole-1-Carboxylic Acid) for Preconcentration and Determination of Rare Earth and Heavy Metals in Water Matrices. *ACS Appl. Mater. Interfaces* **2021**.

(170) Kirchhoff, J. R.; Rohanifar, A.; Shyam Sunder, G. S. Pyrrole-Based Polymers for Metal Extraction, Analysis, and Removal. US 2020/0102410 A1, 2020.

(171) Rohanifar, A.; Alipourasiabi, N.; Shyam Sunder, G. S.; Lawrence, J. G.; Kirchhoff, J. R. Reversible Chelating Polymer for Determination of Heavy Metals by Dispersive Micro Solid-Phase Extraction with ICP-MS. *Microchim. Acta* **2020**, *187* (6). https://doi.org/10.1007/s00604-020-04308-5.

(172) Xia, J.; Psychogios, N.; Young, N.; Wishart, D. S. MetaboAnalyst: A Web Server

for Metabolomic Data Analysis and Interpretation. *Nucleic Acids Res.* **2009**, *37* (SUPPL. 2), 652–660. https://doi.org/10.1093/nar/gkp356.

(173) Westerhuis, J. A.; Hoefsloot, H. C. J.; Smit, S.; Vis, D. J.; Smilde, A. K.; Velzen, E. J. J.; Duijnhoven, J. P. M.; Dorsten, F. A. Assessment of PLSDA Cross Validation. *Metabolomics* **2008**, *4* (1), 81–89. https://doi.org/10.1007/s11306-007-0099-6.

(174) Stringfellow, W. T.; Camarillo, M. K.; Domen, J. K.; Sandelin, W. L.; Varadharajan, C.; Jordan, P. D.; Reagan, M. T.; Cooley, H.; Heberger, M. G.; Birkholzer, J. T. Identifying Chemicals of Concern in Hydraulic Fracturing Fluids Used for Oil Production. *Environ. Pollut.* **2017**, *220*, 413–420. https://doi.org/10.1016/j.envpol.2016.09.082.

(175) Organization, W. H. Polynuclear aromatic hydrocarbons in drinking water.

(176) Cui, D.; Wang, Q.; Wang, Z. C.; Liu, Q.; Pan, S.; Bai, J.; Liu, B. Compositional Analysis of Heteroatom Compounds in Huadian Shale Oil Using Various Analytical Techniques. *Energy and Fuels* **2019**, *33* (2), 946–956. https://doi.org/10.1021/acs.energyfuels.8b03889.

(177) Berrueta, L. A.; Alonso-Salces, R. M.; Héberger, K. Supervised Pattern Recognition in Food Analysis. *J. Chromatogr. A* **2007**, *1158* (1–2), 196–214. https://doi.org/10.1016/j.chroma.2007.05.024.

(178) Drivelos, S. A.; Danezis, G. P.; Halagarda, M.; Popek, S.; Georgiou, C. A. Geographical Origin and Botanical Type Honey Authentication through Elemental Metabolomics via Chemometrics. *Food Chem.* **2021**, *338* (August 2020), 127936. https://doi.org/10.1016/j.foodchem.2020.127936.

(179) Akyon, B.; McLaughlin, M.; Hernández, F.; Blotevogel, J.; Bibby, K. Characterization and Biological Removal of Organic Compounds from Hydraulic Fracturing Produced Water. *Environ. Sci. Process. Impacts* **2019**, *21* (2), 279–290. https://doi.org/10.1039/c8em00354h.

(180) Gromski, P. S.; Muhamadali, H.; Ellis, D. I.; Xu, Y.; Correa, E.; Turner, M. L.; Goodacre, R. A Tutorial Review: Metabolomics and Partial Least Squares-Discriminant Analysis - a Marriage of Convenience or a Shotgun Wedding. *Anal. Chim. Acta* **2015**, *879*, 10–23. https://doi.org/10.1016/j.aca.2015.02.012.

(181) Graymore, M.; Stagnitti, F.; Allinson, G. Impacts of Atrazine in Aquatic Ecosystems. *Environ. Int.* **2001**, *26* (7–8), 483–495. https://doi.org/10.1016/S0160-4120(01)00031-9.

(182) Quillinan, S.; Nye, C.; Engle, M.; Bartos, T. T.; Neupane, G.; Brant, J.; Bagdonas, D.; McLing, T.; McLaughlin, J. F.; Phillips, E.; et al. *Assessing Rare Earth Element Concentrations in Geothermal and Oil and Gas Produced Waters: A Potential Domestic Source of Strategic Mineral Commodities (Final Report)*; United States, 2018. https://doi.org/10.2172/1509037.

(183) Liberatore, H.; Westerman, D.; Allen, J.; Plewa, M.; Wagner, E.; McKenna, A.; Weisbrod, C.; McCord, J.; Liberatore, R.; Burnett, D.; et al. High-Resolution Mass Spectrometry Identification of Novel Surfactant-Derived Sulfur-Containing Disinfection Byproducts from Gas Extraction Wastewater. *Environ. Sci. Technol.* **2020**. https://doi.org/10.1021/acs.est.0c01997.

(184) Liberatore, H. K.; Plewa, M. J.; Wagner, E. D.; Vanbriesen, J. M.; Burnett, D. B.; Cizmas, L. H.; Richardson, S. D. Identification and Comparative Mammalian Cell

Cytotoxicity of New Iodo-Phenolic Disinfection Byproducts in Chloraminated Oil and Gas Wastewaters. *Environ. Sci. Technol. Lett.* **2017**, *4* (11), 475–480. https://doi.org/10.1021/acs.estlett.7b00468.

(185) Emmons, R. V.; Gionfriddo, E. Minimizing Transient Microenvironment-Associated Variability for Analysis of Environmental Anthropogenic Contaminants via Ambient Ionization. *Sci. Total Environ.* **2021**, *775*, 145789. https://doi.org/10.1016/j.scitotenv.2021.145789.

(186) Tsagkaris, A. S.; Nelis, J. L. D.; Ross, G. M. S.; Jafari, S.; Guercetti, J.; Kopper, K.; Zhao, Y.; Rafferty, K.; Salvador, J. P.; Migliorelli, D.; et al. Critical Assessment of Recent Trends Related to Screening and Confirmatory Analytical Methods for Selected Food Contaminants and Allergens. *TrAC - Trends Anal. Chem.* **2019**, *121* (October), 115688. https://doi.org/10.1016/j.trac.2019.115688.

(187) Amine, A.; Mohammadi, H.; Bourais, I.; Palleschi, G. Enzyme Inhibition-Based Biosensors for Food Safety and Environmental Monitoring. *Biosens. Bioelectron.* **2006**, *21* (8), 1405–1423. https://doi.org/10.1016/j.bios.2005.07.012.

(188) Blokland, M. H.; Gerssen, A.; Zoontjes, P. W.; Pawliszyn, J.; Nielen, M. W. F. Potential of Recent Ambient Ionization Techniques for Future Food Contaminant Analysis Using (Trans)Portable Mass Spectrometry. *Food Anal. Methods* **2020**, *13* (3), 706–717. https://doi.org/10.1007/s12161-019-01666-6.

(189) Shelley, J. T.; Badal, S. P.; Engelhard, C.; Hayen, H. Ambient Desorption/Ionization Mass Spectrometry: Evolution from Rapid Qualitative Screening to Accurate Quantification Tool. *Anal. Bioanal. Chem.* **2018**, *410* (17), 4061–4076. https://doi.org/10.1007/s00216-018-1023-9.

(190) Snyder, D. T.; Pulliam, C. J.; Ouyang, Z.; Cooks, R. G. Miniature and Fieldable Mass Spectrometers: Recent Advances. *Anal. Chem.* **2016**, *88* (1), 2–29. https://doi.org/10.1021/acs.analchem.5b03070.

(191) Wu, T.; Wu, X.; Yuan, X.; Wang, Y.; Zhou, W.; Li, W. Rapid Evaluation of Spermidine from 12 Bean Cultivars by Direct Real-Time Mass Spectrometry Analysis. *Molecules* **2018**, *23* (9). https://doi.org/10.3390/molecules23092138.

(192) Farré, M.; Picó, Y.; Barceló, D. Direct Peel Monitoring of Xenobiotics in Fruit by Direct Analysis in Real Time Coupled to a Linear Quadrupole Ion Trap-Orbitrap Mass Spectrometer. *Anal. Chem.* **2013**, *85* (5), 2638–2644. https://doi.org/10.1021/ac3026702.

(193) Gómez-Ríos, G. A.; Vasiljevic, T.; Gionfriddo, E.; Yu, M.; Pawliszyn, J. Towards On-Site Analysis of Complex Matrices by Solid-Phase Microextraction-Transmission Mode Coupled to a Portable Mass Spectrometer: Via Direct Analysis in Real Time. *Analyst* **2017**, *142* (16), 2928–2935. https://doi.org/10.1039/c7an00718c.

(194) Takáts, Z.; Wiseman, J. M.; Gologan, B.; Cooks, R. G. Mass Spectrometry Sampling under Ambient Conditions with Desorption Electrospray Ionization. *Science (80-.).* **2004**, *306* (5695), 471–473. https://doi.org/10.1126/science.1104404.

(195) Na, N.; Zhao, M.; Zhang, S.; Yang, C.; Zhang, X. Development of a Dielectric Barrier Discharge Ion Source for Ambient Mass Spectrometry. *J. Am. Soc. Mass Spectrom.* **2007**, *18* (10), 1859–1862. https://doi.org/10.1016/j.jasms.2007.07.027.

(196) Na, N.; Zhang, C.; Zhao, M.; Zhang, S.; Yang, C.; Fang, X.; Zhang, X. Direct

Detection of Explosives on Solid Surfaces by Mass Spectrometry with an Ambient Ion Source Based on Dielectric Barrier Discharge. *J. Mass Spectrom.* **2007**, *42* (8), 1079–1085. https://doi.org/10.1002/jms.1243.

(197) Hajslova, J.; Cajka, T.; Vaclavik, L. Challenging Applications Offered by Direct Analysis in Real Time (DART) in Food-Quality and Safety Analysis. *TrAC - Trends Anal. Chem.* **2011**, *30* (2), 204–218. https://doi.org/10.1016/j.trac.2010.11.001.

(198) Shelley, J. T.; Hieftje, G. M. Ionization Matrix Effects in Plasma-Based Ambient Mass Spectrometry Sources. *J. Anal. At. Spectrom.* **2010**, *25* (3), 345–350. https://doi.org/10.1039/b923564g.

(199) Newsome, G. A.; Ackerman, L. K.; Johnson, K. J. Humidity Affects Relative Ion Abundance in Direct Analysis in Real Time Mass Spectrometry of Hexamethylene Triperoxide Diamine. *Anal. Chem.* **2014**, *86* (24), 11977–11980. https://doi.org/10.1021/ac503652x.

(200) Newsome, G. A.; Ackerman, L. K.; Johnson, K. J. Humidity Effects on Fragmentation in Plasma-Based Ambient Ionization Sources. *J. Am. Soc. Mass Spectrom.* **2016**, *27* (1), 135–143. https://doi.org/10.1007/s13361-015-1259-y.

(201) Song, L.; Gibson, S. C.; Bhandari, D.; Cook, K. D.; Bartmess, J. E. Ionization Mechanism of Positive-Ion Direct Analysis in Real Time: A Transient Microenvironment Concept. *Anal. Chem.* **2009**, *81* (24), 10080–10088. https://doi.org/10.1021/ac901122b.

(202) Mirabelli, M. F.; Gionfriddo, E.; Pawliszyn, J.; Zenobi, R. Fast Screening of Illicit Drugs in Beverages and Biological Fluids by Direct Coupling of Thin Film

Microextraction to Dielectric Barrier Discharge Ionization-Mass Spectrometry. *Analyst* **2019**, *144* (8), 2788–2796. https://doi.org/10.1039/c8an02448k.

(203) Emmons, R. V; Tajali, R.; Gionfriddo, E. Development, Optimization and Applications of Thin Film Solid Phase Microextraction (TF-SPME) Devices for Thermal Desorption: A Comprehensive Review. *Separations*. 2019. https://doi.org/10.3390/separations6030039.

(204) Gómez-Ríos, G. A.; Pawliszyn, J. Solid Phase Microextraction (SPME)-Transmission Mode (TM) Pushes down Detection Limits in Direct Analysis in Real Time (DART). *Chem. Commun.* **2014**, *50* (85), 12937–12940. https://doi.org/10.1039/c4cc05301j.

(205) Gionfriddo, E.; Gómez-Ríos, G. A. Analysis of Food Samples Made Easy by Microextraction Technologies Directly Coupled to Mass Spectrometry. *J. Mass Spectrom.* **2020**. https://doi.org/10.1002/jms.4665.

(206) Newsome, G. A.; Kavich, G.; Alvarez-Martin, A. Interface for Reproducible, Multishot Direct Analysis of Solid-Phase Microextraction Samples. *Anal. Chem.* **2020**, *92* (6), 4182–4186. https://doi.org/10.1021/acs.analchem.9b05691.

(207) Sisco, E.; Forbes, T. P.; Staymates, M. E.; Gillen, G. Rapid Analysis of Trace Drugs and Metabolites Using a Thermal Desorption DART-MS Configuration. *Anal. Methods* **2016**, *8*, 6494–6499. https://doi.org/10.1002/0470034394.ch9.

(208) Sisco, E.; Robinson, E. L.; Burns, A.; Mead, R. What's in the Bag? Analysis of Exterior Drug Packaging by TD-DART-MS to Predict the Contents. *Forensic Sci. Int.* **2019**, *304*, 109939. https://doi.org/10.1016/j.forsciint.2019.109939.

(209) Helin, A.; Rönkkö, T.; Parshintsev, J.; Hartonen, K.; Schilling, B.; Läubli, T.;

Riekkola, M. L. Solid Phase Microextraction Arrow for the Sampling of Volatile Amines in Wastewater and Atmosphere. *J. Chromatogr. A* **2015**, *1426*, 56–63. https://doi.org/10.1016/j.chroma.2015.11.061.

(210) Herrington, J. S.; German, A. G.; Myers, C.; Stidsen, G.; Bell, D. S. Hunting Molecules in Complex Matrices with SPME Arrows : A Review. **2020**.

(211) Pawliszyn, J. *Handbook of Solid Phase Microextraction*; Chemical Industry Press: Beijing, 2009.

(212) Hutchinson, J. P.; Setkova, L.; Pawliszyn, J. Automation of Solid-Phase Microextraction on a 96-Well Plate Format. *J. Chromatogr. A* **2007**, *1149* (2), 127–137. https://doi.org/10.1016/j.chroma.2007.02.117.

(213) Harris, G. A.; Fernández, F. M. Simulations and Experimental Investigation of Atmospheric Transport in an Ambient Metastable-Induced Chemical Ionization Source. *Anal. Chem.* **2009**, *81* (1), 322–329. https://doi.org/10.1021/ac802117u.

(214) Pawliszyn, J. Development of SPME Devices and Coatings. In *Handbook of Solid Phase Microextraction*; Pawliszyn, J., Ed.; Waltham, 2012; pp 61–97.

(215) Wen, R.; Zeng, D.; Yang, Z.; Jiang, L.; Ma, M.; Chen, B.; Van Beek, T. A. Rapid Analysis of Illegal Cationic Dyes in Foods and Surface Waters Using High Temperature Direct Analysis in Real Time High-Resolution Mass Spectrometry. *J. Agric. Food Chem.* **2018**, *66* (28), 7542–7549. https://doi.org/10.1021/acs.jafc.8b02388.

(216) Gross, J. H. Direct Analysis in Real Time-a Critical Review on DART-MS. *Anal. Bioanal. Chem.* **2014**, *406* (1), 63–80. https://doi.org/10.1007/s00216-013-7316-0.

(217) Guo, J.; Zhang, M.; Liu, J.; Luo, R.; Yan, T.; Yang, T.; Jiang, X.; Dong, M.; Yin,

Y. Evaluation of the Deterioration State of Archaeological Wooden Artifacts: A Nondestructive Protocol Based on Direct Analysis in Real Time – Mass Spectrometry (DART-MS) Coupled to Chemometrics. *Anal. Chem.* **2020**, *92* (14), 9908–9915. https://doi.org/10.1021/acs.analchem.0c01429.

(218) *Direct Analysis in Real Time Mass Spectrometry: Principles and Practices of DART-MS*, 1st ed.; Dong, Y., Ed.; Wiley-VCH Verlag, 2017. https://doi.org/10.1002/9783527803705.

(219) Navare, A. T.; Mayoral, J. G.; Nouzova, M.; Noriega, F. G.; Fernández, F. M. Rapid Direct Analysis in Real Time (DART) Mass Spectrometric Detection of Juvenile Hormone III and Its Terpene Precursors. *Anal. Bioanal. Chem.* **2010**, *398* (7–8), 3005–3013. https://doi.org/10.1007/s00216-010-4269-4.

(220) Borges, D. L. G.; Sturgeon, R. E.; Welz, B.; Curtius, A. J.; Mester, Z. Ambient Mass Spectrometric Detection of Organometallic Compounds Using Direct Analysis in Real Time. *Anal. Chem.* **2009**, *81* (23), 9834–9839. https://doi.org/10.1021/ac901778n.

(221) Gómez-Ríos, G. A.; Mirabelli, M. F. Solid Phase Microextraction-Mass Spectrometry: Metanoia. *TrAC - Trends Anal. Chem.* **2019**, *112*, 201–211. https://doi.org/10.1016/j.trac.2018.12.030.

(222) Pawliszyn, J.; Kudlejova, L.; Risticevic, S.; Vuckovic, D. Solid-Phase Microextraction Method Development. In *Handbook of Solid Phase Microextraction*; 2012; pp 201–249.

(223) Peng, Y.; Gautam, L.; Hall, S. W. The Detection of Drugs of Abuse and Pharmaceuticals in Drinking Water Using Solid-Phase Extraction and Liquid

Chromatography-Mass Spectrometry. *Chemosphere* **2019**, *223*, 438–447. https://doi.org/10.1016/j.chemosphere.2019.02.040.

(224) Ng, K. T.; Rapp-Wright, H.; Egli, M.; Hartmann, A.; Steele, J. C.; Sosa-Hernández, J. E.; Melchor-Martínez, E. M.; Jacobs, M.; White, B.; Regan, F.; et al. High-Throughput Multi-Residue Quantification of Contaminants of Emerging Concern in Wastewaters Enabled Using Direct Injection Liquid Chromatography-Tandem Mass Spectrometry. *J. Hazard. Mater.* **2020**, *398* (April), 122933. https://doi.org/10.1016/j.jhazmat.2020.122933.

(225) Ng, K. T.; Rapp-Wright, H.; Egli, M.; Hartmann, A.; Steele, J. C.; Sosa-Hernández, J. E.; Melchor-Martínez, E. M.; Jacobs, M.; White, B.; Regan, F.; et al. High-Throughput Multi-Residue Quantification of Contaminants of Emerging Concern in Wastewaters Enabled Using Direct Injection Liquid Chromatography-Tandem Mass Spectrometry. *J. Hazard. Mater.* **2020**, *398* (April), 122933. https://doi.org/10.1016/j.jhazmat.2020.122933.

(226) Peng, Y.; Gautam, L.; Hall, S. W. The Detection of Drugs of Abuse and Pharmaceuticals in Drinking Water Using Solid-Phase Extraction and Liquid Chromatography-Mass Spectrometry. *Chemosphere* **2019**, *223*, 438–447. https://doi.org/10.1016/j.chemosphere.2019.02.040.

(227) Wang, X.; Li, X.; Li, Z.; Zhang, Y.; Bai, Y.; Liu, H. Online Coupling of In-Tube Solid-Phase Microextraction with Direct Analysis in Real Time Mass Spectrometry for Rapid Determination of Triazine Herbicides in Water Using Carbon-Nanotubes-Incorporated Polymer Monolith. *Anal. Chem.* **2014**, *86* (10), 4739–4747. https://doi.org/10.1021/ac500382x.

(228) Wang, L.; Zeng, S.; Chen, T.; Qu, H. Direct Analysis in Real Time Mass Spectrometry, a Process Analytical Technology Tool for Real-Time Process Monitoring in Botanical Drug Manufacturing. *J. Pharm. Biomed. Anal.* **2014**, *91*, 202–209. https://doi.org/10.1016/j.jpba.2013.12.034.

(229) Drzyzga, O. Diphenylamine and Derivatives in the Environment: A Review. *Chemosphere* **2003**, *53* (8), 809–818. https://doi.org/10.1016/S0045-6535(03)00613-1.

(230) Márquez-Sillero, I.; Aguilera-Herrador, E.; Cárdenas, S.; Valcárcel, M. Ion-Mobility Spectrometry for Environmental Analysis. *TrAC - Trends Anal. Chem.* **2011**, *30* (5), 677–690. https://doi.org/10.1016/j.trac.2010.12.007.

(231) Sisco, E.; Verkouteren, J.; Staymates, J.; Lawrence, J. Rapid Detection of Fentanyl, Fentanyl Analogues, and Opioids for on-Site or Laboratory Based Drug Seizure Screening Using Thermal Desorption DART-MS and Ion Mobility Spectrometry. *Forensic Chem.* **2017**, *4*, 108–115. https://doi.org/10.1016/j.forc.2017.04.001.

(232) Baumbach, J.; Eiceman, G. Ion Mobility Spectrometry: Arriving On Site and Moving Beyond a Low Profile. *Focal Point* **1999**.

(233) Feng, G.; Hao, Y.; Wu, L.; Chen, S. A Visible-Light Activated [2 + 2] Cycloaddition Reaction Enables Pinpointing Carbon-Carbon Double Bonds in Lipids. *Chem. Sci.* **2020**, *11* (27), 7244–7251. https://doi.org/10.1039/d0sc01149e.

(234) Sunderland, E. M.; Hu, X. C.; Dassuncao, C.; Tokranov, A. K.; Wagner, C. C.; Allen, J. G. A Review of the Pathways of Human Exposure to Poly- and Perfluoroalkyl Substances (PFASs) and Present Understanding of Health Effects.

J. Expo. Sci. Environ. Epidemiol. **2019**, *29* (2), 131–147. https://doi.org/10.1038/s41370-018-0094-1.

(235) Xiao, F. Emerging Poly- and Perfluoroalkyl Substances in the Aquatic Environment: A Review of Current Literature. *Water Res.* **2017**, *124*, 482–495. https://doi.org/10.1016/j.watres.2017.07.024.

(236) Tian, Q.; Sun, M. *Analysis of GenX and Other Per- and Polyfluoroalkyl Substances in Environmental Water Samples*, 1st ed.; Elsevier Inc., 2019; Vol. 11. https://doi.org/10.1016/B978-0-12-815730-5.00014-4.

(237) Janda, J.; Nödler, K.; Brauch, H. J.; Zwiener, C.; Lange, F. T. Robust Trace Analysis of Polar (C2-C8) Perfluorinated Carboxylic Acids by Liquid Chromatography-Tandem Mass Spectrometry: Method Development and Application to Surface Water, Groundwater and Drinking Water. *Environ. Sci. Pollut. Res.* **2019**, *26* (8), 7326–7336. https://doi.org/10.1007/s11356-018-1731-x.

(238) Lind, L.; Zethelius, B.; Salihovic, S.; Van Bavel, B.; Lind, P. M. Circulating Levels of Perfluoroalkyl Substances and Prevalent Diabetes in the Elderly. *Diabetologia* **2014**, *57* (3), 473–479. https://doi.org/10.1007/s00125-013-3126-3.

(239) Cousins, I. T.; Dewitt, J. C.; Goldenman, G.; Herzke, D.; Lohmann, R.; Miller, M.; Ng, C. A.; Scheringer, M.; Vierke, L.; Wang, Z. Environmental Science Processes & Impacts Substances (PFAS) to Protect Human And. **2020**, 1444–1460. https://doi.org/10.1039/D0EM00147C.

(240) Kwiatkowski, C. F.; Andrews, D. Q.; Birnbaum, L. S.; Bruton, T. A.; Dewitt, J. C.; Knappe, D. R. U.; Ma, M. V; Miller, M. F.; Pelch, K. E.; Reade, A.; et al. Scienti Fi c Basis for Managing PFAS as a Chemical Class. **2020**.

https://doi.org/10.1021/acs.estlett.0c00255.

(241) Mulabagal, V.; Liu, L.; Qi, J.; Wilson, C.; Hayworth, J. S. A Rapid UHPLC-MS/MS Method for Simultaneous Quantitation of 23 Perfluoroalkyl Substances (PFAS) in Estuarine Water. *Talanta* **2018**, *190* (May), 95–102. https://doi.org/10.1016/j.talanta.2018.07.053.

(242) World Health Organization. Draft Guidelines for PFOA and PFOS https://www.who.int/teams/environment-climate-change-and-health/water-sanitation-and-health/chemical-hazards-in-drinking-water/per-and-polyfluoroalkyl-substances.

(243) USEPA. Technical Fact Sheet: Drinking Water Health Advisories for Four PFAS (PFOA, PFOS, GenX Chemicals, and PFBS). EPA 822-F-22-002. EPA, Office of Water, Health and Ecological Criteria Division, Washington, DC. **2022**, No. June.

(244) Cousins, I. T.; Dewitt, J. C.; Glüge, J.; Goldenman, G.; Herzke, D.; Lohmann, R.; Ng, C. A.; Scheringer, M.; Wang, Z. The High Persistence of PFAS Is Sufficient for Their Management as a Chemical Class. *Environ. Sci. Process. Impacts* **2020**, *22* (12), 2307–2312. https://doi.org/10.1039/d0em00355g.

(245) DuPont. DuPont GenX Processing Aid for Making Fluoropolymer Resins https://www.chemours.com/Industrial_ Bakery_Solutions/en_GB/assets/downloads/Chemours_GenX_ Brochure_Final_07July2010.pdf (accessed Feb 16, 2023).

(246) Nakayama, S. F.; Yoshikane, M.; Onoda, Y.; Nishihama, Y.; Iwai-Shimada, M.; Takagi, M.; Kobayashi, Y.; Isobe, T. Worldwide Trends in Tracing Poly- and Perfluoroalkyl Substances (PFAS) in the Environment. *TrAC - Trends Anal. Chem.*

2019, *121*, 115410. https://doi.org/10.1016/j.trac.2019.02.011.

(247) Jahnke, A.; Berger, U. Trace Analysis of Per- and Polyfluorinated Alkyl Substances in Various Matrices-How Do Current Methods Perform? *J. Chromatogr. A* **2009**, *1216* (3), 410–421. https://doi.org/10.1016/j.chroma.2008.08.098.

(248) Olomukoro, A. A.; Emmons, R. V.; Godage, N. H.; Cudjoe, E.; Gionfriddo, E. Ion Exchange Solid Phase Microextraction Coupled to Liquid Chromatography/Laminar Flow Tandem Mass Spectrometry for the Determination of Perfluoroalkyl Substances in Water Samples. *J. Chromatogr. A* **2021**, *1651*, 462335. https://doi.org/10.1016/j.chroma.2021.462335.

(249) Cooks, R. G.; Ouyang, Z.; Takats, Z.; Wiseman, J. M. Ambient Mass Spectrometry. *Science (80-.).* **2006**, *311* (5767), 1566–1570. https://doi.org/10.1126/science.1119426.

(250) Lesiak, A. D.; Musah, R. A. Application of Ambient Ionization High Resolution Mass Spectrometry to Determination of the Botanical Provenance of the Constituents of Psychoactive Drug Mixtures. *Forensic Sci. Int.* **2016**, *266* (2016), 271–280. https://doi.org/10.1016/j.forsciint.2016.06.009.

(251) Jastrzembski, J. A.; Sacks, G. L. Solid Phase Mesh Enhanced Sorption from Headspace (SPMESH) Coupled to DART-MS for Rapid Quantification of Trace-Level Volatiles. *Anal. Chem.* **2016**, *88* (17), 8617–8623. https://doi.org/10.1021/acs.analchem.6b01787.

(252) Rýdlová, L.; Prchalová, J.; Škorpilová, T.; Rohlík, B. A.; Čížková, H.; Rajchl, A. Evaluation of Cocoa Products Quality and Authenticity by DART/TOF-MS. *Int. J.*

Mass Spectrom. **2020**, *454*. https://doi.org/10.1016/j.ijms.2020.116358.

(253) Zabalegui, N.; Manzi, M.; Depoorter, A.; Hayeck, N.; Roveretto, M.; Li, C.; Van Pinxteren, M.; Herrmann, H.; George, C.; Monge, M. E. Seawater Analysis by Ambient Mass-Spectrometry-Based Seaomics. *Atmos. Chem. Phys.* **2020**, *20* (10), 6243–6257. https://doi.org/10.5194/acp-20-6243-2020.

(254) Bai, Y.; Zhang, J.; Bai, Y.; Liu, H. Direct Analysis in Real Time Mass Spectrometry Combined with Single-Drop Liquid-Liquid-Liquid Microextraction for the Rapid Analysis of Multiple Phytohormones in Fruit Juice. *Anal. Bioanal. Chem.* **2012**, *403* (8), 2307–2314. https://doi.org/10.1007/s00216-012-5728-x.

(255) Cody, R.; Maleknia, S. D. Coated Glass Capillaries as SPME Devices for DART Mass Spectrometry. *Rapid Commun. Mass Spectrom.* **2020**, *34* (23). https://doi.org/10.1002/rcm.8946.

(256) Li, X.; Ma, W.; Li, H.; Ai, W.; Bai, Y.; Liu, H. Sampling and Analyte Enrichment Strategies for Ambient Mass Spectrometry. *Anal. Bioanal. Chem.* **2018**, *410* (3), 715–724. https://doi.org/10.1007/s00216-017-0658-2.

(257) Albert, A.; Shelley, J. T.; Engelhard, C. Plasma-Based Ambient Desorption/Ionization Mass Spectrometry: State-of-the-Art in Qualitative and Quantitative Analysis. *Anal. Bioanal. Chem.* **2014**, *406* (25), 6111–6127. https://doi.org/10.1007/s00216-014-7989-z.

(258) Olomukoro, A. A.; DeRosa, C.; Gionfriddo, E. Investigation of the Adsorption/Desorption Mechanism of Perfluoroalkyl Substances on HLB-WAX Extraction Phases for Microextraction. *Anal. Chim. Acta* **2023**, *1260*. https://doi.org/10.1016/j.aca.2023.341206.

(259) Lawson, J. *Design and Analysis of Experiments with R*; 2015.

(260) Zhang, Z.; Baixiaofeng. Comparison about the Three Central Composite Designs with Simulation. *Proc. - Int. Conf. Adv. Comput. Control. ICACC 2009* **2009**, No. 3, 163–167. https://doi.org/10.1109/ICACC.2009.48.

(261) Marrubini, G.; Dugheri, S.; Cappelli, G.; Arcangeli, G.; Mucci, N.; Appelblad, P.; Melzi, C.; Speltini, A. Experimental Designs for Solid-Phase Microextraction Method Development in Bioanalysis: A Review. *Anal. Chim. Acta* **2020**, *1119*, 77–100. https://doi.org/10.1016/j.aca.2020.04.012.

(262) Lyon, P. A.; Tomer, K. B.; Gross, M. L. Fast Atom Bombardment and Tandem Mass Spectrometry for Characterizing Fluoroalkanesulfonates. *Anal. Chem.* **1985**, *57* (14), 2984–2989. https://doi.org/10.1021/ac00291a051.

(263) Arsenault, G.; McAlees, A.; McCrindle, R.; Riddell, N. Analysis of Perfluoroalkyl Anion Fragmentation Pathways for Perfluoroalkyl Carboxylates and Sulfonates during Liquid Chromatography/Tandem Mass Spectrometry: Evidence for Fluorine Migration Prior to Secondary and Tertiary Fragmentation. *Rapid Commun. Mass Spectrom.* **2007**, *21* (23), 3803–3814. https://doi.org/10.1002/rcm.3274.

(264) Brase, R. A.; Spink, D. C. Enhanced Sensitivity for the Analysis of Perfluoroethercarboxylic Acids Using LC-ESI-MS/MS: Effects of Probe Position, Mobile Phase Additive, and Capillary Voltage. *J. Am. Soc. Mass Spectrom.* **2020**, *31* (10), 2124–2132. https://doi.org/10.1021/jasms.0c00244.

(265) Box, G. E. P.; Wilson, K. B. On the Experimental Attainment of Optimum Conditions. *J. R. Stat. Soc. Ser. B* **1951**, *13* (1), 1–38.

https://doi.org/10.1111/j.2517-6161.1951.tb00067.x.

(266) Vasiljevic, T.; Gómez-Ríos, G. A.; Pawliszyn, J. Single-Use Poly(Etheretherketone) Solid-Phase Microextraction-Transmission Mode Devices for Rapid Screening and Quantitation of Drugs of Abuse in Oral Fluid and Urine via Direct Analysis in Real-Time Tandem Mass Spectrometry. *Anal. Chem.* **2018**, *90* (1), 952–960. https://doi.org/10.1021/acs.analchem.7b04005.

(267) Watt, L.; Sisco, E. Detection of Trace Drugs of Abuse in Baby Formula Using Solid-Phase Microextraction Direct Analysis in Real-Time Mass Spectrometry (SPME-DART-MS). *J. Forensic Sci.* **2021**, *66* (1), 172–178. https://doi.org/10.1111/1556-4029.14568.

(268) Torbick, N.; Ziniti, B.; Stommel, E.; Linder, E.; Andrew, A.; Caller, T.; Haney, J.; Bradley, W.; Henegan, P. L.; Shi, X. Assessing Cyanobacterial Harmful Algal Blooms as Risk Factors for Amyotrophic Lateral Sclerosis. *Neurotox. Res.* **2018**, *33* (1), 199–212. https://doi.org/10.1007/s12640-017-9740-y.

(269) Delcourt, N.; Claudepierre, T.; Maignien, T.; Arnich, N.; Mattei, C. Cellular and Molecular Aspects of the β-N-Methylamino-l-Alanine (BMAA) Mode of Action within the Neurodegenerative Pathway: Facts and Controversy. *Toxins (Basel).* **2018**, *10* (1). https://doi.org/10.3390/toxins10010006.

(270) Beri, J.; Nash, T.; Martin, R. M.; Bereman, M. S. Exposure to BMAA Mirrors Molecular Processes Linked to Neurodegenerative Disease. *Proteomics* **2017**, *17* (17–18), 17–18. https://doi.org/10.1002/pmic.201700161.

(271) Dunlop, R. A.; Cox, P. A.; Banack, S. A.; Rodgers, K. J. The Non-Protein Amino Acid BMAA Is Misincorporated into Human Proteins in Place of L-Serine

Causing Protein Misfolding and Aggregation. *PLoS One* **2013**, *8* (9), 8. https://doi.org/10.1371/journal.pone.0075376.

(272) Cox, P. A.; Banack, S. A.; Murch, S. J. Biomagnification of Cyanobacterial Neurotoxins and Neurodegenerative Disease among the Chamorro People of Guam. *Proc. Natl. Acad. Sci. U. S. A.* **2003**, *100* (23), 13380–13383. https://doi.org/10.1073/pnas.2235808100.

(273) Baker, T. C.; Tymm, F. J. M.; Murch, S. J. Assessing Environmental Exposure to β-N-Methylamino-l-Alanine (BMAA) in Complex Sample Matrices: A Comparison of the Three Most Popular LC-MS/MS Methods. *Neurotox. Res.* **2018**, *33* (1), 43–54. https://doi.org/10.1007/s12640-017-9764-3.

(274) Bishop, S. L.; Murch, S. J. A Systematic Review of Analytical Methods for the Detection and Quantification of β-: N -Methylamino-l-Alanine (BMAA). *Analyst* **2020**, *145* (1), 13–28. https://doi.org/10.1039/c9an01252d.

(275) Banack, S. A. Methods for the Chemical Analysis of β - N -Methylamino-L-A Lanine : What Is Known and What Remains to Be Determined. **2018**, 184–191. https://doi.org/10.1007/s12640-017-9744-7.

(276) Faassen, E. J. *Presence of the Neurotoxin BMAA in Aquatic Ecosystems: What Do We Really Know?*; 2014. https://doi.org/10.3390/toxins6031109.

(277) Faassen, E. J.; Gillissen, F.; Lürling, M. A Comparative Study on Three Analytical Methods for the Determination of the Neurotoxin BMAA in Cyanobacteria. *PLoS One* **2012**, *7* (5). https://doi.org/10.1371/journal.pone.0036667.

(278) Glover, W. B.; Mash, D. C.; Murch, S. J. The Natural Non-Protein Amino Acid N-β-Methylamino-L-Alanine (BMAA) Is Incorporated into Protein during Synthesis.

Amino Acids **2014**, *46* (11), 2553–2559. https://doi.org/10.1007/s00726-014-1812-1.

(279) Murch, S. J.; Cox, P. A.; Banack, S. A. A Mechanism for Slow Release of Biomagnified Cyanobacterial Neurotoxins and Neurodegenerative Disease in Guam. *Proc. Natl. Acad. Sci. U. S. A.* **2004**, *101* (33), 12228–12231. https://doi.org/10.1073/pnas.0404926101.

(280) Bishop, S. L.; Murch, S. J. A Systematic Review of Analytical Methods for the Detection and Quantification of β-: N -Methylamino-l-Alanine (BMAA). *Analyst* **2020**, *145* (1), 13–28. https://doi.org/10.1039/c9an01252d.

(281) Buszewski, B.; Noga, S. Hydrophilic Interaction Liquid Chromatography (HILIC)-a Powerful Separation Technique. *Anal. Bioanal. Chem.* **2012**, *402* (1), 231–247. https://doi.org/10.1007/s00216-011-5308-5.

(282) Restek Corporation. How to Avoid Common Problems with HILIC Methods https://www.restek.com/en/technical-literature-library/articles/how-to-avoid-common-problems-with-hilic-methods/.

(283) Beach, D. G.; Kerrin, E. S.; Quilliam, M. A. Selective Quantitation of the Neurotoxin BMAA by Use of Hydrophilic-Interaction Liquid Chromatography-Differential Mobility Spectrometry-Tandem Mass Spectrometry (HILIC-DMS-MS/MS). *Anal. Bioanal. Chem.* **2015**, *407* (28), 8397–8409. https://doi.org/10.1007/s00216-015-9012-8.

(284) Needham, S. R.; Brown, P. R.; Duff, K.; Bell, D. Optimized Stationary Phases for the High-Performance Liquid Chromatography-Electrospray Ionization Mass Spectrometric Analysis of Basic Pharmaceuticals. *J. Chromatogr. A* **2000**, *869* (1–

2), 159–170. https://doi.org/10.1016/S0021-9673(99)00986-3.

(285) Santasania, C. T.; Bell, D. S. Mechanisms of Interaction Responsible for Alternative Selectivity of Fluorinated Stationary Phases. *LC-GC Eur.* **2016**, *29* (2), 86–92.

(286) Bell, D. S.; Jones, A. D. Solute Attributes and Molecular Interactions Contributing to "U-Shape" Retention on a Fluorinated High-Performance Liquid Chromatography Stationary Phase. *J. Chromatogr. A* **2005**, *1073* (1–2), 99–109. https://doi.org/10.1016/j.chroma.2004.08.163.

(287) Cudjoe, E.; Pawliszyn, J. Optimization of Solid Phase Microextraction Coatings for Liquid Chromatography Mass Spectrometry Determination of Neurotransmitters. *J. Chromatogr. A* **2014**, *1341*, 1–7. https://doi.org/10.1016/j.chroma.2014.03.035.

(288) Bell, D. S. Solute Attributes and Molecular Interactions Contributing to Retention on a Fluorinated High-Performance Liquid Chromatography Stationary Phase, The Pennsylvania State University, 2005.

(289) U.S. Department of Health and Human Services; Food and Drug Organization. *Bioanalytical Method Validation Guidance for Industry*; 2018; Vol. 1043.

(290) Restek Corporation. How do instrinsically base-deactivated phases work? https://www.restek.com/en/technical-literature-library/articles/how-do-intrinsically-base-deactivated-phases-work/.

(291) Restek Corporation. Underivatized Amino Acids Analysis in Baby Formula on Raptor Polar X https://www.restek.com/en/pages/chromatogram-view/LC_FF0579.

(292) Cooper, W. T.; Smith, P. L. Retention Mechanisms in Cyanopropyl Normal Bonded Phase High-Performance Liquid Chromatographic Columns. *J. Chromatogr. A* **1986**, *355* (C), 57–74. https://doi.org/10.1016/S0021-9673(01)97303-0.

(293) Linford, M. R.; Jensen, D. S.; Clark, J.; Teutenberg, T. Elevated Temperatures in Liquid Chromatography, Part III: A Closer Look at the van 't Hoff Equation. *LCGC North Am.* **2012**, *30* (12), 1052–1057.

(294) Reichardt, C.; Welton, T. *Solvents and Solvent Effects in Organic Chemistry: Fourth Edition*; 2010. https://doi.org/10.1002/9783527632220.

(295) Bell, D. S.; Cramer, H. M.; Jones, A. D. Rational Method Development Strategies on a Fluorinated Liquid Chromatography Stationary Phase: Mobile Phase Ion Concentration and Temperature Effects on the Separation of Ephedrine Alkaloids. *J. Chromatogr. A* **2005**, *1095* (1–2), 113–118. https://doi.org/10.1016/j.chroma.2005.08.004.

(296) Wells, M. J. M. Handling Large Volume Samples: Applications of SPE to Environmental Matrices. In *Solid-phase extraction: Principles, applications and techniques*; 2000; pp 97–123.

(297) Horváth, C. *High-Performance Liquid Chromatography: Advances and Perspectives*; Horváth, C., Ed.; Academic Press: New York, 1980. https://doi.org/doi.org/10.1016/C2013-0-10805-7.

(298) Morris, H. R.; Al-Sarraj, S.; Schwab, C.; Gwinn-Hardy, K.; Perez-Tur, J.; Wood, N. W.; Hardy, J.; Lees, A. J.; McGeer, P. L.; Daniel, S. E.; et al. A Clinical and Pathological Study of Motor Neurone Disease on Guam. *Brain* **2001**, *124* (11),

2215–2222. https://doi.org/10.1093/brain/124.11.2215.

(299) Murch, S. J.; Cox, P. A.; Banack, S. A.; Steele, J. C.; Sacks, O. W. Occurrence of β-Methylamino-L-Alanine (BMAA) in. ALS/PDC Patients from Guam. *Acta Neurol. Scand.* **2004**, *110* (4), 267–269. https://doi.org/10.1111/j.1600-0404.2004.00320.x.

(300) Brand, L. E. Human Exposure to Cyanobacteria and BMAA. In *Amyotrophic Lateral Sclerosis*; 2009; Vol. 10, pp 85–95. https://doi.org/10.3109/17482960903273585.

(301) Roney, B. R.; Renhui, L.; Banack, S. A.; Murch, S.; Honegger, R.; Cox, P. A. Consumption of Fa Cai Nostoc Soup: A Potential for BMAA Exposure from Nostoc Cyanobacteria in China? In *Amyotrophic Lateral Sclerosis*; 2009; Vol. 10, pp 44–49. https://doi.org/10.3109/17482960903273031.

(302) Waidyanatha, S.; Ryan, K.; Sanders, J. M.; Mcdonald, J. D.; Wegerski, C. J.; Doyle-eisle, M.; Garner, C. E. Disposition of β - N -Methylamino- L -Alanine (L-BMAA), a Neurotoxin , in Rodents Following a Single or Repeated Oral Exposure. *Toxicol. Appl. Pharmacol.* **2018**, *339* (December 2017), 151–160. https://doi.org/10.1016/j.taap.2017.12.008.

(303) Banack, S. A.; Murch, S. J. Multiple Neurotoxic Items in the Chamorro Diet Link BMAA with ALS/PDC. In *Amyotrophic Lateral Sclerosis*; 2009; Vol. 10, pp 34–40. https://doi.org/10.3109/17482960903278451.

(304) Wu, X.; Wu, H.; Gu, X.; Zhang, R.; Ye, J.; Sheng, Q. Biomagnification Characteristics and Health Risk Assessment of the Neurotoxin BMAA in Freshwater Aquaculture Products of Taihu Lake Basin, China. *Chemosphere* **2019**,

229, 332–340. https://doi.org/10.1016/j.chemosphere.2019.04.210.

(305) Sighinolfi, G.; Clark, S.; Blanc, L.; Cota, D.; Rhourri-Frih, B. Mass Spectrometry Imaging of Mice Brain Lipid Profile Changes over Time under High Fat Diet. *Sci. Rep.* **2021**, *11* (1), 1–14. https://doi.org/10.1038/s41598-021-97201-x.

(306) Godage, N. H.; Cudjoe, E.; Chau, T.; Gionfriddo, E. Quantitative Determination of Pesticides in Human Plasma Using Bio-SPME-LC–MS/MS: A Robust Tool to Assess Occupational Exposure to Pesticides. *Anal. Bioanal. Chem.* **2023**, No. 0123456789. https://doi.org/10.1007/s00216-023-04589-8.

(307) Bonfiglio, R.; King, R. C.; Olah, T. V.; Merkle, K. The Effects of Sample Preparation Methods on the Variability of the Electrospray Ionization Response for Model Drug Compounds. *Rapid Commun. Mass Spectrom.* **1999**, *13* (12), 1175–1185. https://doi.org/10.1002/(SICI)1097-0231(19990630)13:12<1175::AID-RCM639>3.0.CO;2-0.

(308) Lage, S.; Burian, A.; Rasmussen, U.; Costa, P. R.; Annadotter, H.; Godhe, A.; Rydberg, S. BMAA Extraction of Cyanobacteria Samples: Which Method to Choose? *Environ. Sci. Pollut. Res.* **2016**, *23* (1), 338–350. https://doi.org/10.1007/s11356-015-5266-0.

(309) Li, A.; Fan, H.; Ma, F.; McCarron, P.; Thomas, K.; Tang, X.; Quilliam, M. A. Elucidation of Matrix Effects and Performance of Solid-Phase Extraction for LC-MS/MS Analysis of β-N-Methylamino-l-Alanine (BMAA) and 2,4-Diaminobutyric Acid (DAB) Neurotoxins in Cyanobacteria. *Analyst* **2012**, *137* (5), 1210–1219. https://doi.org/10.1039/c2an15887f.

(310) Al-Sammak, M. A.; Hoagland, K. D.; Snow, D. D.; Cassada, D. Methods for

Simultaneous Detection of the Cyanotoxins BMAA, DABA, and Anatoxin- A in Environmental Samples. *Toxicon* **2013**, *76*, 316–325. https://doi.org/10.1016/j.toxicon.2013.10.015.

(311) Lendor, S.; Olkowicz, M.; Boyaci, E.; Yu, M.; Diwan, M.; Hamani, C.; Palmer, M.; Reyes-Garcés, N.; Gómez-Ríos, G. A.; Pawliszyn, J. Investigation of Early Death-Induced Changes in Rat Brain by Solid Phase Microextraction via Untargeted High Resolution Mass Spectrometry: In Vivo versus Postmortem Comparative Study. *ACS Chem. Neurosci.* **2020**, *11* (12), 1827–1840. https://doi.org/10.1021/acschemneuro.0c00270.

(312) Cudjoe, E.; Bojko, B.; Delannoy, I.; Saldivia, V.; Pawliszyn, J. Solid-Phase Microextraction: A Complementary InVivo Sampling Method to Microdialysis. *Angew. Chemie - Int. Ed.* **2013**, *52* (46), 12124–12126. https://doi.org/10.1002/anie.201304538.

(313) Lendor, S.; Hassani, S. A.; Boyaci, E.; Singh, V.; Womelsdorf, T.; Pawliszyn, J. Solid Phase Microextraction-Based Miniaturized Probe and Protocol for Extraction of Neurotransmitters from Brains in Vivo. *Anal. Chem.* **2019**, *91* (7), 4896–4905. https://doi.org/10.1021/acs.analchem.9b00995.

(314) Defaix, C.; Solgadi, A.; Pham, T. H.; Gardier, A. M.; Chaminade, P.; Tritschler, L. Rapid Analysis of Glutamate, Glutamine and GABA in Mice Frontal Cortex Microdialysis Samples Using HPLC Coupled to Electrospray Tandem Mass Spectrometry. *J. Pharm. Biomed. Anal.* **2018**, *152*, 31–38. https://doi.org/10.1016/j.jpba.2018.01.039.

(315) Lendor, S.; Hassani, S. A.; Boyaci, E.; Singh, V.; Womelsdorf, T.; Pawliszyn, J.

Solid Phase Microextraction-Based Miniaturized Probe and Protocol for Extraction of Neurotransmitters from Brains in Vivo. *Anal. Chem.* **2019**, *91* (7), 4896–4905. https://doi.org/10.1021/acs.analchem.9b00995.

(316) Bag, M. A.; Valenzuela, L. M. Impact of the Hydration States of Polymers on Their Hemocompatibility for Medical Applications: A Review. *Int. J. Mol. Sci.* **2017**, *18* (8). https://doi.org/10.3390/ijms18081422.

(317) Souza-Silva, É. A.; Reyes-Garcés, N.; Gómez-Ríos, G. A.; Boyaci, E.; Bojko, B.; Pawliszyn, J. A Critical Review of the State of the Art of Solid-Phase Microextraction of Complex Matrices III. Bioanalytical and Clinical Applications. *TrAC - Trends Anal. Chem.* **2015**, *71*, 249–264. https://doi.org/10.1016/j.trac.2015.04.017.

(318) Vuckovic, D.; Zhang, X.; Cudjoe, E.; Pawliszyn, J. Solid-Phase Microextraction in Bioanalysis: New Devices and Directions. *Journal of Chromatography A*. Elsevier B.V. 2010, pp 4041–4060. https://doi.org/10.1016/j.chroma.2009.11.061.

(319) Tarazona, K.; Béziat, N. S.; Cebrián-torrejón, G.; Gros, O.; De, A. P.; Harynuk, J. J. Metabolomic Analysis of Secondary Metabolites from Caribbean Crab Gills Using Comprehensive Two-Dimensional Gas Chromatography - Time-of-Flight Mass Spectrometry — New Inputs for a Better Understanding of Symbiotic Associations in Crustaceans. *J. Chromatogr. Open* **2022**, *2* (August), 100069. https://doi.org/10.1016/j.jcoa.2022.100069.

(320) Guo, K.; Zhao, Z.; Luo, L.; Wang, S.; Zhang, R.; Xu, W.; Qiao, G. Ecotoxicology and Environmental Safety Untargeted GC-MS Metabolomics Reveals the Metabolic Responses in the Gills of Chinese Mitten Crab (Eriocheir Sinensis)

Subjected to Air-Exposure Stress. *Ecotoxicol. Environ. Saf.* **2022**, *231*, 113159. https://doi.org/10.1016/j.ecoenv.2021.113159.

(321) Oliveira, A. P.; Lopes, A. C.; Silva, M.; Andrade, P. B.; Valentão, P. Exploring Montagu's Crab: Primary and Secondary Metabolites and Enzyme Inhibition. *Arab. J. Chem.* **2019**, *12* (8), 4017–4025. https://doi.org/10.1016/j.arabjc.2016.03.007.

(322) Craig, H. D.; Jenkins, T. F.; Johnson, M. T.; Walker, D. M.; Dobb, D. E.; Pepich, B. V. Method Development and Laboratory Intercomparison of an RP-HPLC-UV Method for Energetic Chemicals in Marine Tissues. *Talanta* **2019**, *198* (November 2018), 284–294. https://doi.org/10.1016/j.talanta.2019.02.005.

(323) Rupp, H. S.; Stuart, J. S.; Hurlbut, J. A. Liquid Chromatography/Tandem Mass Spectrometry Analysis of Chloramphenicol in Cooked Crab Meat. *J. AOAC Int.* **2005**, *88* (4), 1155–1159. https://doi.org/10.1093/jaoac/88.4.1155.

(324) Matuszewski, B. K.; Constanzer, M. L.; Chavez-Eng, C. M. Strategies for the Assessment of Matrix Effect in Quantitative Bioanalytical Methods Based on HPLC-MS/MS. *Anal. Chem.* **2003**, *75* (13), 3019–3030. https://doi.org/10.1021/ac020361s.

(325) Glover, W. B.; Liberto, C. M.; McNeil, W. S.; Banack, S. A.; Shipley, P. R.; Murch, S. J. Reactivity of β-Methylamino-L-Alanine in Complex Sample Matrixes Complicating Detection and Quantification by Mass Spectrometry. *Anal. Chem.* **2012**, *84* (18), 7946–7953. https://doi.org/10.1021/ac301691r.

(326) Diaz-parga, P.; Goto, J. J.; Krishnan, V. V. On the Differential Roles of Mg2+, Zn2+, and Cu2+ in the Equilibrium of β-N-Methyl-Amino-L-Alanine (BMAA)

and Its Carbamates. *Neurotox. Res.* **2021**, *39* (1), 6–16.

https://doi.org/10.1007/s12640-019-00157-0.

Appendix A

Supporting Information for Chapter 3

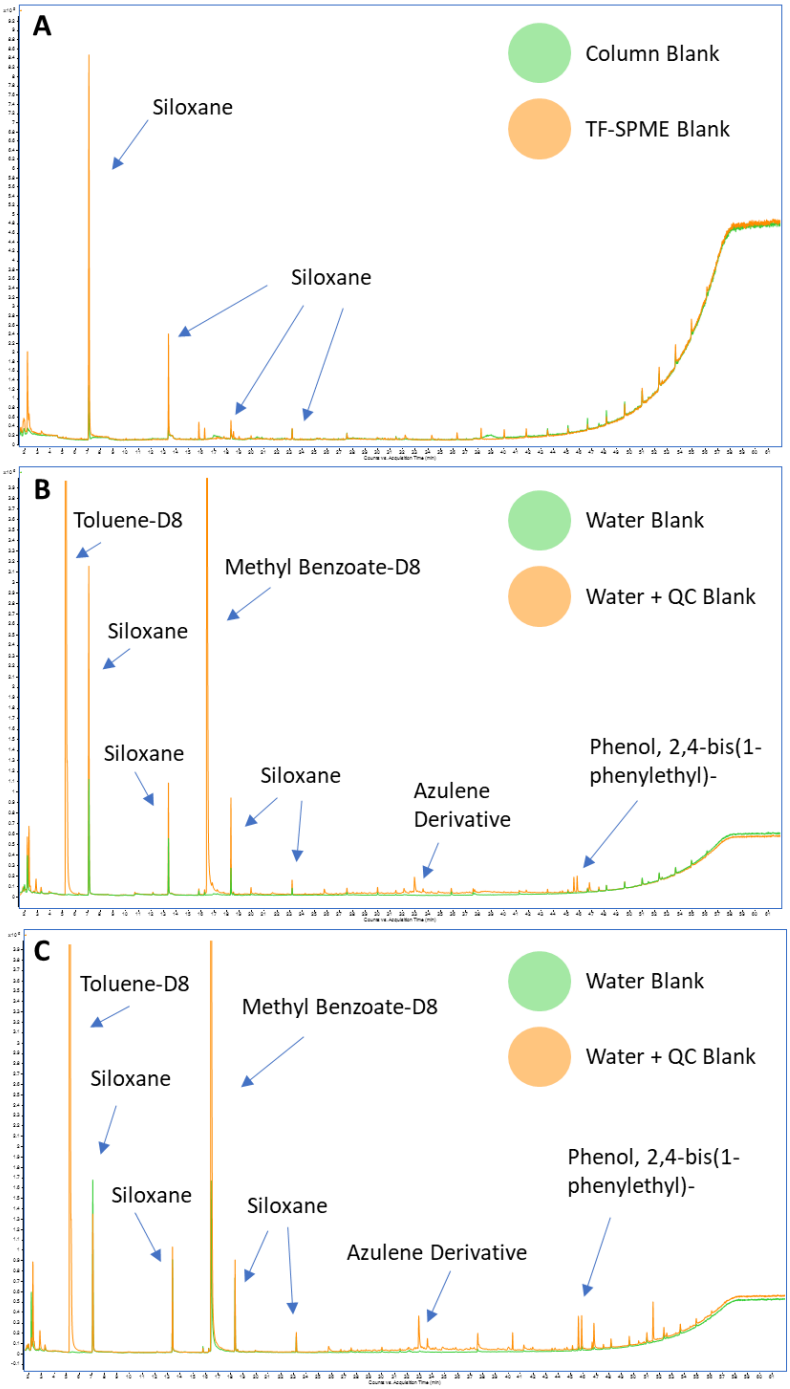

Figure A-1 Overlaid chromatograms of a) GC-MS blank and TF-SPME-GC-MS blank b) DI-TFME analysis with and without QC compound loading c) HS-TFME analysis with and without QC compound loading.

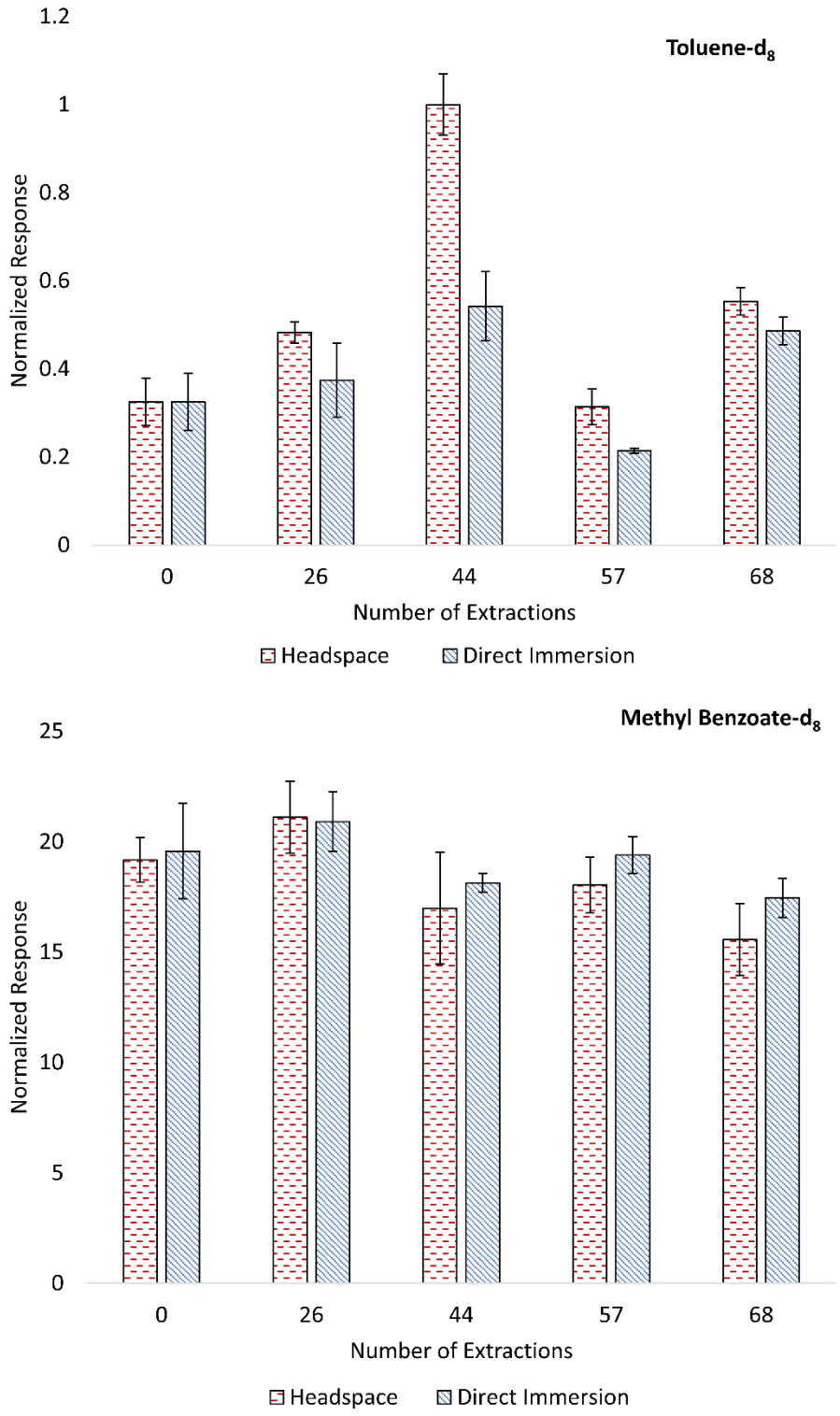

Figure A-2 Reproducibility of QC compounds (toluene-d_8 and methyl benzoate-d_8) loaded onto the TF-SPME device. The loading procedure involved a 5 min DI extraction at room temperature and 600 rpm from 9 ml of ultrapure water spiked with the two QC compounds at 500 µg L^{-1}.

Table A.1 Sample PW 1 characterization.

RT	Compound	MF	Area	ΔRI	Extraction Mode
3.81	1,4-Dioxane	92	104754	42	DI & HS
4.16	Butanenitrile, 2-methyl-	91	160090	49	DI & HS
5.15	Toluene	87	57154	19	DI & HS
6.04	Cyclopentanol, 1-methyl-	89	159767	11	DI & HS
6.17	Hexane, 3-methyl-4-methylene-	87	139936	84	HS
7.11	Heptane, 2,6-dimethyl-	89	96088	41	DI & HS
7.36	Cyclohexane, 1,1,3-trimethyl-	88	156671	79	DI & HS
8.11	Heptane, 2,3-dimethyl-	92	118962	69	HS
8.74	Cyclohexane, 1,2,3-trimethyl-, (1.alpha.,2.beta.,3.alpha.)-	84	74531	29	DI
9.74	2-Hexanol, 2,5-dimethyl-, (S)-	81	369259	57	DI & HS
9.93	4-Octen-3-one	83	74732	53	DI & HS
10.30	Heptane, 2,3,5-trimethyl-	90	198764	94	HS
10.99	Octane, 2,6-dimethyl-	96	676202	49	DI & HS
10.99	Octane, 3,6-dimethyl-	95	255323	49	DI
11.24	Heptane, 3-ethyl-2-methyl-	94	667006	56	DI & HS
11.69	Cyclohexane, 1,1,2,3-tetramethyl-	89	478763	21	DI & HS
11.87	Cyclohexene, 3-methyl-6-(1-methylethyl)-	80	123281	1	HS
12.40	Cyclohexane, 1-methyl-4-(1-methylethyl)-, trans-	86	124672	0	DI & HS
12.79	Cyclopentane, 1-methyl-3-(2-methylpropyl)-	91	736819	30	HS
12.79	Cyclohexane, (2-methylpropyl)-	90	445274	29	DI & HS
13.15	2-Heptanol, 2,6-dimethyl-	94	2384786	53	DI & HS
13.38	2-Octanol, 2-methyl-	89	962787	6	DI & HS
14.12	Decane, 4-methyl-	96	1132092	27	DI & HS
14.40	Cyclohexane, butyl-	89	309752	46	DI & HS
15.15	Naphthalene, decahydro-	90	323623	46	DI & HS
15.48	1-Ethyl-2,2,6-trimethylcyclohexane	79	334803	11	HS
15.84	Cyclohexane, 1,1,3,5-tetramethyl-, cis-	82	411910	100	HS
15.94	1-Methylcyclooctanol	80	502273	46	DI
16.13	Tetrahydrocarvone	81	315818	63	DI
17.48	Naphthalene, decahydro-2-methyl-	94	1054965	34	DI & HS
17.50	Decane, 3,7-dimethyl-	85	493156	43	DI & HS
18.68	Naphthalene, decahydro-1,5-dimethyl-	82	369642	56	DI & HS
19.11	Naphthalene, decahydro-2,6-dimethyl-	90	651121	42	DI & HS
19.86	1H-Indene, 2,3-dihydro-1,1,3-trimethyl-	84	106759	35	HS
20.10	Undecane, 2,6-dimethyl-	96	1794760	30	DI & HS
20.35	Cyclohexane, 2-butyl-1,1,3-trimethyl-	92	677282	50	DI & HS
20.83	Cyclohexane, hexyl-	86	216181	37	DI & HS
21.52	Tridecane, 5-methyl-	88	164004	84	DI
21.52	Dodecane, 4-methyl-	86	421049	16	HS
21.76	Tridecane, 7-methyl-	94	2051679	75	DI & HS
22.52	Tridecane	83	230894	12	DI
23.01	Tridecane, 6-methyl-	91	641251	30	DI & HS
23.19	Naphthalene, 1,2,3,4-tetrahydro-1-methyl-	88	2639008	50	DI
24.10	Cyclohexane, 1,1'-methylenebis-	79	221792	80	HS
24.21	Tridecane, 2-methyl-	83	164518	15	DI
24.40	Tridecane, 3-methyl-	80	152852	95	DI
24.55	Dodecane, 2,6,10-trimethyl-	95	2335859	57	DI & HS

RT	Compound	MF	Area	ΔRI	Extraction Mode
24.74	1(2H)-Naphthalenone, 3,4-dihydro-	88	597308	46	DI
25.16	Tetradecane	88	463742	13	DI & HS
26.21	Ethanone, 1-(2,3-dihydro-1H-inden-5-yl)-	81	135052	99	DI
26.71	2,6,10-Trimethyltridecane	97	2E+06	98	DI & HS
26.8	Decahydro-1,1,4a,5,6-pentamethylnaphthalene	83	280389	34	DI & HS
26.93	Tetradecane, 3-methyl-	80	89996	22	DI
27.65	Pentadecane	90	434042	57	DI
28.1	2,4-Di-tert-butylphenol	87	328432	36	DI
29.73	Hexadecane	88	409173	13	DI
31.09	Pentadecane, 2,6,10-trimethyl-	91	2E+06	31	DI & HS
31.29	Cyclohexane, decyl-	86	244510	17	DI & HS
32.34	Pentadecane, 2,6,10,14-tetramethyl-	98	3E+06	51	DI & HS
33.54	Cyclohexane, undecyl-	79	198688	12	DI
34.52	Hexadecane, 2,6,10,14-tetramethyl-	96	2E+06	55	DI & HS
35.06	Heptadecane, 2-methyl-	79	318350	88	DI
35.9	1,2-Benzenedicarboxylic acid, bis(2-methylpropyl) ester	91	310211	32	DI & HS
36.35	Nonadecane	85	267252	12	DI
37.08	Anthracene, 2-methyl-	85	301290	41	HS
37.09	Phenanthrene, 2-methyl-	86	310437	41	HS
39.24	Phenanthrene, 3,6-dimethyl-	86	184178	43	DI & HS
44.55	Methyl dehydroabietate	78	46921	90	HS
45.18	Tetracosane	86	199933	8	DI & HS
46.74	Pentacosane	86	99453	7	HS
51.76	Octacosane	84	147668	5	HS

Table A-2 Sample PW 2 characterization.

RT	Compound	MF	Area	ΔRI	Extraction Mode
2.85	1,4-Dioxane	78	119613	42	DI & HS
3.21	Butanenitrile, 2-methyl-	97	513359	50	DI & HS
3.66	Pyridine	96	1E+06	87	DI
4.91	2-Hexenal, (E)-	93	946722	18	DI & HS
6.03	1-Octene, 3,3-dimethyl-	83	379406	95	DI
6.36	2-Pentanone, 3-ethyl-	95	137300	46	DI & HS
6.73	2-Heptanone	86	114762	8	HS
6.73	2-Hexanone, 4-methyl-	91	207014	56	DI & HS
6.85	2-Cyclohexen-1-ol	82	85192	42	DI
7.12	2-Hexanone, 5-methyl-	88	189651	67	DI
7.27	Octane, 2-methyl-	93	438719	8	DI & HS
7.59	Octane, 3-methyl-	97	392263	17	DI & HS
8.28	Benzene, 1,3-dimethyl-	88	70606	19	HS
8.29	p-Xylene	87	79769	19	DI
8.32	Cyclohexane, 1-ethyl-4-methyl-, cis-	85	622739	52	HS
8.33	1-Octene, 6-methyl-	89	326553	47	DI
8.69	Nonane	98	1E+06	17	DI & HS
9.57	Octane, 2,5-dimethyl-	97	328573	36	DI & HS
9.76	Cyclohexane, propyl-	85	2E+06	51	HS
9.94	Octane, 2,6-dimethyl-	98	3E+06	46	DI & HS
9.99	Octane, 3,6-dimethyl-	98	3E+07	47	HS
10.12	Heptane, 3-ethyl-2-methyl-	94	1E+06	51	DI & HS

RT	Compound	MF	Area	ΔRI	Extraction Mode
10.34	Cyclopentane, 1-methyl-3-(2-methylpropyl)-	90	2E+06	12	HS
10.68	Octane, 4-ethyl-	92	1E+06	2	DI & HS
10.9	Nonane, 5-methyl-	93	2E+06	8	HS
10.97	Nonane, 4-methyl-	96	2E+06	10	DI & HS
11.1	Nonane, 2-methyl-	94	1E+06	14	DI & HS
11.46	Benzene, 1,2,3-trimethyl-	76	64952	45	DI
11.51	m-Menthane, (1S,3S)-(+)-	86	6E+06	0	HS
11.73	Cyclohexane, 1-methyl-2-propyl-	92	2E+06	58	DI & HS
11.86	Cyclohexane, 1-methyl-4-(1-methylethyl)-, trans-	86	273366	10	DI & HS
12.02	Cyclooctane, 1,2-dimethyl-	87	7E+06	91	HS
12.38	Decane	99	5E+06	15	DI & HS
12.62	Benzene, 1-methyl-4-propyl-	93	556995	99	HS
12.76	cis-1-Ethyl-3-methyl-cyclohexane	81	251838	70	DI & HS
12.97	o-Cymene	81	49531	25	DI & HS
13.43	Cyclohexane, butyl-	94	2E+06	48	DI & HS
13.54	Benzene, 1-methyl-3-(1-methylethyl)-	80	198989	8	HS
13.73	Nonane, 3,7-dimethyl-	89	1E+07	54	HS
13.77	1-Ethyl-2,2,6-trimethylcyclohexane	79	476419	35	DI & HS
13.95	Benzene, 1,4-diethyl-	81	59499	60	HS
14.18	Nonane, 2,3-dimethyl-	79	127683	67	DI & HS
14.23	Naphthalene, decahydro-	90	660799	46	DI
14.27	Naphthalene, decahydro-, trans-	93	9E+06	45	HS
14.3	Decane, 5-methyl-	90	1E+06	6	DI
14.35	Nonane, 2,5-dimethyl-	85	6E+06	72	HS
14.42	Decane, 4-methyl-	94	1E+06	9	DI
14.55	Acetophenone	88	269093	35	DI
14.58	Decane, 2-methyl-	96	2E+06	14	DI & HS
14.77	Decane, 3-methyl-	95	2E+06	20	DI & HS
14.9	Cyclohexane, 1,1,3,5-tetramethyl-, cis-	82	736527	99	DI & HS
15.12	5-Undecene	78	6E+06	42	HS
15.43	Cyclohexane, (1,2-dimethylpropyl)-	77	2E+07	40	HS
15.52	1,2,4-Trithiolane	87	466863	70	DI
15.76	Undecane	99	1E+07	15	DI & HS
15.97	Benzene, 1-methyl-4-(1-methylpropyl)-	85	176319	34	DI & HS
16.09	Naphthalene, decahydro-2-methyl-	95	3E+06	51	DI
16.26	Undecane, 5-methyl-	92	1E+06	33	DI & HS
16.39	Thiophene, 2-pentyl-	75	849138	71	HS
16.56	Decane, 3,7-dimethyl-	94	3E+06	40	DI & HS
16.81	Cyclohexane, pentyl-	92	2E+06	44	DI & HS
17.41	Decane, 2,5-dimethyl-	88	2E+06	68	DI
17.64	Undecane, 4-methyl-	86	6E+06	11	HS
17.67	Nonane, 5-butyl-	85	1E+07	87	HS
17.73	Benzene, (1-methylbutyl)-	82	425720	37	HS
17.75	Undecane, 2-methyl-	93	3E+06	15	DI
17.93	Undecane, 3-methyl-	93	2E+06	21	DI & HS
18.27	Naphthalene, decahydro-1,5-dimethyl-	82	1E+06	41	DI & HS
18.34	Naphthalene, decahydro-2,6-dimethyl-	84	1E+07	39	HS
18.48	3-Hexen-1-ol, propanoate, (Z)-	79	5E+06	98	HS
18.73	1H-Indene, 2,3-dihydro-1,1,3-trimethyl-	84	402464	45	HS
18.84	Dodecane	98	1E+07	14	DI & HS
19.21	Undecane, 2,5-dimethyl-	96	1E+07	28	DI
19.34	Undecane, 2,6-dimethyl-	94	6E+07	33	HS

RT	Compound	MF	Area	ΔRI	Extraction Mode
19.36	Cyclohexane, 2-butyl-1,1,3-trimethyl-	88	2E+06	56	DI & HS
19.94	Cyclohexane, hexyl-	91	2E+06	39	DI & HS
20.16	Undecane, 4-ethyl-	81	343843	2	DI & HS
20.37	Dodecane, 5-methyl-	88	973096	5	DI & HS
20.51	Dodecane, 4-methyl-	86	1E+06	10	DI & HS
20.67	Dodecane, 2-methyl-	94	2E+06	16	DI & HS
20.9	Tridecane, 7-methyl-	91	1E+07	76	DI
21.63	3-Methyl-4-isopropylphenol	80	667056	36	DI
21.69	Tridecane	95	5E+06	13	DI & HS
21.75	Naphthalene, 1,2,3,4-tetrahydro-1-methyl-	85	3E+06	75	DI
21.8	1,1'-Bicyclohexyl	78	788721	37	DI & HS
22.19	Benzene, cyclohexyl-	84	2E+06	35	HS
22.57	Naphthalene, 1,2,3,4-tetrahydro-1,1,6-trimethyl-	76	263227	81	DI & HS
22.84	Heptylcyclohexane	89	2E+06	34	DI & HS
23.03	Tridecane, 6-methyl-	87	774486	1	DI & HS
23.11	Tridecane, 5-methyl-	88	826618	4	DI & HS
23.28	Tridecane, 4-methyl-	78	2E+06	11	HS
23.41	Tridecane, 2-methyl-	92	2E+06	15	DI & HS
23.58	Tridecane, 3-methyl-	91	2E+06	22	DI & HS
23.6	1(2H)-Naphthalenone, 3,4-dihydro-	96	4E+06	34	DI
23.74	Dodecane, 2,6,10-trimethyl-	90	1E+07	57	HS
25.21	Cyclohexane, 1-(1,5-dimethylhexyl)-4-methyl-	78	1E+06	25	DI & HS
25.56	Cyclohexane, octyl-	89	3E+06	28	DI & HS
25.67	Tetradecane, 5-methyl-	84	462755	4	DI
25.88	2,6,10-Trimethyltridecane	92	1E+07	42	DI & HS
25.9	Decahydro-1,1,4a,5,6-pentamethylnaphthalene	86	3E+06	29	HS
25.97	Tetradecane, 4-methyl-	94	1E+06	16	DI & HS
26.87	Pentadecane	93	3E+06	12	DI & HS
26.98	2,4-Di-tert-butylphenol	76	220870	50	DI
27.99	Pentadecane, 7-methyl-	79	3E+06	1	DI
28.11	n-Nonylcyclohexane	89	5E+06	24	DI
28.24	Pentadecane, 4-methyl-	88	857979	10	DI
28.55	Pentadecane, 3-methyl-	85	924432	23	DI
28.58	Phenylglyoxylic Acid, 3-methylbutyl ester	76	115296	57	DI
29.25	Hexadecane	91	3E+06	12	DI & HS
30.32	Pentadecane, 2,6,10-trimethyl-	94	1E+07	30	DI & HS
30.53	Cyclohexane, decyl-	82	1E+06	18	DI
30.69	Hexadecane, 2-methyl-	84	719689	17	DI
31.59	Pentadecane, 2,6,10,14-tetramethyl-	97	2E+07	52	DI & HS
32.82	Cyclohexane, undecyl-	80	966341	13	DI
32.88	Heptadecane, 2-methyl-	80	508777	19	DI
33.03	Heptadecane, 3-methyl-	78	822898	26	DI
33.66	Octadecane	92	2E+06	9	DI & HS
33.8	Hexadecane, 2,6,10,14-tetramethyl-	97	2E+07	55	DI & HS
34.98	Dodecylcyclohexane	80	798050	8	DI
35.7	Nonadecane	93	2E+06	9	DI
35.77	n-Tridecylcyclohexane	79	355747	68	DI
38.11	Phenanthrene, 1,7-dimethyl-	85	781485	16	DI
38.35	Phenanthrene, 3,6-dimethyl-	82	271328	28	DI & HS
40.53	Phenanthrene, 2,3,5-trimethyl-	76	30007	27	HS
41.3	Docosane	90	976458	19	DI & HS
42.99	Tricosane	95	536371	32	HS

RT	Compound	MF	Area	ΔRI	Extraction Mode
44.64	Tetracosane	96	984614	47	HS
46.24	Pentacosane	93	2E+06	64	DI & HS
47.76	Hexacosane	90	879422	86	DI & HS
54.64	Octacosane, 2-methyl-	79	360887	34	DI

Table A.3 Sample PW 3 characterization.

RT	Compound	MF	Area	ΔRI	Extraction Mode
3.14	Methanesulfonyl chloride	82	747	-	HS
6.89	Iodine	99	6E+07	-	DI
7.47	Ethylbenzene	86	94026	27	DI
8.31	Styrene	86	20899	5	DI
9.34	Methane, diiodo-	96	8E+06	-	DI & HS
9.94	Octane, 2,6-dimethyl-	94	165653	46	DI & HS
9.94	Octane, 3,6-dimethyl-	92	148215	46	DI
10.12	Heptane, 3-ethyl-2-methyl-	96	327576	51	DI & HS
10.18	trans-2,4-Dimethylthiane, S,S-dioxide	78	117847	-	HS
10.67	Octane, 4-ethyl-	83	152404	2	HS
10.95	Nonane, 4-methyl-	82	86238	10	HS
11.43	Cyclohexane, 1,1,3-trimethyl-	80	251040	59	HS
11.5	Cyclohexane, 1-methyl-4-(1-methylethyl)-, trans-	80	47754	0	DI & HS
11.72	Cyclohexane, 1-methyl-2-propyl-	84	517734	58	HS
11.74	Benzonitrile	81	133605	24	DI
12.08	Indane	87	16447	55	DI
12.16	Cyclooctane, 1,5-dimethyl-	86	541690	87	HS
12.73	Decane, 2,4-dimethyl-	80	32745	76	DI
13.13	Decane, 4-methyl-	84	195969	29	DI & HS
13.43	Cyclohexane, butyl-	84	123865	48	DI & HS
13.77	1-Ethyl-2,2,6-trimethylcyclohexane	88	231391	35	DI & HS
14.22	Naphthalene, decahydro-, trans-	91	227588	47	DI & HS
14.23	Naphthalene, decahydro-	91	121944	46	DI
14.29	Tetrahydrocarvone	80	219217	91	HS
14.56	Benzonitrile, 2-methyl-	79	43990	6	DI
14.89	Cyclohexane, 1,1,3,5-tetramethyl-, cis-	81	418544	98	DI & HS
15.14	Indan, 1-methyl-	83	67726	26	DI & HS
16.08	Naphthalene, decahydro-2-methyl-	96	994008	51	DI & HS
16.8	Cyclohexane, pentyl-	80	166292	44	HS
18.26	Naphthalene, decahydro-1,5-dimethyl-	87	807423	42	HS
18.26	Naphthalene, decahydro-2,6-dimethyl-	86	391559	42	DI & HS
19.19	Undecane, 2,5-dimethyl-	89	423385	28	HS
19.19	Undecane, 2,6-dimethyl-	88	235328	28	DI
19.34	Cyclohexane, 2-butyl-1,1,3-trimethyl-	92	509650	56	DI & HS

RT	Compound	MF	Area	ΔRI	Extraction Mode
20.58	Methane, triiodo-	88	1E+06	-	DI & HS
21.47	Naphthalene, 2-methyl-	79	35259	52	DI
21.79	1,1'-Bicyclohexyl	77	187176	37	HS
22.38	Furan, 2,5-dibutyl-	78	159403	2	DI & HS
22.56	Naphthalene, 1,2,3,4-tetrahydro-1,1,6-trimethyl-	78	147741	81	HS
23.19	Cyclohexane, 1,1'-methylenebis-	81	158197	84	DI & HS
23.69	Dodecane, 2,6,10-trimethyl-	82	396531	55	HS
30.54	Dodecane, 1-iodo-	87	257291	30	DI & HS
31.56	Pentadecane, 2,6,10,14-tetramethyl-	82	753205	50	DI & HS
32.51	Atrazine	78	74866	49	DI
33.76	Hexadecane, 2,6,10,14-tetramethyl-	85	673905	53	DI
38.39	Cyclic octaatomic sulfur	89	85383	-	DI & HS
39.49	Heneicosane	87	111763	13	HS
41.28	Docosane	93	267306	20	HS
42.99	Tricosane	95	640604	31	HS
44.64	Tetracosane	91	764872	47	DI & HS
46.22	Pentacosane	95	856357	65	DI & HS
47.19	2-Methylpentacosane	84	111304	51	HS
47.75	Hexacosane	94	997907	86	DI & HS
48.82	3-Methylhexacosane	81	113106	66	HS
50.11	2-Methylheptacosane	82	93001	99	HS
50.26	3-Methylheptacosane	84	128673	91	HS
51.65	Cholest-5-en-3-ol (3.beta.)-, acetate	78	249296	16	DI

Appendix B

Supporting Information for Chapter 4

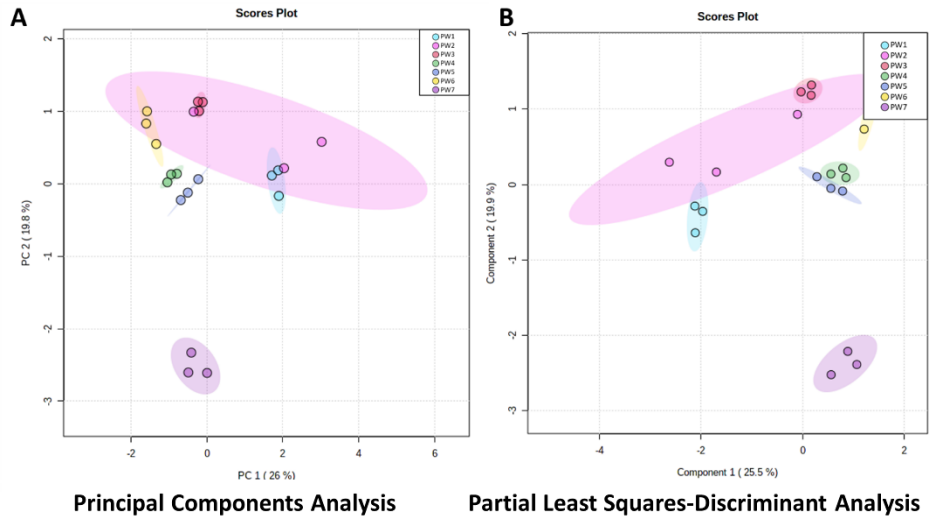

Figure B-1 Plot of organic soluble headspace extraction data analyzed by a) PCA and b) PLS-DA. As the overlap and variance of these data were greater than the other data sets, it was excluded from the final data evaluation.

Table B.1 List of organic solubles characterized in PW samples. Compounds listed are all statistically significant in discriminating each sample from another. Significant p-values ($p < 0.05$; $-\log(p) > 0.77$) are listed along with the identity of the characterized compound.

Compound	-log(p)
3-Buten-2-one, 4-phenyl-, E-	15.20
Tridecane, 5-methyl-	14.32
Methane, diiodo-	13.83
Cyclopentanone, 2-methyl-	13.21
2-Pentanone	12.33
Pyridine	11.98
Octadecane	11.27
Decane, 5,6-dipropyl-	10.69
Tetradecane, 4-methyl-	10.47
Hexadecane, 2-methyl-	10.21
Octacosane	9.94
1-Nonanol, 4,8-dimethyl-	9.78
Naphthalene, decahydro-2-methyl-	9.75
Nonane, 4-methyl-	9.46
7,9-Di-tert-butyl-1-oxaspiro(4,5)deca-6,9-diene-2,8-dione	9.24
1-Dodecanamine, N,N-dimethyl-	9.15
Ethanone, 1-(2-furanyl)-	9.04
Cyclopentane, 1-methyl-3-(2-methylpropyl)-	8.92
2-Heptanol, 2,6 dimethyl-	8.54
Cyclohexane, octyl-	8.50
4-Hexen-3-one, 5-methyl-	8.27
Phenol, 2,4-bis(1-phenylethyl)-	8.18
Benzene, 1,4-diethyl-2-methyl-	8.17
o-Cymene	8.17
Hexanoic acid, 2-ethyl-, methyl ester	8.02
Methane, triiodo-	7.64
Cyclopentanone	7.38
Decane, 3-8-dimethyl-	7.32
Octadecanoic acid	7.28
Pentadecane, 2,6,10,14-tetramethyl-	6.92
Cyclohexane, hexyl-	6.64
Octasulfur	6.57
1,2,4-Trithiolane	6.53
Cyclopentanol, 1-methyl-	6.45
Naphthalene, decahydro-	5.95
Nonane, 5-butyl-	5.75
n-Nonylcyclohexane	5.61

Compound	-log(p)
Docosane	5.51
2-Pentanol, 2-methyl-	5.44
1,2-Benzenedicarboxylic acid, bis(2-methylpropyl) ester	5.38
Phenanthrene, 3,6-dimethyl-	5.34
Tetrahydrocarvone	5.33
Hexadecane, 2,6,10,14-tetramethyl-	5.31
1H-Inden-1-one, 2,3-dihydro-	5.29
Dodecylcyclohexane	5.13
Cyclohexane, 20butyl-1,1,3-trimethyl-	4.90
Triacontane	4.88
Nonacosane	4.59
Hentriacontane	4.58
Cyclohexane, 1,1'-methylenebis-	4.51
Butanenitrile, 2-methyl-	4.33
Naphthalene, decahydro-1,5-dimethyl-	4.16
Heptanal	4.13
Decane, 2-methyl-	4.05
Nonane	3.95
Benzothiazole	3.83
Tricosane	3.80
cis-1-Ethyl-3-methyl-cyclohexane	3.48
Naphthalene, 1,2,3,4-tetrahydro-1,1,6-trimethyl-	3.41
Toluene	3.23
1,4-Dioxane	3.20
Cyclohexane, decyl-	3.05
1H-Indene, 2,3-dihydro-1,1,3-trimethyl-	2.93
Decahydro-1,1,4a,5,6-pentamethylnaphthalene	2.84
Hexacosane	2.78
Phenanthrene, 2-methyl-	2.68
Cyclohexane, 1,1,2,3-tetramethyl-	2.39
2-Heptanol, 2-methyl-	2.29
4,4-Dimethyl octane	2.23
Indane	2.21
Cyclohexane, undecyl-	2.20
Heneicosane	2.18
Cholest-5-en-3-ol (3.beta.)-, acetate	2.12
Iodine	2.12
Decane, 3,7-dimethyl-	2.11
Diethyl Phthalate	2.09
Atrazine	2.07
Benzonitrile, 2-methyl-	2.06
Chloroiodomethane	1.95

Compound	-log(p)
2,2,4-Trimethyl-1,3-pentanediol diisobutyrate	1.90
Benzene, 1,3-dimethyl-	1.89
Heptacosane	1.83
Pentadecane	1.75
Tetracosane	1.61

Table B.2 Elements characterized in PW samples. Metals listed are all statistically significant in discriminating each sample from another source location. Significant p-values ($p < 0.05$; $-\log(p) > 0.77$) are listed along with the name of the element.

Element	-log(p)	Element	-log(p)
Mn	16.59	Eu	8.24
Mg	14.14	V	8.02
Cu	13.05	Gd	7.46
Se	11.95	Pb	6.98
Ag	11.91	Ce	6.31
Rb	10.28	Cd	5.97
Ga	10.21	La	5.37
Co	10.14	Nd	4.74
Ba	9.95	Sm	3.76
Dy	9.92	Zn	3.27
Cs	9.13	Cr	3.12
Yb	8.51		

Appendix C

Supporting Information for Chapter 7

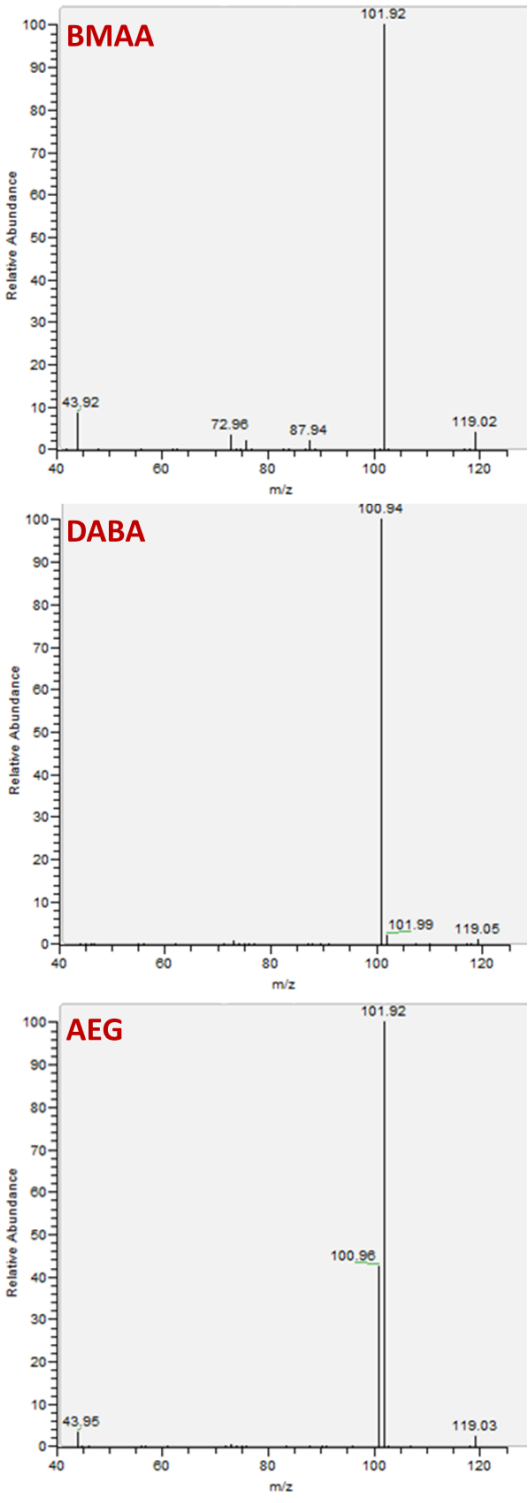

Figure C-1 Mass spectra of all target analytes.

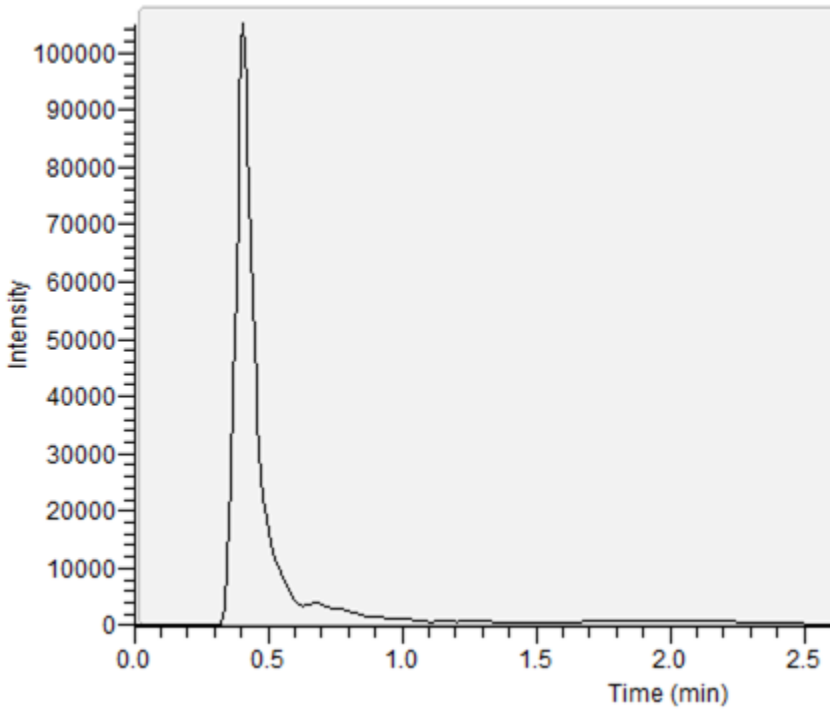

Figure C-2 Representative Pinnacle DB IBD chromatogram of BMAA and DABA. Conditions: gradient 1, mobile phase 1. Evaluated conditions did not permit retention.

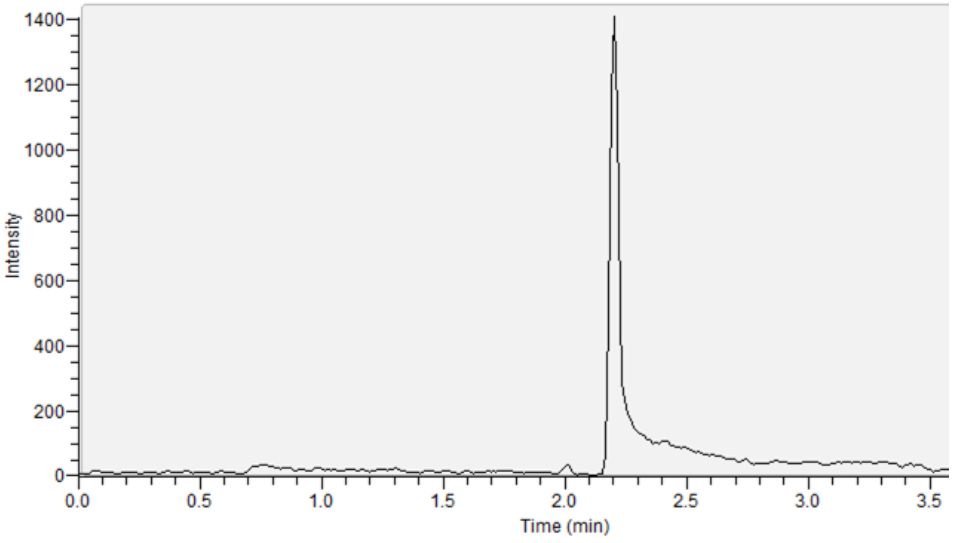

Figure C-3 Representative Raptor Polar X chromatogram BMAA and DABA. Conditions: gradient 1, mobile phase 1. Retention of the analytes was achieved; however, no separation was observed using the conditions outlined in the study.

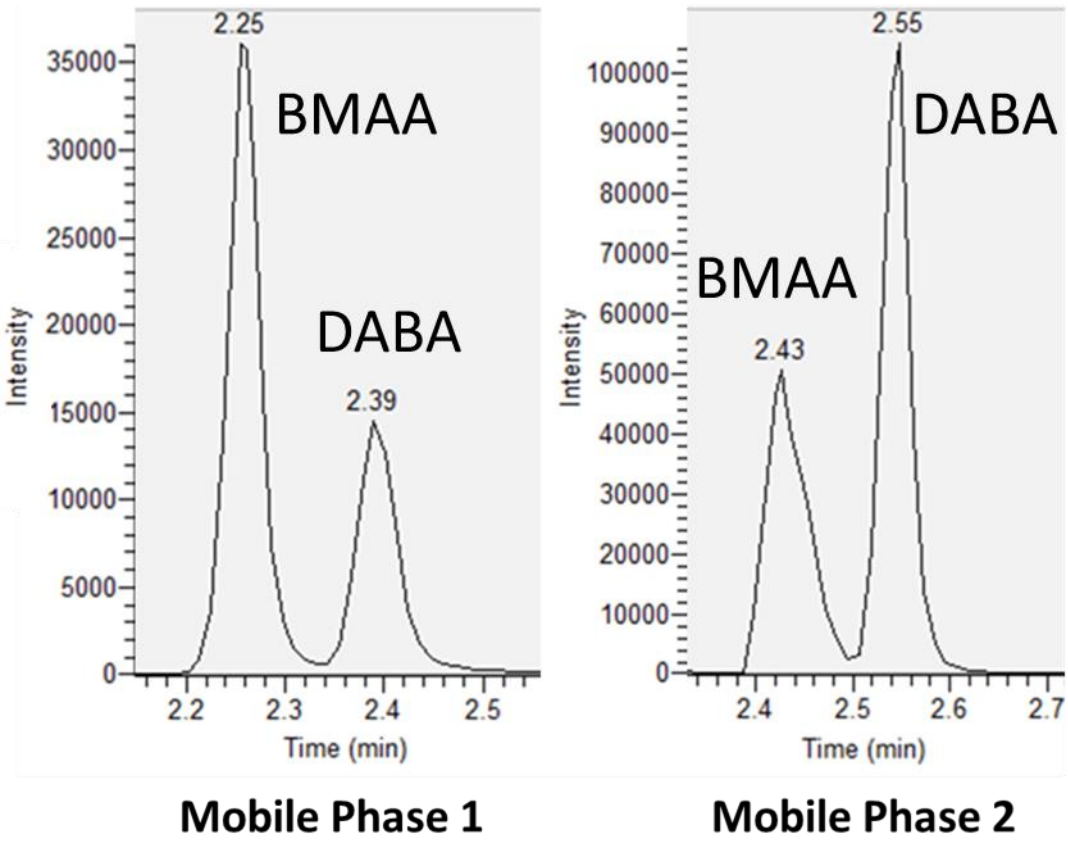

Figure C-4 Chromatograms obtained on the Pinnacle DB Cyano column with gradient 4 and both evaluated mobile phases. It was observed that mobile phase 2, with ACN as its organic composition, demonstrated lower resolution but higher response for the studied analytes.

Table C.1 Global mass spectrometric parameters.

Parameter	Value
Spray Voltage (kV)	4
Source Temperature (°C)	290
Sheath Gas (AU)	20
Aux Gas (AU)	30
Sweep Gas (AU)	30
Capillary Temperature (°C)	270
Capillary Voltage (V)	9
Tube Lens (V)	20

Table C.2 Compound-specific mass spectrometric parameters.

Compound	Parent (*m/z*)	Quantifier (*m/z*)	Qualifier (*m/z*)	CE
BMAA	119	102	44	25
DABA	119	101	-	25
AEG	119	102	44	25
L-serine-d_3	109	91	-	22
L-BMAA-d_3	122	104	-	25

Table C.3 Separation factors and resolutions calculated for the separation of BMAA and DABA using the Pinnacle DB Cyano column.

	Gradient	Separation Factor	Resolution
Mobile Phase 1 (MeOH-based)	1	1.2	5.5
	2	1.0	1.8
	3	1.0	2.2
	4	1.1	2.6
Mobile Phase 2 (ACN-based)	1	1.2	4.0
	2	-	-
	3	1.0	1.3
	4	-	-